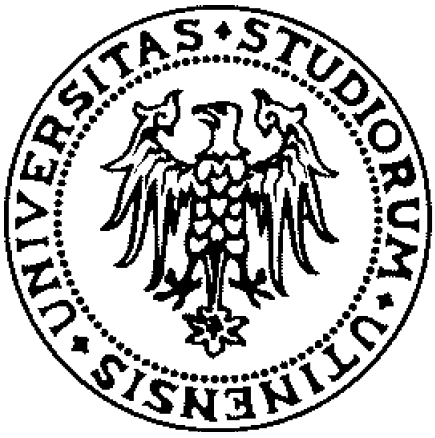

Università degli Studi di Udine

Dipartimento di Ingegneria Elettrica Gestionale e Meccanica
Dottorato in Ingegneria Industriale e dell'Informazione
– XXIV Ciclo –

Tesi di Dottorato

Dynamics and control of flexible-links mechanisms

Relatore:
Prof. Alessandro Gasparetto

Dottorando:
Ing. Paolo Boscariol

Correlatore:
Ing. Vanni Zanotto

Coordinatore:
Prof. Roberto Rinaldo

alla Dani

Desidero ringraziare il prof. Gasparetto, relatore di questa tesi, per la grande disponibilità e cortesia dimostratemi fin dal primo momento in cui ho iniziato a far parte del suo gruppo di ricerca.

Un ringraziamento di cuore va a Vanni Zanotto, per avermi fornito costantemente una mole incredibile di stimoli, di idee e di consigli nel corso degli anni in cui ho avuto il privilegio di lavorare con lui. Non avrò mai la possibilità di ringraziarlo sufficientemente per avermi considerato alla pari di un fratello minore.

Un grazie va anche a Renato ed Albano, allo stesso tempo amici e colleghi. Il loro aiuto, i loro consigli e la loro cortesia hanno reso tutto più facile e divertente.

Contents

Abstract **v**

Sommario **vii**

1 Introduction **1**
- 1.1 FLM dynamics 4
- 1.2 Control of FLM 6
  - 1.2.1 MPC control for FLM 9
- 1.3 Contribution 11

2 Dynamic models of FLM **13**
  - 2.0.1 Kinematics 14
  - 2.0.2 Differential equations of motion 19

3 Simulations **23**
- 3.1 SL: static model 24
- 3.2 4R: static model 27
- 3.3 5R: static model 30
- 3.4 SL: dynamic model 32
  - 3.4.1 2 node SLM: Simulink 36
  - 3.4.2 2 and 3 FEM single link 43
- 3.5 4-bar linkage 48
- 3.6 5 link dynamic model 55

4 MPC **63**
4.1 Closed-loop control . . . 63
4.1.1 Closed-loop control . . . 66
4.2 Predictive control . . . 71
4.2.1 MPC with linear models . . . 73
4.3 Unconstrained MPC . . . 76
4.3.1 State-space models with embedded integrator . . . 76
4.3.2 Predictive control of MIMO system . . . 83
4.4 Constrained MPC . . . 87
4.4.1 The receding horizon concept . . . 87
4.4.2 Control law . . . 94
4.4.3 Formulation as minimum square . . . 98

5 HIL testbed for FLM **103**
5.1 Introduction . . . 103
5.1.1 HIL systems . . . 103
5.2 Reference mechanism . . . 107
5.3 HIL implementation . . . 111
5.4 Validation . . . 114
5.4.1 Validation with PI . . . 114
5.4.2 Validation with LQ . . . 115

6 MPC Results **125**
6.1 MPC control of a four-bar linkage . . . 125
6.2 Reference mechanism . . . 126
6.3 Linear model . . . 128
6.3.1 Accuracy of the linearized model . . . 129
6.3.2 State observer . . . 131
6.3.3 Simulation results . . . 132
6.3.4 Robustness . . . 137
6.4 Tuning parameters . . . 140
6.4.1 PID control . . . 143
6.5 Trajectory tracking and vibration suppression in a 5-link mechanism 145
6.5.1 Reference mechanism . . . 145
6.5.2 Linearized model . . . 147
6.5.3 Tracking in the joint space . . . 149
6.5.4 Effects of the reference lookahead and control tuning . . . 151

6.5.5 Evaluation of robustness . . . 157
6.5.6 End-effector trajectory tracking . . . 159
6.5.7 End effector tracking of a closed trajectory . . . 166
6.5.8 Conclusions . . . 168
6.6 Experimental validation . . . 170
6.6.1 Experimental setup . . . 170
6.7 State observer . . . 171
6.8 Experimental results . . . 173
6.9 Experimental results: comparison between MPC and LQ performance . . . 177
6.10 Conclusion . . . 179

Conclusion **181**

Appendix: Finite Elements for the analysis of elastic beams **183**

A Appendix: Finite Elements for the analysis of elastic beams **183**
A.1 FEM beams . . . 183
A.1.1 The beam element . . . 183
A.1.2 Stiffness matrix . . . 186
A.1.3 Equivalent nodal loads . . . 187
A.1.4 The beam element . . . 189
A.1.5 Artbitrary Orientation . . . 193
A.1.6 Matrices for the 6 d.o.f. beam . . . 194

Abstract

This thesis deals with modeling, Real-Time simulation and model-based control strategies for flexible-link mechanisms. The dynamic model under consideration is based on Finite Element Method (FEM) and Equivalent Rigid Link System (ERLS). Such model is used for the simulation and for the design of closed-loop controls systems for a single-link mechanism, a four-bar linkage and a five-link mechanism. The resulting nonlinear model is used to perform both off-line and Hardware-In-the-Loop (HIL) simulations.

A whole chapter of this work is devoted to the development and experimental validation of a HIL testbed of a single-link planar mechanism with high flexibility and affected by gravity. The experimental validation of the proposed HIL simulator is performed by comparing the response of the real and of the simulated system using the same real-time controller. The comparison shows a good agreement of results.

Moreover two MPC (Model Predictive Control) strategies are investigated as an effective strategy to control both the position and the vibration in flexible-link manipulators. The investigation involves the single-link mechanism, the 4-bar linkage and the five-link manipulator. For the latter, also the ability to track a prescribed trajectory for the end-effector in investigated. Again, for the five-link mechanism, the effect of the choice of different primitives for the trajectory planning algorithm is evaluated trough simulations, as well as the optimal choice for control's tuning parameters. Robustness of the proposed control system is investigated trough several numerical experiments.

In the last part of this work experimental results are proposed to show the

superior capabilities of MPC to perform high-speed movements with limited vibration trough the comparison with traditional control strategies.

Sommario

In questa tesi vengono affrontate diverse problematiche relatice alla modellizzazione, alla simulzione in tempo reale a al controllo di meccanismi articolati a membri flessibili. La formulazione del modello dinamico utilizzato in questo lavoro è basata sulle tecniche ad elementi finiti (FEM) e sul concetto di Equivalent Rigid Link System (ERLS). Tale modello viene sfruttato oer la sumulazione e lo sviluppo di controlli in catena chiusa per tre tipologie di meccanismi: il singolo link, il quadrilatero ed il pentalatero articolato. I risultati presenti riguardano sia simulazioni off-line che simulazioni ottenute secondo l'approccio Hardware-In-the-Loop (HIL).

Un intero capitolo è infatti dedicato allo sviluppo ed alla validazione sperimentale di un banco di prova HIL per un meccanismo planare a singolo link, sottoposto agli effetti della gravità. La validazione sperimentale viene effettuata comparando la risposta del sistema simulato e del sistema reale ottenute sfruttando il medesimo dispositivo hardware di controllo. Tali risultati sperimentali confermano la validità dell'approccio Hardware-In-the-Loop e l'accuratezza del banco di prova sviluppato.

La seconda parte di questo lavoro è dedicata allo sviluppo di tecniche di controllo predittivo per meccanismi a membri flessibili. In particolare, vengono analizzate due architetture MPC (Model Predictive Control) per il controllo simultaneo di posizione e vibrazione di meccanismi flessibili. Tale analisi viene effettuata utilizzando i meccanismi a singolo link, il quadrilatero ed il pentalatero articolato. Nel caso dell'ultimo meccanismo viene inoltre verificata la possibilità di utilizzare il controllo MPC per l'inseguimento di traiettorie dell'end-effector.

I criteri per la scelta dell'algoritmo di pianificazione della traiettoria dell'end-effector e dei parametri di tuning del sistema di controllo MPC vengono investigati a partire da risultati ottenuti in simulazione. Risultati sperimentali vengono riportati nella parte finale di questo lavoro, confermando la superiorità in termini di accuratezza del moto e riduzione delle vibrazioni ottenibili tramite l'utilizzo di tecniche di controllo predittivo, rispetto a quanto ottenibile tramite tecniche di controllo classiche.

1 Introduction

The use of robots has become a necessity in almost all industrial fields. Robots are used for a variety of tasks like assembling circuit boards, installing the circuit boards onto the chassis of electronics, inspection, testing, pick and place, welding, soldering, spray painting and many others. The reasons for their use is the need of performing operations with high speed and precision, producing therefore higher volumes of goods with lower costs.

High speed operation is a reoccurring target in the design and in the operation of robotic manipulator, for clear economic reasons. Also maximizing the ration between the weight of the payload and of the whole manipulator is a common objective of the robot design. Last but not least, lower power consumption is also a profitable target for industries, also if it can be thought that reduced power consumption is often used just as an efficient marketing strategy. It can be reasonably evaluated that the electrical power used by robots in most industrial environments represents just a barely noticeable fraction of the power dissipated by all the production chain, if the environmental costs of obtaining and moving the raw materials used for the production are taken into account. However this considerations should not discourage roboticists who focus on the reduction of power consumption.

Given the impossibility of performing high-speed motion without large actuators and bulky manipulators, as in the traditional approach of most robot producers, a common trend of robot design is to develop lightweight robots also for industrial operations, not only for weight critical tasks, such as outer space explorations. Lightweight robots usually present high flexibility in their links, for obvious reasons. Such flexibility, if neglected or poorly controlled, can lead

to major worsening in the accuracy of positioning and motion, to high mechanical stresses, and also to instability. Therefore, special techniques must be used to achieve safer and more precise operation.

During the last 30 years, a large effort has been made by both the academic and the industrial worlds to offer solutions to the aforementioned problems. Several approaches have been explored, focusing on the main tasks of:

- dynamical modelling
- control
- trajectory planning

Dynamical modelling refers to all the techniques used to obtain a mathematical description of the dynamics of a given physical object. Such goal can be originated from physical considerations, such as Newton's laws, or Euler-Lagrange equations, or from numerical analysis, as sported by the approach based on numerical estimation. The importance of the investigation of dynamical models goes beyond the use of its results for mere practical reasons: to the author's opinion, it represents one, albeit small, step to be taken along the path that leads to a deeper knowledge of the nature.

The problem of finding accurate and profitable dynamic models for elastic manipulators is certainly the most important aspect of FLM studies. Much has been done in the last decades, so that literally hundreds of different possibilities have been investigated. Again a very large number of control techniques have been tested as an effective way of moving with accuracy and speed lightweight robots. This of course does not mean that there is no more chances of bringing significant advances in this field. Moreover, the development of accurate dynamic models is strictly related to the problem of control, since most of the really effective control strategies for this class of mechanisms are actually model-based, meaning that the design of the control system is based on the dynamics of the plant to be controlled. Moreover, the development of control strategies cannot abstract from the use of numerical simulations, which are the first use of dynamic models.

For the same reason, the development of dynamic models is often merged with various aspects of software development, since the target of modelling in robotics if often to produce a working simulator, hopefully with real-time capability. Real-time execution of mechanisms simulators is a topic that is

constantly gaining interest, in the wake of the over increasing of computational power sported by PC manufacturers.

A HIL simulator is a valuable tool to give an evaluation of the performance of the control unit under investigation, in particular it can be used to test its real-time capability. Many modern control techniques, such the very popular Model Predictive Control, are very demanding in term of computational power, so their Real-Time implementation can be very critical when high bandwidth and highly complex processes are involved. The proposed device can be used also to perform an in-depth analysis of the robustness of the control system under test. In many application, especially when model-based control is concerned, it is necessary to evaluate how the control unit would behave in the presence of mismatches between the modeled and the real plant. These test can be easily implemented with the aid of a Hardware-In-the-Loop simulator of the plant, simply by adding some parametric mismatches, nonlinearities, noise, etc. to the simulation model. Among the advantages of the use of HIL simulators, lower implementation costs must be mentioned. Generally, and also in the case under consideration here, the cost of the hardware needed to set-up a simulator like the proposed one is one fraction of the cost of building a real prototype. Moreover, it should be noticed that a careful design of an HIL test-bench allows to perform a seamless transition from the HIL to the traditional experimental setup, in the case that the HIL simulator has the very same physical connection to the control unit.

Also the trajectory planning strategies are covered by a large interest, again as testified by a long list of papers and books on the topic. Moreover, the problem of trajectory planning and the problem of control are very strictly related. Often the approaches used by researchers on trajectory (or in general, motion) planning make extensive use of results coming from control literature. Looking form a further perspective, both of these two problems can be enclosed in the framework of optimization. Therefore, any advance in one of the two direction is of possible use for the other topic.

This dissertation focuses mainly on dynamical modelling and on closed-loop control of flexible link mechanisms. The problem of trajectory tracking is barely touched in the last chapter.

All the designs and simulation presented here originate form an highly accurate nonlinear dynamic model of planar FLM with an arbitrary number of links. The development of such model is based on the principle of virtual works and on finite-element discretization using Euler-Bernoulli beams. The original

development of this model belongs to Giovagnoni, and has been published for the first time in [1].

1.1 Dynamics of flexible-link manipulators

Dynamics of flexible-link mechanism is a topic that has received a wide interests in robotics literature. One of the seminal works on dynamics of this class of mechanisms has been developed by Book, and dates back to 1974 [2]. A brief analysis on the state of the art on modelling of FLM is conducted here, a more complete overview can be found in the review paper [3].

It should be pointed out that robotic systems with flexible link are systems with an infinite number of degrees of freedom, therefore the computation of their dynamics requires to adopt some discretization strategies to bring the dynamic computation to a finite number of DOFs. This is not true if only flexibility at the joints is present, since this kind of effect can be efficiently represented with discrete and concentrated flexible elements, such as springs.

A popular choice is to use the assumed mode formulation, in which the link flexibility is represented by a truncated finite modal series. The main drawback of this method is the difficulty of finding modes for link with non-regular cross section and multi-link manipulators [4].

Another popular approach involves Finite Element Method (FEM), in which the infinite dimension problem is discretized by using some FEM models, the most popular being Euler-Bernoulli beam elements. The use of Timoshenko beams is less frequent, since it allows to perform a better description of the dynamics of FLM only for short links.

In the following some of the most important works are reported, making a distinction between single, and multi-link manipulators.

Single-link manipulators

The assumed method mode uses a truncated finite modal series in terms of spatial mode eigen functions and time-varying mode amplitudes to represent links deformation. A large number of works on the topics has been done, since there are several ways to chose link boundary conditions and mode eigenfunction. AMM together with Lagrangian dynamics is very popular. Some notable works on the topics are [5], [6], [7], [8], [9], [10].

AMM has been used together with other formulation, such as Newton-Euler formulation in [11], or Hamilton's principle in [12].

The works reported so far, as well as the vast majority of papers on FLM dynamics, refer only to manipulators with revolute joints. Among the few works including prismatic joints, [13], [14] and [15] should be cited.

The use of FEM discretization has gained popularity in the 90's, as testified by the notable works by Nagarayan and Turcic [16, 17] and Bricout [18]. An Equivalent Rigid Links System (ERLS) has been developed by Chang and Gannon [19]. ERLS formulation has been used also in [20, 1], i.e. the formulation used for the simulation and control design in this dissertation. As it will be explained in greater details in chapter 2, the formulation by Giovagnoni is based on the virtual work principle. Lagrangian dynamics with FEM discretization is a quite popular approach, as testified by some works such as [21],[22], [23], [24]. All the papers cited so far deals with planar mechanisms. Analysis of 3D mechanisms appears to be less popular: among the few works available on the subject, [25] deals with a single-link mechanism, while [26] deals with a spatial robot with a flexible prismatic link.

Another frequently adopted strategy for the modeling of FLM is the lumped parameter model. This approach tries to describe the dynamics of FLM using concentrated elements of mass and elasticity, often substituting a continuous flexible elements with a set of rigid elements kept together by flexible elements. Some notable works in this field are [27], [28], [29].

Multi-link manipulators

Describing the dynamics of a flexible two-link manipulator is not a simple task, since basic models are usually not sufficiently accurate. This happens because, as shown by Milford and Ashokanathan [30], the eigenfrequencies of a two-link FLM can vary up to 30 % as the manipulators sweeps across its range of motion. Thus a large number of different approaches have been proposed. Among them, [31] and [32] uses a Lagrangian based finite dimension model with assumed mode method. Morris and Madani in [33], [34] and [35] develop the equation of motion for a two-link manipulator using the Lagrange-Euler formulation and assumed method mode. On the other hand Lee showed in [36] that conventional Lagrangian modeling of FLM is not very accurate for links with rotation, and therefore he proposed a new approach to solve this problem. Newton-Euler formulation together with finite element method has been investigated by Rosado in [37] and [38].

Cannon and Schimtz also showed in [5] that multi-link manipulators cannot

be described by a linearized model when dealing with large displacement, since the influence of nonlinearities change significantly with the robot configuration. For this class of mechanism a popular approach is based on Lagrangian dynamics, as testified, among others, by the works [39, 2] by Book, [40] by Siciliano, [41] by Chedmail et. al., [42] by Arteaga. Moreover, Asada et. al. proposed in [43] an approach based on assumed mode model for a n-link robot using a special moving coordinate systems called virtual rigid link coordinates.

FEM is used by Bayo in [6] considering Timoshenko beams including nonlinear Coriolis and Centrifugal effects for the elastic behavior. The same nonlinear terms are also included in the model by Giovagnoni [1], which has the benefit of considering the fully coupled dynamics of both rigid and flexible motion of a planar FLM with an arbitrary number of revolute joints. The same model can also include rigid elements. Such modeling is based on virtual work principle, FEM with Euler-Bernoulli beams, and ERLS principle. This model has been recently extended to 3D mechanisms in the work by Vidoni et. al. [44]. Such investigation deals with a 3 links flexible robot, and the proposed model is compared with the results from ADAMS software. Other works on mechanisms moving in a 3D environment are [45] by Beres and Sasiadek and [46] by Beres et al. Here Lagrangian finite elements approach and Denavit-Hartemberg method is used. Among the others, [47] should be cited as one of the few (if not only) paper focusing on modeling of five-bar linkages.

1.2 Control strategies for flexible-link manipulators

The literature on control of flexible-link mechanism is very extended. Almost any kind of control strategy has been tested in simulation and experimentally on flexible manipulators. Among the many possible variations, PID, optimal control, adaptive control, feedforward control, nonlinear control and in general model-based control systems have been used. Model-based control is the most popular approach, the necessity of this choice is motivated in [46]. Here only a brief analysis of the state of the art of FLM mechanisms is given, since a complete analysis would could be worth of thesis itself. Extensive reviews on the topic can be found in [3] and [48] by Benosmand and Vey.

Both feedforward and feedback strategies have been studied. The first have the advantage of not needing sensors for direct measurement of plant behavior,

but in general they lack the robustness of some feedback controllers. Moreover the design of a feedforward inverse filter is made difficult by the fact that the inverse transfer function of a non-minimum phase system is unstable. This problem can be overcome by designing a stable controller which approximate the inverse transfer function of the plant [49]. Feedback controller can instead, using sensor and more or less sophisticate estimators, track the control of the plant even in the presence of disturbances or unmodeled dynamics. The most common tasks are:

- end-effector regulation
- point-to-point motion
- joint trajectory tracking
- end-effector trajectory tracking

The last topic appears to be the most difficult one, since the nonminimum phase character of FLMs. Other control schemes applied to flexible robots include PID (and its numerous variations), computed torque control, active damping control, adaptive control, neural network based control, lead-lag control, sliding mode control, stable inversion in the frequency domain, stable inversion in the time domain, algebraic control, optimal and robust control, input shaping control and boundary control.

Single link manipulators

The most frequently adopted testbench for control system for FLMs is the single-link mechanisms. This is due to the fact that dynamic modelling is less critical, and also to the fact that this kind of mechanisms is easier to build. Computed torque is used by Looke et al. [50], Kwon and Book [51]. Adaptive control is also quite popular, as testified by the works of Menq and Chen [52], Feliu et al. [53, 54], Yang et al. [55, 56].

Some papers, such as Rattan and Feliu [57] and Karray [58] deals with robust control. This class of controllers can be used efficiently with FLMs since they provide a way to overcome the effects of a less than perfect dynamic model, as it sometimes happens in optimal control. Anyway, optimal control has also been deeply studied, since it can be easily adopted for MIMO systems. Some example includes Pal et al. [59] and Lee [25, 60]. Another approach. which has been developed for the position control of flexible mechanisms, takes advantage of

input shaping techniques. The key idea is to feed the mechanisms with inputs (forces and/or torques) with a particular shape and with precise timing, in order to avoid the excitation of system resonance. The idea is originated from the posicast control developed back in 1957 by Smith [61]. Input shaping is used by Singhose et al. in [62, 63], by Liu et al. in [64], by Rhim and Book in [65], just to report some examples. It should be pointed out that input shaping techniques, besides being a very elegant solution, often lack in robustness to modeling errors.

An emerging approach to the solution of vibration problems is the use of of smart materials. In particular, piezoelectric actuator can be used together with traditional electric motors to improve vibration damping. This topic is dealt with in [66, 67] by Choi et al. with robust control. The motor controls the rigid motion, while the piezoceramic actuators provide a proper vibration damping. A similar approach is also investigated by Ge et al. in [68]

Multi-link manipulators

As for single-link manipulators, two-link robots have been often used as test-benches for the development of control strategies for FLMs. Some solutions are briefly described in this section. Computed torque control is considered in [69] by Bayo, in [70] by Cheong et al., and in [71]. An application of sliding control is reported in [72, 73] by Zhang et al., while the simpler approach of PD control is favored by Yigit in [74]. Many other approaches can be found in literature, but tracking all of them is beyond the purpose of this short literature review.

Concerning manipulators with more than two links, the application of non-linear feedback PID feedforward and Lyapunov stabilization to a six dof flexible manipulator in [75] should be cited. A five bar manipulator with only one flexible link is controlled by a LQR regulator plus an input shaping approach in [76] by Boyer et al. A five bar linkage with all the moving links with flexibility is treated using PID control by Gallina et al. in [77]. Sliding mode control based on pole assignment is developed by Utkin in [78]. Neural network control can also be effective with FLMs, as shown in [79] by Isogai et al. Also model-free control can be a good choice for flexible multi-link manipulators, and this topic is dealt with in [80, 81, 68, 82]. Adaptive control is applied to a four-bar linkage by Trevisani in [83, 84]. Optimal control is used in [25], in [35] and in [85], just to cite some significant works. Of particular interest is also robust control, which can be a very effective solution to the design of control system

and state observer for FLM. The ability to take into account the modeling error has proven to work quite well with flexible manipulators, as testified by papers such as [86, 87, 88, 89].

1.2.1 MPC control for FLM

Model Predictive Control (MPC) refers to a family of control algorithms that compute an optimal control sequence based on the knowledge of the plant and on the feedback information. The dynamic system, together with a set of constraints, is used as the basis of an optimization problem.

MPC is gaining a wider diffusion in different industrial applications, an interesting report about this specific matter can be found in [90]. This kind of control has been first employed in large chemical factories, but in recent years has experienced a wider diffusion to other industrial fields. For examples Chen [91] has recently proposed the use of MPC control in a ball mill grinding process, while Perez [92] deals with control of a rudder roll stabilization control for ships. Other interesting results on MPC control of high-bandwidth systems are [93], [94] and [95].

The availability of more powerful embedded platforms in the last years has encouraged the development of embedded MPC control systems suitable to fast-dynamic plants. For example Hassapis [96] has developed a multicore PC-based embedded MPC control, while FPGA has been chosen by Ling [97] and He [98].

The literature on MPC as an effective vibration reduction strategy in flexible systems is very limited, and one of the aim of this thesis and of the research that led to it is to fill the gaps in literature.

In the paper [99], MPC is used to control position and vibrations in a single-link flexible link without gravity. The mechanisms sports both an electric actuator which moves the hub, both a piezoelectric actuator to improve the damping of the closed-loop system. FEM discretization and assumed mode method are used to derive a linear state-space model with which dynamics prediction is performed. Good performance is shown to be achievable trough experimental results.

Another paper that should be cited is [100] by Zmeu et al. Again, a single-link manipulator not affected by gravity is considered. In this paper a MPC controller is used to control vibrations in a flexible rotating beam through electric motor and piezo-ceramic actuators. Two independent unconstrained controllers are used to control the angular hub position and the tip of the beam.

Plant dynamic model is developed using artificial neural networks (ANN). Both numerical and experimental results are reported.

In a very recent paper, [101] Bossi et al. conducted an experimental analysis on a single-link FLM not affected by gravity. A linear model is used, and its parameters are obtained trough an off-line procedure. Results are compared with a LQR, and the superior performance of MPC for tracking a step of hub angular position is shown.

The last paper worth of notice is, to the author's best knowledge, [102] by Fan and De Silva. In this paper the dynamic model is nonlinear and based on Euler-Lagrange equations of motion, however the model prediction is performed on a locally linearized model. System identification for unknown payload is introduced as well using a prediction-error method (PEM). Results are provided trough a two-link manipulator unaffected by gravity. Constraints are handled only on control action, by means of saturation functions.

The Author, together with Gasparetto and Zanotto, has developed further works on the predictive control of flexible-links mechanisms. The first example is paper [103], in which the constrained predictive control of a single-link mechanisms affected by gravity is investigated. The dynamic model used for simulation is nonlinear, and the controller design is based on a linearized model. Simulation results provide the evidence that this kind of controller easily outperforms classical controllers such as PID with gravity compensation. An evaluation of the accuracy of the linearized model is provided as well. An experimental validation is provided in [104], where a prototype of a single-link mechanism with gravity is controlled by a real-time MPC. It is shown there that MPC can provide better vibration damping and wider motion excursion than a LQG controller with integral action based on the same dynamic model. MPC is used here together with a Kalman state observer that does not require for elastic displacement to be measured. The only measured value available to the state observer is the angular position of the link.

Concerning other mechanisms, the control of a four-bar linkage is addressed in [105] and in [106]. Here a four-link mechanisms with three flexible link is controlled by a constrained predictive controller. Also a robustness analysis of the controller to parametric mismatches is present in paper [105], together with an evaluation of the accuracy of both the linearized model and the state observer. Some simulation results are also used to show the effect of changing the tuning parameters. Paper [107] gives more insight in the development of the aforementioned state observer. Joint control and end-effector trajectory

tracking for a five-bar flexible linkage is the topic of papers [108] and [109]. The first work presents a deep investigation of the use of MPC control for tracking a desired performance for multi-actuated flexible linkages. An analysis of the robustness to modeling error is conducted, together with a study of the effects of the length of the prediction and control horizons on the accuracy of end effector position tracking. The effects of choosing different trajectories planning algorithms are analyzed, in order to find the one that maximizes the position accuracy. A similar approach is exploited in [109], but here a closed trajectory in the operative space is taken as a test case.

Some other works by the Author deal with the development of HIL simulators of flexible-links mechanisms, such as [110] and [111]. The proposal is to use the HIL real-time simulation as an effective testbench for the development and the tuning of control systems. The simulator takes advantage of a software implementation of a highly accurate nonlinear dynamic model of a single link FLM, which allow to reach not only real-time, but also faster-than real-time operation.

1.3 Contribution

This thesis builds upon and adds to the general body of knowledge surrounding flexible-link mechanisms, focusing on dynamic modelling and control of this class of mechanisms. Specifically, this thesis contributes to the following:

- provides a simulation framework for the development of numerical tests of closed-loop control systems for planar multi-link FLM
- provides an experimental framework, in the form of an Hardware-In-the-Loop simulator for a single-link flexible mechanism. This testbench has been validated experimentally and used with profit for the development of Real-Time control systems
- provides an extensive investigation of the performance that can be obtained by the use of Model Predictive Control strategy for the simultaneous position and vibration control of flexible-link mechanisms. The impact on closed-loop dynamics of control tuning parameters and of trajectory planning algorithms for FLM is investigated as well
- provides an experimental validation of the use of a Real-Time MPC control on a FLM affected by gravity

2

Dynamic models of flexible-link manipulators

In the past 40 years modeling, dynamics and control of flexible-links mechanisms have been a central topic in robotics. The fact that accurate dynamic and control of vibration phenomena would allow to design and build robots with reduced weight and higher operative speed has been the main reason of this popularity. Accurate modeling of both single and multi-body flexible links mechanism have been studied in a great deal of works, extensive reviews of the results obtained so far can be found in [112, 113, 114, 3]. Among the different approaches to dynamics modeling, Finite Element Method (FEM) has been the most popular. This approach, which is based on the discretization of elastic deformation into a finite set of nodal displacements, have been used in [115, 116, 16, 17, 117, 1, 118]. Some authors have also proposed description of flexible mechanisms making use of modal coordinates in places of physical coordinates (see [119, 20, 120]). Other approaches to the dynamic analysis and characterization of planar as well as spatial mechanism can be found in [121, 122].

In this section a detailed description of a dynamic model for flexible-link mechanism is given. The derivation of the model follows the work proposed by Giovagnoni in [1]. The motivation behind the choice of this particular model among the others available in literature is motivated by its accuracy, which has been experimentally evaluated in a large number of works, such as [47] and [123].

2.0.1 Kinematics

First, let us consider a flexible links mechanism composed by an arbitrary number of links. Each link can be subdivided into another arbitrary number of finite elements. The motion of the whole mechanisms can be separated into two components. The first one describes the motion of an equivalent rigid-body mechanism, the second one describes the elastic motion, referred to the nodes of the equivalent rigid-body mechanisms. We can refer to the 'rigid motion' as the motion of the ERLS (Equivalent Rigid-Link System). This procedure has been developed first by Chang and Hamilton in [124]. The formulation under investigation here employs, other than the ERLS concept, the principle of virtual works.

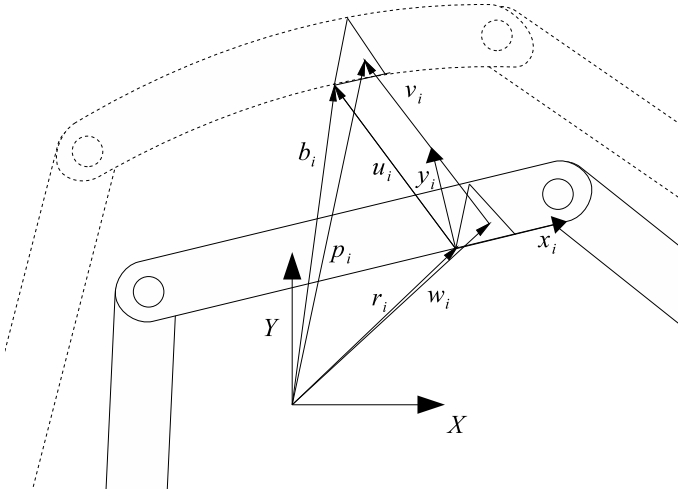

Figure 2.1: Kinematic definitions

We can define the following vectors:

- $\mathbf{r}_i$ is the vector of the position of the nodes of the i-th element of the ERLS;
- $\mathbf{u}_i$ is the vector of the nodal elastic displacement;
- $\mathbf{b}_i$ is the vector of the position of the nodes.

The vector of positions $\mathbf{b}_i$ is linked to $\mathbf{r}_i$ and $\mathbf{u}_i$ trough:

$$\mathbf{b}_i = \mathbf{r}_i + \mathbf{u}_i \tag{2.1}$$

since the motion of the nodes of each elastic element is evaluated as the superimposition of the rigid and of the elastic motion.

In the same way, also the following vectors can be defined:

- $\mathbf{w}_i$ is the vector that measures the position of a generic point belonging to the ERLS
- $\mathbf{v}_i$ is the vector of the displacement of the point to which $\mathbf{w}_i$ refers, measured from the ERLS
- $\mathbf{p}_i$ is the vector obtained from the relation:

$$\mathbf{p}_i = \mathbf{w}_i + \mathbf{v}_i \tag{2.2}$$

All the vectors just defined are measured in the global reference frame $\{X, Y, Z\}$, but they can be also described in the local reference frame connected to the i-th element of the ERLS, $\{x_i, y_i, z_i\}$. The conversion from local to global reference frame can be easily done by noticing that the two reference frame are linked to each other trough the vector q, which is the vector of the generalized coordinates of the equivalent rigid-link system.

In order to evaluate the the position vector p_i for each configuration, the following relation can be used:

$$\mathbf{p}_i = \mathbf{w}_i + \mathbf{R}_i(q)\mathbf{N}_i(x_i, y_i, z_i)\mathbf{T}_i(q)\mathbf{u}_i \tag{2.3}$$

in which $\mathbf{T}_i$ is the global-to-local rotation matrix, defined for the i-th element of the ERSL. In the previous pages, this matrix has been defined as T_{LG}. The corresponding local-to-global transformation matrix is taken as $\mathbf{R}_i$. Both these matrices depends only on the vector of free coordinates $\mathbf{q}$, i.e. on the position of the whole equivalent rigid-body mechanisms. Here we point out that $\mathbf{T}_i$ is a block-diagonal matrix, while $\mathbf{R}_i$ is a square matrix. $\mathbf{N}_i$ is the matrix of the shape function corresponding to the i-th element, and it allows to evaluate the displacement of all the points belonging to each link, as a function of its nodal displacements. If each finite element is modeled as a 6 d.o.f. element whose length is L, taking s as the longitudinal coordinate in the local reference frame, $\mathbf{N}_i$ can be calculated as:

$$\mathbf{N}_i = \begin{bmatrix} 1-\frac{s}{L} & 0 & 0 & \frac{s}{L} & 0 & 0 \\ 0 & 1-3\left(\frac{s}{L}\right)^2+2\left(\frac{s}{L}\right)^3 & s-2\frac{s^2}{L}+\frac{s^3}{L^2} & 0 & 3\left(\frac{s}{L}\right)^2-2\left(\frac{s}{L}\right)^3 & -\frac{s^2}{L}+\frac{s^3}{L^2} \end{bmatrix} \tag{2.4}$$

The principle of virtual works can be used only if virtual strains and virtual displacements are considered together with real strains and real displacements. Virtual displacements can be obtained by taking the variations of eq. (2.2):

$$\delta\mathbf{p}_i = \delta\mathbf{w}_i + \delta\mathbf{v}_i \tag{2.5}$$

The infinitesimal displacements of the rigid-body mechanism are evaluated using the shape matrix $\mathbf{N}_i$:

$$\delta\mathbf{w}_i = \mathbf{R}_i\mathbf{N}_i(x_i, y_i, z_i)\mathbf{T}_i\delta\mathbf{r}_i \tag{2.6}$$

The second term $\delta\mathbf{v}_i$ in eq. (2.5) depends on both the virtual displacements $\delta\mathbf{u}_i$ of the nodes and on the vector of infinitesimal variations of free coordinates, $\delta\mathbf{q}$:

$$\delta\mathbf{v}_i = \delta\mathbf{R}_i\mathbf{N}_i(x_i, y_i, z_i)\mathbf{T}_i\mathbf{u}_i + \delta\mathbf{R}_i\mathbf{N}_i(x_i, y_i, z_i)\mathbf{T}_i\mathbf{u}_i + \mathbf{R}_i\mathbf{N}_i(x_i, y_i, z_i)\mathbf{T}_i\delta\mathbf{u}_i \tag{2.7}$$

The complete expression for the virtual displacements and for the velocities at the i-th element, both referred to the global reference frame $\{X, Y, Z\}$ are:

$$\delta\mathbf{p}_i = \mathbf{R}_i\mathbf{N}_i(x_i, y_i, z_i)\mathbf{T}_i\delta\mathbf{r}_i + \delta\mathbf{R}_i\mathbf{N}_i(x_i, y_i, z_i)\mathbf{T}_i\mathbf{u}_i + \mathbf{R}_i\mathbf{N}_i(x_i, y_i, z_i)\delta\mathbf{T}_i\mathbf{u}_i + \\ + \mathbf{R}_i\mathbf{N}_i(x_i, y_i, z_i)\mathbf{T}_i\delta\mathbf{u}_i \tag{2.8}$$

$$\dot{\mathbf{p}}_i = \mathbf{R}_i\mathbf{N}_i(x_i, y_i, z_i)\mathbf{T}_i\dot{r}_i + \dot{\mathbf{R}}_i\mathbf{N}_i(x_i, y_i, z_i)\mathbf{T}_i\mathbf{u}_i + \mathbf{R}_i\mathbf{N}_i(x_i, y_i, z_i)\dot{\mathbf{T}}_i\mathbf{u}_i + \\ + \mathbf{R}_i\mathbf{N}_i(x_i, y_i, z_i)\mathbf{T}_i\dot{\mathbf{u}}_i \tag{2.9}$$

Also the accelerations $\ddot{\mathbf{w}}_i$ of the equivalent rigid body are linked to the nodal accelerations $\ddot{\mathbf{r}}_i$ trough the the shape matrix $\mathbf{N}_i$:

$$\ddot{\mathbf{w}}_i = \mathbf{R}_i\mathbf{N}_i(x_i, y_i, z_i)\mathbf{T}_i\ddot{\mathbf{r}}_i \tag{2.10}$$

Therefore the acceleration of a point inside the i-th element can be calculating by taking the second time derivative of equation (2.5) together with eq. (2.10):

$$\ddot{\mathbf{p}}_i = \mathbf{R}_i\mathbf{N}_i(x_i, y_i, z_i)\mathbf{T}_i\ddot{\mathbf{r}}_i + 2(\dot{\mathbf{R}}_i\mathbf{N}_i(x_i, y_i, z_i)\mathbf{T}_i + \mathbf{R}_i\mathbf{N}_i(x_i, y_i, z_i)\dot{\mathbf{T}}_i)\dot{\mathbf{u}}_i$$

$$+(\ddot{\mathbf{R}}_i\mathbf{N}_i(x_i,y_i,z_i)\mathbf{T}_i + 2\dot{\mathbf{R}}_i\mathbf{N}_i(x_i,y_i,z_i)\dot{\mathbf{T}}_i + \mathbf{R}_i\mathbf{N}_i(x_i,y_i,z_i)\ddot{\mathbf{T}}_i)\mathbf{u}_i \quad (2.11)$$

Some simplification to the formula just written can be applied by using isoparametric elements, as in [125]. It can be shown that this choice of formulation brings:

$$(\delta\mathbf{R}_i\mathbf{N}_i(x_i,y_i,z_i)\mathbf{T}_i + \mathbf{R}_i\mathbf{N}_i(x_i,y_i,z_i)\delta\mathbf{T}_i)\mathbf{u}_i = 0; \quad (2.12)$$

$$(\dot{\mathbf{R}}_i\mathbf{N}_i(x_i,y_i,z_i)\mathbf{T}_i + \mathbf{R}_i\mathbf{N}_i(x_i,y_i,z_i)\dot{\mathbf{T}}_i)\mathbf{u}_i = 0; \quad (2.13)$$

$$(\ddot{\mathbf{R}}_i\mathbf{N}_i(x_i,y_i,z_i)\mathbf{T}_i + 2\dot{\mathbf{R}}_i\mathbf{N}_i(x_i,y_i,z_i)\dot{\mathbf{T}}_i + \mathbf{R}_i\mathbf{N}_i(x_i,y_i,z_i)\ddot{\mathbf{T}}_i)\mathbf{u}_i = 0; \quad (2.14)$$

It should be pointed out that the choice just made makes the dynamic model suitable only in the case of small elastic displacements. The resulting simplified expressions for the virtual displacements and the real acceleration inside the i-th element are:

$$\delta\mathbf{p}_i = \mathbf{R}_i\mathbf{N}_i(x_i,y_i,z_i)\mathbf{T}_i\delta\mathbf{r}_i + \mathbf{R}_i\mathbf{N}_i(x_i,y_i,z_i)\mathbf{T}_i\delta\mathbf{u}_i \quad (2.15)$$

$$\ddot{\mathbf{p}}_i = \mathbf{R}_i\mathbf{N}_i(x_i,y_i,z_i)\mathbf{T}_i\ddot{\mathbf{r}}_i + \mathbf{R}_i\mathbf{N}_i(x_i,y_i,z_i)\mathbf{T}_i\ddot{(}\mathbf{u}_i) + 2(\dot{\mathbf{R}}_i\mathbf{N}_i(x_i,y_i,z_i)\mathbf{T}_i$$
$$+\mathbf{R}_i\mathbf{N}_i(x_i,y_i,z_i)\dot{\mathbf{T}}_i)\dot{\mathbf{u}}_i \quad (2.16)$$

This allows to keep the coupling between the ERLS motion and vibration. Real and virtual strains are now calculated, as they are needed to complete the expression onf the virtual work:

$$\epsilon_i = \mathbf{B}_i(x_i,y_i,z_i)\mathbf{T}_i\mathbf{u}_i \quad (2.17)$$

$$\delta\epsilon_i = \mathbf{B}(x_i,y_i,z_i)\delta\mathbf{T}_i\mathbf{u}_i\mathbf{B}_i(x_i,y_i,z_i)\mathbf{T}_i\delta\mathbf{B}_i(x_i,y_i,z_i) \quad (2.18)$$

in which $\mathbf{B}_i(x_i,y_i,z_i)$ is the strain-displacement matrix. Infinitesimal displacements and rotations at the node can be expressed as the sum of the infinitesimal elastic displacements and of the infinitesimal displacements of the ERLS for the i-th element:

$$d\mathbf{b} = d\mathbf{u} + d\mathbf{r} \quad (2.19)$$

The use of ERLS allows to eliminate the dependence of $\delta\mathbf{b}$ from $\delta\mathbf{r}$ using the matrix of sensibility coefficients $\mathbf{S}(\mathbf{q})$. Therefore we obtain:

$$d\mathbf{r} = \mathbf{S}(\mathbf{q})d\mathbf{q} \tag{2.20}$$

$$\dot{\mathbf{r}} = \mathbf{S}(\mathbf{q})\dot{\mathbf{q}} \tag{2.21}$$

$$\ddot{\mathbf{r}} = \mathbf{S}(\mathbf{q})(\ddot{\mathbf{q}}) + \dot{\mathbf{S}}(\mathbf{q}, \dot{\mathbf{q}})\dot{\mathbf{q}} \tag{2.22}$$

The matrix of sensibility coefficients is function of the vector of free coordinates $\mathbf{q}$, and it expresses the relation between $\dot{\mathbf{q}}$ and $\dot{\mathbf{r}}$, as in eq. (2.21). On the other hand, eq. (2.22) relates the second derivative of nodal rigid-body acceleration to the first and second derivative of $\mathbf{q}$. Thus, from eq. (2.19) and (2.21), $\boldsymbol{b}$ can be expressed in matrix form as:

$$d\mathbf{b} = \begin{bmatrix} \mathbf{I} & \mathbf{S} \end{bmatrix} \begin{bmatrix} d\mathbf{u} \\ d\mathbf{q} \end{bmatrix} \tag{2.23}$$

It should be noticed that the equation written above introduces some redundancies. Given a configuration $d\mathbf{b}$ for infinitesimal nodal displacements, it corresponds to more sets of increments $[d\mathbf{u}^T, d\mathbf{q}^T]$. In order to solve the redundancy, e elements of $d\mathbf{u}$ must be forced to zeros. Partitioning $d\mathbf{u}^T$ into two parts, i.e. into its independent and zeroed part, and applying the same partitioning to $\mathbf{S}$, we can obtain a non-redundant expression for $d\mathbf{b}$:

$$d\mathbf{b} = \begin{bmatrix} \mathbf{I} & \mathbf{S}_{in} \\ 0 & \mathbf{S}_0 \end{bmatrix} \begin{bmatrix} d\mathbf{u}_{in} \\ d\mathbf{q} \end{bmatrix} \tag{2.24}$$

$\mathbf{S}_{in}$ has size $(n-e)\times(e)$, while $\mathbf{S}_0$ has e rows and e columns. The coefficient matrix in eq. (2.24) must be invertible, therefore:

$$det\mathbf{S}_0 \neq 0$$

Therefore, a correct ERLS definition must ensure that the sensitivity coefficients matrix of those elastic d.o.f. which are forced to zero, must be non-singular for all the configuration of the ERLS during the motion. Moreover, also non-zeros $d\mathbf{q}$ must be possible in each configuration of the ERLS. This implied that the generalized coordinates of the ERLS must be chosen in a way that no singular configuration is encountered.

We should also point out that matrices $\mathbf{S}$, $\mathbf{T}_i$, $\mathbf{R}_i$ and their time derivatives are a function of the free coordinates and of the geometry of the ERLS. Therefore, once a procedure for solving the kinematics of the ERLS is available, all the cited matrices can be evaluated.

In the next subsection we will develop the differential equations of motion, which involve $\mathbf{R}_i$, $\dot{(\mathbf{R})}_i$, $\mathbf{T}_i$, $\dot{\mathbf{T}}_i$, $\mathbf{S}$ and $\dot{\mathbf{S}}$.

2.0.2 Differential equations of motion

The development of the equation of motion can be started from the virtual work principle for an undamped system. The damping will be introduced later, using Rayleigh's model. According to Rayleigh's theory, the damping is directly proportional to both thew mass matrix and the stiffness matrix. We can write the principle of virtual work as:

$$\delta W^{inertia} + \delta W^{elastic} + \delta W^{external} = 0 \tag{2.25}$$

in which the virtual work of external forces $\delta W^{external}$ takes into account also for the gravity force. A more explicit definition of the previous equation is:

$$\sum_i \int_{v_i} \delta \mathbf{p}_i^T \ddot{\mathbf{p}}_i dv + \sum_i \int_{v_i} \delta {\epsilon_i}^T \mathbf{D}_i \epsilon_i dv = \sum_i \int_{v_i} \delta {\mathbf{p}_i}^T \mathbf{g} \rho_i dv + (\delta \mathbf{u}^T + \delta \mathbf{r}^T)\mathbf{q} \tag{2.26}$$

in which:

- $\mathbf{D}_i$ is the stress-strain matrix for the i-th element
- ρ_i is the linear density of mass for the i-th element
- v_i is the volume of the i-th element
- $\mathbf{g}$ is the vector of gravity loads
- $\mathbf{f}$ is the vector of generalized forces applied to the nodes (forces and torques)

Using into the last equation (2.15),(2.16),(2.17) and (2.18), one can find:

$$\sum_i \int_{v_i} [\delta \mathbf{u}_i^T \mathbf{T}_i^T \mathbf{N}_i^T \mathbf{R}_i^T + \delta \mathbf{r}_i^T \mathbf{T}_i^T \mathbf{N}_i^T \mathbf{R}_i^T][\mathbf{R}_i \mathbf{N}_i \mathbf{T}_i \ddot{\mathbf{r}}_i + \mathbf{R}_i \mathbf{N}_i \mathbf{T}_i \ddot{\mathbf{u}}_i + 2(\dot{\mathbf{R}}_i \mathbf{N}_i \dot{\mathbf{T}}_i)\mathbf{u}_i]\rho_i dv$$

$$+ \sum_i \int_i (\delta \mathbf{u}_i^T \mathbf{T}_i^T \mathbf{B}_i^T + \mathbf{u}_i^T \delta \mathbf{T}_i^T \mathbf{B}_i^T) \mathbf{D}_i \mathbf{B}_i \mathbf{T}_i \mathbf{u}_i dv$$

$$= \sum_i \int_{v_i} (\delta \mathbf{u}_i^T \mathbf{T}_i^T \mathbf{N}_i^T \mathbf{R}_i^T + \delta \mathbf{r}_i^T \mathbf{T}_i^T \mathbf{N}_i^T \mathbf{R}_i^T) \mathbf{g} \rho_i dv + (\delta \mathbf{u}^T + \delta \mathbf{r}^T) \mathbf{f} \qquad (2.27)$$

The equation above contains some contribution, which can be expanded as:

- the mass matrix: $\mathbf{M}_i = \int_{v_i} \mathbf{T}_i^T \mathbf{N}_i^T \mathbf{R}_i^T \mathbf{R}_i \mathbf{N}_i \rho_i dv$
- the stiffness matrix: $\mathbf{K}_i = \int_{v_i} \mathbf{T}_i^T \mathbf{B}_i^T \mathbf{D}_i \mathbf{B}_i \mathbf{T}_i dv$
- the vector of external forces due to gravity: $\mathbf{f}_{gi} = \int_{v_i} \mathbf{T}_i^T \mathbf{N}_i^T \mathbf{R}_i^T \mathbf{g} \rho_i dv$
- the first matrix of Coriolis contributions: $\mathbf{M}_{G1i} = \int_{v_i} \mathbf{T}_i^T \mathbf{N}_i^T \mathbf{R}_i^T \mathbf{R}_i \mathbf{N}_i \mathbf{T}_i \rho_i dv$
- the second matrix fo Coriolis contribution: $\mathbf{M}_{G1i} = \int_{v_i} \mathbf{T}_i^T \mathbf{N}_i^T \mathbf{R}_i^T \mathbf{R}_i \mathbf{N}_i \dot{\mathbf{T}}_i \rho_i dv$

The quantity $\delta \mathbf{T}_i^T$ can be rewritten as the product between a virtual angular displacement and each columns of the rotation sub-matrices of the principal diagonal of $\mathbf{T}_i^T$:

$$\delta \mathbf{T}_i^T = \delta \phi_i \mathbf{T}_i^T \qquad (2.28)$$

$\delta \phi_i$ is a block-diagonal matrix, just as $\delta \mathbf{T}_i^T$ and its transpose $\delta \mathbf{T}_i$. Moreover, it is a function of the virtual rotation of the i-th coordinate system and thus it could also be defined in terms of sensitivity coefficients and virtual increments $\delta \mathbf{q}$. Now, using the equations above, eq. (2.27) can be rewritten as:

$$\sum_i \delta \mathbf{u}_i^T \mathbf{M}_i (\ddot{\mathbf{r}}_i + \ddot{\mathbf{u}}_i) + 2 \sum_i \delta \mathbf{u}_i^T (\mathbf{M}_{G1i} + \mathbf{M}_{G2i}) \dot{\mathbf{u}}_i + \sum_i \delta \mathbf{r}_i^T \mathbf{M}_i (\ddot{\mathbf{r}}_i + \ddot{\mathbf{u}}_i)$$

$$+2 \sum_i \delta \mathbf{r}_i^T (\mathbf{M}_{G1i} + \mathbf{M}_{G2i}) \dot{\mathbf{u}}_i + \sum_i \delta \mathbf{u}_i^T \mathbf{K}_i \mathbf{u}_i + \sum_i \mathbf{u}_i^T \delta \phi_i \mathbf{K}_i \mathbf{u}_i$$

$$= \sum_i (\delta \mathbf{u}_i^T + \delta \mathbf{r}_i^T) \mathbf{f}_{gi} + (\delta \mathbf{u}^T + \delta \mathbf{r}^T) \mathbf{f} \qquad (2.29)$$

Nodal elastic virtual displacements $\delta \mathbf{u}$ an virtual displacements of the ERLS are completely independent fro each other. Therefore the relation above con be spitted into two parts:

$$\delta \mathbf{u}^T \mathbf{M} (\ddot{\mathbf{r}} + \ddot{\mathbf{u}}) + 2 \delta \mathbf{u}^T (\mathbf{M}_{G1} + \mathbf{M}G2) \dot{\mathbf{u}} + \delta \mathbf{u}^T \mathbf{K} \mathbf{u} = \delta \mathbf{u}^T (\mathbf{f}_g + \mathbf{f}) \qquad (2.30)$$

$$\delta\mathbf{r}^T\mathbf{M}(\ddot{\mathbf{r}}+\ddot{\mathbf{u}})+2\delta\mathbf{r}^T(\mathbf{M}_{G1}+\mathbf{M}_{G2})\dot{\mathbf{u}}+\sum_i \mathbf{u}_i^T\delta\phi_i\mathbf{K}_i\mathbf{u}_i=\delta\mathbf{r}^T(\mathbf{f}_G+\mathbf{f}) \quad (2.31)$$

Equation (2.30) expresses the nodal equilibrium, while eq. (2.31) expresses the overall equilibrium. When considering the equilibrium of elastic forces with respect to all others in eq. (2.30), and substituting into eq. (2.31), this latter can be rewritten as:

$$\sum_i \mathbf{u}_i^T\delta\phi_i\mathbf{K}_i\mathbf{u}_i-\sum_i \delta\mathbf{r}_i^T\mathbf{u}_i=0 \quad (2.32)$$

Such expression shows that the term $\sum_i \mathbf{u}_i^T\delta\phi_i\mathbf{K}_i\mathbf{u}_i$ is (2.31) can be neglected, since $u_i\delta\phi_i$ is small in comparison to $\delta\mathbf{r}_i^T$, as a consequence of the choice of considering only small deformations.

Now, the virtual displacements of the ERLS can be expressed using the sensitivity coefficient matrix $\mathbf{S}$ trough:

$$\delta\mathbf{r}^T=\delta\mathbf{q}^T\mathbf{S}^T \quad (2.33)$$

In this way, it is possible to eliminate all the virtual displacements of generalized coordinates of the system. Doing this leads to:

$$\mathbf{M}(\ddot{\mathbf{r}}+\ddot{\mathbf{u}})+2(\mathbf{M}_{G1}+\mathbf{M}_{G2})\dot{\mathbf{u}}+\mathbf{K}\mathbf{u}=\mathbf{f}_g+\mathbf{f} \quad (2.34)$$

$$\mathbf{S}^T\mathbf{M}(\ddot{\mathbf{r}}+\ddot{\mathbf{u}})+2\mathbf{S}^T(\mathbf{M}_{G1}+\mathbf{M}_{G2})\dot{\mathbf{u}}=\mathbf{S}^T(\mathbf{f}_g+\mathbf{f}) \quad (2.35)$$

In practical situation some kind of damping must be introduced into the system. Using Rayleigh's model, we introduce the coefficients α and β into eq. (2.34) and (2.35), leading to:

$$\mathbf{M}(\ddot{\mathbf{r}}+\ddot{\mathbf{u}})+2(\mathbf{M}_{G1}+\mathbf{M}_{G2})\dot{\mathbf{u}})+\alpha\mathbf{M}\dot{\mathbf{u}}+\beta\mathbf{K}\dot{\mathbf{u}}+\mathbf{K}\mathbf{u}=\mathbf{f}_g+\mathbf{f} \quad (2.36)$$

$$\mathbf{S}^T\mathbf{M}(\ddot{\mathbf{r}}+\ddot{\mathbf{u}})+2\mathbf{S}^T(\mathbf{M}_{G1}+\mathbf{M}_{G2})+\alpha\mathbf{S}^T\mathbf{M}\dot{\mathbf{u}}=\mathbf{S}^T(\mathbf{f}_g+\mathbf{f}) \quad (2.37)$$

The value of Rayleigh damping coefficients α and β can be determined experimentally. The acceleration $\ddot{\mathbf{r}}$ can be rewritten as in eq. (2.22):

$$\ddot{\mathbf{r}} = \mathbf{S}\ddot{\mathbf{q}} + \left(\sum_k \dot{q} \frac{\partial \mathbf{S}}{\partial q_k} \right) \dot{\mathbf{q}} \tag{2.38}$$

Therefore, eq. (2.36) and (2.37) can be rewritten as:

$$\mathbf{M}\ddot{\mathbf{u}} + \mathbf{M}\mathbf{S}\ddot{\mathbf{q}} = \mathbf{t}(\mathbf{u}, \dot{\mathbf{u}}, \mathbf{q}, \dot{\mathbf{q}}) \tag{2.39}$$

$$\mathbf{S}^T\mathbf{M}\ddot{\mathbf{u}} + \mathbf{S}^T\mathbf{M}\mathbf{S}\ddot{\mathbf{q}} = \mathbf{S}^T\mathbf{t}(\mathbf{u}, \dot{\mathbf{u}}, \mathbf{q}, \dot{\mathbf{q}}) \tag{2.40}$$

The two equations above can be grouped together in a single matrix form, which will be used for the software implementation of the model. Further information will be given in the chapter of this work which deals with the Hardware-In-the-Loop (HIL) implementation of such model. The term $\mathbf{t}$ accounts for all the forces acting on the mechanism, except for those directly linked with the second derivative of the generalized coordinates $\mathbf{q}$ and $\mathbf{u}$.

$$\begin{bmatrix} \mathbf{M}_{in} & (\mathbf{MS})_{in} \\ \left(\mathbf{S}^T\mathbf{M}\right)_{in} & \mathbf{S}^T\mathbf{MS} \end{bmatrix} \begin{bmatrix} \ddot{\mathbf{u}}_{in} \\ \ddot{\mathbf{q}} \end{bmatrix} = \begin{bmatrix} \mathbf{t}_{in} \\ \mathbf{S}^T\mathbf{t} \end{bmatrix} \tag{2.41}$$

In this equation, zeroed elastic degrees of freedom are eliminated, as expressed by the use of the subscript 'in'. The matrix expression (2.41) shows clearly the coupling between the elastic acceleration of the free coordinates of the ERLS. It represents a system of ordinary differential equations (ODE): once it has been converted to the first order (by augmenting the 'state' variable), the dynamics of the FLM can be solved using a standard ode solver. Extensive simulation conducted using Matlab environment, shows that the `ode45` solver is a good candidate, since it shows a good trade-off between speed of computation and stability of solution. The ode solver `ode23tb` has shown to be a valuable tool when stiffer problems are encountered. In general, variable step solvers should be preferred to fixed step solvers.

3

Simulation results: static and dynamic models of flexible-links mechanisms

In this chapter a more deep insight to the static and dynamic model for flexible-link mechanisms will be given. In particular, the focus will be set on the development of the software tool that has been written by the author in order to produce accurate results. All the software modules analyzed in this chapter has been developed by means of Matlab. All the software has been targeted at computational efficiency. The numerical efficiency of multibody dynamics simulation software is a topic of large interest in the research community, as testified by the paper [126] which cites 877 references up to 2003. As it will be shown in the last section of this chapter, the Author has been able to develop a simulator whose efficiency has lead to a Real-Time (and in some cases also Faster-Than-Real-Time) implementation. Such software has been used by the same author as the basis of an Hardware-In-the-Loop workbench.

Along this chapter we will see in deeper details how to implement a static and dynamic model compliant with the theoretical development presented in chapter 2. The mechanisms under investigation are all planar flexible-link mechanisms. In particular, the Author has developed the static and dynamic models for:

- Single-link mechanism
- 4 bar mechanism
- 5 bar mechanism

In this way, the analysis includes the simplest FLM (the single link), a closed-loop mechanism with 1 rigid degree of freedom, and a closed-chain mechanism

with two rigid degrees of freedom. The resulting models will be used for both the design and the simulation of innovative closed-loop control strategies for FLMs. The results of this study will be presented in chapter 5.

3.1 Static model for a single-link mechanism

The first mechanism under analysis is the single-link mechanism. It is made up by a simple metal rode, connected to a chassis using a rotational joint. Therefore the angular position of the mechanism is represented by the scalar quantity q, while its elastic behavior is described by a set of nodal displacements, which are included in the vector **u**. The size of vector **u** depends on the number of finite element used to discretize the elastic behavior of the mechanisms. Since we are now focusing on a static model, we will analyze the elastic displacement of the single link mechanism for a given angular position q and for a given vector of external loads f.

The parameters of the beam are:

	symbol	value
Young's modulus	E	200×10^9 [Pa]
Beam width	a	6×10^{-3} [m]
Beam thickness	b	6×10^{-3} [m]
Length	L	0.7 [m]
Mass/unit of length	m	0.282 [kg/m]

Table 3.1: Characteristics of the FLM

In this case the angle link can be described as a single link with 6 elastic d.o.f., i.e. the structure can be discretized using only one finite element. It should be pointed out that, in order to solve the static problem, some mechanical constraints must be taken into account. In particular, the two displacements along the x and y axis of the first node must be forced to zero, since these two displacements are inhibited by the rotation joint. Then, according to the ERLS theory, one more displacement must be forced to zero, since the ERLS has one degree of freedom, q. We can choose one of the remaining 4 elastic d.o.f, in this case the choice made is to force to zero the rotational displacement at the first node. The elastic displacement can be calculated using the following relation:

$$\mathbf{u}_G = \begin{bmatrix} u_{x1}^G \\ u_{y1}^G \\ u_{z1}^G \\ u_{x2}^G \\ u_{y2}^G \\ u_{z2}^G \end{bmatrix} = \mathbf{K}_G^{-1}\mathbf{F}_G \tag{3.1}$$

in which $\mathbf{u}_G$, $\mathbf{K}_G$ $\mathbf{F}_G$ are the vector of nodal displacement, the matrix of stiffness and the vector of external loads due to gravity force, respectively. All these quantities are measured in the global reference frame. The three constraints described above can be taken into account by removing the first tree elements of $\mathbf{u}_G$ and $\mathbf{F}_G$, and by removing the first three rows and columns of $\mathbf{K}_G$. The resulting quantities are: $\mathbf{u}_G^*$, $\mathbf{F}_G^*$ and $\mathbf{K}_G^*$. Therefore we obtain:

$$\mathbf{u}_G^* = \begin{bmatrix} u_{x2}^G \\ u_{y2}^G \\ u_{z2}^G \end{bmatrix} = \left(\mathbf{K}_G^*\right)^{-1}\mathbf{F}_G^* \tag{3.2}$$

Given the angular position of the link and the mechanical data of the link (length, mass, stiffness, etc..), the stiffness matrix $\mathbf{K}_L$ in the local reference frame can be calculated. At the same way, the vector of nodal loads (referred to the local reference frame) due to gravity can be calculated as:

$$\mathbf{F}_P = \begin{bmatrix} L/2 & 0 \\ 0 & L/2 \\ 0 & L^2/12 \\ L/2 & 0 \\ 0 & L/2 \\ 0 & -L^2/12 \end{bmatrix} \mathbf{F}_{grav}^L = \begin{bmatrix} L/2 & 0 \\ 0 & L/2 \\ 0 & L^2/12 \\ L/2 & 0 \\ 0 & L/2 \\ 0 & -L^2/12 \end{bmatrix} m\mathbf{R}_{LG} \begin{bmatrix} 0 \\ -g \end{bmatrix} \tag{3.3}$$

in which L is the length of the link, m is its mass per unit of length, and g is the gravity acceleration constant. In order to bring the relation into the global reference frame, it is necessary to use the local-to-global rotation matrix $\mathbf{T}_{GL}$. We find:

$$\mathbf{K}_G = \mathbf{T}_{GL}\mathbf{K}_L\mathbf{T}_{LG}; \tag{3.4}$$

$$\mathbf{F}_{pG} = \mathbf{T}_{GL}\mathbf{F}_{pL}\mathbf{T}_{LG}; \tag{3.5}$$

If other external forces are included in the modal, we can refer them to the global reference frame and put them in the vector of external forces (and torques) $\mathbf{F}_{ext}$:

$$\mathbf{F}_{ext} = [{F_x}^1, {F_y}^1, {F_z}^1, {F_x}^2, {F_y}^2, {F_z}^2]^T$$

Such vector has six elements, since the considered model has been described with 6 nodal displacement. The vector of all the forces acting on the link is therefore:

$$\mathbf{F}_G = \mathbf{F}_{pG} + \mathbf{F}_{ext} \tag{3.6}$$

As a matter of example, if $q = 45$ deg, and adding the force ${F_y}^2 = -10N$, we obtain the following nodal displacements: ${u_x}^2 = 27$ mm, ${u_y}^2 = -27$ mm, ${u_z}^2 = -0.0183$ rad. To plot the profile of the deformed link, the interpolation functions (2.4) must be used. Care must be taken, since this matrix applies to the displacements measured in the local reference frame. In order to calculate them, the global-to-local rotation matrix must be used, trough the relation: $\mathbf{u}_G = \mathbf{T}_{LG}\mathbf{u}_L$. The result is: ${u_x}^2 = 0$, ${u_y}^2 = -38.2$ mm , ${u_z}^2 = -0.0813$ rad. A graphic representation of the deformed link for an external load of -10 N applied vertically at the free end of the link.

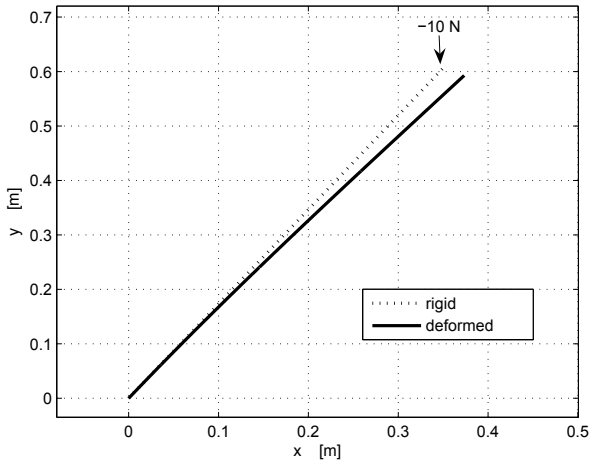

Figure 3.1: Elastic deformation of a single link mechanism with an external load F_y = -10 N applied to the free end

3.2 4-bar mechanism: static analysis

The four link mechanism is the simplest closed-loop planar mechanism that can be built using only rotational joints. It is made up by four link, including the ground link. It is a single degree-of-freedom mechanism (if only rigid motion is taken into account), since the position of one link univocally determines the position of the other two links. The results presented in this section have been obtained by discretizing the links with 2 finite elements for the longest link, and with one finite element for the other two links. The ground link is considered to be perfectly rigid.

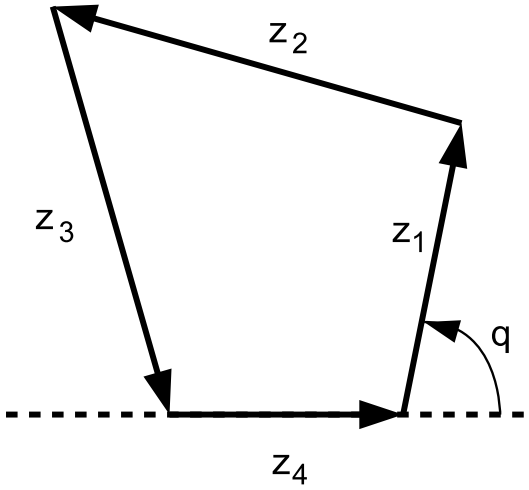

Figure 3.2: Position vectors for the four-bar mechanism under investigation

The mechanism under investigation has the following link lengths: $L_1 = 0.35965$ m, $L_2 = 0.372285$ m, $L_3 = 0.525$ m, while the distance between the two ground link joint is $L_4 = 0.632$ m. Each element has a square section, whose width is 6 mm, and the mass per unit of length is $273 * 10^{-3}$ Kg/m. The calculation of the static deformation of the mechanism has been obtained using a Matlab script.

Here we describe in detail ho to evaluate the stiffness matrix an the vector of gravity load. First of all, the the matrices for each link are evaluated. Care must be taken when evaluating the stiffness matrix for the third link, since it has been discretized by 2 finite elements. Therefore such matrix can be evaluated by adding two matrices calculated as in eq. (A.1.6) after 'translating' the second

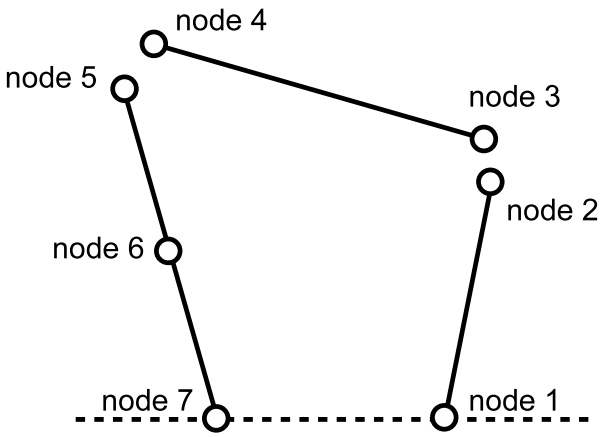

Figure 3.3: Finite element discretization for the 4-bar mechanism

matrices, as represented in figure 3.4. This procedure allows to take into account the continuity constraints between the two finite elements belonging to the third link.

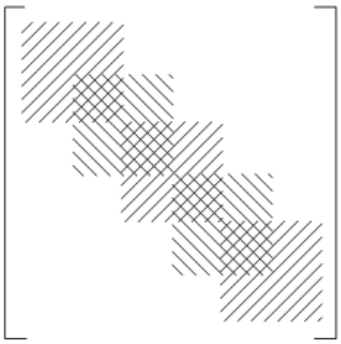

Figure 3.4: Matrix assembling for multi-element discretization

The first and second link has 6 elastic d.o.f, the third has 9 d.o.f, if we consider the separately. If we connect them to form a 4-bar mechanism, the following constraints must be considered:

- the coincidence of node 2 and 3, which implies ${u_2}^x = {u_3}^x$ e ${u_2}^y = {u_3}^y$
- the coincidence of node 3 and 4, therefore: ${u_4}^x = {u_5}^x$ e ${u_4}^y = {u_5}^y$

So the nonzero elastic displacements are:

$$\mathbf{u} = [{u_1}^x, {u_1}^y, {u_1}^z, {u_2}^x = {u_3}^x, {u_2}^y = {u_3}^y, {u_2}^z, {u_3}^z, {u_4}^x = {u_5}^x,$$

$$, {u_4}^y = {u_5}^y, {u_4}^z, {u_5}^z, {u_6}^x, {u_6}^y, {u_6}^z, {u_7}^x, {u_7}^y, {u_7}^z]$$

Moreover, other 4 constraints are considered, in order to take into account the two rotational joints that connect node 1 and 5 to the gornd link:

- ${u_1}^x = {u_1}^y = 0$ because of the rotational joint at node 1
- ${u_7}^x = {u_7}^y = 0$ because of the rotational joint at node 7
- ${u_2}^x$=0, since the ERLS formulation requires to force to zero one d.o.f. for each rigid degree of freedom

The last choice is in general arbitrary, but the choice made has proved to avoid singular configurations during simulations.

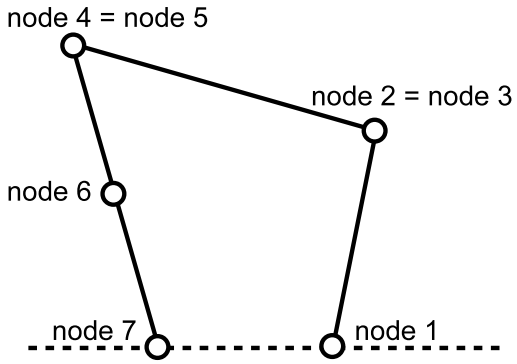

Figure 3.5: Nodes after the imposition of constraints

The solution of the static problem has been obtained using some Matlab script. As a matter of example, in table 3.2 the calculated nodal displacements for a 4-link mechanism under gravity, taking $q = \pi/6$ as the position of the mechanism.

Nodal displacements [mm] and [rad]	
${u_1}^x$	-0.08481
${u_2}^y$	-0.001509
${u_2}^z$	0.08411
${u_3}^z$	0.2744
${u_4}^x$	-0.0008715
${u_4}^y$	-0.0009271
${u_4}^z$	-0.2748
${u_5}^z$	0.1950
${u_6}^x$	0.03376
${u_6}^y$	-0.01874
${u_6}^z$	-0.01917
${u_7}^z$	-0.01954

Table 3.2: Nodal displacement in the 4-bar linkage with $q = \pi/6$

3.3 Static analysis of a 5-bar linkage

The third kind of mechanism under investigation in this work is the planar five-bar mechanisms. It is made up by 4 bars, connected using only revolute joints. Again, the ground link (which is considered as the fifth link) is considered to be perfectly rigid. Such mechanisms has 2 rigid d.o.f., as testified by Grubler's equation: $n_{GDL} = 3(m-1) - 2c_1 - c_2$. n_{GDL} is the number of d.o.f, m is the number of links, while c_1 and c_2 are the number of class 1 and class 2 joints, respectively. The revolute joint belong to class 2. The links nomenclature has been chosen as it can be seen in figure A.4. The two rigid d.o.f., $\mathbf{q} = [q_1, q_2]$ are used to describe to the angular position of the first and fourth link measured from the chassis. This is a natural choice, since usually the motion of the whole mechanisms is controlled by means of two actuators mounted on the chassis. Mounting the motors directly on the chassis in fact allows to reduce to the minimum the size of the actuated mass. This kind of mechanism can be used for high-speed manipulation tasks within a planar workspace, as in EULA's PacDrive D2 Robot (figure 3.6).

In order to keep to the minimum the size of the static problem, each link has been discretized using a single finite element. Therefore, the number of d.o.f. before assembling the structure is 24. Assembling the structure reduces the number of degrees of freedom to 14. Other d.o.f. must be forced to zero, according to ERLS theory. In this case it has been chosen to force to zero the displacement along the x and the y axis at the node that connects the second

Figure 3.6: EULA PacDrive D2 robot

and the third link.

As for the single-link and the four-bar linkage, a set of Matlab routines has been developed to evaluate the static deformation under external loads. As a matter of example, the following mechanisms has been modeled: all the links are 70 cm long, they are made of steel, and the section of the links is square, with a 6 mm side. The external forces taken into consideration are the gravity force, and a 10 Nm load applied horizontally at the meeting point of the second and the third link. The force vector is shown in figure 3.9 as F_y.

In this case the magnitude of the displacement is similar to the previous case, and it can be noticed that all the links belonging to the mechanism undergoes to the effects of a force applied to a generic point of the mechanisms.

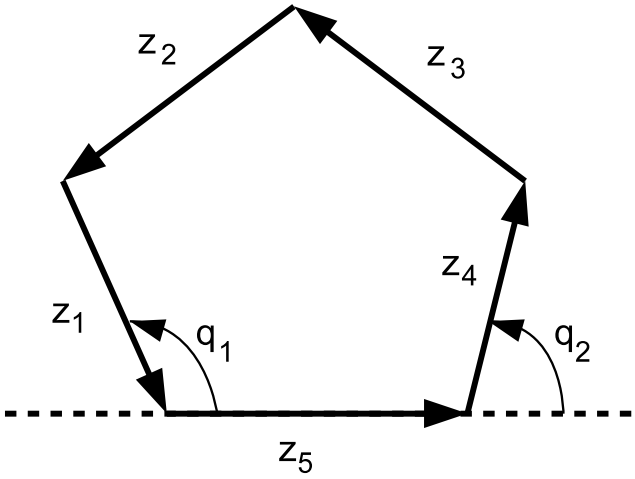

Figure 3.7: Position vectors for the 5-link mechanism

3.4 Simulation of Dynamic models: single-link

In this section the results of the application of the dynamic model presented in Chapter 1 will be presented. Such model will be implemented for three basic FLM: single-link, four-bar linkage and five-link mechanism. The resulting simulators have been used extensively during the development of this work for the numerical and experimental validation of closed-loop control strategies for the aforementioned mechanisms. Such results will pre presented in Chapter 5.

The first mechanisms under consideration is, as obvious, the single link mechanisms (SLM). In order to describe correctly the dynamics of a SLM discretized with a single finite element (therefore with 2 nodes) constrained to the chassis with an ideal rotoidal joint, we must first choose the right number of nonzero elastic displacements. As already seen in the previous chapter, the vector of elastic displacements (in the global reference frame), is composed of 6 elements if only one finite element is used:

$$\mathbf{u}_G = [{u_x}^1, {u_y}^1, {u_z}^1, {u_x}^2, {u_y}^2, {u_z}^2] \tag{3.7}$$

The static model of the SLM is described simply by the vector $[\mathbf{u}_G, \mathbf{q}]$, but in order to include the dynamics, we must augment such vector so that it will include also the change rate of $\mathbf{u}_G$ and $\mathbf{q}$. Therefore the dynamics of the system is must include also the terms of velocities and accelerations [$\dot{\mathbf{u}}$, $\ddot{\mathbf{u}}$, $\dot{\mathbf{q}}$ e $\ddot{\mathbf{q}}$]. We

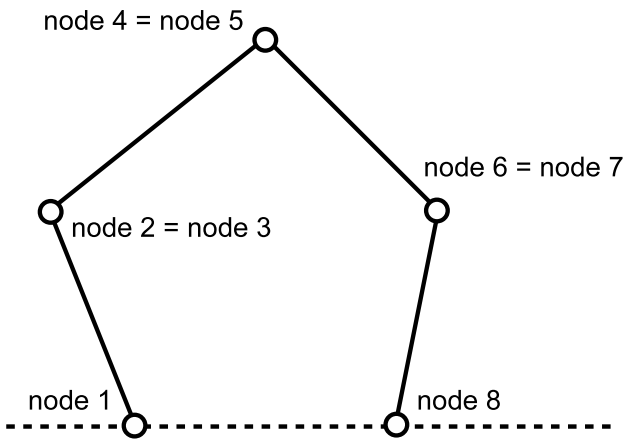

Figure 3.8: Nodal discretization for the whole mechanism

can can refer to the relations already presented in chapter one:

$$\mathbf{M}\ddot{\mathbf{u}} + \mathbf{MS}\ddot{\mathbf{q}} = t(\mathbf{u}, \dot{\mathbf{u}}, \mathbf{q}, \dot{\mathbf{q}}) \tag{3.8}$$

$$\mathbf{S}^T\mathbf{M}\ddot{\mathbf{u}} + \mathbf{S}^T\mathbf{M}\ \mathbf{S}\ddot{\mathbf{q}} = \mathbf{S}^T t(\mathbf{u}, \dot{\mathbf{u}}, \mathbf{q}, \dot{\mathbf{q}}) \tag{3.9}$$

which can be rewritten in the more compact matrix form:

$$\begin{bmatrix} \mathbf{M}_{in} & (\mathbf{MS})_{in} \\ \left(\mathbf{S}^T\mathbf{M}\right)_{in} & \mathbf{S}^T\mathbf{MS} \end{bmatrix} \begin{bmatrix} \ddot{\mathbf{u}}_{in} \\ \ddot{\mathbf{q}} \end{bmatrix} = \begin{bmatrix} \mathbf{t}_{in} \\ \mathbf{S}^T\mathbf{t} \end{bmatrix} \tag{3.10}$$

This formula shows how the dynamics of a FLM can be computed as a function of the vector $\mathbf{t}$, which depends on $\mathbf{u}$, $\dot{\mathbf{u}}$, $\mathbf{q}$ and $\dot{\mathbf{q}}$. This shows that the dynamics of the system can be made explicit as a nonlinear relation whose state space vector is $\mathbf{x}$:

$$\mathbf{x} = \begin{bmatrix} \dot{\mathbf{u}} \\ \dot{\mathbf{q}} \\ \mathbf{u} \\ \mathbf{q} \end{bmatrix}$$

The vector $\mathbf{x}$ can be used to evaluate $\ddot{\mathbf{u}}$ e $\ddot{\mathbf{q}}$ using the relation:

$$\mathbf{M}_m\dot{\mathbf{x}} = \mathbf{M}_1\mathbf{x} + \mathbf{f}_g + \mathbf{f} \tag{3.11}$$

in which:

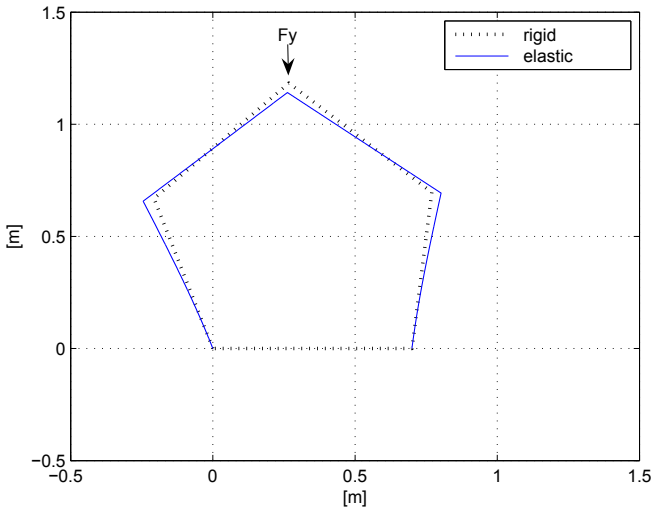

Figure 3.9: Static deformation of a 5-bar linkage under gravity and external loads

$$\mathbf{M}_m = \begin{bmatrix} \mathbf{M} & \mathbf{MS} & 0 & 0 \\ \mathbf{S}^T\mathbf{M} & \mathbf{S}^T\mathbf{MS} & 0 & 0 \\ 0 & 0 & \mathbf{I} & 0 \\ 0 & 0 & 0 & \mathbf{I} \end{bmatrix}$$

$$\mathbf{M}_1 = \begin{bmatrix} -2\mathbf{M}_{G1} - 2\mathbf{M}_{G2} - \alpha\mathbf{M} - \beta\mathbf{K} & -\mathbf{M}\dot{\mathbf{S}} & -\mathbf{K} & 0 \\ \mathbf{S}^T(-2\mathbf{M}_{G1} - 2\mathbf{M}_{G2} - \alpha\mathbf{M}) & \mathbf{S}^T\mathbf{M}\dot{\mathbf{S}} & 0 & 0 \\ \mathbf{I} & 0 & 0 & 0 \\ 0 & \mathbf{I} & 0 & 0 \end{bmatrix}$$

while $\mathbf{f}_g$ is the vector of the equivalent nodal forces due to gravity and $\mathbf{f}$ is the vector of the generalized external forces. For the definition of the other matrices involved, such as $\mathbf{M}$, $\mathbf{K}$ and so on, refer to Chapter 1. The explicit calculation of the state vector $\mathbf{x}$ can be obtained simply by multiplying both terms of equation 3.11 for the inverse of $\mathbf{M}_1$:

$$\dot{\mathbf{x}} = \mathbf{M}_m^{-1}\mathbf{M}_2\mathbf{x} + \mathbf{M}_m^{-1}[\mathbf{f}_g + \mathbf{f}] \tag{3.12}$$

It must be pointed out that the previous equation cannot be solved in this form, since that up to now the proper constraints on the displacement vector

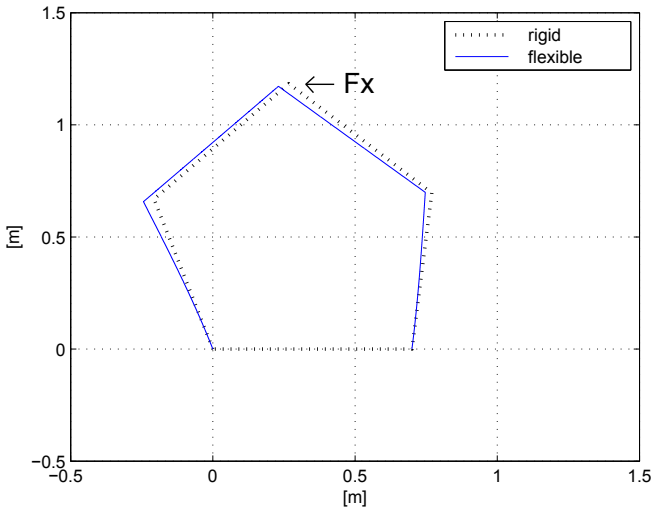

Figure 3.10: Static deformation of a 5-bar mechanism under a 10 N load applied to the end-point

have not been included yet [1]. From the ERLS theory, and following the most common choice, we chose to force to zero all the three displacements of the first node, i.e. the node which is linked to the chassis with a rotational joint. Therefore the constrained dynamics can be expressed in terms of the first time derivative of the space vector $\mathbf{x}^*$:

$$\dot{\mathbf{x}}^* = \begin{bmatrix} \ddot{\mathbf{u}}_1 \\ \ddot{\mathbf{u}}_2 \\ \ddot{\mathbf{u}}_3 \\ \ddot{\mathbf{q}} \\ \dot{\mathbf{u}}_1 \\ \dot{\mathbf{u}}_2 \\ \dot{\mathbf{u}}_3 \\ \dot{\mathbf{q}} \end{bmatrix} = \mathbf{M}_m{}^{-1^*}(\mathbf{M}_1\mathbf{x}^* + \mathbf{f}_g{}^* + \mathbf{f}^*)$$

The symbol * is used to show that the constraints to the nodal displacements have been considered. Therefore from the size of vectors $\mathbf{x}$, $\mathbf{f}_g$ and $\mathbf{f}$, which is $[14 \times 1]$, we arrive to the size of $\mathbf{x}^*$, $\mathbf{f}_g^*$ and $\mathbf{f}^*$ which is $[8 \times 1]$, since $\mathbf{x}^*$ comprises three elastic displacements and one angular postion, plus their time derivatives. Matrices $\mathbf{M}_m$ and $\mathbf{M}_1$ also change accordingly to the size of $[8 \times 8]$.

In this way we have developed a simple way to evaluate a matrix description

of the dynamics system. As evident form the relations above, in order to evaluate the model for a particular angular position q and a speed $\dot{\mathbf{q}}$, it is needed to evaluate matrices $\mathbf{M}_m$ and $\mathbf{M}_1$, and in particular the inverse of $\mathbf{M}_m$ matrix. The computation of such inverse matrix is crucial to the time required for the simulation of the model, and also for its numerical stability and accuracy. This topic will be dealt with in greater detail in Chapter 4.

3.4.1 Simulink model for the 2 node SLM

The Matlab package Simulink has been chosen to develop the dynamic model of all the simulators presented in this work. In particular, the simulators have been implemented using S-functions, which allow to define custom Simulink blocks using M o C code. The integration of such S-function routines can be preformed easily using Matlab built-in integrators, such as ode45 or ode23.

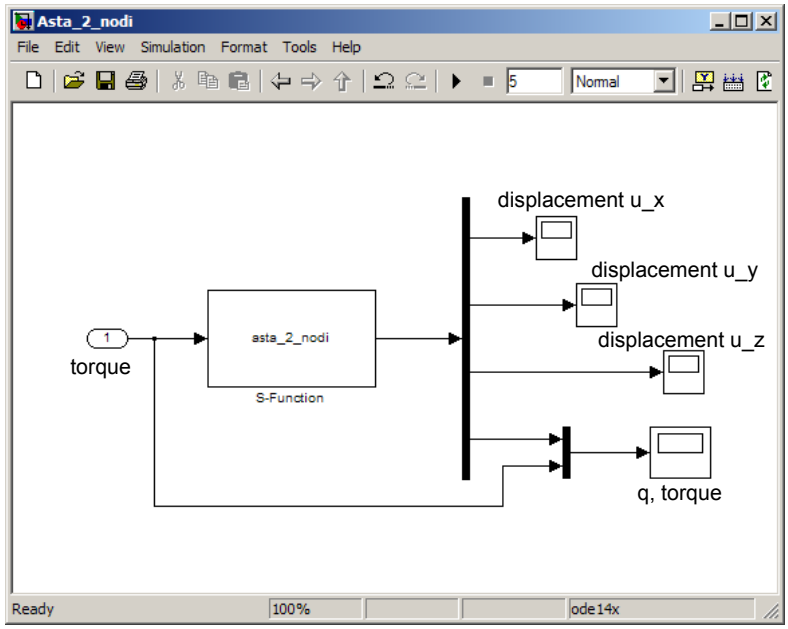

Figure 3.11: Simulink model for single link mechanism, discretized with a single finite element

Figure (3.11) shows a Simulink program that implements the dynamic simulator of the 2 node SLM. The actual simulator is included in the block "asta 2 nodi", and it receives as input the torque applied to the mechanism. The four scopes on the right side are used to plot the time evolution of the three elastic

displacement and of the position of the mechanism. The s-function included in the main block can be written using different languages, such as C, Matlab, Fortran. In this case, as for all the other simulators presented in this work, C code has been chosen. It has been noticed that C code routines require less time to perform a simulation than Matlab code routines. The speed increment has been evaluated to be at least 5 times in most cases. This is a fundamental requirements for Real-Time systems. The simulator presented in this section, can perform in Faster-Than-Real-Time, meaning that the time required for performing a full simulation is shorter than the length of the simulated time. As the result of a large number of trials, the aforementioned model can perform a 5 seconds simulation in around two seconds. The same model written using Matlab code, requires around 6 seconds to complete the simulation. All this data have been measured using Windows XP, which is a non Real-Time environment.

The choice of Matlab-Simulink environment has also the advantage of allowing to compile the model with a standard C compiler, such as the popular Microsoft .NET. The compiled code can be run on different platforms, such as Real-Time OS. The Real-Time simulator has been run for several tests on both Matlab's Real-Time Windows Target and National Instruments Real-Time LabVIEW OS. This topic will be dealt with in greater details in Chapter 5.

Here we briefly recall the implementation and the basic operation of a software simulator built around an s-function. The structure of an s-function is very simple, since it recalls the definition of a dynamic system of the type:

$$\begin{aligned} \dot{x} &= Ax + Bu \\ y &= Cx + Du \end{aligned}$$

Vector x represent a state vector, while u represents the input variable to the model, while y represent the output vector. Using one of the Matlab built-in ode solvers (such as the popular ode45), the s-function is executed following the flowchart shown in Figure (3.12).

During the first phase, i.e. the initialization of the model, the software evaluates the state vector at the time $t = 0$. Considering the SLM, the static model is used to evaluate the position and the displacements along the mechanism at the initial configuration of choice. The state vector at $t = 0$ has the form:

$$x_0 = \begin{bmatrix} 0 & 0 & 0 & 0 & u_1(0) & u_2(0) & u_3(0) & q(0) \end{bmatrix}$$

The only value chosen by the user is the initial angular position of the link, $q(0)$, while the displacements at the same time are evaluated using the relation

$\mathbf{u}_G = {\mathbf{K}_G}^{-1}\mathbf{f}_G$. After this calculation, the output vector at time $t = 0$ is evaluated. After that, the first integration is performed by the ode solver, allowing to evaluate the x and y vector at time $t = 0 + \delta t$. The the integration and the evaluation of the outputs is repeated several times, up to the completion of the simulation scenario chosen by the user. A proper choice of the size of the integration step is fundamental to achieve good precision and an acceptable simulation time. For non Real-Time simulations a variable step solver has proven to provide a good accuracy with limited computational requirements. For most of the simulation presented in this chapter and in the following ones, ode23tb routine has been used. For the real-time application, the fixed-step solver ode14x has been used instead, using a step time no longer than 1 ms.

The results of some simulations are reported in the following, concerning the free evolution of the model with nonzero initial condition, i.e., in this case, an initial angular position $q = -\pi/3$. The SLM is composed by a 70 cm long steel beam with square section 6 mm wide. The evolution of the model is reported in Figures (3.13) and (3.14).

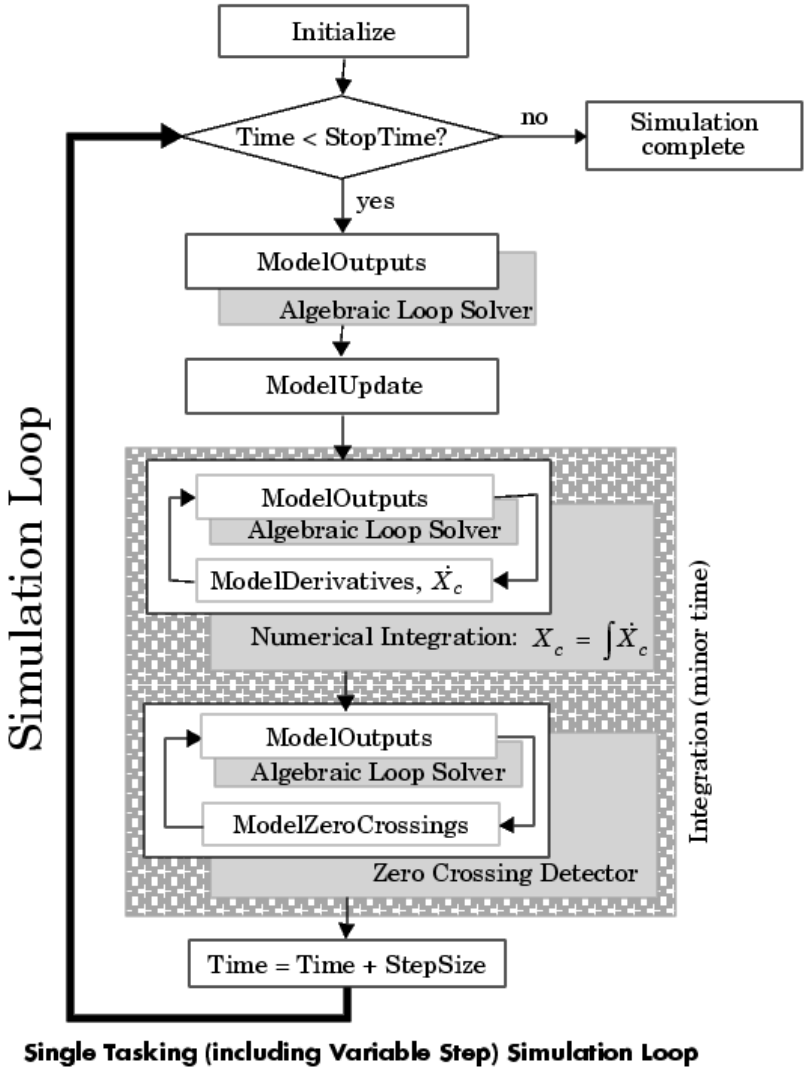

Figure 3.12: S-function: execution flowchart

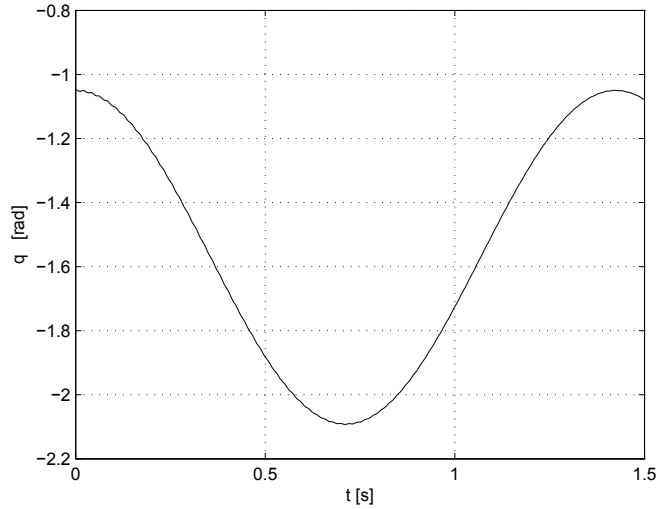

Figure 3.13: Free response of the single-link mechanisms with initial condition $q_0 = -\pi/3$: rigid displacement q

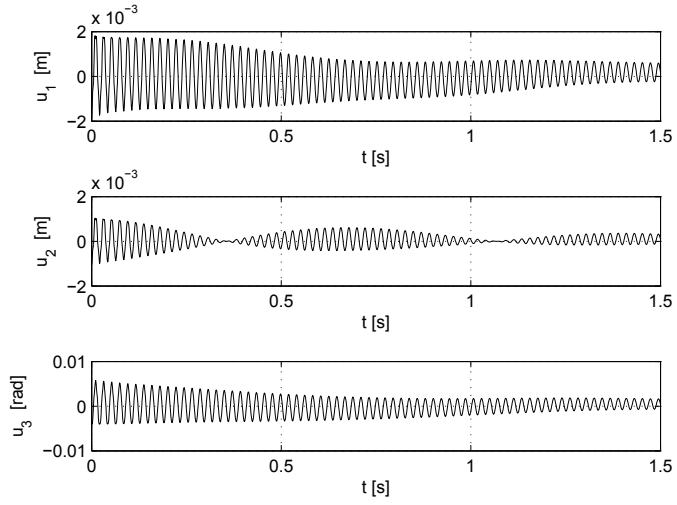

Figure 3.14: Free response of the single-link mechanisms with initial condition $q_0 = -\pi/3$: elastic displacements u_1, u_2 and u_3

As it can be easily seen form Figures (3.13) and (3.13), the beam behaves like a flexible pendulum, since the angular coordinate q evolves like a slightly perturbed sinusoidal function. It should also be noticed that the magnitude of the elastic displacements cannot be neglected even if no torque is applied to the mechanism.

Figures (3.15), (3.16), (3.17) shows insted the response to a finite torque stimulus applied to the rotational joint. The model starts from the rest condition ($q = -\pi/2$), while a 1 Nm torque is applied from time 0.1 s to time 0.2 s:

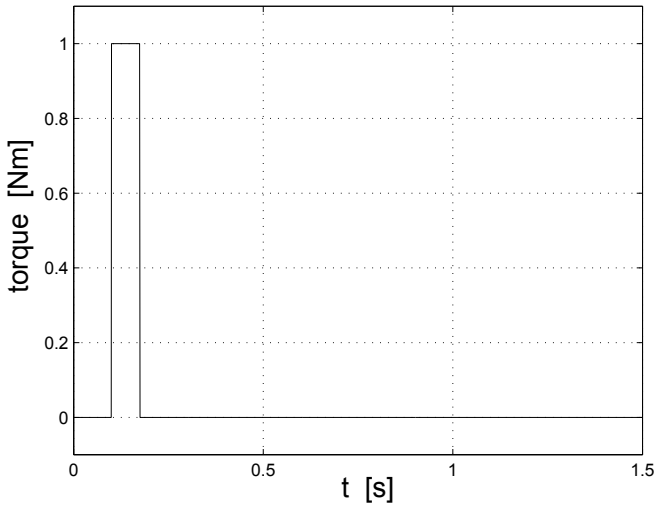

Figure 3.15: Torque impulse applied to the FLM

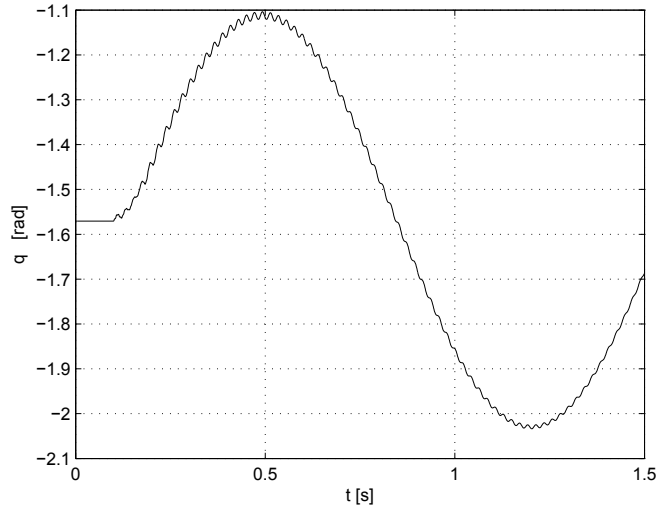

Figure 3.16: Forced response: angular position q

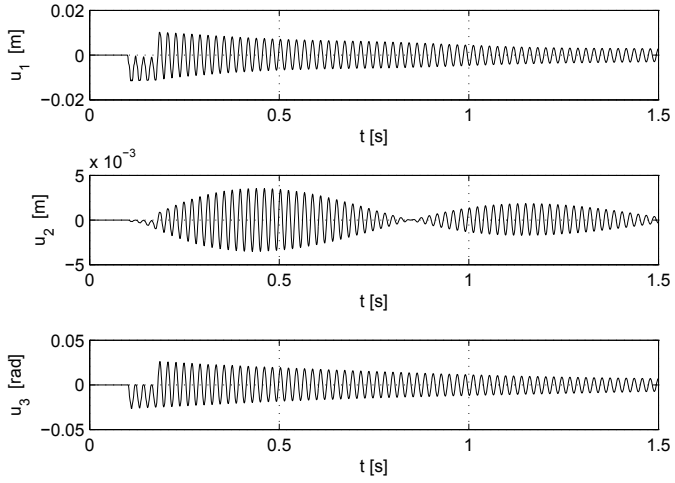

Figure 3.17: Forced response: elastic displacements

3.4.2 Simulink model for the 3 and 4 node SLM

A larger number of finite elements can be used to improve the accuracy of the dynamic model. The accuracy is directly proportional to the number of finite elements, but a finer discretization also brings an in increment in the computational weight of the model. As it will be addressed in the following chapters, one to three finite elements are usually a good compromise between the accuracy of the model and its speed. Let's now compare the results obtainable with 1, 2 and 3 finite elements. In the first case there are 3 nonzero elastic displacements, with 2 FE there are 6 nonzero displacement, and 9 nonzero displacements with 3 FE.

Here some results are included to show the difference between the use of 1 or 2 finite elements. The torque applied in both cases is plotted in figure (3.18):

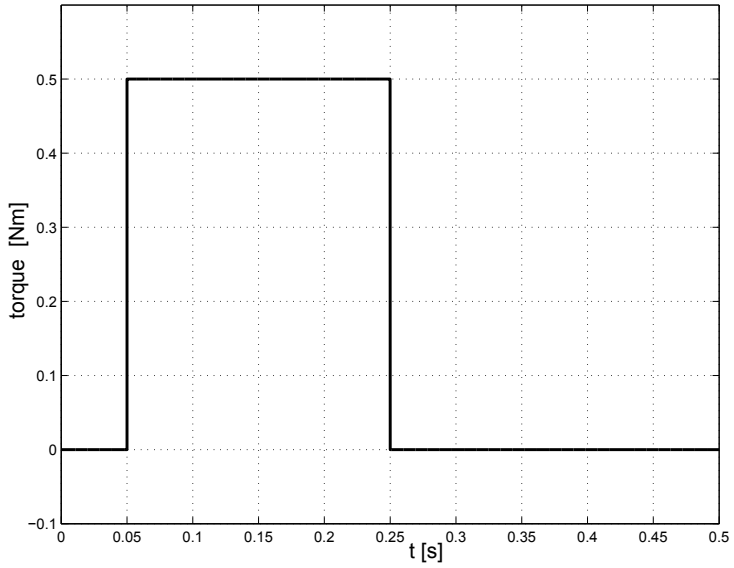

Figure 3.18: Applied torque

The resulting displacement along the three axes in the local reference frame is plotted in figures (3.19, 3.20,3.21):

A non negligible difference in the response between the two model is present, both concerning the amplitude and the number of vibrational modes. Using the same procedure, also a comparison of 3 node and 4 node beams is presented

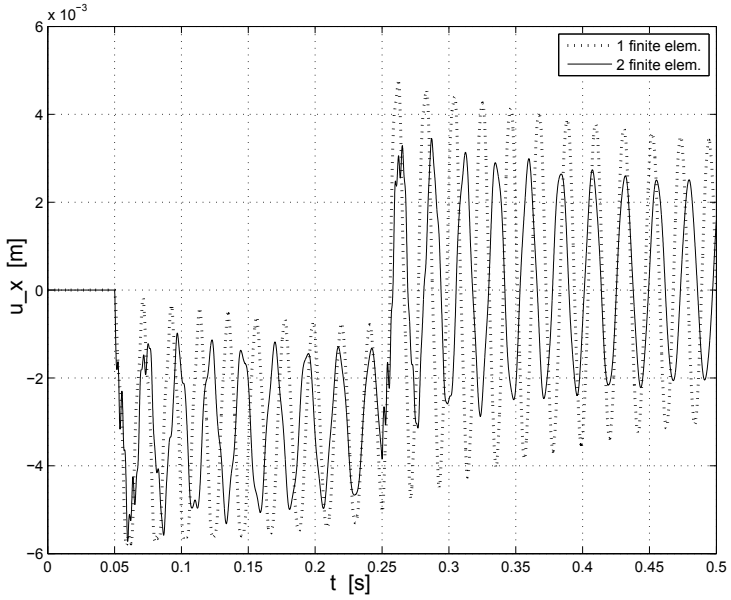

Figure 3.19: Elastic displacement with 1 and 2 finite elements: elastic displacement u_x

here. The operative conditions are the same as in the previous simulations. Results are plotted in figures (3.22,3.23,3.24).

Very similar results are shown in figures (3.22,3.23,3.24), meaning that the "distance" between the 1 FE model and the 2 FE element model is greater than the "distance" between the 2 FE and the 3 FE model. Therefore the single link model has never been used in the numerical and experimental results shown in the following chapters.

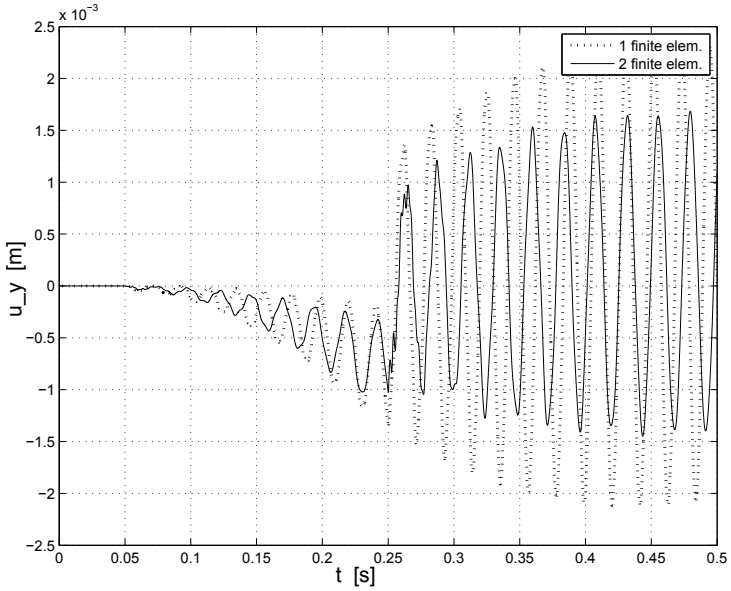

Figure 3.20: Elastic displacement with 1 and 2 finite elements: elastic displacement u_y

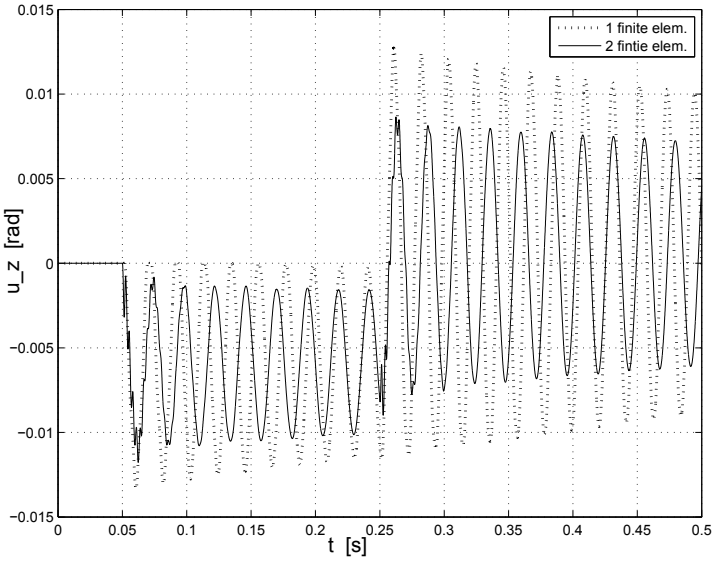

Figure 3.21: Elastic displacement with 1 and 2 finite elements: elastic displacement u_z

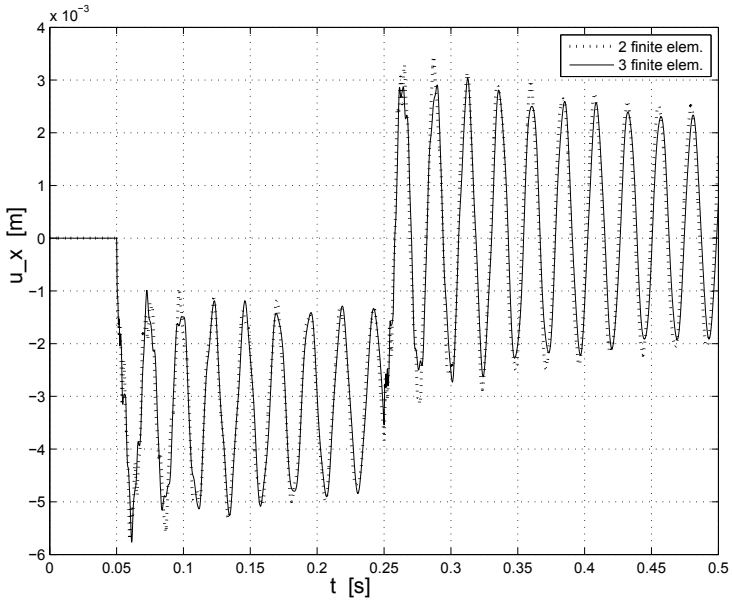

Figure 3.22: Elastic displacement with 2 and 3 elements discretization: elastic displacement u_x

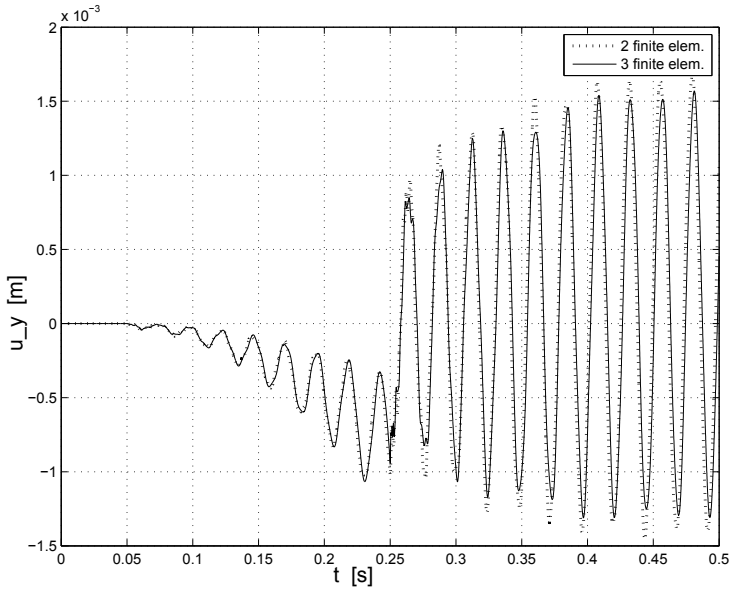

Figure 3.23: Elastic displacement with 2 and 3 elements discretization: elastic displacement u_y

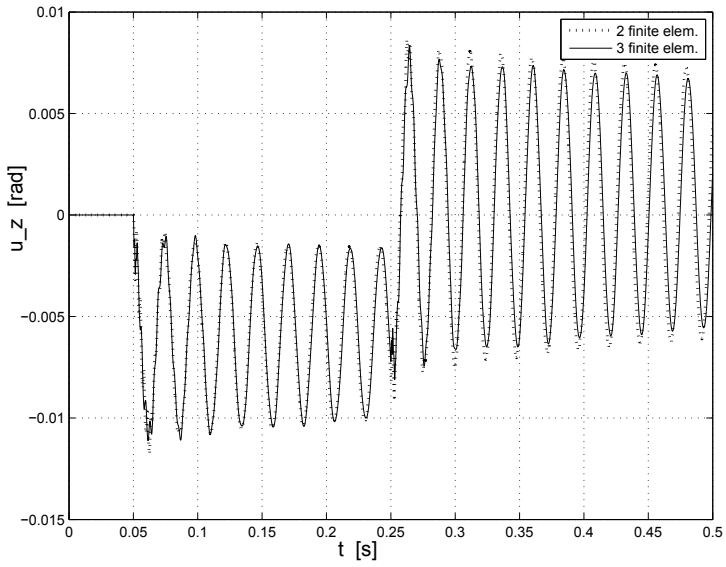

Figure 3.24: Elastic displacement with 2 and 3 elements discretization: elastic displacement u_z

3.5 4-bar linkage: dynamic model

The structure of the code used for the 4-bar linkage simulator is the same as the one used for the single-link mechanism. The only substantial difference is the inclusion of a routine that evaluates the position and speed kinematics of the ERLS. This routine is necessary since the evaluation of the matrices describing the dynamic model of the mechanism depend on both the angular position and on the velocity of each moving link. The choice of the number of finite elements and of the kinematic constraints is the same as the one chosen for the static simulator presented before in the same chapter. Some simulation results are presented here, in order to show both the free response and to a finite non periodic torque solicitation. In particular, plots will report the response in terms of the free coordinate q and of the tree elastic displacements at the 6th node (see figure 3.25), i.e. the displacement at the midspan of the longest link, which we will refer as u_9, u_{10} and u_{11}.

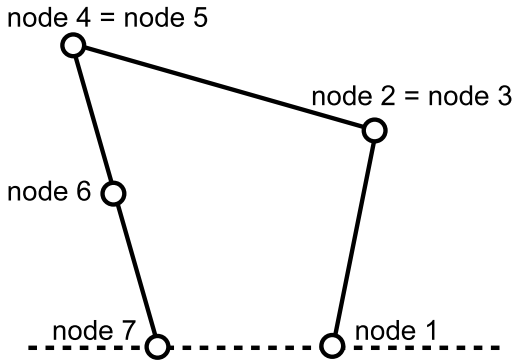

Figure 3.25: Four-bar mechanisms: finite element discretization

The simulink model, which is based as for the SLM on a C coded s-function, is shown in figure 3.26.

Free response

In order to show the free response of the 4-bar linkage, the mechanism is left free to swing from the initial position $q_0 = \pi/2$, without applying any torque to the crank. The results of this simulation are plotted in figures (3.27,3.28,3.29), wich shows the elastic displacements at the midspan of the follower link.

The evolution of crank angular position, as in figure (3.30), is that under the gravity force load, the mechanism "falls" toward the left:

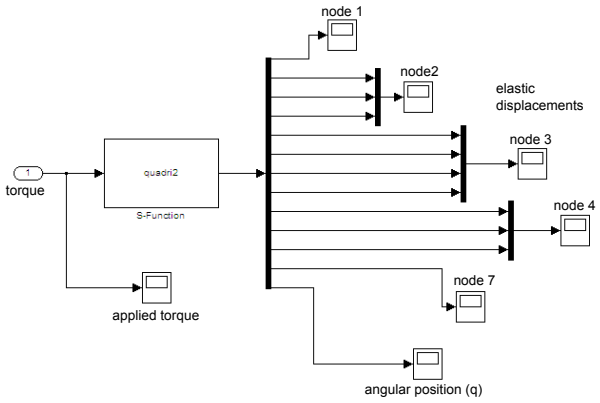

Figure 3.26: Simulink model for the flexible 4-bar mechanisms

As it can be seen, the magnitude of the elastic displacement is quite small. This is because the mechanism has a closed kinematic chain, therefore is stiffer than an open-chain mechanism with the same number of degree of freedom.

Forced response

Now we want to investigate the behavior of the mechanism under an additional external force. In order to do this, the simulator is fed with a torque solicitation of amplitude 1.5 Nm and 200 ms duration. The initial configuration is the same as in the previous simulation, $q_0 = \pi/2$. The torque is plotted in figure (3.32).

The evolution of the free coordinate q and of the elastic deformation at node 6 is plotted in figures (3.32,3.33,3.34,3.35).

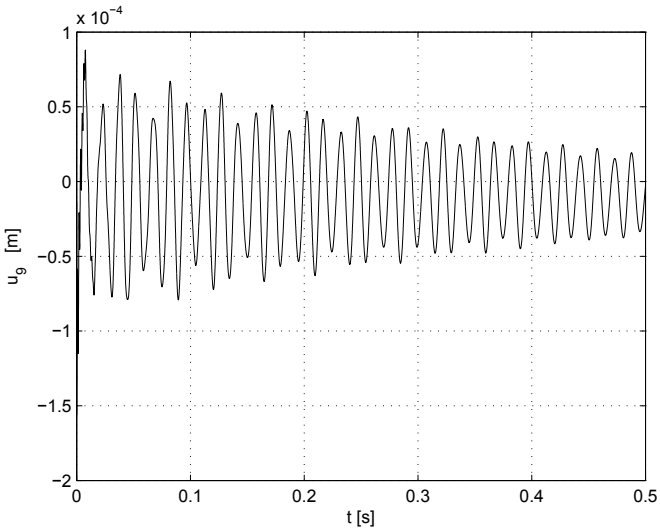

Figure 3.27: Free response: elastic displacement u_9 along the x axis

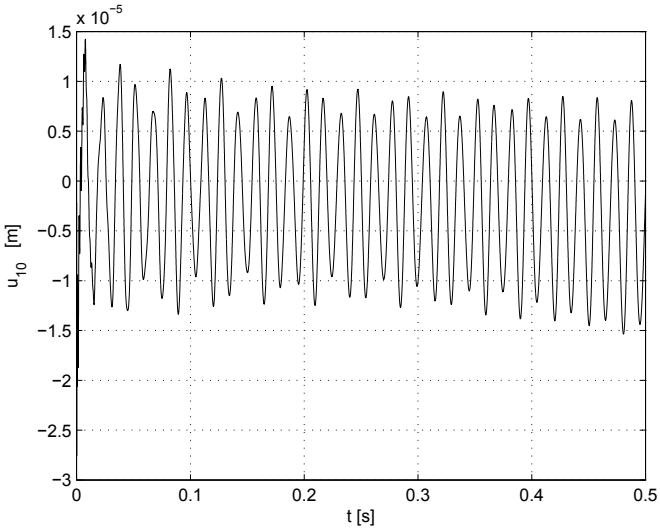

Figure 3.28: Free response: elastic displacement u_{10} along the y axis

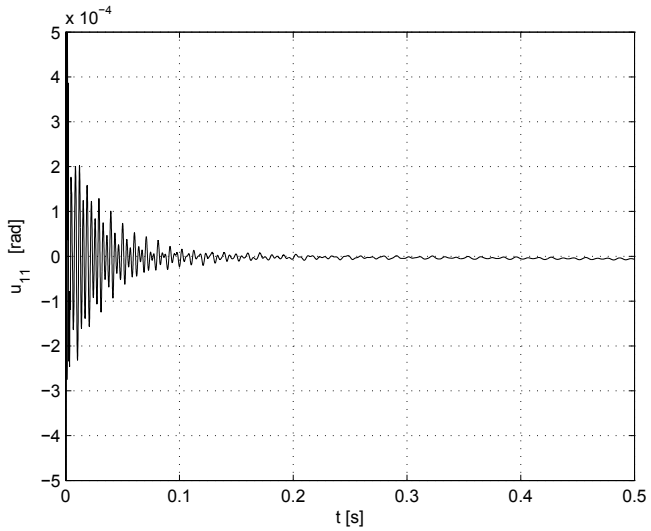

Figure 3.29: Free response: elastic displacement u_{11} along the z axis

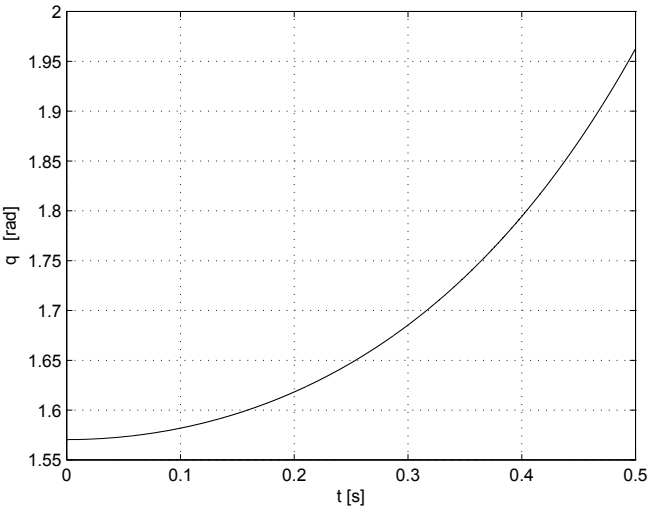

Figure 3.30: Free response: crank position q

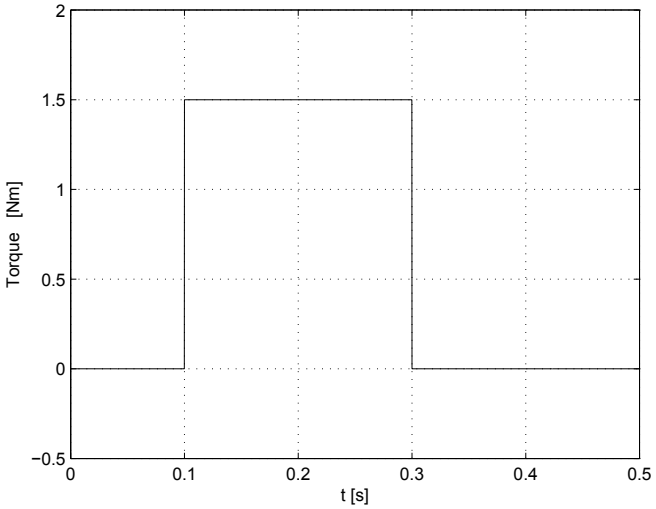

Figure 3.31: Torque sollicitation

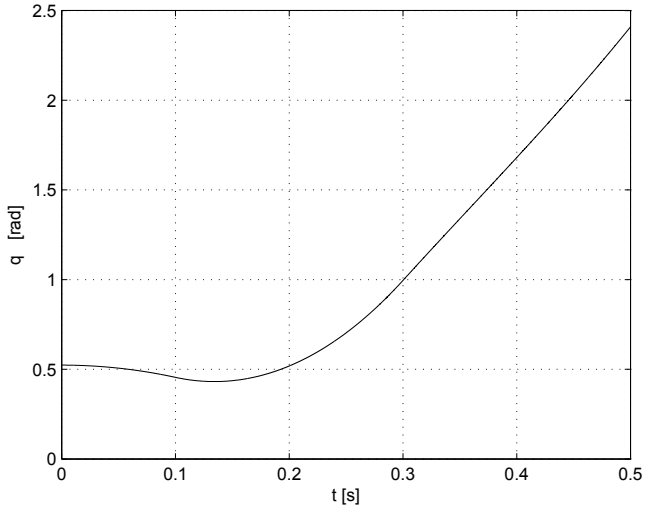

Figure 3.32: Angular position of the crank, q

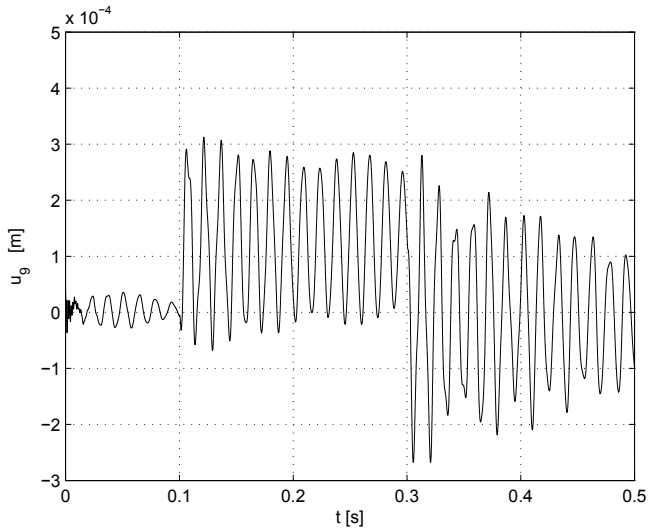

Figure 3.33: Elastic displacement at the 6^{th} node: u_9 along the x axis

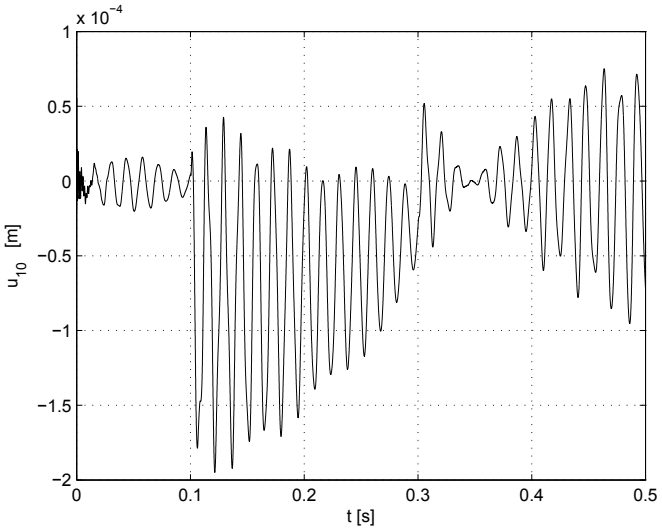

Figure 3.34: Elastic displacement at the 6^{th} node: u_{10} along the y axis

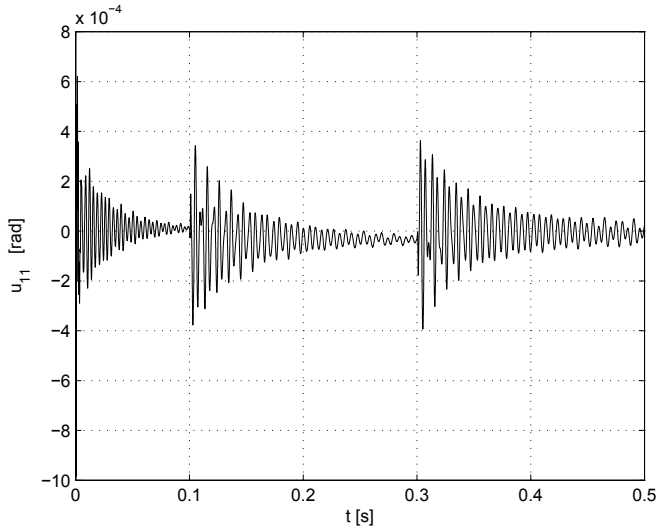

Figure 3.35: Elastic displacement at the 6^{th} node: u_{11} along the z axis

3.6 Dynamic model for the 5 link mechanism

The same procedure and the same program structure used for the 4-bar linkage has been adopted to develop the dynamic simulator for a five-bar linkage. For the results presented here, the longest link (in this case the second link, counting clockwise) has been discretized with 2 finite elements. In this way, we can describe with higher accuracy the elastic behavior of such link. In particular, the elastic displacements at the midspan of such link will be addressed in the plots presented in this section. The resulting node disposition can be seen in Figure (3.36):

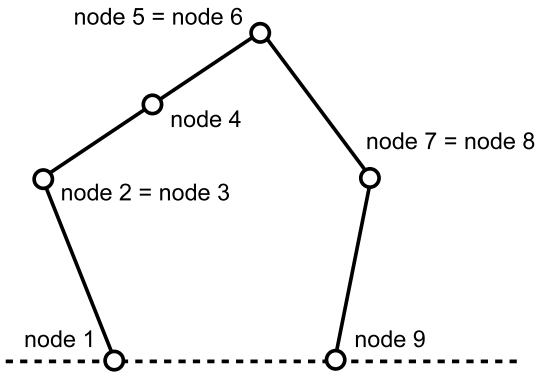

Figure 3.36: 5 bar mechanism: finite element discretization

As already done before for the static model, the following elastic displacements are forced to zero:

- the two displacements along x ed y axes at node 9, because of the rotational joint
- the two displacements along x ed y axes at node 9, to take into account the rotational joint
- the two displacements along x ed y axes at node $5 = 6$

The latest choice is actually the result of a trial-and-error procedure, since it has been noticed that this choice allows to avoid singular points which could create numerical problems during the simulation of the dynamics of the mechanism.

The geometric and structural properties of the simulated mechanism are reported here:

- Length of the links: $L_1 = 0.4$ m, $L_2 = 0.7$ m, $L_3 = 0.565$ m, $L_4 = 0.5$ m
- Distance between node 1 and 9: $d = 0.5m$
- Area of the section of the links: $A = 1.1025 \times 10^{-4}\ m^2$
- Young's modulus: $E = 2 \times 10^{11} Pa$
- Mass density if the links: $\rho = 7850 Kg/m^2$

Free evolution

As already done for the single-link and the four-bar mechanism, the free evolution of the simulated mechanism is investigated here. The results presented here refers to a simulation whose initial position for the two cranks are $q_1 = 2/3\pi$ and $q_2 = \pi/2$. The only external force acting on the mechanism is the gravity load.

The evolution of the positions of the two cranks are shown in figure (3.37), while the elastic displacements at node 4 are plotted in figures (3.38, 3.39, 3.40). Results are shown for a 500 ms time span.

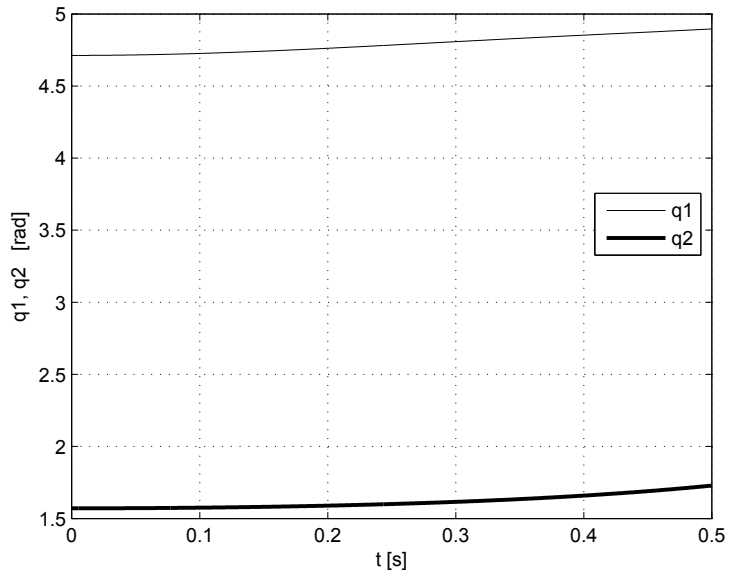

Figure 3.37: Free response with initial conditions: $q_1(0) = 2/3\pi$ and $q_2(0) = \pi/2$: angular positions q_1 and q_2

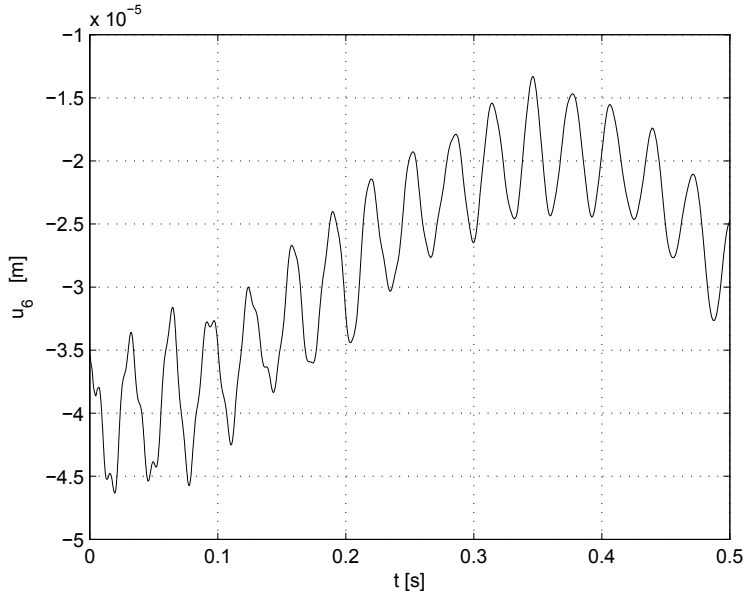

Figure 3.38: Free response eith initial conditions: $q_1(0) = 2/3\pi$ and $q_2(0) = \pi/2$: elastic displacement u_6

Forced evolution

The response of the dynamic simulator to the torques exerted by the two actuators located at node 1 and node 9 is here investigated. It has been chose to impose a constant torque whose value is 4 Nm from $t = 100$ ms to $t = 250$ ms for the first actuator. The second one produces a torque whose amplitude is 5 Nm from $t = 100$ ms to $t = 300$ ms. Otherwise both torques are equal to zero. The evolution of the torques is plotted in figure 3.41. Also gravity is included in the model. The closed-loop behavior of a similar mechanism will be investigated in greater detail in chapter 5, where an advanced control technique will be tested using the simulator of the 5-bar linkage.

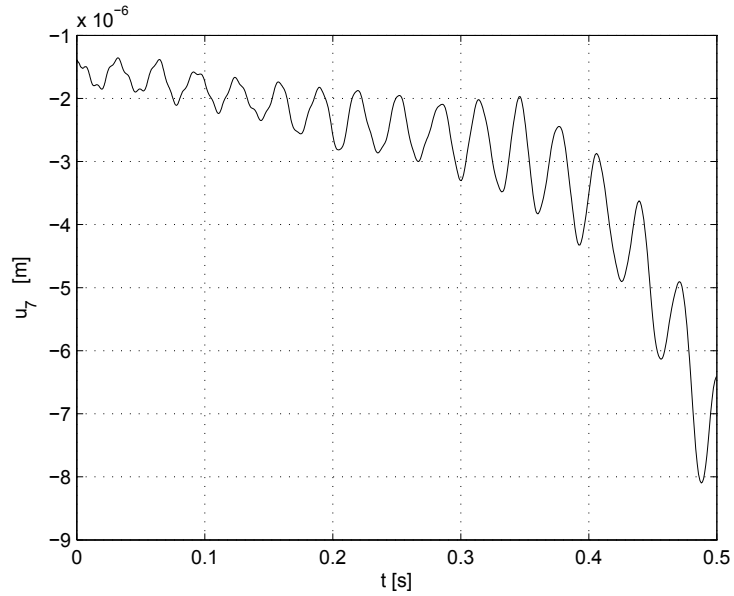

Figure 3.39: Free response eith initial conditions: $q_1(0) = 2/3\pi$ and $q_2(0) = \pi/2$: elastic displacement u_7

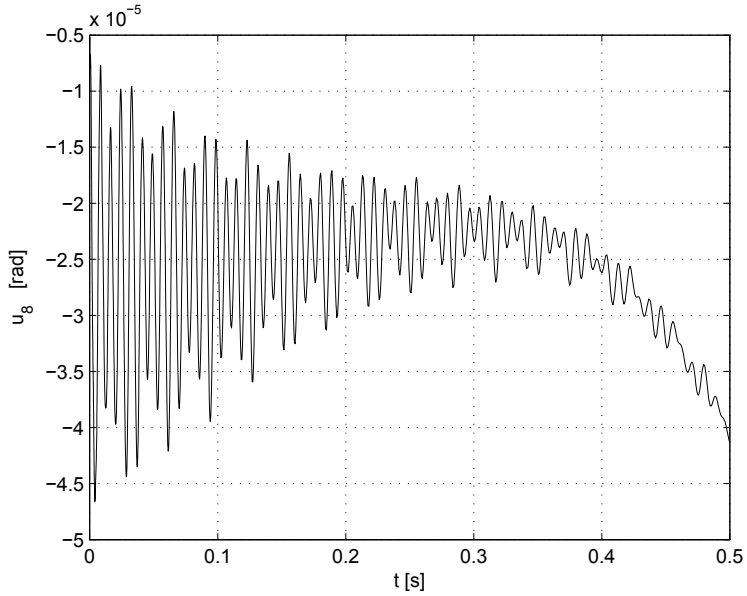

Figure 3.40: Free response with initial conditions: $q_1(0) = 2/3\pi$ and $q_2(0) = \pi/2$: elastic displacmenet u_8

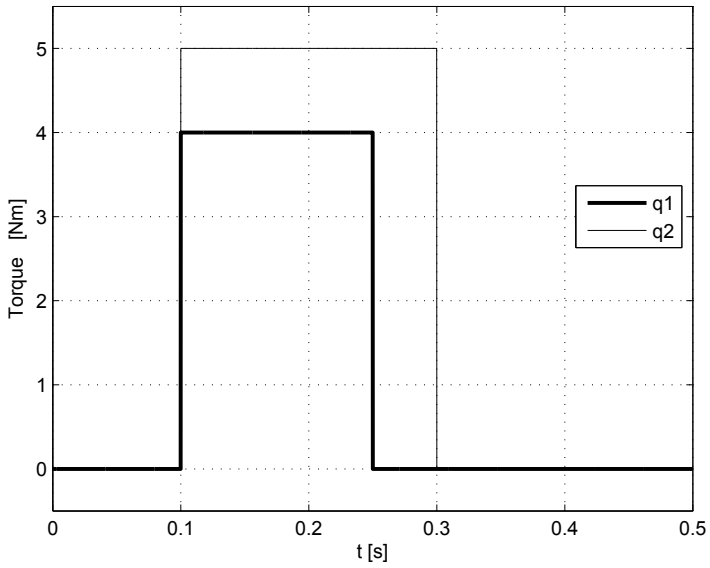

Figure 3.41: Torque sollicitations to the two cranks

The mechanisms evolves from the initial condition $q_1 = 2/3\pi$, $q_2 = \pi/6$: during the first part the mechanisms "falls" toward the right beccause of gravity, but as soon as the two torques are nonzero, the mechanisms starts moving in the opposite direction. The position of the cranks are plotted in figure (3.42)

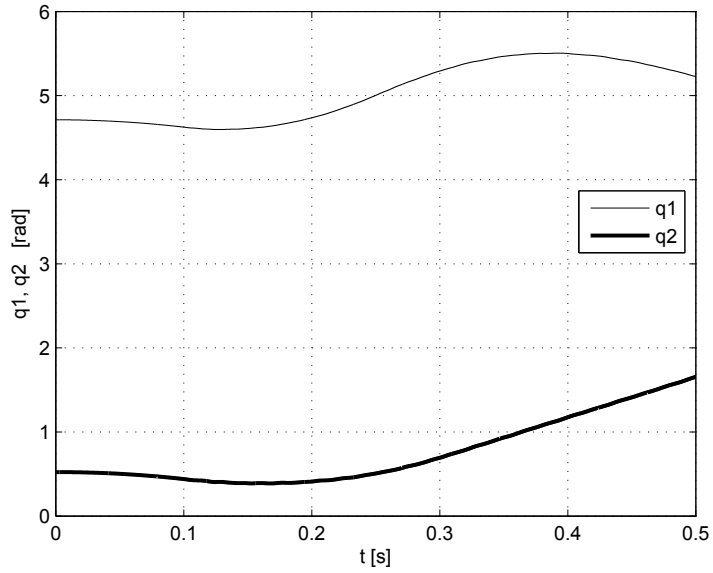

Figure 3.42: Evolution of angular positions q_1 and q_2

The three elastic displacement at the midspan of the second link are q_6, q_7 e q_8. They represents the three components of the displacement at node 4 along x, y and z axis, respectively. Their evolution is depicted in figures (3.43,3.44,3.45).

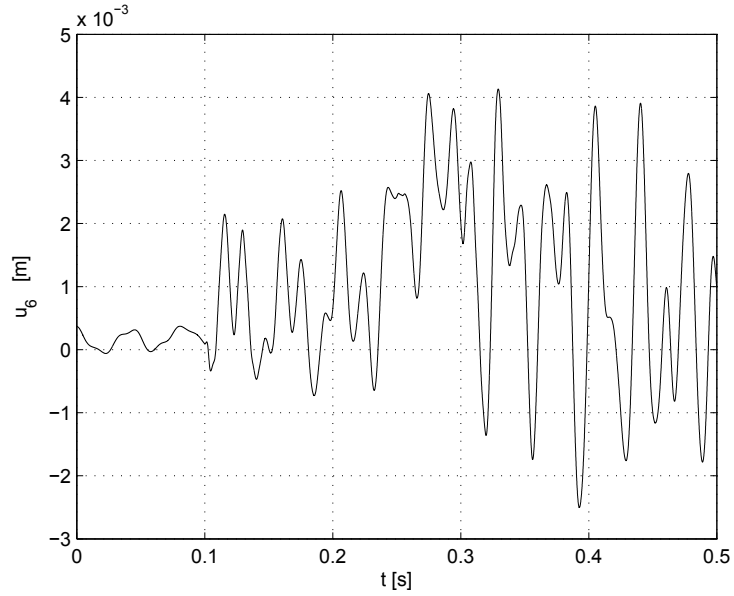

Figure 3.43: Elastic displacement alog the x axis at the midspan of the second link

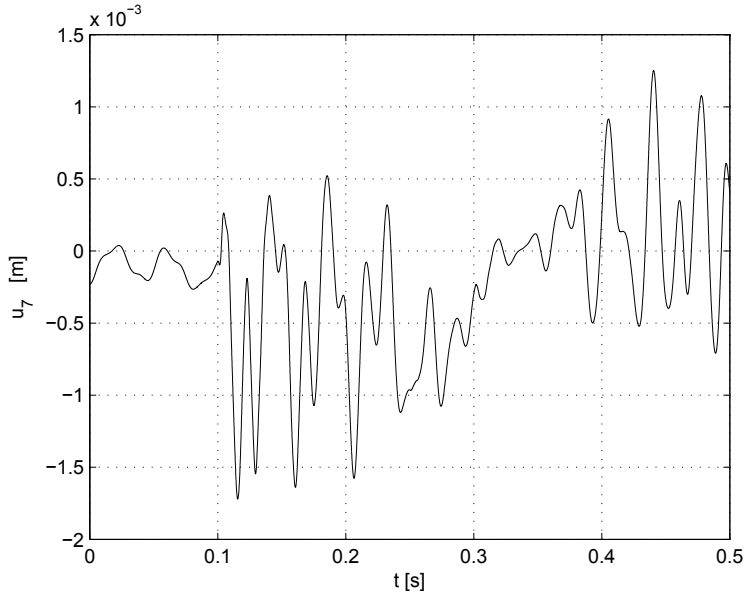

Figure 3.44: Elastic displacement alog the y axis at the midspan of the second link

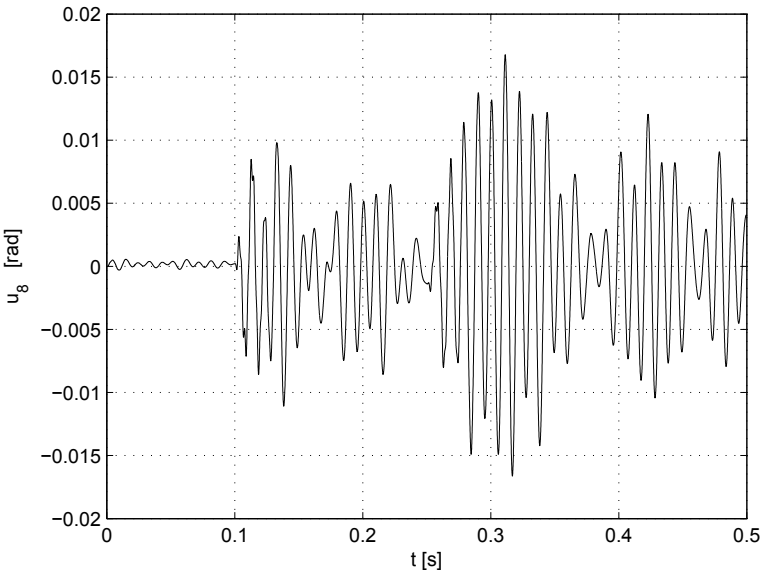

Figure 3.45: Elastic displacement alog the z axis at the midspan of the second link

4 Model Predictive Control

In this chapter an overview of the basics of Model Predictive Control will be given. In order to introduce the reader to the topics of control of mechanical systems, some general concepts of closed-loop control will be given. A general overview of closed-loop control can be found on classic books such as [127], [128],[129].

4.1 Control of robotic manipulators

The problem of control of mechanisms consists on finding a way to compute the generalized forces that the actuator should supply in order to perform with prescribed accuracy a pre-defined task. This task is of crucial importance in modern robotics, where high-speed motion, precision, low power consumption and safety are ever present goals. As it should be evident, the design of proper control techniques are even more important for mechanisms with flexible elements (links and/or joints), since their non-minimum phase behavior [130] and their being in most cases underactuated system [131] make their control a true challenge if high performance is required.

In most cases the tasks for mechanical systems are specified in the operative space, i.e. using a set of kinematic quantities (position, velocity, acceleration) referred to the end-effector of the manipulator. On the other end, the motion of the mechanisms is performed using the actuators, which are mounted usually on the joints of the robot. The two tasks are quite different, since in the two cases different problems must be overcome [132]. Therefore in the literature the two problems are referred as *control in the operative space* and *control in the*

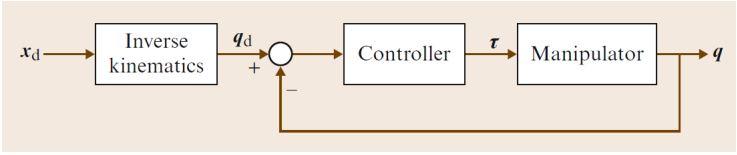

Figure 4.1: Generic control in the joint space

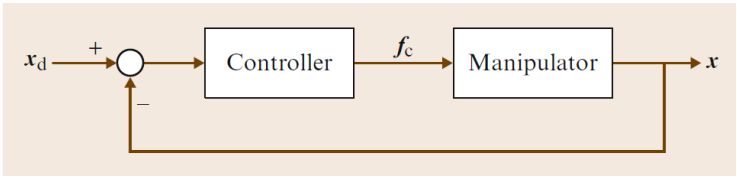

Figure 4.2: Generic control in the operative space

joint space [133]. The difference between the two control approaches is made evident in figures (4.1) and (4.2).

As it is evident in figure (4.1), the control in the joint space requires the use of a kinematic inversion algorithms, i.e. an algorithm which allows to evaluate the trajectory in the joint space from its equivalent in the operative spaace. This work deals exclusively with control in the joint space, as the vast majority of works available on flexible-link mechanisms [48].

The dynamics of robot manipulator, in the absence of external forces on the end effector, without static friction and distributed flexibility, can be described as:

$$\mathbf{B}(\mathbf{q})\ddot{\mathbf{q}} + \mathbf{C}(\mathbf{q}, \dot{\mathbf{q}})\dot{\mathbf{q}} + \mathbf{F}_v\dot{\mathbf{q}} + \mathbf{g}(\mathbf{q}) = \tau \tag{4.1}$$

in which $\mathbf{B}$, $\mathbf{C}$, $\mathbf{F}_v$, $\mathbf{g}$ are the terms related to inertia, to Coriolis contribution, to dynamic friction and to gravity, respectively. The control system has the objective of evaluating the best values for the generalized torques τ in order to guarantee a motion $\mathbf{q}(t)$ so that:

$$\mathbf{q}(t) = \mathbf{q}_d(t)$$

being $\mathbf{q}_d(t)$ the desired trajectory for all joints of the mechanism, which can be evaluated, in most cases, using a kinematic inversion algorithm. The vector of positions of the actuators $\mathbf{q}_m$ are linked to the joint position vector $\mathbf{q}$ trough the following relation:

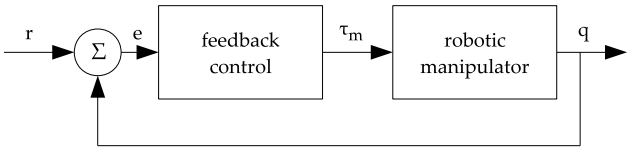

Figure 4.3: Feedback control

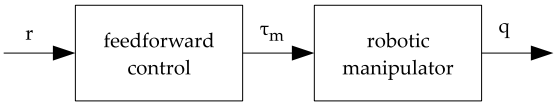

Figure 4.4: Feedforward control

$$\mathbf{K}_r \mathbf{q} = \mathbf{q}_m \tag{4.2}$$

where $\mathbf{K}_r$ is a diagonal matrix that takes into account for all the reduction gears normally used in robotic manipulators. If $\mathbf{K}_r$ is a diagonal matrix, it means that each joint can be moved independently from all the other one belonging to the manipulator. Using relation (4.2), the vector of motor torques τ_m generated by the actuators can be computed as:

$$\tau_m = {\mathbf{K}_r}^{-1} \tau \tag{4.3}$$

The quantity τ_m is usually computed by a control system, using the data coming from one or more sensor for each joint. This is the case in which measures are available is indicated as *feedback control* (see fig. 4.3), while when measures are not used or not available, we speak of *feedforward control* (see fig 4.4). While feedforward control can be an effective strategy for the control of robotic systems, it is not dealt with in this work.

Another distinction can be made between control systems for robotic manipulators with just one or multiple actuators. The generation of a control input can be made independently for each actuated joint, or in a coordinated manner. In the first case, the effect of a joint movement on another joint is treated simply as a disturbance, while in the latter the coupling effects between joints are taken into account by the control system. Both of this approaches are legit, the choice between the two of them is demanded on the control designer. The approach used along this work belongs to the second class (coordinated control), meaning that the single closed-loop control developed for the five-link mechanisms moves both the actuators in a coordinated manner, since it relies

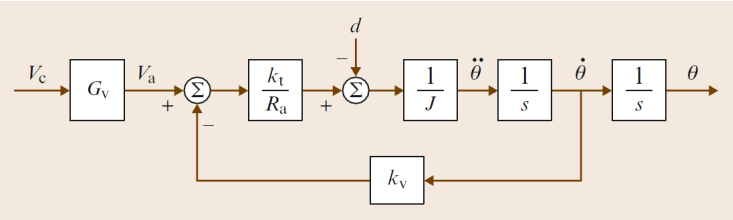

Figure 4.5: Block diagram of a single joint actuation system

on a precise knowledge of the effects of both the actuators on the dynamics of the whole mechanism.

4.1.1 Closed-loop control

In the simplest case, a robotic manipulator can be interpreted as being composed by n independent systems, i.e. each joint can be controlled independently using a SISO controller. Let us consider the case in which the manipulator is controlled using rotary DC motors, as often happens in practical situations. Therefore each joint can be represented by the block diagram represented in figure (4.5)

In this block diagram θ is the angular position of the joint, J is the inertia at the joint, R_a is the armature resistance, and k_t and k_v are, respectively, the torque and motor constants. Furthermore, G_v denotes the voltage gain of the power amplifier so that the reference input is the input voltage V_c of the amplifier instead of the armature voltage V_a. It has also been assumed that the mechanical (viscous) friction coefficient can be neglected with respect to the electrical coefficient. Now the input-output transfer function of the motor can be written as:

$$M(s) = \frac{km}{s(1 + sT_m)}$$

where $k_m = G_v/k_v$ and $T_m = R_a J/k_v k_t$ are, respectively, the voltage-to-velocity gain and the time constant of the motor. To guide selection of the control structure, start by noticing that an effective rejection of the disturbance d on the output θ is ensured by a large value of the amplifier before the point of intervention of the disturbance and by the presence of an integral action in the controller so as to cancel the effect of the gravitational component on the output at the steady state (i. e., constant θ). Therefore the use of a proportional–integral (PI) control system is a good choice.

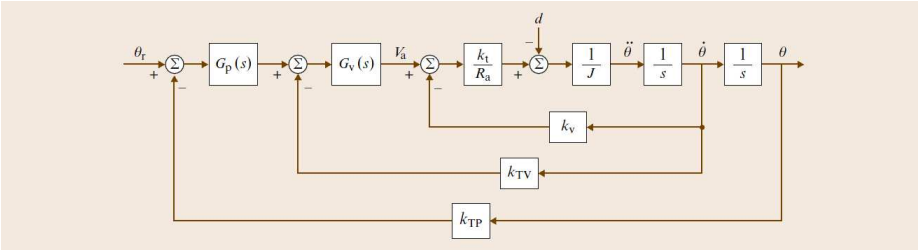

Figure 4.6: Generic control for each independent joint

In this case, as shown in figure (4.5), the control action with position and velocity feedback is characterized by:

$$G_p(s) = K_P \tag{4.4}$$

$$G_v(s) = K_V \frac{1 - sT_v}{s} \tag{4.5}$$

where $G_p(s)$ and $G_v(s)$ correspond to the position and velocity control actions, respectively. It is worth noticing that the inner control action $G_v(s)$ is in a form of proportional-integral (PI) control to achieve zero error in the steady state under a constant disturbance d. This choice of controller brings an important advantage: the resulting closed-loop transfer function is:

$$\frac{\Theta(s)}{\Theta_r(s)} = \frac{\frac{1}{k_{TP}}}{1 + \frac{sk_{TV}}{K_P k_{TP}} + \frac{s^2}{k_m K_P k_{TP} K_V}} \tag{4.6}$$

It can be noticed that equation 4.6 represents a second order system like:

$$W(s) = \frac{\frac{1}{k_{TP}}}{1 + \frac{2\varsigma s}{\omega_n} + \frac{s^2}{\omega_n^2}}$$

Therefore, trough a proper choice of the control system parameters, all the values of the natural frequency ω_n and of the damping ς can be obtained. For more reference on the choice of such parameters, refer to [133].

PD control with gravity compensation

Another control strategy that can be applied to robotic manipulators, and also to flexible-link ones [134], is the proportional-derivative control with gravity compensation. Such a controller is introduced here, since a similar approach

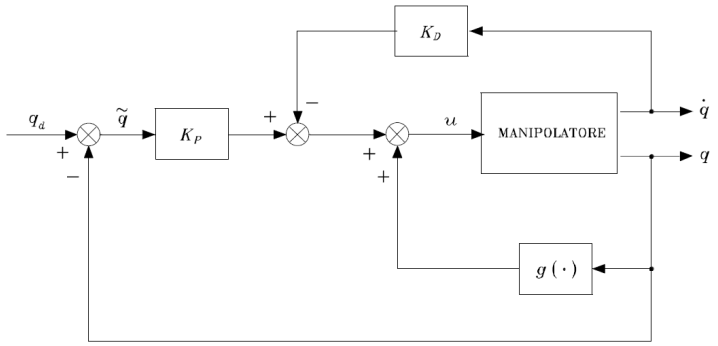

Figure 4.7: PD control with gravity compensation: block diagram

has been used for some of the simulation work presented in chapter 6, where the effects of gravity compensation is investigated together with PID and MPC control. The structure of the controller is presented in the block diagram 4.1.1

The structure of the control is quite simple: q_d is the desired set-point for the joint position q, while $\widetilde{q}$ is the tracking error. K_p and K_d are the proportional and derivative gains, respectively. The block diagram $g(\cdot)$ represents a generic function that implements the gravity compensation, i.e. it provides the value of the torque needed to compensate the effects of gravity for the actual position q. Therefore the control action is:

$$u = g(q) + K_p\widetilde{q} - K_D\dot{q} \tag{4.7}$$

in which the (nonlinear) gravity compensation term is shown together with proportional and derivative terms. This kind of controller has some advantages, such as the property of global asymptotic stability for positive values of K_P and K_D. In order for this to occur, the gravity compensation must be perfect, otherwise the aforementioned property cannot be proved.

Optimal Control

Optimal control is a popular choice for the design of closed-loop controllers, both for rigid and flexible-link manipulators. This kind of controller is quite appealing for the control of mechanism and manipulators, since it can be easily applied to MIMO plants with linear models. Nonlinear plants can be treated as well, but in this work it has been chosen to focus on controls based on linear models. Moreover, its design is based on a cost function, which can be chosen to enhance

some properties of the closed-loop system. Therefore, as a matter of example, an optimal control can be chosen to be optimal in the sense of: minimum time execution [135] of the task, minimum effort (or 'cheap control') [136], minimum energy [137], minimum jerk [138]. Moreover also mixed performance indexes can be considered, such as minimum time-energy [139], and constraints can be introduced as well [140]. Other variants such as robust control have been very popular in the last years [141], counting also some implementation for flexible-link manipulators [142], [86].

Here some basics on LQ (linear quadratic control) will be given, since it can be useful to understand the derivation of unconstrained MPC given in the next pages. Moreover this kind of controller has been used to obtain both numerical and experimental results presented in chapter 6. The literature on optimal control is very large, some excellent references are [128], [143], [144], [145].

In the traditional LQG (Linear Quadratic Gaussian) control it is assumed that the plant to be controlled can be represented (if not perfectly, with a sufficient level of confidence) by a known linear time invariant (LTI) model, and that the measurement noise and disturbances are stochastic processes with known properties. Therefore the plant model can be written as:

$$\begin{aligned} \dot{x} &= Ax + Bu + w_d \\ y &= Cx + w_n \end{aligned} \tag{4.8}$$

where w_d and w_m are the disturbance and measurement noise, respectively. As it should be familiar to the reader, x, y and u are the state, the output and the input to the plant, respectively. The LQG control problem is: find the optimal control $u(t)$ which minimizes the cost function J:

$$J = E\left\{ \lim_{t\to\infty} \frac{1}{T} \int_0^T \left[x^T Q x + u^T R u \right] dt \right\} \tag{4.9}$$

where Q and R are positive definite weighting matrices. This control is called LQG, since the model is linear, the cost function is quadratic and the noise is Gaussian. The solution of this control problem can be found using the Separation Theorem: first the optimal control problem is solved (as in LQR control - Linear Quadratic Regulator) without considering noise. In that case the problem has a simple solution in the form of a state feedback law:

$$u(t) = -K_r x(t) \tag{4.10}$$

in which K_r is a constant state feedback matrix, whose computation does not depend on w_d and w_n. The following step is to find an optimal estimate $\hat{x}$ of the state x, in order to minimize the expected value $E\left\{[x-\hat{x}]^T[x-\hat{x}]\right\}$. The optimal state estimation can be achieved trough Kalman filtering techniques, and it is independent form Q and R. Once the two problems are solved independently, the feedback regulator can be applied as: $u(t) = -K_r\hat{x}$, being $\hat{x}$ the state estimation provided by the state observer.

The LQR control problem consists on finding the feedback law for a given nonzero initial state of the plant $x(0)$ that brings the state back to $x = 0$ along a path which optimizes a given performance index. In the case that the performance index is:

$$J_r = \int_0^\infty \left[x(t)^T Q x(t) + u(t)^T R u(t)\right] dt \tag{4.11}$$

the optimal solution is, for any initial state, $u(t) = -K_r x(t)$, where:

$$K_r = R^{-1}B^T X \tag{4.12}$$

and X is the solution of the algebraic Riccati equation:

$$A^T X + XA - XBR^{-1}B^T X + Q = 0 \tag{4.13}$$

The Kalman filter has the same structure of a classic (such as Luneberger) state observer:

$$\dot{\hat{x}} = A\hat{x} + Bu + K_f(y - C\hat{x}) \tag{4.14}$$

where the optimal value of the gain matrix K_f is given by:

$$K_f = YC^T V^{-1} \tag{4.15}$$

with Y solution of the algebraic Riccati equation:

$$YA^T + AY - YC^T V^{-1} CY + W = 0 \tag{4.16}$$

being W and V the power spectral density matrix of disturbance and measurement noise, respectively. Such value for K_f ensure the minimization of $E\left\{[x-\hat{x}]^T[x-\hat{x}]\right\}$.

Combining optimal state estimation and optimal state feedback yields to the definition of a feedback control as described in figure 4.8

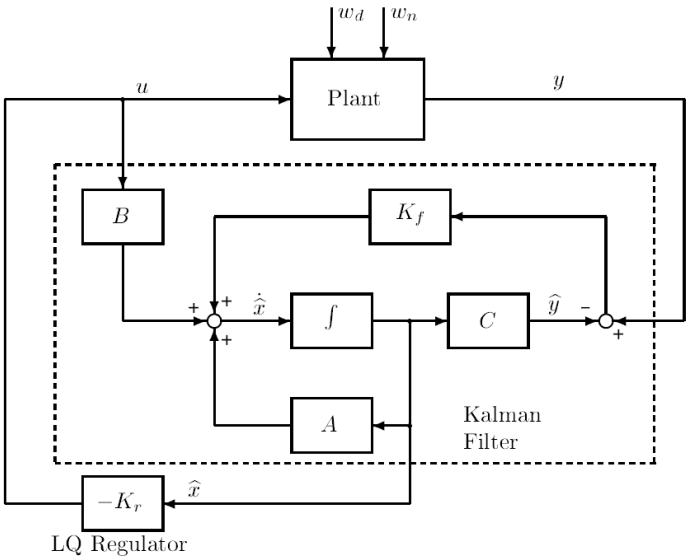

Figure 4.8: LQG control: block diagram

4.2 Predictive control strategy

A predictive control strategy is, generally speaking, a control loop strategy based on a prediction model, which allows to compute a control action based also on a forecast of the plant evolution. This is a general definition, which is needed to classify the large number of predictive controllers which has been developed since the seminal work of Richalet [146], which is dated back to 1978. Just to give an idea of the importance of this class of control systems in both literature and industrial applications, it is sufficient to say that the paper [90] reports around 100 industrial applications up to 2002, or that the book [147] has been cited more than 2000 times since year 2000.

The main idea behind model predictive control is to optimize a metric of the forecast of process behavior. The forecasting is done, explicitly or not, using a plant model, therefore the prediction model is the key element of such controller. As obvious, models are never perfect, so feedback is still necessary. In all the formulations of predictive control, the dynamic prediction is done in open-loop [147].

The most common choice for MPC is to use linear models. The earliest choices were to use input/output, step or impulse response models [146, 148, 149]. The use of simple model has been motivated by the appeal of simpler

models to control practitioners in industry. However, the most recent technology for linear MPC is based almost entirely on state-space models:

$$\begin{cases} \dot{\mathbf{x}} = \mathbf{A}\mathbf{x} + \mathbf{B}\mathbf{u} \\ \mathbf{y} = \mathbf{C}\mathbf{x} + \mathbf{D}\mathbf{u} \end{cases}$$

or the equivalent discrete-time:

$$\begin{cases} \mathbf{x}_{j+1} = \mathbf{A}\mathbf{x}_j + \mathbf{B}\mathbf{u}_j \\ \mathbf{y}_{j+1} = \mathbf{C}\mathbf{x}_j + \mathbf{D}\mathbf{u}_j \end{cases}$$

in which $\mathbf{x}(t)$, $\mathbf{y}(t)$ and $\mathbf{u}(t)$ are the system state, output and input, respectively, and j is the discrete time step. Both continuous time and discrete-time can be used. Without abuse of notation, here continuous and discrete-time models will be indicated by the same matrix triplet (**A,B,C**). The popularity of state-space formulation for MPC is motivated by several reasons, such as the easy extension form SISO to MIMO problems, or the availability of efficient software tools for the analysis and Real-Time computation. Moreover, the choice of state-space model allows to easily interface with the classical formulation of optimal control (LQ) and Kalman filtering. From a theoretical prospective, the significant shift in formulation from the LQ framework came from the introduction of constraints, particularly on input variable:

$$\begin{cases} \dot{\mathbf{x}} = \mathbf{A}\mathbf{x} + \mathbf{B}\mathbf{u} \\ \mathbf{y} = \mathbf{C}\mathbf{x} + \mathbf{D}\mathbf{u} \\ \mathbf{D}\mathbf{u} \leq d \\ \mathbf{H}\mathbf{y} \leq h \end{cases}$$

or:

$$\begin{cases} \mathbf{x}_{j+1} = \mathbf{A}\mathbf{x}_j + \mathbf{B}\mathbf{u}_j \\ \mathbf{y}_{j+1} = \mathbf{C}\mathbf{x}_j + \mathbf{D}\mathbf{u}_j \\ \mathbf{D}\mathbf{u}_j \leq d \\ \mathbf{H}\mathbf{y}_j \leq h \end{cases}$$

in which **D**, **H** are the constraints matrices and **d**, **h** are positive vectors. The constraints region boundaries are straight lines. Optimization over inputs subject to hard constraints leads immediately to nonlinear control, and that departure from the well-understood and well-tested linear control theory provided practitioners with an important, new control technology and motivated researchers to better understand this new framework. Certainly optimal control with constraints was not a new concept in the 1970s, but the moving horizon implementation of these open-loop optimal control solutions subject to constraints at each sample time was the new twist that had not been fully investigated.

The use of nonlinear models in MPC is motivated by the possibility of improving control by improving the quality of the forecasting.

Determining the settings in which the use of nonlinear models for forecasting delivers improved control performance is still an open issue. For continuous processes maintained at nominal operating conditions and subject to small disturbances, the potential improvement would appear small. For processes operated over large regions of the state space the advantages of nonlinear models appear larger. The numerical results presented in the last part of this work are also meant as an evidence of the fact that an MPC based on a linear plant can be efficiently used for flexible-link mechanisms undergoing large displacements.

Regardless of the model form and identification method, for tutorial purposes we represent the nonlinear model inside the MPC controller also in state-space form:

$$\begin{aligned}\dot{\mathbf{x}} &= f(\mathbf{x}, \mathbf{u}) \\ \mathbf{y} &= g(\mathbf{x}) \\ \mathbf{u} &\in \mathcal{U} \\ \mathbf{x} &\in \mathcal{X}\end{aligned}$$

or:

$$\begin{aligned}\mathbf{x}_{j+1} &= f(\mathbf{x}_j, \mathbf{u}_j) \\ \mathbf{y}_j &= g(\mathbf{x}_j) \\ \mathbf{u}_j &\in \mathcal{U} \\ \mathbf{x}_j &\in \mathcal{X}\end{aligned}$$

If the model is nonlinear, there is no advantage in keeping the constraints as linear inequalities, so we consider the constraints as membership in more general regions $\mathcal{U}$, $\mathcal{X}$.

4.2.1 MPC with linear models

Given the complexity and the relative lack of general results for nonlinear predictive control, in this thesis we will focus entirely on linear MPC. Here, in order to properly introduce the predictive control strategy, we focus on formulating MPC as an infinite horizon optimal control strategy with a quadratic performance criterion. We use the following discrete time model of the plant:

$$\begin{aligned}\mathbf{x}_{j+1} &= \mathbf{A}\mathbf{x}_j + \mathbf{B}(\mathbf{u}_j + \mathbf{d}) \\ \mathbf{y}_j &= \mathbf{C}\mathbf{x}_j + \mathbf{p}\end{aligned}$$

The affine terms $\mathbf{d}$ and $\mathbf{p}$ serve the purpose of adding integral control. They may be interpreted as modeling the effect of constant disturbance influencing the input and the output, respectively.

Assuming that the state of the plant is perfectly measured, we define MPC as the feedback law $\mathbf{u}_j = p(\mathbf{x}_j)$ that minimizes:

$$\Phi = \frac{1}{2}\sum_{j=0}^{\infty}(\mathbf{y}_i - \bar{\mathbf{y}})'\mathbf{Q}(\mathbf{y}_i - \bar{\mathbf{y}}) + (\mathbf{u}_i - \bar{\mathbf{u}})'\mathbf{R}(\mathbf{u}_i - \bar{\mathbf{u}}) + \Delta\mathbf{u}_j{}'\mathbf{S}\mathbf{u}_j \qquad (4.17)$$

In which $\Delta\mathbf{u}_j = \mathbf{u}_j - \mathbf{u}_{j-1}$. The matrices $\mathbf{Q}$, $\mathbf{R}$ and $\mathbf{S}$ are assumed to be symmetric positive definite. When the complete state of the plant is not measured, as is almost always the case, the addition of a state estimator is necessary. The vector $\bar{\mathbf{y}}$ is the desired output target and $\bar{\mathbf{u}}$ is the desired input target, assumed for simplicity to be time invariant. In many industrial applications, the desired targets are calculated as a steady-state economic optimization at the plant level. In these cases, the desired targets are normally constant between plant optimizations, which are performed on a slower time scale than the one at which the MPC controller operates. As discussed by Bitmead et al. [150] in the context of generalized predictive control (GPC), one can pose these types of tracking problems within the LQ framework by augmenting the state of the system to describe the evolution of the reference signal and posing an LQ problem for the combined system.

For a time invariant set point, the. steady-state aspect of the control problem, is to determine appropriate values of $(\mathbf{y}_s, \mathbf{x}_s, \mathbf{u}_s)$. Ideally, $\mathbf{y}_s = \bar{\mathbf{y}}$ and $\mathbf{u} = \bar{\mathbf{u}}$. Process limitations and constraints, however, may prevent the system from reaching the desired steady state. The goal of the target calculation is to find the feasible triple $(\mathbf{y}_s, \mathbf{x}_s, \mathbf{u}_s)$ such that $\mathbf{y}_s$ and $\mathbf{u}_s$ are as close as possible to $\bar{\mathbf{y}}$ and $\bar{\mathbf{u}}$. We address the target calculation below.

$$\Phi = \frac{1}{2}\sum_{j=0}^{\infty}\mathbf{z}_j'\mathbf{Q}\mathbf{z}_j + \mathbf{v}_j'\mathbf{R}\mathbf{v}_j + \Delta\mathbf{v}_j'\mathbf{S}\Delta\mathbf{v}_j \qquad (4.18)$$

The original criterion (4.17) can he recovered from (4.18) by making the mowing substitutions:

$$\begin{aligned}\mathbf{z}_j &\leftarrow \mathbf{y}_j - \mathbf{C}\mathbf{x}_s - \mathbf{p}_s\\ \mathbf{w}_j &\leftarrow \mathbf{x}_j - \mathbf{x}_s\\ \mathbf{v}_j &\leftarrow \mathbf{u}_j - \mathbf{u}_s\end{aligned}$$

in which $\mathbf{y}_s$, $\mathbf{x}_S$ and $\mathbf{u}_s$ are the steady states satisfying the following relation:

$$\begin{aligned}\mathbf{x}_s &= \mathbf{A}\mathbf{x}_s + \mathbf{B}(\mathbf{u}_s + \mathbf{d})\\ \mathbf{y}_s &= \mathbf{C}\mathbf{x}_s\mathbf{p}\end{aligned}$$

By using deviation variables, we treat separately the steady-state and the dynamic elements of the control problem, thereby simplifying the overall analysis of the controller. The dynamic aspect of the control problem is to control $(\mathbf{y}\ ,\ \mathbf{x}\ ,\ \mathbf{u})$ to the steady-state values $(\mathbf{y}_s, \mathbf{x}_s, \mathbf{u}_s)$ in the face of constraints, which are assumed not to be active at steady state, i.e. the origin is in the strict interior of $\mathcal{X}$, $\mathcal{U}$. As it will be addressed in more detail later, when the constraints are not active, the feedback law is a linear quadratic regulator. With the addition of inequality constraints however, an analytic form for $\mathbf{p}(\mathbf{w}_j)$ may not exist. For cases in which an analytics solution is unavailable, the feedback law is obtained by repeatedly solving the optimal control problem. This strategy allows us to consider only the encountered sequence of measured states rather than the entire state space. For a further discussion, see Mayne [151].

If we consider only linear constraints on the input, input velocity and outputs of the form:

$$\begin{aligned} \mathbf{u}_{min} &\leq \mathbf{D}\mathbf{u}_k \leq \mathbf{u}_{max} \\ -\Delta_u &\leq \Delta\mathbf{u}_k \leq \Delta_u \\ \mathbf{y}_{min} &\leq \mathbf{C}\mathbf{x}_k \leq \mathbf{y}_{max} \end{aligned} \tag{4.19}$$

we formulate the regulator as the solution of the following infinite horizon optimal control problem:

$$\min_{[\mathbf{w}_k, \mathbf{v}_k]} \Phi(\mathbf{x}_j) = \frac{1}{2}\sum_{j=0}^{\infty} \mathbf{z}_j'\mathbf{Q}\mathbf{z}_j + \mathbf{u}_j'\mathbf{R}\mathbf{u}_j + \Delta\mathbf{u}_j'\mathbf{S}\Delta\mathbf{u}_j \tag{4.20}$$

subject to the constraints:

$$\begin{aligned} \mathbf{w}_0 &= \mathbf{x}_j - \mathbf{x}_s \\ \mathbf{v}_{j-1} &= \mathbf{u}_{j-1} - \mathbf{u}_s \\ \mathbf{w}_{k+1} &= \mathbf{A}\mathbf{w}_k + \mathbf{B}\mathbf{v}_k \\ \mathbf{z}_k &= \mathbf{C}\mathbf{w}_k \\ \mathbf{u}_{min} - \mathbf{u}_s &\leq \mathbf{u}_{max} - \mathbf{u}_s \\ -\Delta_u &\leq \Delta\mathbf{v}_k \leq \Delta_u \\ \mathbf{y}_{min} - \mathbf{y}_s &\leq \mathbf{C}\mathbf{w}_k \leq \mathbf{y}_{max} - \mathbf{y}_s \end{aligned}$$

Combining the solution of the target tracking problem and the constrained regulator, we define the MPC algorithm as follows:

1. Obtain an estimate of the state and the disturbances $\Rightarrow (\mathbf{x}_j, \mathbf{p}, \mathbf{d})$
2. Determine the steady-state target $\Rightarrow (\mathbf{y}_s, \mathbf{x}_s, \mathbf{u}_s)$
3. Let $\mathbf{u}_j = \mathbf{v}_j + \mathbf{u}_s$
4. Repeat for $j \leftarrow j + 1$

4.3 Unconstrained Model Predictive Control

In this section an unconstrained formulation of MPC control will be introduced. The theoretical aspects have been taken from the excellent book by Wang [152]. This kind of formulation as been used as the basis for the development of the control systems whose performance are investigated in Chapter 6. This formulation has been chosen among the several available in literature for its clarity and its straightforward implementation. In order to give the clearest explanation of this formulation, the application to Single-Input Single-Output (SISO) plants will be initially dealt with. As it will be evident, the extension to SIMO, MISO and MIMO systems is quite straightforward.

4.3.1 State-space models with embedded integrator

As already highlighted before, the design of an MPC controller is based on a mathematical object, i.e. the dynamic model of the controlled plant. For the vast majority of the MPC formulation, and for the case under consideration here, such dynamical model should belong to the class of linear time-invariant systems with state space representation. In general all the linear-time invariant systems can be put into their state-space representation, also using commonly available software tools such as Matlab. Therefore the choice of this class of systems does not introduce severe constraints on the controlled plant. For the ease of calculation and for the improvements on real-time computation, discrete-time LTI systems with state-space representation is used widely, but similar results are available for continuous-time systems. This kind of formulation, as we will see in the next pages, allows to evaluate in a very straightforward manner the forecast on plant future evolution. On the other hand it should be noticed that different formulations are available in literature using different inner prediction model. In particular, MPC refers to predictive control using state-space model, while GPC (Generalized Predictive Control) [153, 154] refers to the implementation trough transfer functions. A state-space model has always an equivalent formulation as a transfer function (and vice versa), but the state-space formulation is more appealing when dealing with MIMO systems, or in general when dealing with systems represented by a large number of state variable, such as in the cases analized in this work.

MPC of SISO systems

Let's first introduce the formulation of a discrete-time SISO systems:

$$x_m(k+1) = A_m x_m(k) + B_m u(k) \tag{4.21}$$

$$y_m(k) = C_m x_m(k) \tag{4.22}$$

in which u is the input variable (or the control variable); y_i is the output of the system, while x_m is the state-space vector whose dimension is n_1. k represents the time. The development of the formulation of MPC of choice requires to add an integrator to the model above. This can be done simply by adding to the cited formulation a terms that links directly the output $y(k)$ with the input $u(k)$ trough:

$$y(k) = C_m x_m(k) + D_m u(k)$$

In the case under investigation, matrix D_m equals zero, i.e. we deal only with strictly proper models. This choice complies with the representation of linearized models that will be introduced in Chapter 6. Evaluating the difference at both sides of eq. 4.21 one obtains:

$$x_m(k+1) - x_m(k) = A_m(x_m(k) - x_m(k-1)) + B_m(u(k) - u(k-1))$$

We express the change of the state vector as:

$$\Delta x_m(k+1) = x_m(k+1) - x_m(k) \qquad \Delta x_m(k) = x_m(k) - x_m(k-1)$$

and the change of the control variable as:

$$\Delta u(k) = u(k) - u(k-1)$$

These are the increments of variables $x_m(k)$ e $u(k)$. By operating a change of variables, the incremental state space becomes:

$$x_m(k+1) = A_m x_m(k) + B_m u(k) \tag{4.23}$$

It should be noticed that the input of the model is the very same $u(k)$, as in the classic state space system. The next step is to make explicit the relationship

between the state vector $x_m(k)$ and the output $y(k)$. The correct procedure for this task is:

$$x(k) = \begin{bmatrix} \Delta x_m(k)^T & y(k) \end{bmatrix}^T$$

in which the symbol ^{T} represents the matrix transpose. We highlight that:

$$y(k+1) - y(k) = C_m(x_m(k+1) - x_m(k)) = C_m \Delta x_m(k+1) =$$

$$= C_m A_m \Delta x_m(k) + C_m B_m \Delta u(k) \tag{4.24}$$

By using eq. 4.23 together with eq. 4.24 the following state-space model can be computed:

$$\overbrace{\begin{bmatrix} \Delta x_m(k+1) \\ y(k+1) \end{bmatrix}}^{x(k+1)} = \overbrace{\begin{bmatrix} A_m & o_m^T \\ C_m A_m & 1 \end{bmatrix}}^{A} \overbrace{\begin{bmatrix} \Delta x_m(k) \\ y(k) \end{bmatrix}}^{x(k)} + \overbrace{\begin{bmatrix} B_m \\ C_m B_m \\ 8 \end{bmatrix}}^{B} \Delta u(k)$$

$$y(k) = \overbrace{\begin{bmatrix} o_m & 1 \end{bmatrix}}^{C} \begin{bmatrix} \Delta x_m(k) \\ y(k) \end{bmatrix} \tag{4.25}$$

in which $o_m = \overbrace{\begin{bmatrix} 0 & 0 & \dots & 0 \end{bmatrix}}^{n_1}$.

The triplet (A, B, C) is referred as augmented model, and it will be used as the basic building block for unconstrained MPC.

The following step is to find a way to evaluate the prediction on the outputs as a function of the future values of the control variable, in order to find the optimal sequence of control variables. This prediction (and optimization) is defined for a time window whose length is equal to N_p discrete time steps. Again the formulation refers to SISO systems, but the results are valid also for MIMO systems.

State and output prediction

Let's assume that at the sampling time k_i, $k_i > 0$, a measure of $x(k_i)$ is available. The value of $x(k_i)$ describes the actual state of the plant. In most cases such value is not directly available: it will be shown later in this chapter how to deal with these cases. The future trajectory of the control is

$$\begin{bmatrix} \Delta u(k_i) & \Delta u(k_i+1) & \dots & \Delta u(k_i+N_c-1) \end{bmatrix}$$

in which N_c is called *control horizon*. It should be highlighted that the length of N_c is the number of values which define univocally the future evolution of

the plant. From a given $x(k_i)$, the prediction of the states of the plant is made for N_p future samples. Therefore N_p is the *prediction horizon*. We indicate the future states of the plant as:

$$\left[\begin{array}{ccccccc} x(k_i+1|k_i) & x(k_i+2|k_i) & \dots & x(k_i+m|k_i) & \dots & x(k+i+N_p|k_i) \end{array}\right]$$

in which $x(k_i+m|k_i)$ is the prediction of the state vector at time k_i+m evaluated starting form $x(k_i)$. The length of the control horizon N_c is typically chosen to be less (or at most equal) to the prediction horizon N_p. The forecast on the plant dynamics is evaluated using the model (A, B, C) sequentially, using the sequence of values that will be assumed by the control variable:

$$\begin{array}{l} x(k+1|k_i) = Ax(k_i) + B\Delta u(k_i) \\ x(k+2|k_i) = Ax(k_i+1|k) + B\Delta u(k_i+1) \\ = A_2 x(k_i) + AB\Delta u(k_i) + Bu(k_i+1) \\ \vdots \\ x(k+N_p) = A^{N_p}x(k_i) + A^{N_p-1}B\Delta u_k(k_i) + A^{N_p-2}B\Delta u(k_i+1) \\ + \ldots + A^{N_p-N_c}B\Delta u(k_i+N_c-1) \end{array} \tag{4.26}$$

Using eq. (4.22) in the equation above, one obtains the prediction of the output:

$$\begin{array}{l} y(k_i+1|k_i) = CAx(k_i) + CB\Delta u(k_i) \\ y(k_i+2|k_i) = CA^2x(k_i) + CAB\Delta u(k_i) + CB\Delta u(k_i+1) \\ y(k_i+3|k_i) = CA^3x(k_i) + CA^2B\Delta u(k_i) + CAB\Delta u(k_i+1) + CB\Delta u(k_i+2) \\ \vdots \\ y(k_i+N_p|k_i) = CA^{N_p}x(k_i) + CA^{N_p-1}B\Delta u(k_i) + CA^{N_p-2}B\Delta u(k_i+1) \\ + \ldots + CA^{N_p-N_c}B\Delta u(k_i+N_c-1) \end{array} \tag{4.27}$$

It should be noticed that the prediction are formulated from the state available at time k_i, which is $x_m(k_i)$, and from the future changes of the control $\Delta u(k_i+j)$, with $j = 0, 1, ...Nc-1$:

$$Y = \left[\begin{array}{ccccc} y(k_i+1|k_i) & y(k_i+2|k_i) & y(k_i+3|k_i) & \dots & y(k_i+N_p|k_i) \end{array}\right]^T$$

$$\Delta U = \left[\begin{array}{ccccc} \Delta u(k_i) & \Delta u(k_i+1) & \Delta u(k_i+2) & \dots & \Delta u(k_i+N_c-1) \end{array}\right]^T$$

The length of Y is N_p, while ΔU has N_c elements. Putting together eq. (4.26) with eq. (4.27) in a single matrix expression, we obtain:

$$Y = Fx(k_i) + \Phi\Delta U \tag{4.28}$$

in which

$$F = \begin{bmatrix} CA \\ CA^2 \\ CA^3 \\ \vdots \\ CA^{N_p} \end{bmatrix}$$

$$\Phi = \begin{bmatrix} CB & 0 & 0 & \dots & 0 \\ CAB & CB & 0 & \dots & 0 \\ CA^2B & CAB & CB & \dots & 0 \\ \vdots & & & & \\ CA^{N_p-1}B & CA^{N_p-2}B & CA^{N_p-3}B & \dots & CA^{N_p-N_c}B \end{bmatrix}$$

Optimization

Given a set-point $r(k_i)$ a the sampling time k_i, it is assumed that this value will be kept constant for the whole duration of the optimization window. Under this assumption, an optimization problem can be formulated in order to evaluate the optimal vector of increments of the control variable, i.e. ΔU, in order to minimize a metric of the error between the set-point and the predicted output. Given the vector of set-point values:

$$R_s^T = \overbrace{\begin{bmatrix} 1 & 1 & \dots & 1 \end{bmatrix}}^{N_p} r(k_i)$$

the cost function J is defined as:

$$J = (R_s - Y)^T (R_s - Y) + \Delta U^T \bar{R} \Delta U \tag{4.29}$$

The first term has the function of minimizing the distance between the predicted output and the set-point signal, while the second one is aimed at minimizing the changes of the control variable. R is a diagonal matrix built as: $\bar{R} = r_w I_{N_c \times N_c} \quad (r_w \geq 0)$. r_w it's the tuning parameter that allows to adapt the response of the closed-loop system. If $r_w = 0$, the cost function (4.29) can be read in this way: the aim off the optimization problem is to minimize the error $(R_s - Y)^T (R_s - Y)$ without caring about the amplitude of ΔU. Meanwhile choosing for r_w to be large allows to penalize large values of ΔU and still to minimize also the error $(R_s - Y)^T (R_s - Y)$. As in most optimization problems based on a quadratic function, a proper choice of the weights values is the result of a trade-off. Once that the cost function J is defined trough the choice of

weights, the vector of optimal controls ΔU which minimizes J can be calculated using equation (4.28), starting form:

$$J = (R_s - Fx(k_i))^T(R_s - Fx(k_i)) - 2\Delta U^T\Phi^T(R_s - Fx(k_i)) + \Delta U^T(\Phi^T\Phi\bar{R})\Delta U \tag{4.30}$$

Expressing the first derivative of J as a function of ΔU:

$$\frac{\partial J}{\partial \Delta U} = -2\Phi^T(R_s - Fx(k_i)) + 2(\Phi^T\Phi + \bar{R})\Delta U \tag{4.31}$$

the necessary condition for the minimum of J is:

$$\frac{\partial J}{\partial \Delta U} = 0$$

from which the optimal value of ΔU can be calculated as:

$$\Delta U = (\Phi^T\Phi + \bar{R})^{-1}\Phi^T(R_s - Fx(k_i)) \tag{4.32}$$

if we assume that the quantity $(\Phi^T\Phi + \bar{R})^{-1}$ exists. Matrix $(\Phi^T\Phi + \bar{R})^{-1}$ is usually called *Hessian matrix*. It should be noticed that R_s is the vector containing the values of the set-point signal in the form:

$$R_s^T = \overbrace{\begin{bmatrix} 1 & 1 & \dots & 1 \end{bmatrix}}^{N_p} r(k_i) = \bar{R}_s r(k_i)$$

in which:

$$R_s^T = \overbrace{\begin{bmatrix} 1 & 1 & \dots & 1 \end{bmatrix}}^{N_p}$$

The solution of the optimal control problem is linked to the set-point signal $r(k_i))$ and to the state variable $x(k_i)$ trough the following:

$$\Delta U = (\Phi^T\Phi + \bar{R})^{-1}\Phi^T(\bar{R}_s r(k_i) - Fx(k_i)) \tag{4.33}$$

Closed-loop system

By analyzing the equations derived above, it can be noticed that at time k_i the optimal value of vector ΔU is calculated as:

$$\Delta U = (\Phi^T\Phi + \bar{R})^{-1}\Phi^T(\bar{R}_s r(k_i) - Fx(k_i))$$

in which the contributions $(\Phi^T\Phi + \bar{R})^{-1}\Phi^T\bar{R}_s$ e $(\Phi^T\Phi + \bar{R})^{-1}\Phi^T F$ depends simply on the parameters of the dynamic model. Therefore, for a time-invariant system, such values are constant matrices. Moreover, from the principle of receding horizon, only the first value of ΔU at time k_i is actually used in the closed-loop control. Therefore:

$$\begin{aligned}\Delta u(k_i) &= \overbrace{\begin{bmatrix} 1 & 0 & \dots & 1 \end{bmatrix}}^{N_c} \left(\Phi^T\Phi + \bar{R}\right)^{-1} \Phi^T(\bar{R}_s r(k_i) - Fx(k_i)) \\ &= K_y r(k_i) - K_{mpc}x(k_i)\end{aligned} \tag{4.34}$$

in which K_y is the first element of:

$$(\Phi^T\Phi + \bar{R})^{-1}\Phi^T\bar{R}_s$$

and K_{mpc} is the first row of:

$$(\Phi^T\Phi + \bar{R})^{-1}\Phi^T F$$

Equation (4.34) represents the state feedback of a linear time invariant model. The matrix of feedback gains is K_{mpc}. Therefore, using the augmented model:

$$x(k+1) = Ax(k) + B\Delta u(k)$$

the closed-loop system can be obtained by substituting equation (4.34) into the expression of the augmented system:

$$x(k+1) = Ax(k) - BK_{mpc}x(k) + BK_y r(k) \tag{4.35}$$

$$= (A - BK_{mpc})x(k) + BK_y r(k) \tag{4.36}$$

Therefore the eigenvalues of the closed-loop system can be evaluated from the closed-loop characteristic equation:

$$det\left[\lambda I - (A - BK_{mpc})\right] = 0$$

Because of the peculiar structure of matrices C and A, the last column of F is equal to $\bar{R}_s$, which equals $\begin{bmatrix} 1 & 1 & \dots & 1 \end{bmatrix}^T$, therefore K_y equals the last element of K_{mpc}. By noticing the state vector $x(k_i) = \begin{bmatrix} \Delta x_m(k)^T & y(k) \end{bmatrix}^T$, and using the definition of K_y, it can be written that $K_{mpc} = \begin{bmatrix} Kx & Ky \end{bmatrix}$,

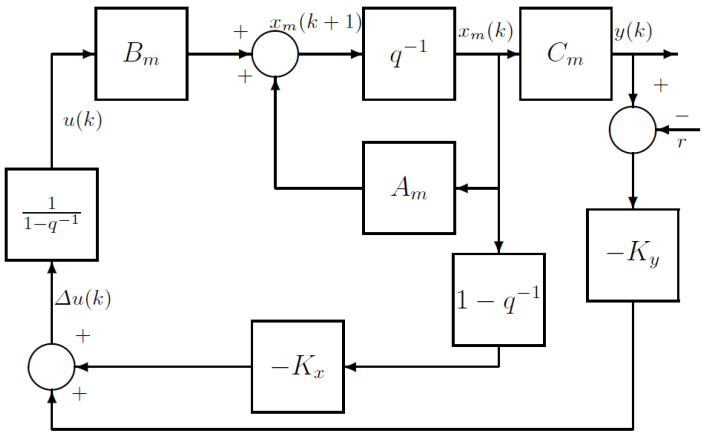

Figure 4.9: Block diagram of discrete-time model predictive control

where K_x is the vector of feedback gains connected to $\Delta x_m(k)$, while K_y equals to the feedback gain to be applied to the output $y(k)$.

In this way the block diagram in figure (4.9) is completely defined. The block q^{-1} represents the backward shift operator. Such diagram shows the structure of a discrete time MPC with integral action. The block $\frac{1}{1-q^{-1}}$ is the discrete time integrator.

4.3.2 Predictive control of MIMO system

In the previous pages the development of MPC control structure for SISO system ha been dealt with for the sake of simplicity. That formulation can be extended naturally also to systems with more than one input and/or output, trough a careful use of the state-space representation.

We assume that the plant has m inputs, q outputs and n_1 states. It is also assumed that the number of output is less or equal to the number if inputs, i.e. $q \leq m$. Otherwise the formulation that will be shown here will not allow to control independently every output with a zero steady-state error. In order to make the formulation more general, also the effects of noise are added to the plant:

$$x_m(k+1) = A_m x_m(k) + B_m u(k) + B_d \omega(k) \tag{4.37}$$

$$y(k) = C_m x_m(k) \tag{4.38}$$

in which $\omega(k)$ is the input disturbance, modeled as an integrated white noise. This implies that the input noise $\omega(k)$ is related to the white noise with zero average $\epsilon(k)$ as in the equation:

$$\omega(k) - \omega(k-1) = \epsilon(k) \tag{4.39}$$

It should be noticed that, form eq. (4.37), also the following relation holds:

$$x_m(k) = A_m x_m(k-1) + B_m u(k-1) + B_d \omega(k-1) \tag{4.40}$$

By defining $\Delta x_m(k) - x_m(k-1)$ and $\Delta u(k) - u(k-1)$, and than subtracting eq. (4.40) to eq. (4.37) we arrive at:

$$\Delta x_m(k+1) = A_m \Delta x_m(k-1) + B_m u(k-1) + B_d \omega(k-1) \tag{4.41}$$

In order to relate the output $y(k)$ to the state variable $\Delta x_m(k)$, we can deduce that:

$$\Delta y(k+1) = C_m \Delta x_m(k+1) = C_m A_m \Delta x_m(k) + C_m B_m \Delta u(k) + C_m B_d \epsilon(k)$$

in which $\Delta y(k+1) = y(k+1) - y(k)$. By choosing the new state variable $x(k) = \left[\Delta x_m(k)^T y(k)^T\right]^T$ one obtains:

$$\begin{bmatrix} \Delta x_m(k+1) \\ y(k+1) \end{bmatrix} = \begin{bmatrix} A_m & o_m^T \\ C_m A_m & I_{q\times q} \end{bmatrix} \begin{bmatrix} \Delta x_m(k) \\ y(k) \end{bmatrix} + \begin{bmatrix} B_m \\ C_m B_m \end{bmatrix} \Delta u(k) + \begin{bmatrix} B_d \\ C_m B_d \end{bmatrix} \epsilon(k)$$

$$y(k) = \begin{bmatrix} o_m & I_{q\times q} \end{bmatrix} \begin{bmatrix} \Delta x_m(k) \\ y(k) \end{bmatrix} \tag{4.42}$$

in which $I_{q\times q}$ is an identity matrix of size $q \times q$, being q the number of outputs. o_m is a matrix whose size is $q \times n_1$ with all null entries. In eq. (4.42), A_m, B_m e C_m have size $n_1 \times n_1$, $n_1 \times m$ and $q \times n_1$, respectively. In order to get a simpler notation, we indicate eq. (4.42) as:

$$\begin{aligned} x(k+1) &= Ax(k) + B\Delta u(k) + B_\epsilon \epsilon(k) \\ y(k) &= Cx(k) \end{aligned} \tag{4.43}$$

in which A, B e C are the same as in the incremental formulation presented in eq. (4.42). In the following, the dimension of the augmented state space will be indicated as $n = n_1 + q$. Now there are two more aspects that should be investigated: the eigenvalues of the augmented model, and the realization of the model in the state-space.

Eigenvalues if the augmented model

The characteristic equation of the augmented model is:

$$\rho(\lambda) = \det \begin{bmatrix} \lambda I - A_m & o_m^T \\ -C_m A_m & (\lambda I - 1) I_{q\times q} \end{bmatrix} = (\lambda - 1)^q \det(\lambda I - A_m) = 0 \quad (4.44)$$

in which has been used the property of block triangular matrices of having a determinant that equals the product of the determinants of the two matrices on the principal diagonal. Therefore, the eigenvalues of the augmented model are the eigenvalues of the original dynamic model plus q eigenvalues $\lambda = 1$. This implied that the model includes q integrators. This feature allows to include integral action to the MPC.

Solution of MPC for MIMO systems

The extension to MIMO problems is quite straightforward, the only things to pay more attention to are the size of the state, of the control and of the output vectors. Let's define the vector Y ΔU as:

$$\Delta U = \begin{bmatrix} \Delta u(k_i)^T & \Delta u(k_i+1)^T & \dots & \Delta u(k_i+N_c-1)^T \end{bmatrix}$$

$$Y = \begin{bmatrix} u(k_i+1|k_i)^T & y(k_i+2|k_i)^T & y(k_i+3|k_i)^T & \dots & y(k_i+N_p|k_i)^T \end{bmatrix}$$

Using model (A, B, C), the forecast on the evolution is calculated sequentially starting from the values that will be ideally assumed by the control vector:

$$\begin{aligned}
x(k_i+1|k_i) &= Ax(k_i) + B\Delta u(k_i) + B_d\epsilon(k_i) \\
x(k_i+2|k_i) &= Ax(k_i+1|k_i) + B\Delta u(k_i+1) + B_d(k_i+1|k_i) \\
&= A^2x(k_i) + AB\Delta u(k_i) + B\Delta u(k_i+1) \\
&\quad + AB_\epsilon\epsilon(k_i) + B_d\epsilon(k_i+1|k_i) \\
&\vdots \\
x(k_i+N_p|k_i) &= A^{N_p}x(k_i) + A^{N_p-1}B\Delta u(k_i) + A^{N_p-2}B\Delta u(k_i+1) \\
&\quad + A^{N_p-N_c}B\Delta u(k_i+N_c-1) + A^{N_p-1}B_d\epsilon(k_i)6 \\
&\quad + A^{N_p-2}B_d\epsilon(k_i+1|k_i) + \dots B_d\epsilon(k_i+N_p-1|k_i)
\end{aligned}$$

It is also assumed that $\epsilon(k)$ is a white signal with zero average, and that the predicted value of $\epsilon(k_i+i|k_i)$ is zero. The prediction of the state and of the output are calculated as the expected values of their respective values, therefore the effect of noise on the prediction is null. For sake of simplicity, the expected value symbol is omitted from there to the end of the section.

$$Y = Fx(k_i) + \Sigma\Delta U \tag{4.45}$$

with

$$F = \begin{bmatrix} CA \\ CA^2 \\ CA^3 \\ \vdots \\ CA^{N_p} \end{bmatrix}$$

$$\Phi = \begin{bmatrix} CB & 0 & 0 & \dots & 0 \\ CAB & CB & 0 & \dots & 0 \\ CA^2B & CAB & CB & \dots & 0 \\ \vdots & & & & \\ CA^{N_p-1}B & CA^{N_p-2}B & CA^{N_p-3}B & \dots & CA^{N_p-N_c}B \end{bmatrix}$$

The optimal control in its incremental form for the lenght of the optimization window can be calculated as:

$$\Delta U = (\Sigma^T\Sigma + \bar{R})^{-1}(\Sigma^T\bar{R}_s r(k_i) - \Sigma F x(k_i)) \tag{4.46}$$

in which matrix $\Sigma^T\Sigma$ has size $mN_c \times mN_c$, $\Sigma^T F$ has size $mN_c \times n$, while $\Sigma^T\bar{R}_s$ equals the last q columns of $\Sigma^T F$. The weight matrix $\bar{R}$ is a block matrix composed by m blocks, with the same size of $\Sigma^T\Sigma$. The set-pint signal is $r(k_i) = \begin{bmatrix} r_1(k_i) & r_2(k_i) & \dots & r_q(k_i) \end{bmatrix}^T$, i.e. it is made by the q set-point signals referred to the q outputs.

By using the receding horizon principle, the first m values of ΔU are used to express the optimal incremental control:

$$\begin{aligned} \Delta u(k_i) &= \overbrace{\begin{bmatrix} I_m & o_m & \dots & o_m \end{bmatrix}}^{N_c} \left(\Phi^T\Phi + \bar{R}\right)^{-1} \left(\Phi^T\bar{R}_s r(k_i) - \Phi^T F x(k_i)\right) \\ &= K_y r(k_i) - K_{mpc} x(k_i) \end{aligned} \tag{4.47}$$

in which I_m and o_m are, respectively, the identity and the null matrices of size $m \times m$.

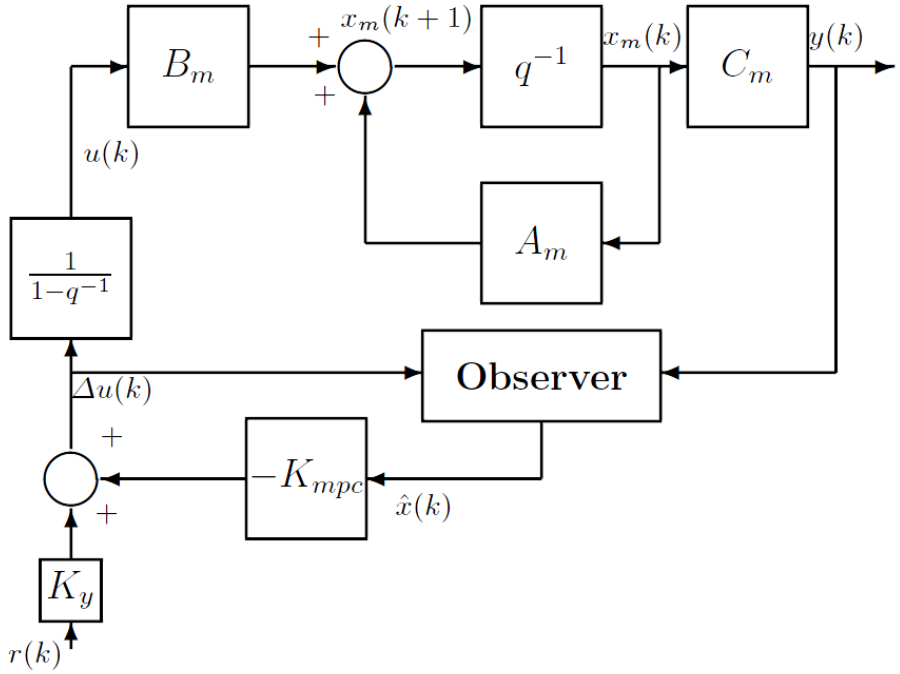

Figure 4.10: Unconstrained MPC with state observer: block diagram

4.4 MPC: Constrained formulation

In this section the MPC formulation proposed by Maciejowski [147] will be recalled. Comparing tho the formulation presented in the previous part of this chapter, some new concepts, such as the difference between reference and set-point signals will be introduced. Such design has been used for obtaining some of the results presented in chapter 6.

4.4.1 The receding horizon concept

Figure (4.11) represents the basic concepts of predictive control. As previously done, we refer now to a single-input single-output controlled plant. It is also assumed to work with a discrete time plant and controller, with time denoted by variable k. The output of the plant is $y(k)$, and the figure represents the past evolution (prior to time k) of the output. In the same figure also the set-point trajectory is shown, i.e. the trajectory that the output should follow. The value of the set-point at time t is represented by $s(t)$. The reference trajectory is

in general different from the set-point trajectory. The first is defined from the output $y(k)$ as the trajectory that the plant should follow to reach optimally the set-point. Therefore the choice of a proper reference trajectory plays an important role for the definition of the closed-loop response. Typically it is convenient that the reference trajectory approaches the set-point along an exponential trajectory. Therefore a 'time constant' for this exponential function can be defined. Therefore let T_{ref} indicate this parameter. If the tracking error at current time is:

$$\epsilon(k) = s(k) - y(k) \tag{4.48}$$

the reference trajectory can be defined so that the error i steps later is:

$$\epsilon(k+i) = e^{-iT_s/T_{ref}}\epsilon(k) \tag{4.49}$$

$$= \lambda^i \epsilon(k) \tag{4.50}$$

in which T_s is the sampling time and $A = e^{-T_s/T_{ref}}$. It should be noticed that$0 < \lambda < 1$. Therefore the reference trajectory can be defined as:

$$r(k+i|k) = s(k+i) - \epsilon(k+i) \tag{4.51}$$

$$= s(k+i) - e^{-iT_s/T_{ref}}\epsilon(k) \tag{4.52}$$

The notation $r(k+i|k)$ indicates that the reference trajectory depends on the conditions found at time k. It is possible to make other choices for the reference trajectory, as a matter of example, it can be imposed for the trajectory to be a straight line which meets the value of the set-point at a given time.

Let's again assume that the inner prediction model is linear also for this simulation. This brings many benefits in terms of theoretical treatment and in terms of computational efforts. It will be shown in chapter 6 that this choice allows to obtain very good results in all the test cases under consideration. It is also assumed that a measure of $y(k)$ is available when the choice of the value of $u(k)$ is made. This requires for the inner prediction model to be strictly proper, i.e. that $y(k)$ does depend on the past values of u: $u(k-1), u(k-2), \ldots$, but not on $u(k)$.

In the simplest case the input trajectory can be chosen so that the output is going to reach the set-point at the end of the prediction horizon, i.e. at time

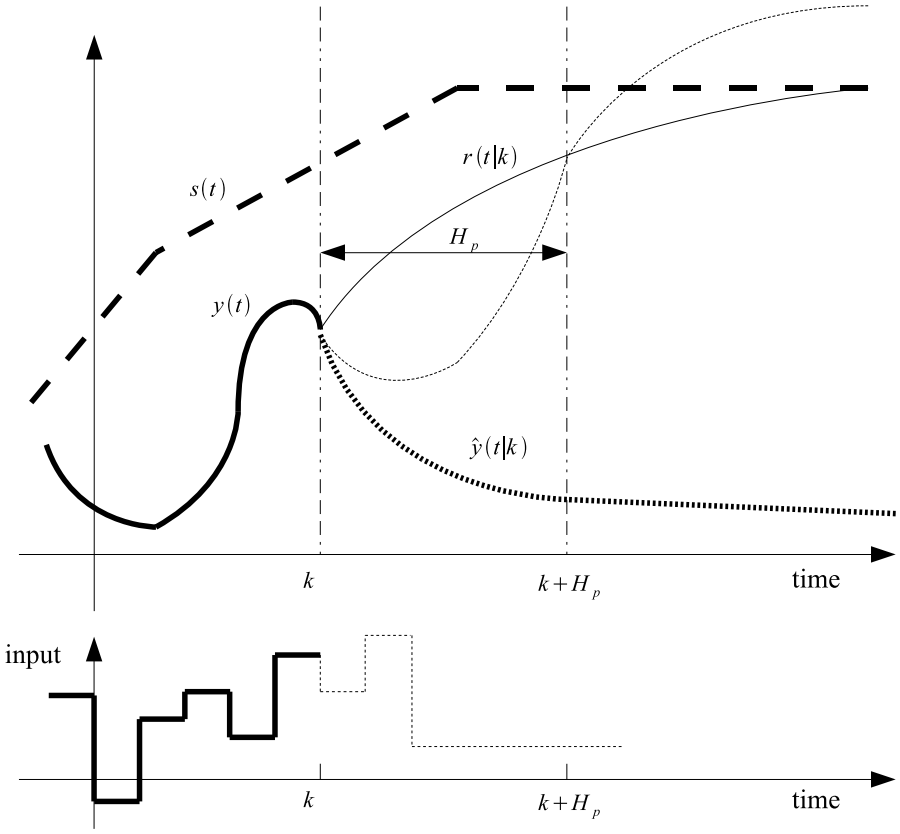

Figure 4.11: Predictive control: the basic idea

$k+H_p$ (being H_p and H_c the prediction and the control horizon, respectively). In this way, borrowing Richalet's notation [155], we implement a single coincident point at time $k + H_p$. There are certainly infinite trajectories of the input $u(k|k) \quad , u(k+1|k) \quad , \ldots \quad , u(k+H_p-1|k)$ that can satisfy this goal, we just need to chose one, such as the one with less effort, as an example.

Figure (4.11) for example shows that the input changes only for three steps, and after that it remains constant. In this situation, we need to evaluate only three values: $u(k|k)$, $u(k+1|k)$, $u(k+2|k)$. In the same way we could impose for the input variable to remain constant for all the prediction horizon:

$$u(k|k) = u(k+1|k) = \ldots = u(k+H_p-1|k)$$

Under this circumstance, it is needed to evaluate only a scalar value, which is $u(k|k)$; since we have to satisfy only the condition $y(k + H_p|k) = r(k + Hp|k)$, the solution to the problem is unique. Anyway, for any length of the the control trajectory under evaluation, only its first value if supplied to the plant. Therefore, let us impose $u(k) = u(k|k)$. At the following sampling time, the whole procedure composed by the measure of the output, the prediction, the evaluation of the input trajectory is repeated. After that, a new measure of $y(k + 1)$ is available, therefore we define a new trajectory for the reference $r(k+i|k+1)$ with $(i = 2, 3, \ldots)$; we operate a forecast on the horizon $k+i+1$, with $i = 1, 2, 3, \ldots, H_p$, therefore a new $u(k + 1 + i|k + 1)$, with $i = 0, 1, ..., Hp - l$ can be evaluated. At last, the new input is fed to the plant: $u(k + 1) = u(k+1|k+1)$. Since the length of the horizon remains constant, but the horizon 'slides' forward, such strategy is referred as *receding horizon*.

Evaluation of optimal control

In the simplest case of a single coincidence point and of a single parameter to choose in order to define the future evolution of the input, an unique solution to the control problem exists. More generally, more than one coincidence point could exist along the prediction horizon, and it might even happen that all the points $k+1, k+2, \ldots, k+H_p$ are coincidence points. Anyway, it is often found that greater the number of coincidence points is, the greater the number of unknown parameters, making the exact evaluation of the solution impossible. In this case it is necessary to perform an approximation. The most common choice is to look for a minimum square solution, i.e. a solution which minimizes the sum of the square of errors:

$$\sum_{i \in P} [r(k+1|k) - \hat{y}(k+1|k)]^2$$

in which P indicates the set of indexes i corresponding to the requested coincidence points.

Should the simplest problem considered here, i.e. a the case with a single coincidence point located at $k + H_p$ and with only $u(k|k)$ to be determined. Conceptually, the following procedure can be used. The embedded model can be used for predicting the free response $\hat{y}_f(k + H_p|k)$, which is the value of the plant output at the coincidence point in the situation that the input remains always at the value $u(k-1)$.

Should $S(H_p)$ represent the response of the plant to a step signal after H_p steps after the application of such stimulus, the predicted output at time $k+H_p$ is:

$$\hat{y}(k + H_p|k) = \hat{y}_f(k + H_p|k) + S(H_p)\Delta\hat{u}(k|k) \tag{4.53}$$

in which:

$$\Delta\hat{u}(k|k) = \hat{u}(k|k) - u(k-1) \tag{4.54}$$

shows the variation from the actual input $u(k-1)$ to the predicted input $\hat{u}(k|k)$. The target is to obtain:

$$\hat{y}(k + H_p|k) = r(k + H_p|k) \tag{4.55}$$

therefore the optimal variation of the input signal is:

$$\Delta\hat{u}(k|k) = \frac{r(k + H_p|k) - \hat{y}_f(k + H_p|k)}{S(H_p)} \tag{4.56}$$

Prediction

A way to calculate the prediction of the future control variable $z(k+1|i)$ from the estimation of the actual state plant $x(k|k)$ must be found to solve the control problem. For ease of calculation, we base the formulation on the last input $u(k-1)$ and on the estimation of its possible future variations $\Delta\hat{u}(k+i|k)$. This is conceptually the same approach which uses an incremental form for the prediction model, as for the formulation by Wang [152] already presented in the previous section of this chapter.

Let's consider the simplest case in which the whole state vector is measured, i.e. $x(k|k) = x(k) = y(k)$ (therefore $C_y = I$), and in the absence of measurement noise. The prediction of the plant future evolution is obtained by iterating the plant model:

$$\hat{x}(k+1|k) = Ax(k) + B\hat{u}(k|k) \tag{4.57}$$

$$\hat{x}(k+2|k) = Ax(k+1|k) + B\hat{u}(k+1|k) \tag{4.58}$$

$$= A^2x(k) + AB\hat{u}(k|k) + B\hat{u}(k+1|k) \tag{4.59}$$

$$\vdots$$

$$\hat{x}(k+H_p|k) = A\hat{x}(k+H_p-1|k) + B\hat{u}(k+H_p-1|k) \tag{4.60}$$

$$= A^{H_p}x(k) + A^{H_p-1}B\hat{u}(k|k) + \ldots + B\hat{u}(k+H_p-1|k) \tag{4.61}$$

The input will change only at the time steps $k, k+1, \ldots, k+H_u-1$, and it will remain constant afterwards. Therefore:

$$\hat{u}(k+i|k) = \hat{u}(k+H_u-1) \quad per \quad H_u \leq i \leq H_p - 1$$

Our aim is to express the prediction in terms of $\Delta\hat{u}(k+i|k)$. We remember that $\Delta\hat{u}(k+k|k) = \hat{u}(k+i|k) - \hat{u}(k+i-1|k)$ and that at time k, $u(k-1)$ is known. Therefore:

$$\begin{gathered}
\hat{u}(k|k) = \Delta\hat{u}(k|k) + u(k-1) \\
\hat{u}(k+1|k) = \Delta\hat{u}(k+1|k) + \Delta\hat{u}(k|k) + u(k-1) \\
\vdots \\
\hat{u}(k+H_u-1|k) = \Delta\hat{u}(k+H_u-1|k) + \ldots + \Delta\hat{u}(k|k) + u(k-1)
\end{gathered}$$

and

$$\begin{gathered}
\hat{x}(k+1|k) = Ax(k) + B\left[\Delta\hat{u}(k|k) + u(k-1)\right] \\
\hat{x}(k+2|k) = A^2x(k) + AB\left[\Delta\hat{u}(k|k) + u(k-1)\right] \\
+B\underbrace{\left[\Delta\hat{u}(k+1|k) + \Delta\hat{u}(k|k) + u(k-1)\right]}_{\hat{u}(k+1|k)}
\end{gathered}$$

$$= A^2x(k) + (A+I)B\Delta\hat{u}(k|k) + B\Delta u(k+1|k) + (A+I)Bu(k-1)$$
$$\vdots$$
$$\hat{x}(k+H_u|k) = A^{H_u}x(k) + (A^{H_u-1} + \ldots + A + I)B\Delta\hat{u}(k|k)$$
$$\cdots = +B\Delta\hat{u}(k+H_u-1|k) + (A^{H_u-1} + \ldots + A + I)Bu(k-1)$$

Notice the change here:

$$\hat{x}(k+H_u+1|k) = A^{H_u+1}x(k) + (A^{H_u} + \ldots + A + I)B\Delta\hat{u}(k|k)$$
$$\ldots + (A+I)B\Delta\hat{u}(k+H_u-1|k)$$
$$\cdots$$
$$\hat{x}(k+H_p|k) = A^{H_p}x(k) + (A^{H_p-1} + \ldots + A + I)B\Delta y(k|k)$$
$$\ldots + (A^{H_p-H_u} + \ldots + A + I)B\Delta u(k+H_u-1|k)$$
$$+(A^{H_p-1} + \ldots + A + I)Bu(k-1)$$

Rewriting all in matrix form:

$$\begin{bmatrix} \hat{x}(k+1|k) \\ \vdots \\ \hat{x}(k+H_u|k) \\ \hat{x}(k+H_u+1|k) \\ \vdots \\ \hat{x}(k+H_p|k) \end{bmatrix} = \underbrace{\begin{bmatrix} A \\ \vdots \\ A^{H_u} \\ A^{H_u+1} \\ \vdots \\ A^{H_p} \end{bmatrix} x(k) + \begin{bmatrix} B \\ \vdots \\ \sum_{i=0}^{H_u-1} A^iB \\ \sum_{i=0}^{H_u} A^iB \\ \vdots \\ \sum_{i=0}^{H_p-1} A^iB \end{bmatrix} u(k-1) +}_{past}$$
$$\underbrace{\begin{bmatrix} B & \cdots & 0 \\ AB+B & \cdots & 0 \\ \vdots & \ddots & \vdots \\ \sum_{i=0}^{H_u-1} A^iB & \cdots & B \\ \sum_{i=0}^{H_u} A^iB & \cdots & AB+B \\ \vdots & \vdots & \vdots \\ \sum_{i=0}^{H_p-1} A^iB & \cdots & \sum_{i=0}^{H_p-H_u} A^iB \end{bmatrix} \begin{bmatrix} \Delta\hat{u}(k|k) \\ \vdots \\ \Delta\hat{u}(k+H_u-1|k) \end{bmatrix}}_{future} \tag{4.62}$$

The controlled variable prediction can be evaluated trough:

$$\hat{z}(k+1|k) = C_z\hat{x}(k+1|k) \tag{4.63}$$

$$\hat{z}(k+2|k) = C_z\hat{x}(k+2|k) \tag{4.64}$$

$$\dots$$

$$\hat{z}(k+H_p|k) = C_x\hat{x}(k+H_p|k) \tag{4.65}$$

or

$$\begin{bmatrix} \hat{z}(k+1|k) \\ \vdots \\ \hat{z}(k+H_p|k) \end{bmatrix} = \begin{bmatrix} C_z & 0 & \cdots & 0 \\ 0 & C_z & \cdots & 0 \\ \vdots & \vdots & \ddots & \vdots \\ 0 & 0 & \cdots & C_z \end{bmatrix} \begin{bmatrix} x(k+1|k) \\ \vdots \\ x(k+H_p|k) \end{bmatrix} \tag{4.66}$$

A little note on equation (4.62) must be made. Such equation includes the evaluation of A^i, with sometimes large values of i. This can lead to serious numerical problem, especially in the case of an unstable plant, in which case some entries of matrix A^i are very large in comparison with some others. This effect worsen with the increase of i. The most convenient strategy is to operate one iteration at time.

4.4.2 MPC control law

The formulation of an MPC control law must of course be originated from a cost function to be minimized by the same control. Among the large number of choices available, here the following function is taken into consideration:

$$V(k) = \sum_{i=H_w}^{H_p} \|\hat{z}(k+i|k) - r(k+1)\|^2_{Q(i)} + \sum_{i=0}^{H_u-1} \|\Delta u(k+i|k)\|^2_{R(i)} \tag{4.67}$$

Which can be rewritten as:

$$V(k) = \|\mathcal{Z} - \mathcal{T}(k)\|^2_{\mathcal{Q}} + \|\Delta\mathcal{U}(k)\|^2_{\mathcal{R}} \tag{4.68}$$

with

$$\mathcal{Z}(k) = \begin{bmatrix} \hat{z}(k+H_w|k) \\ \vdots \\ \hat{z}(k+H_p|k) \end{bmatrix} \qquad \mathcal{T}(k) = \begin{bmatrix} \hat{r}(k+H_w|k) \\ \vdots \\ \hat{r}(k+H_p|k) \end{bmatrix}$$
$$\Delta\mathcal{U}(k) = \begin{bmatrix} \Delta\hat{u}(k|k) \\ \vdots \\ \Delta\hat{u}(k+H_u-1|k) \end{bmatrix} \tag{4.69}$$

The weigh matrices $\mathcal{Q}$ and $\mathcal{R}$ are composed by:

$$\mathcal{Q} = \begin{bmatrix} \mathcal{Q}(H_w) & 0 & \cdots & 0 \\ 0 & \mathcal{Q}(H_w+1) & \cdots & 0 \\ \vdots & \vdots & \ddots & \vdots \\ 0 & 0 & \cdots & \mathcal{Q}(H_p) \end{bmatrix} \tag{4.70}$$

$$\mathcal{R} = \begin{bmatrix} \mathcal{R}(0) & 0 & \cdots & 0 \\ 0 & \mathcal{R}(1) & \cdots & 0 \\ \vdots & \vdots & \ddots & \vdots \\ 0 & 0 & \cdots & \mathcal{R}(H_p) \end{bmatrix} \tag{4.71}$$

Recalling that $\mathcal{Z}$ has the form:

$$\mathcal{Z}(k) = \Psi x(k) + \Upsilon u(k-1) + \Theta\Delta\mathcal{U}(k) \tag{4.72}$$

with appropriate matrices Ψ, Υ and Θ. Let's define:

$$\mathcal{E}(k) = \mathcal{T}(k) - \Psi x(k) - \Upsilon u(k-1) \tag{4.73}$$

This vector can be thought as measure of the 'tracking error', since it expresses the difference between the desired trajectory and the 'free response' of the system, i.e. the the response of the system in absence of future changes of the input. This happens when $\Delta\mathcal{U}(k) = 0$. If $\mathcal{E}(k)$ was effectively equal to zero, it might be chosen that $\Delta\mathcal{U}(k) = 0$.

It can be stated that:

$$V(k) = \|\Theta\Delta\mathcal{U}(k) - \mathcal{E}(k)\|^2_{\mathcal{Q}} + \|\Delta U(k)\|^2_{\mathcal{R}} \tag{4.74}$$

$$= \left[\Delta\mathcal{U}(k)^T\Theta^T - \mathcal{E}(k)^T\right]\mathcal{Q}\left[\Theta\Delta\mathcal{U}(k) - \mathcal{E}(k)\right] + \Delta\mathcal{U}(k)^T\mathcal{R}\Delta\mathcal{U}(k) \tag{4.75}$$

$$= \mathcal{E}(k)^T \mathcal{Q}\mathcal{E}(k) - 2\Delta\mathcal{U}(k)^T \Theta^T \mathcal{Q}\mathcal{E}(k) + \Delta\mathcal{U}(k)^T \left[\Omega^T \mathcal{Q}\Theta + \mathcal{R}\right] \Delta\mathcal{U}(k) \quad (4.76)$$

If $V(k)$ has the form:

$$V(k) = const - \Delta\mathcal{U}(k)^T \mathcal{G} + \Delta\mathcal{U}(k)^T \mathcal{H}\Delta\mathcal{U}(k) \quad (4.77)$$

with

$$\mathcal{G} = 2\Theta\mathcal{Q}\mathcal{E}(k) \quad (4.78)$$

and

$$\mathcal{H} = \Theta^T \mathcal{Q}\Theta + \mathcal{R} \quad (4.79)$$

and both $\mathcal{G}$ and $\mathcal{H}$ are not a function of $\Delta\mathcal{U}(k)$, the optimal value of $\Delta\mathcal{U}(k)$ can be calculated by the null condition on the gradient of $V(k)$. From eq. (4.77) it is found that:

$$\Delta_{\Delta\mathcal{U}(k)} V = -\mathcal{G} + 2\mathcal{H}\Delta\mathcal{U}(k) \quad (4.80)$$

therefore the set of optimal future control changes is:

$$\Delta\mathcal{U}(k)_{opt} = \frac{1}{2}\mathcal{H}^{-1}\mathcal{G} \quad (4.81)$$

It should be noticed that in practical situations only the first value of this vector is actually fed to the plant, according to the receding horizon principle. Therefore, if the plant has l inputs, we use only the first l rows of the vector $\Delta\mathcal{U}(k)_{opt}$. Such vector can be represented as:

$$\Delta u(k)_{opt} = \left[\begin{array}{cc} I_l, & \underbrace{0_l, \ldots, 0_l}_{(H_u-1)times} \end{array}\right] \Delta\mathcal{U}(k)_{opt} \quad (4.82)$$

in which I_l is the identity matrix of size $l \times l$ and 0_l is a zero matrix with size $l \times l$. It must be highlighted also that here $\Delta u(k)_{opt}$ can be used here instead of $\hat{u}(k|k)_{opt}$, since we have found a solution which is applied at time k. It might happen that the solution just found corresponds to a stationary point which is not the minimum. By taking the derivative of the gradient of $\Delta_{\Delta\mathcal{U}(k)V}$ (4.80) with respect to a $\Delta\mathcal{U}(k)$ the Hessian of V is obtained:

$$\frac{\partial^2 V}{\partial\Delta\mathcal{U}(k)^2} = 2\mathcal{H}(\Theta^T \mathcal{Q}\Theta + \mathcal{R}) \quad (4.83)$$

It has been chosen that $Q(i) \geq 0$ for every i, and this imples that $\Theta^T \mathcal{Q} \Theta \geq 0$. Therefore if $\mathcal{R} > 0$, the Hessian is positive definite, which guarantees that the solution found before is the minimum of V. This applies when $\mathcal{R}(i) > 0$ per ogni i.

If it is chosen that $\mathcal{R} = 0$ for some (or all) the i, it happens that $\mathcal{R} \geq 0$, but not that $\mathcal{R} > 0$. If $\mathcal{R} = 0$, it is necessary that $\Theta Q^T \mathcal{Q} \Theta > 0$ for the existence of a minimum and for the existence of $\mathcal{H}^{-1}$.

In the other cases, i.e. when $\mathcal{R} \geq 0$, it must be checked that $\Theta^T \mathcal{Q} \Theta + \mathcal{R} > 0$.

4.4.3 Formulation as minimum square

The optimal solution, as found in eq. (4.81), should not be evaluated by taking the inverse of $\mathcal{H}$. Matrix Θ and $\mathcal{H}$ are rarely well conditioned. Therefore particular numerical procedures should be used. The easiest way is to define a minimum square problem. Since $\mathcal{Q} \geq 0$ and $\mathcal{R} \geq 0$, we can use matrices $S_{\mathcal{Q}}$ e $S_{\mathcal{R}}$ which are the respective 'square roots':

$$S_{\mathcal{Q}}^T S_{\mathcal{Q}} = \mathcal{Q} \qquad S_{\mathcal{R}}^T S_{\mathcal{R}} = \mathcal{R}$$

Without going into details, $\Delta\mathcal{U}(k)_{opt}$ is the minimum square solution of equation:

$$\left[\begin{array}{c} S_{\mathcal{Q}}\ \Theta\Delta\mathcal{U}(k) - \mathcal{E}(k) \\ s_{\mathcal{R}}\Delta\mathcal{U}(k) \end{array} \right] = 0 \tag{4.84}$$

or, equivalently of:

$$\left[\begin{array}{c} S_{\mathcal{Q}}\Theta \\ s_{\mathcal{R}} \end{array} \right] = \mathcal{U}(k) = \left[\begin{array}{c} S_{\mathcal{Q}}\mathcal{E}(k) \\ 0 \end{array} \right] \tag{4.85}$$

Equations in the form $A\theta = b$ can be solved efficiently using the QR algorithm. If using Matlab, the syntax is: $\theta_{opt} = A\backslash b$.

Remembering that:

$$\Delta u(k)_{opt} = [I_l, 0_l, \ldots, 0_l]\, \mathcal{H}^{-1}\Theta^T\mathcal{Q}\mathcal{E}(k) \tag{4.86}$$

and:

$$\mathcal{E}(k) = \mathcal{T}(k) - \Psi x(k) - \Upsilon u(k-1) \tag{4.87}$$

The only part of the solution which changes at every time step is the tracking error $\mathcal{E}(k)$. Therefore an unconstrained predictive control system can be represented as in figure (4.12). The block labeled as K_{MPC} is defined by:

$$K_{MPC} = [I_l, 0_l, \ldots, 0_l]\, \mathcal{H}^{-1}\Theta^T\mathcal{Q} \tag{4.88}$$

We point out that the 'correct' way of computing KMPC is (again using MATLAB notation, including the ':' operator to pick out the first l rows of the solution):

$$K_{full} = \left[\begin{array}{c} S_{\mathcal{Q}}\Theta \\ S_{\mathcal{R}} \end{array} \right] \backslash \left[\begin{array}{c} S_{\mathcal{Q}} \\ 0 \end{array} \right] \tag{4.89}$$

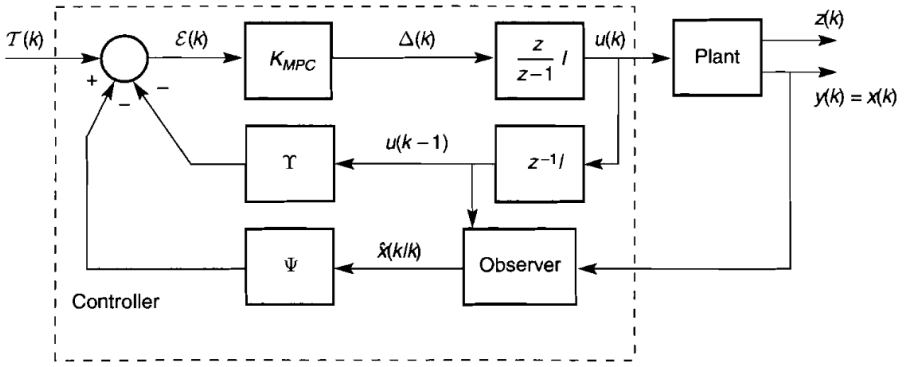

Figure 4.12: Structure of unconstrained control

$$K_{MPC} = K_{full}(1 : l, :) \tag{4.90}$$

It is clear from the figure that the controller is a linear time-invariant system in this case. So it is possible to compute its frequency response, stability margins etc. Note that the controller is, in general, dynamic. It is not just 'state feedback', except under very special circumstances (refer to previous section). The matrix K_s that can be computed computed by the Model Predictive Control Toolbox function smpccon is related to K_{MPC} as follows:

$$K_s = K_{MPC} \begin{bmatrix} \begin{bmatrix} I \\ I \\ \vdots \\ I \end{bmatrix}, -\Psi, -\Upsilon \end{bmatrix} \tag{4.91}$$

so that:

$$\Delta u(k)_{opt} = K_s \begin{bmatrix} \mathcal{T}(k) \\ x(k) \\ u(k-1) \end{bmatrix} \tag{4.92}$$

Constrained Formulation

Here we deal with the case when constraints are present. Inequality constraints are imposed on the control vector $u(k)$, on its change rate $\Delta u(k)$ and on plant controlled outputs $z(k)$ as:

$$\begin{array}{c} \Delta u_{min} \leq \Delta u(k) \leq \Delta u_{max} \\ u_{min} \leq u(k) \leq u_{max} \\ z_{min} \leq z(k) \leq z_{max} \end{array} \qquad k \in [1, 2, \ldots, H_p]\,; \tag{4.93}$$

or, taking the whole horizon as 3 vectors:

$$\begin{array}{c} \Delta\mathcal{U}_{min} \leq \Delta\mathcal{U} \leq \Delta\mathcal{U}_{max} \\ \mathcal{U}_{min} \leq \mathcal{U} \leq \mathcal{U}_{max} \\ \mathcal{Z}_{\min} \leq \mathcal{Z}(k) \leq \mathcal{Z}_{max} \end{array} \tag{4.94}$$

The constraints of Equation (4.94) can always be written as:

$$E \left[\begin{array}{c} \Delta\mathcal{U}(k) \\ 1 \end{array} \right] \leq 0 \tag{4.95}$$

$$F \left[\begin{array}{c} \mathcal{U}(k) \\ 1 \end{array} \right] \leq 0 \tag{4.96}$$

$$G \left[\begin{array}{c} \mathcal{Z}(k) \\ 1 \end{array} \right] \leq 0 \tag{4.97}$$

Now all the constraints must be expressed as function of $\Delta\mathcal{U}$. Suppose that F has the form:

$$F = [F_1, F_2, \ldots, F_{H_u}, f]$$

where each F_i is of size $q \times m$ and f has size $q \times 1$, so that (4.96) can be written as:

$$\sum_{i=1}^{H_u} F_i \hat{u}(k+i-1|k) + f \leq 0$$

Since

$$\hat{u}(k+i-1|k) = u(k-1) + \sum_{j=0}^{i-1} \Delta\hat{u}(k+j|k)$$

we can write (4.96) as

$$\begin{array}{l} \sum_{j=1}^{H_u} F_j \Delta\hat{u}(k|k) + \sum_{j=2}^{H_u} F_j \Delta\hat{u}(k|k) + \ldots + F_{H_u} \Delta\hat{u}(k+H_u-1|k) \\ + \sum_{j=1}^{H_u} F_j u(k-1|k) + f \leq 0 \end{array}$$

Now define $F_i = \sum_{j=1}^{H_u} F_j$ and $F = [F_1, \ldots, F_{H_u}]$. Then (4.96) can be written as:

$$F\Delta\mathcal{U} \leq -F_1 u(k-1) - f \tag{4.98}$$

where the right-hand side vector is known at time k. In this way equation (4.96) has been converted on a linear inequality constraint on $\Delta\mathcal{U}(k)$.

A similar thing must be done also for eq. (4.97). Using eq. (4.72), (4.97) can be rewritten as:

$$G\begin{bmatrix} \Psi x(k) + \Upsilon u(k-1) + \Theta\Delta\mathcal{U}(k) \\ 1 \end{bmatrix} \leq 0$$

Now letting $G = [\Gamma, g]$ where g is the last column of G, this is the same as:

$$\Gamma\left[\Psi x(k) + \Upsilon u(k-1)\right] + \Gamma\Theta\Delta\mathcal{U}(k) + g \leq 0$$

or

$$\Gamma\left[\Psi x(k) + \Upsilon u(k-1)\right] \leq -\Gamma\Theta\Delta\mathcal{U}(k) - g \tag{4.99}$$

The last step is to put eq. (4.95) in the form:

$$W\Delta\mathcal{U}(k) \leq w \tag{4.100}$$

Assembling inequalities (4.98),(4.99) and (4.100) yields to:

$$\begin{bmatrix} F \\ \Gamma\Theta \\ W \end{bmatrix} \Delta U(k) \leq \begin{bmatrix} -F_i u(k-1) - f \\ -\Gamma\left[\Psi x(k) + \Upsilon u(k-1) - g\right] \\ w \end{bmatrix} \tag{4.101}$$

The cost function to be minimized is the same stated before, i.e. $V(k)$. Therefore the optimization problem to solve can be formulated as:

$$minimize \qquad \Delta\mathcal{U}(k)^T(H)\Delta\mathcal{U}(k) - \mathcal{G}^T\Delta\mathcal{U}(k) \tag{4.102}$$

subject to the inequality (4.101). Noticing that the problem has the form

$$\min_\theta \frac{1}{2}\theta^T\Psi\theta + \phi^T\theta \tag{4.103}$$

subject to:

$$\Omega\theta \leq \omega \tag{4.104}$$

which is a standard optimization problem, known as quadratic programming (QP in short) and many standard algorithms are available for solving it

efficiently. Moreover, since $\mathcal{H} \geq 0$, the problem is also convex, meaning that the cost function has only has one minimum. Therefore there is no chance that a local minimum is mistaken as a global minimum. The choice and the development of the solution procedure are not dealt with in this work, since it would go beyond the purposes of this thesis. The simulation presented in the last chapter have been implemented with the aid of Matlab's Model Predictive Control Toolbox, which represents a very valuable tool for the control system designer.

5 Development of a Hardware-in-the-Loop testbed for FLMs

5.1 Introduction

This chapter deals with the development and the experimental validation of a Hardware-In-the-Loop (HIL) simulator of flexible-link mechanisms. The core of the simulator is a highly accurate FEM nonlinear dynamic model of planar mechanisms. The accuracy of the proposed simulator is proved by comparing the response of the virtual model with the response of the real mechanism by using the same real controller. Results are provided by the use of classical controllers real-time capability of the dynamic model is guaranteed by a symbolic manipulation of the equations that describe the mechanism, in order to avoid the numerical inversion of the large mass matrix of the system.

5.1.1 Hardware-In-the-Loop systems

Real-Time systems can be used efficiently for the development and the fast prototyping phased during the development of a control system. Let's consider a basic example of this approach, the development of a car engine control unit (CU). The traditional approach for this kind of product is:

1. Software implementation of the engine's dynamic model
2. Software implementation of the control system
3. Software simulation of the closed-loop system (engine+CU)

4. Hardware implementation of the control system

5. Experimental tests using the CU prototype and the engine

For the first two steps a simulation suite can be used (such as Matlab Simulink), or low-level languages can be used (like C or Fortran) to develop the simulators for both the plant and the control unit. During this phase, an unlimited number of tests can be run, experimenting different control systems and different implementation of the engine simulators. This phase usually leads to the choice and definition of a proper control system. Just after that, a physical prototype of the CU must be developed, in order to verify its correct functionality. The last phase can easily lead to big problems, since it is necessary to effectively control the real car engine. This kind of experimental tests are usually expensive both in terms of time and money. At the same time, some particular testing conditions are hard to replicate, such as extreme environmental conditions or operation in case of faulty device. Moreover, the experimental testbed is in many case prone to mechanical failure, especially if improper control actions are taken. A possible solution to all this problems is the use of Hardware-In-the-Loop (HIL) systems. The Hardware-In-the-Loop approach consists of the use of a simulated real-time model of the plant, whose accuracy and complete I/O replication of the real plant allows to substitution of the plant with the simulator. In this way, a seamless transition from pure simulation to full hardware tests can be implemented. In particular, a HIL simulator is a valuable tool for the tuning of closed-loop control strategies for this class of mechanisms, since it allows to reduce the safety risks and the time needed to fine tune the real-time controllers. The experimental tests of control strategies for vibration reduction in flexible-link mechanisms (FLMs) give rise to some technical problems. FLMs are quite prone to mechanical failure, which occurs, for example, if strong torques warp the links as a consequence of an unsuitable control strategy. This also represents a potential safety risk for the operator. Replacing a broken link is a time-consuming task, since it is needed to attach a new strain gauge bridge to the beam, and to calibrate the strain gauge amplifier. Moreover the small differences often encountered between two links can reduce the reproducibility of the experiments.

One way to solve the problem can be found in Hardware-In-the-Loop (HIL) simulation. This technology allows the complete and right interaction of a real device (the controller) with a simulated one (the FLM).

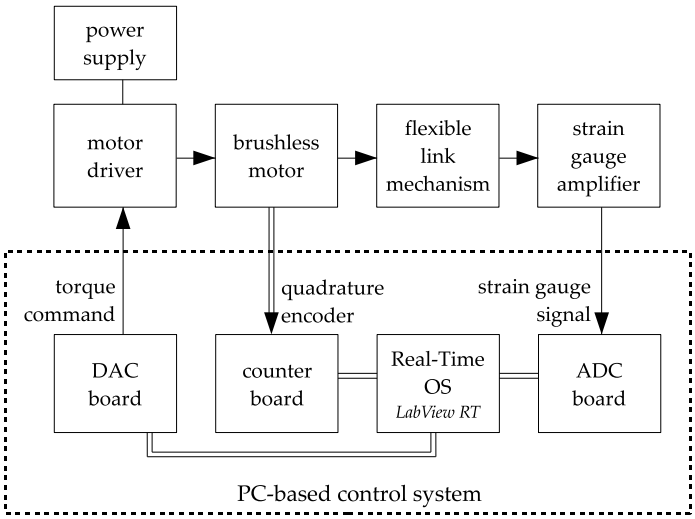

Figure 5.1: Experimental tests: traditional approach
8

In this case, the software that implements the dynamics of a flexible-link mechanism can be executed on a PC-based device and, through an I/O interface, the interaction with the real control system can be established. By using this method, many tests to get a suitable tuning of the control device can be done without involving the real mechanism, thus reducing the risk of mechanical failure as a result of an improper setup. A HIL simulator is a valuable tool to give an evaluation of the performance of the control unit under investigation, in particular it can be used to test its real-time capability. Many modern control techniques, such the very popular Model Predictive Control, are very demanding in term of computational power, so their Real-Time implementation can be very critical when high bandwidth and high complexity processes are involved. The proposed device can be used also to perform an in-depth analysis of the robustness of the control system under test. In many application, especially when model-based control is concerned, it is necessary to evaluate how the control unit would behave in the presence of mismatches between the modeled and the real plant. These test can be easily implemented with the aid of a Hardware-In-the-Loop simulator of the plant, simply by adding some parametric mismatches, nonlinearities, noise, etc. to the simulation model. Among the advantages of the use of HIL simulators, lower implementation costs must be mentioned. Generally, and also in the considered case, the cost of the hardware

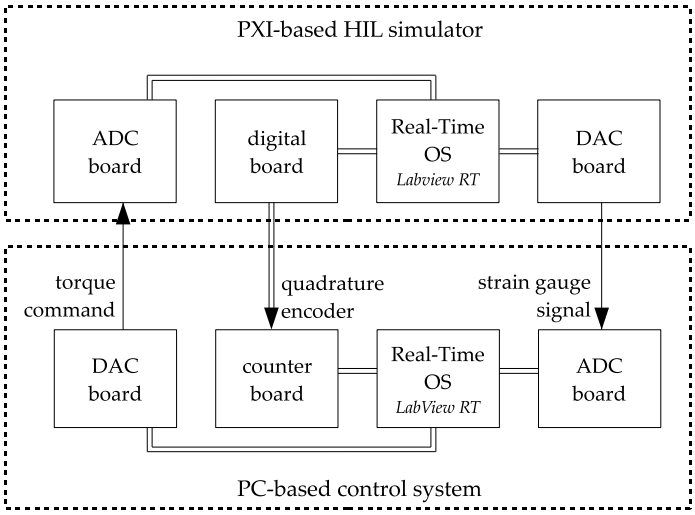

Figure 5.2: Experimental tests: Hardware-In-the-Loop approach

needed to set-up a simulator like the proposed one is one fraction of the cost of building a real prototype. Moreover, it should be noticed that a careful design of an HIL test-bench allows to perform a seamless transition from the HIL to the traditional experimental setup, in the case that the HIL simulator has the very same physical connection to the control unit.

Other advantages of the HIL approach are:

- reproducibility of experiments
- the ability to perform tests which would otherwise be impossible, impractical and unsafe
- a shorter time required for experimental testing
- testing the effects of component faults
- long-term durability testing

Hardware-In-the-Loop technology is experiencing a wide diffusion in many industrial fields, in the wake of its early but successful introduction in the aerospace [156] and automotive [157] research areas. More recently many papers have been written on the subject of HIL simulator for mechatronic systems, such as [158, 159] on the use of HIL in machine tool design, [160] on the design

of mobile robots and [161, 162, 163] on the analysis and synthesis of robotic systems. However, to the authors' best knowledge, there are no papers available in literature on the development or the use of Hardware-In-the-Loop simulators for mechanisms with link flexibility.

One requirement of the dynamic model used for the HIL simulation is the Real-Time capability, since it is necessary to make it interact with real-world signals, as the input and outputs of the control system are used in the feedback loop. This is a challenging problem, since the FLM dynamic model is both nonlinear and high order. It involves large and badly conditioned matrices whose computation requires a large amount of resources [126]. Moreover, the structure of the model and its parameters make the dynamic equation ill-conditioned.

The proposed simulation can also be used for Real-Time SIL (Software-In-the-Loop) simulations [164, 165]. This strategy involves the interaction of two software devices, that in this case would simulate the mechanism and the control unit, respectively. This approach, while certainly valid, is less useful for our purposes than the HIL approach, since our target is to provide a full validation of the hardware implementation of the control system. In fact, unlike the SIL, the HIL technology allows to test the control unit as a whole system, composed by its hardware components (processor, memory ,I/O devices) and its firmware.

Next section provides a brief explanation of the FLM dynamic model, while the main characteristics of the test bench are exposed in detail. In Section 3, some details of the Real-Time implementation will be introduced. In the fourth section, the experimental results are presented. Here the validity of this approach is investigated by comparing the response of the HIL simulator with the response of the FLM to the same real controller. Two classical control strategy are tested: a usual PI controller and an Optimal LQY regulator.

Here two well-known control strategies are applied to the simplest flexible-link mechanism, namely the 1-link FLM, but the authors' aim is to address their future work to extending the capabilities of the proposed simulator to the 4-link FLM already analyzed in [106] and to use such a simulator to test the capabilities of the Model-Predictive Control proposed in [105, 103].

5.2 Reference mechanism

The mechanism for the HIL simulation is a flexible-link manipulator. The link is a square-section metal rod actuated by a brushless AC motor. It can swing in

Table 5.1: Structural and dynamics characteristics of the flexible rod

	Symbol	Value
Young's modulus	E	$230 \cdot 10^9$ [Pa]
Flexural stiffness	EJ	191.67 [Nm^4]
Beam width	a	$1 \cdot 10^{-2}$ [m]
Beam thickness	b	$1 \cdot 10^{-2}$ [m]
Mass/unit length	m	0.7880 [kg/m]
Flexible Link length	l	1.5 [m]
Strain sensor position	s	0.75 [m]
First Rayleigh damping constant	α	$4.5 \cdot 10^{-1}$ [s^{-1}]
Second Rayleigh damping constant	β	$4.2 \cdot 10^{-5}$ [s^{-1}]

the vertical plane and its rigid configuration depends on the angular position q. The FLM prototype is depicted in Figure 6.51. The Structural and dynamics characteristics of the flexible mechanism can be found in Table 6.4.

Evidence of exhaustive experimental tests allows to choose the suitable number of finite elements needed to describe the mechanism's dynamics accurately. The main frequencies of the flexible rod have been inferred by analyzing the spectrum of the vibration when the rod is excited by tapping its end with a steel hammer. This experimental data is then compared with the response of the HIL simulator to the same stimulus. Such conditions can be reproduced by locking the rotation of the rigid degree of freedom q and providing a sequence of impulsive forces to the last node of the FLM.

Figure 5.2 shows the results of this comparison. The black line draws the FFT of the strain-gauge signal, acquired through a Hottinger Baldwin Messtechnik KWS 3073 amplifier. The gray line shows the FFT of the corresponding displacement of the HIL simulator, for the node at the mid-span of the link.

Experimental tests allow to choose the correct number of finite elements and show that just 4 elements can describe the overall dynamics of the link with good accuracy, as proved in Fig. 5.2. The HIL simulator can take into account, with negligible errors, the first three modes of the real mechanism (namely 4.5 Hz, 28 Hz, 81 Hz) and, with lesser but still sufficient precision, the modes at 167 Hz and 274 Hz. It should be pointed out that the modes of high order are less important for the description of the elasto-dynamics of FLM, since they have a very fast decay-time. As such, the resulting nodal displacement is a vector of

Figure 5.3: The mechanisms used for experimental tests

12 elements:

$$\mathbf{u} = \begin{bmatrix} u_1 & u_2 & u_3 & \dots & u_{11} & u_{12} \end{bmatrix}' \tag{5.1}$$

The strain measured can be directly linked to the angular displacement u_6, located at the third node, as it can be seen in Fig. 5.5. From this choice of finite elements, the state vector $\mathbf{x}$ that describes the system has 26 components, and the size of the mass matrix of the whole dynamic system (see Eq. (2.10)) is 26×26.

The accuracy of the Hardware-In-the-Loop simulator has been increased including the non-ideal behavior of the real plant. Additive white Gaussian

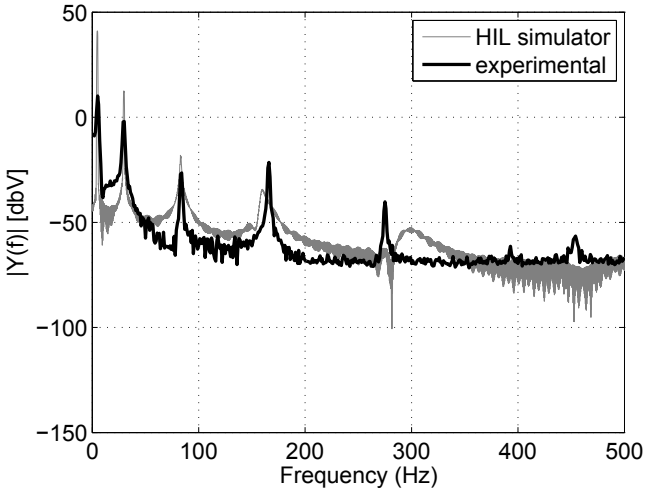

Figure 5.4: Frequency spectrum of strain signal: comparison between experimental results and HIL simulation

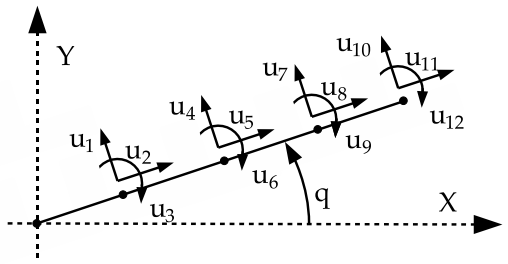

Figure 5.5: Finite-element discretization: nodal displacements

noise have been added to both the simulated strain-gauge signal and to the simulated signal of the encoder. The contribution on strain-gauge signal is crucial, since this kind of signal is affected by large amount of noise, due to the strain-gauge amplifier high gain. Moreover this signal is highly affected by the noise irradiated by the motor driver power supply. The gain of the simulated strain gauge amplifier has been set to 200, meaning that an elastic displacement of 0.01 radians would produce an analog signal with 2 Volts amplitude.

The dynamics of the motor driver and of the actuator have been modeled as a first order low-pass filter with time constant τ_m, and the moment of inertia of the motor J_m has also been included. Such values, which are reported in

Table 5.2: Dynamic characteristics of the actuator

	Symbol	Value
Motor time constant	τ_m	3 [ms]
Motor shaft inertia	J_m	0.0021 $[kg\ m^2]$
Coulomb friction coefficient	μ	0.1
Driver torque analog command gain	G_d	0.4 $[Nm]/[V]$

Table 2, have been evaluated experimentally to refine the accuracy of the simulated dynamic model. The two Rayleigh damping coefficients listed in Table 1 have been also determined experimentally, by comparing the decay time of the vibration of the real mechanism with the one of the HIL simulator.

5.3 HIL implementation

The goal of the Hardware-In-the-Loop simulator is to make the real controller and the simulated model interact with each other, without any need of change on the structure and/or the tuning of the controller. As such, the dynamic model must meet two main requirements: (a) high accuracy (b) real-time (RT) capability. The accuracy allows to mask the virtual model to the controller and, undoubtedly, allows to make the experiments consistent. The dynamic model described above has been investigated by the same authors and its accuracy has been demonstrated in recent papers by comparing the results of several experimental tests with the corresponding simulation's results [47].

The need for the RT capacity arises from the mentioned interaction between real and simulated signals. This requires the dynamic model running on the RT target must have a constant updating frequency to allow the correct synchronization among the signals. These constraints ask for some algebraic manipulations on the dynamic model.

We briefly recall the matrix formulation for the dynamics of a planar flexible-link mechanisms (see Chapter II):

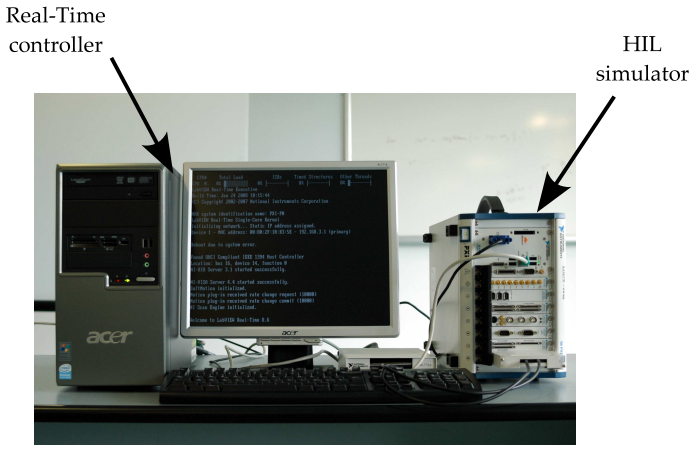

Figure 5.6: The HIL test bench: PXI-based simulator and Real-Time controller

$$\begin{bmatrix} \mathbf{f} \\ \mathbf{S}^T\mathbf{f} \end{bmatrix} = \begin{bmatrix} -2\mathbf{M}_G - \alpha\mathbf{M} - \beta\mathbf{K} & -\mathbf{M}\dot{\mathbf{S}} & -\mathbf{K} \\ \mathbf{S}^T(-2\mathbf{M}_G - \alpha\mathbf{M}) & -\mathbf{S}^T\mathbf{M}\dot{\mathbf{S}} & 0 \end{bmatrix} \begin{bmatrix} \dot{\mathbf{u}} \\ \dot{\mathbf{q}} \\ \mathbf{u} \end{bmatrix} + \begin{bmatrix} \mathbf{M} & \mathbf{I} \\ \mathbf{S}^T\mathbf{M} & \mathbf{S}^T \end{bmatrix} \begin{bmatrix} \mathbf{g} \\ \mathbf{F} \end{bmatrix} \tag{5.2}$$

The last equation can be rewritten as:

$$\begin{bmatrix} \mathbf{M} & \mathbf{MS} & \mathbf{0} & \mathbf{0} \\ \mathbf{S}^T\mathbf{M} & \mathbf{S}^T\mathbf{MS} & \mathbf{0} & \mathbf{0} \\ \mathbf{0} & \mathbf{0} & \mathbf{I} & \mathbf{0} \\ \mathbf{0} & \mathbf{0} & \mathbf{0} & \mathbf{I} \end{bmatrix} \begin{bmatrix} \ddot{\mathbf{u}} \\ \ddot{\mathbf{q}} \\ \dot{\mathbf{u}} \\ \dot{\mathbf{q}} \end{bmatrix} = \begin{bmatrix} \mathbf{M} & \mathbf{I} \\ \mathbf{S}^T\mathbf{M} & \mathbf{S}^T \\ \mathbf{0} & \mathbf{0} \\ \mathbf{0} & \mathbf{0} \end{bmatrix} \begin{bmatrix} \mathbf{g} \\ \mathbf{F} \end{bmatrix} +$$

$$+ \begin{bmatrix} -2\mathbf{M}_G - \alpha\mathbf{M} - \beta\mathbf{K} & -\mathbf{M}\dot{\mathbf{S}} & -\mathbf{K} & \mathbf{0} \\ \mathbf{S}^T(-2\mathbf{M}_G - \alpha\mathbf{M}) & -\mathbf{S^T}\mathbf{M}\dot{\mathbf{S}} & \mathbf{0} & \mathbf{0} \\ \mathbf{I} & \mathbf{0} & \mathbf{0} & \mathbf{0} \\ \mathbf{0} & \mathbf{I} & \mathbf{0} & \mathbf{0} \end{bmatrix} \begin{bmatrix} \dot{\mathbf{u}} \\ \dot{\mathbf{q}} \\ \mathbf{u} \\ \mathbf{q} \end{bmatrix}$$

or, in a more compact form:

$$\tilde{\mathbf{M}}(\mathbf{x}, t)\dot{\mathbf{x}} = \mathbf{\Phi}(\mathbf{x}, \mathbf{F}, t) \tag{5.3}$$

where:

$$\mathbf{x} = [\dot{\mathbf{u}}, \dot{\mathbf{q}}, \mathbf{u}, \mathbf{q}]^T$$

and

$$\mathbf{\Phi}(\mathbf{x},\mathbf{F},t)=\begin{bmatrix}\mathbf{M} & \mathbf{I}\\ \mathbf{S}^T\mathbf{M} & \mathbf{S}^T\\ \mathbf{0} & \mathbf{0}\\ \mathbf{0} & \mathbf{0}\end{bmatrix}\begin{bmatrix}\mathbf{g}\\ \mathbf{F}\end{bmatrix}+\begin{bmatrix}-2\mathbf{M}_G-\alpha\mathbf{M}-\beta\mathbf{K} & -\mathbf{M}\dot{\mathbf{S}} & -\mathbf{K} & \mathbf{0}\\ \mathbf{S}^T(-2\mathbf{M}_G-\alpha\mathbf{M}) & -\mathbf{S^T}\mathbf{M}\dot{\mathbf{S}} & \mathbf{0} & \mathbf{0}\\ \mathbf{I} & \mathbf{0} & \mathbf{0} & \mathbf{0}\\ \mathbf{0} & \mathbf{I} & \mathbf{0} & \mathbf{0}\end{bmatrix}\mathbf{x}$$

$$\tilde{\mathbf{M}}(\mathbf{x},t)=\begin{bmatrix}\mathbf{M} & \mathbf{MS} & \mathbf{0} & \mathbf{0}\\ \mathbf{S}^T\mathbf{M} & \mathbf{S}^T\mathbf{MS} & \mathbf{0} & \mathbf{0}\\ \mathbf{0} & \mathbf{0} & \mathbf{I} & \mathbf{0}\\ \mathbf{0} & \mathbf{0} & \mathbf{0} & \mathbf{I}\end{bmatrix}$$

From Eq.(5.3), it can be seen that the updating equation of the dynamic system involves a large, non-linear and time-dependent matrix, $\tilde{\mathbf{M}}(\mathbf{x},\mathbf{t})$, which needs to be inverted at every iteration.

$$\dot{\mathbf{x}}=\tilde{\mathbf{M}}(\mathbf{x},t)^{-1}\mathbf{\Phi}(\mathbf{x},\mathbf{F},t) \tag{5.4}$$

It should be point out that, owing to the specific choice of the constraints on the flexible displacements $\mathbf{u}$, the matrix $\tilde{\mathbf{M}}$ is always nonsingular.

To speed up the computation of $\dot{\mathbf{x}}$ and improve the updating time, it is necessary to make explicit the vector $\dot{\mathbf{x}}$, by computing its components algebraically. This operation can be done off-line and improves the updating time drastically, since the computation of Eq.(9) becomes a mere numerical substitution during the run-time operations. The main drawback of this approach is that a large amount of memory is required to memorize all the components of the vector.

An optimized C-code routine corresponding to Eq. (5.4) further improves the real-time (or even faster-than-real-time) capacity.

The RT simulation of the whole system, including sensors, actuators and drivers runs on a National Instruments PXI device. It integrates a standard PC-based CPU with a high performance I/O board, so it is well suited for both control and measurement applications.

In particular, the HIL simulator has been implemented on a 1042Q PXI chassis with a PXI-8110 controller, a PXI-6259 analog I/O board and a PXI-6602 counter board, all made by National Instruments®.

The dynamic equation, originally written in C language, can be easily included in a LabVIEW RT project.

In order to evaluate the maximum refresh frequency of the HIL simulator, a large number of tests has been done. The aim was at evaluation of the maximum time required for the computation of equation (5.4).

The results show that the mean time required is $\overline{T} = 0.61831428$ ms, evaluated with the precision of 4×10^{-8} s. As a consequence, the model's refresh frequency for all the experimental tests presented in this paper has been set to 1 kHz. This sampling frequency is sufficient to describe with a good accuracy all the first seven modes of vibration of the flexible link. The computational weight of the model could be reduced by using a more efficient programming technique, for example by using Fortran instead of C code. However, the main limit to the approach proposed here is the computational burden of the symbolic computation of the explicit form of eq. (5.4). So far, using Matlab routines on a standard PC, the author has succeeded only at computing the explicit dynamics for a single flexible link, since all the attempts on trying to replicate the procedure for a flexible four-bar linkage have failed, due to the greater complexity of the equation involved for such mechanisms. However better results might be obtained in the future in the wake of the use of a more powerful hardware platform or of a more suitable software.

5.4 Experimental validation of the HIL simulator

A set of experimental tests has been conducted to prove the effectiveness of the HIL simulator. In particular, the simulator has been validated by using classical controllers while the comparison between the open-loop responses of the real and the simulated plant is necessary missing. This depends on the gravity force that makes unstable the plant. It must be pointed out that, for each experimental test, the same (real) controller has been used both for the real mechanism and the simulated one, without any change on its setup. In the next subsection the simulator is validated by comparing the step response of the real and the simulated mechanism, when the controller implements a simple PI regulator. After that, the same comparison is done by using a LQY regulator.

5.4.1 Validation with PI closed-loop position control

In this section, the real controller implements a simple PI regulator with a feed-forward gravity-compensation action. The block diagram of the control system is depicted in Fig. (5.7). Figure (5.8) shows the comparison between the angular position of the real mechanism and the HIL simulator. The reference signal is a 3 degrees wide step. It can be seen that the two positions are almost equal.

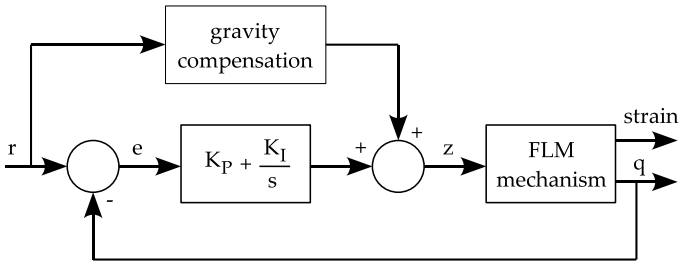

Figure 5.7: PI position control: control diagram

In Figs. (5.9) and (5.10) the torque commands and the strain gauge signals are compared, respectively. In Fig. (5.9), the small difference between the real and the simulated signals is due to the approximation of the link curvature with the nodal displacement u_6. All the figures demonstrate the effectiveness of the HIL simulator. As such, it can simulate with a good accuracy the behavior of the real mechanism. A PID control system might have been used as well, but the choice of a simple PI control has been motivated for its damping properties: a less damped system is more demanding on the accuracy of the HIL test bench.

5.4.2 Validation with LQ closed-loop position and vibration control

In this section a further proof of the accuracy of the Hardware-In-the-Loop simulator is given, by comparing with each other the responses of the real and the HIL-simulated plant by using a LQ position-vibration controller with an integral action. A graphic representation of the control's loop structure is shown in Fig. (5.11).

Owing to the space constraints of this paper, just a basic overview of this controller will be given. A complete explanation of this controller can be found in [128].

The design of such a controller is based on a linear state-space model of the FML which has been obtained through a classical linearization procedure of Eq.(5.3). The resulting state-space model can be written as:

$$\begin{cases} \dot{\mathbf{x}}(t) = \mathbf{A}\mathbf{x}(t) + \mathbf{B}\mathbf{z}(t) \\ \mathbf{y}(t) = \mathbf{C}\mathbf{x}(t) \end{cases} \tag{5.5}$$

where $\mathbf{A} \in \mathbb{R}^{26} \times \mathbb{R}^{26}$, $\mathbf{B} \in \mathbb{R}^{26} \times \mathbb{R}^{1}$, $\mathbf{C} \in \mathbb{R}^{2} \times \mathbb{R}^{26}$ are time-invariant matrices.

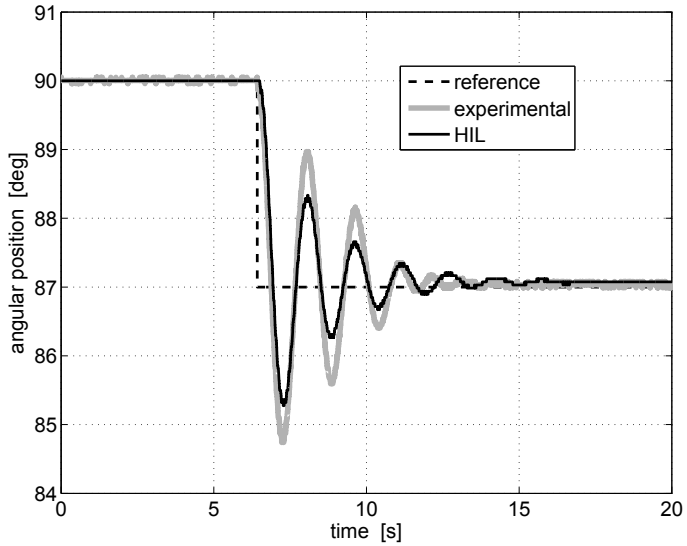

Figure 5.8: PI position control: experimental validation of the angular position closed-loop response

In order to provide an integral action to the controller, the state-space model must be augmented. The tracking error can be defined so that its time derivative obeys the following differential equation:

$$\dot{\mathbf{w}} = \mathbf{r}(r) - \mathbf{y}(t) = \mathbf{r}(t) - \mathbf{C}\mathbf{x}(t) \tag{5.6}$$

where $\mathbf{r}(t)$ is the desired trajectory that the plant output $\mathbf{y}(t)$ should follow. In this way $\mathbf{w}(t)$ is the integral of the tracking error. An augmented state vector $\hat{\mathbf{x}}$ can be defined such as: $\hat{\mathbf{x}} = \begin{bmatrix} \mathbf{x} \\ \mathbf{w} \end{bmatrix}$, then the augmented state equation is:

$$\dot{\hat{\mathbf{x}}}(t) = \underbrace{\begin{bmatrix} \mathbf{A} & 0 \\ -\mathbf{C} & 0 \end{bmatrix}}_{\hat{\mathbf{A}}} \hat{\mathbf{x}} + \underbrace{\begin{bmatrix} \mathbf{B} \\ 0 \end{bmatrix}}_{\hat{\mathbf{B}}} \mathbf{z} + \underbrace{\begin{bmatrix} 0 \\ \mathbf{r} \end{bmatrix}}_{\mathbf{d}} \tag{5.7}$$

while the augmented output equation is:

$$\mathbf{y} = \underbrace{\begin{bmatrix} \mathbf{C} & 0 \end{bmatrix}}_{\hat{\mathbf{C}}} \hat{\mathbf{x}} \tag{5.8}$$

The LQY controller calculates the optimal control sequence $\tau(t)$ which minimizes the performance index J, defined as:

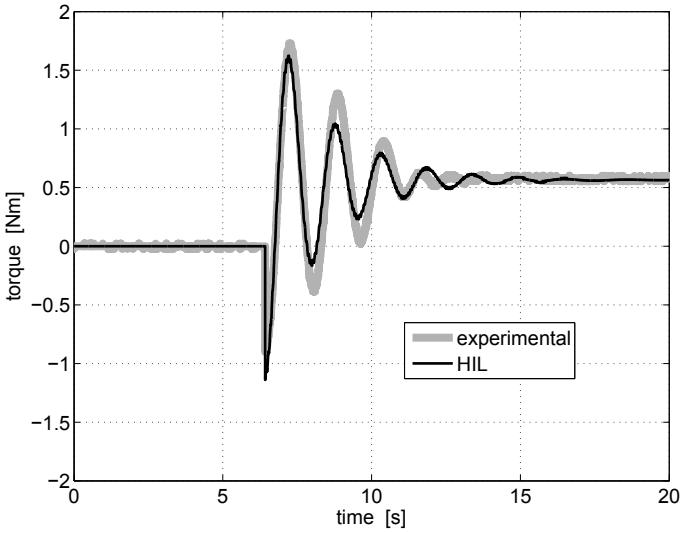

Figure 5.9: PI position control: experimental validation of the torque closed-loop response

$$J = \frac{1}{2}\int_0^\infty \left\{ (\mathbf{y}-\mathbf{r})^T \mathbf{Q}_y (\mathbf{y}-\mathbf{r}) + \mathbf{w}^T \mathbf{Q}_w \mathbf{w} + \mathbf{z}^T \mathbf{R} \mathbf{z} \right\} dt \tag{5.9}$$

The first term inside the integral minimizes the absolute value of the tracking error of free coordinate q and the elastic displacement, whereas the second takes into account the absolute value of integral error of q. The last one minimizes the system input, namely the torque applied to the link. $\mathbf{Q}_y$ is a diagonal matrix of weights, while $\mathbf{Q}_w$ and $\mathbf{R}$ are simple scalar values. The value of the control variable can be found as:

$$z(t) = -\mathbf{K}_x \mathbf{x} - \mathbf{K}_w w + \mathbf{K}_r \mathbf{r} \tag{5.10}$$

where the optimal value of the gain matrices $\mathbf{K}_x$, $\mathbf{K}_w$, $\mathbf{K}_r$ are found through the solution of the algebraic Riccati equation. The control strategy explained above can be applied only when a measure of the whole state $\mathbf{x}$ is available. In this application, there are only two measured values, so that a state observer must be used. Here a standard Kalman asymptotic estimator has been chosen. An estimation of $\mathbf{x}(k)$ and $\mathbf{x}_m(k)$ (where $\mathbf{x}(k)$ is the state of the plant model and $\mathbf{x}_m(k)$ is the state of the measurement noise model) can be computed from the measured output $\mathbf{y}_m(k)$ through:

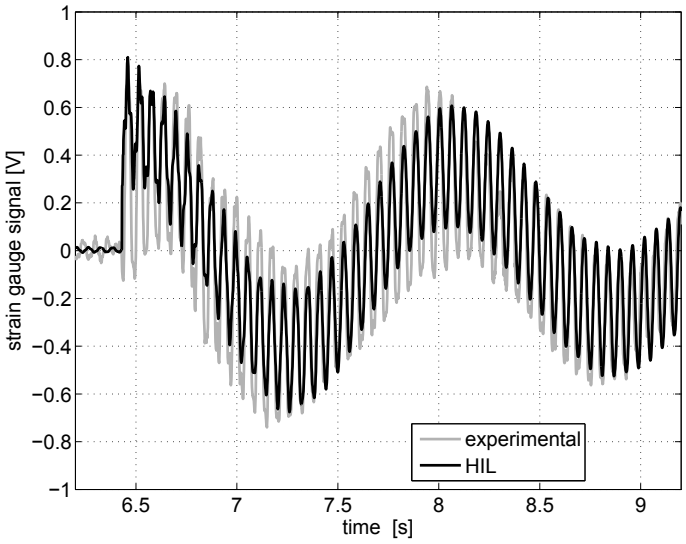

Figure 5.10: PID position control: experimental validation of the strain gauge signal closed-loop response - detailed view of the transient

$$\begin{bmatrix} \hat{\mathbf{x}}(k|k) \\ \hat{\mathbf{x}}_m(k|k) \end{bmatrix} = \begin{bmatrix} \hat{\mathbf{x}}(k|k-1) \\ \hat{\mathbf{x}}_m(k|k-1) \end{bmatrix} + \mathbf{L}(\mathbf{y}_m(k) - \hat{\mathbf{y}}_m(k))$$

$$\begin{bmatrix} \hat{\mathbf{x}}(k+1|k) \\ \hat{\mathbf{x}}_m(k+1|k) \end{bmatrix} = \begin{bmatrix} \mathbf{A}\hat{\mathbf{x}}(k|k) + \mathbf{B}\mathbf{z}(k) \\ \tilde{\mathbf{A}}\hat{\mathbf{x}}_m(k|k) \end{bmatrix} \tag{5.11}$$

$$\hat{\mathbf{y}}_m(k) = \mathbf{C}_m\hat{\mathbf{x}}(k|k-1)$$

The gain matrix $\mathbf{L}$ is designed by using Kalman filtering techniques, see [127].

The response of the HIL simulator and of the mechanism when the LQ position and vibration control is used are reported in Figs. (5.12 – 14) and in Figs. (5.15 – 17). Two different tunings of the control system have been used to show how the HIL simulator can respond to different control parameters.

LQ control: experimental validation

The first experimental validation using the LQ optimal control with integral action is done using the following tuning parameters: $\mathbf{Q}_y = \begin{bmatrix} 1000 & 0 \\ 0 & 50 \end{bmatrix}$ and $\mathbf{Q}_w = 100$.

The initial position of the mechanism is 90 deg., and the reference signal is

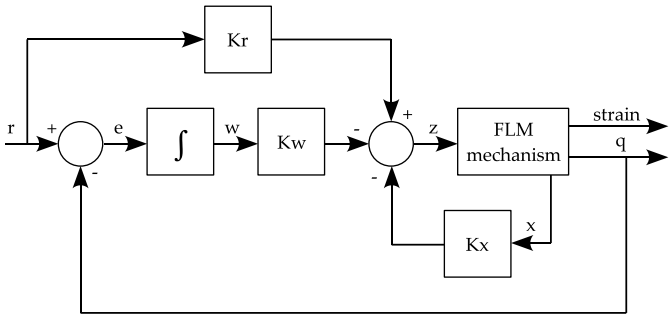

Figure 5.11: LQY with integral action position and vibration control: control diagram

a step that moves form 90 to 94 degrees. The response of the mechanism and the HIL simulator are compared in Fig. 13. As it can be seen, the responses are very similar each other. The small discrepancies are the result of the limited accuracy of the brushless motor torque control. A more accurate comparison would require to effectively measure the torque produced by the actuator.

The values of the torque computed by the real-time control system are compared in Fig. 14. Again, the accuracy of the HIL simulator is confirmed by the likeness of the two torque profiles.

The accuracy of the proposed Hardware-In-the-Loop simulator in terms of vibration response is shown in Fig. 15.

It should be noted that the LQ controller needs the HIL simulator have a higher level of accuracy comparing to the requirements of the previous PI control, since it also relies on the elastic displacement for the computation of the control action.

The second experimental validation is done by setting the following parameters: $\mathbf{Q}_y = \begin{bmatrix} 500 & 0 \\ 0 & 100 \end{bmatrix}$ and $\mathbf{Q}_w = 50$.

As it can be seen from Figs. 5.15,5.16,5.17, the likeness of the two responses exhibited in the previous test is kept at the same level also after altering the tuning of the control system. Some discrepancies are visible in figures 5.14 and 5.17, in particular it can be seen that the amplitude of the vibration is not perfectly reproduced by the HIL simulator. This behavior, that was not detected using the PID control system (see fig. 5.10), might be due to both some inevitable mismatches between the model and the actual mechanisms, both to the less then perfect state estimation, that is reflected trough the controller's

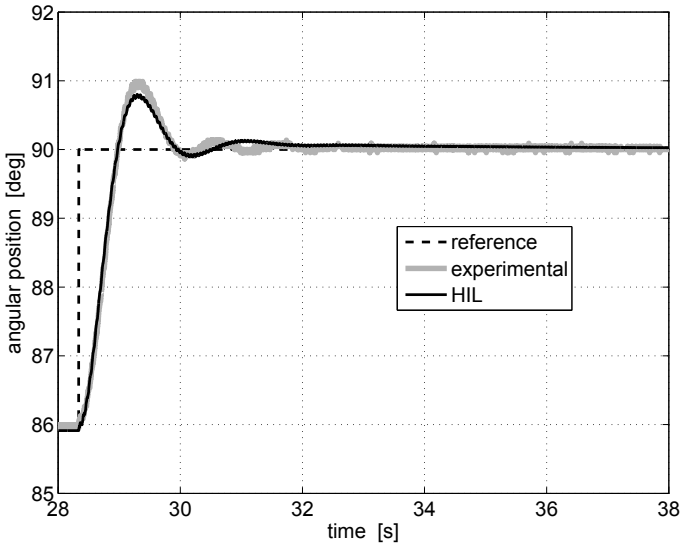

Figure 5.12: Optimal control: experimental validation of the angular position closed-loop response

action to the closed-loop response.

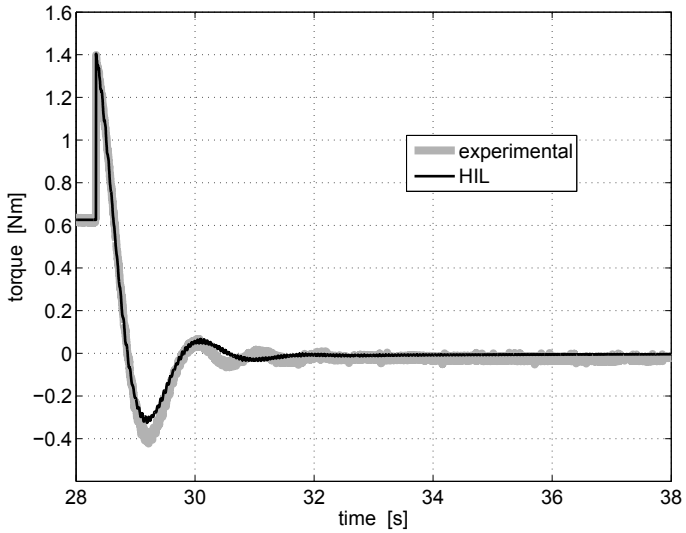

Figure 5.13: Optimal control: experimental validation of the torque closed-loop response

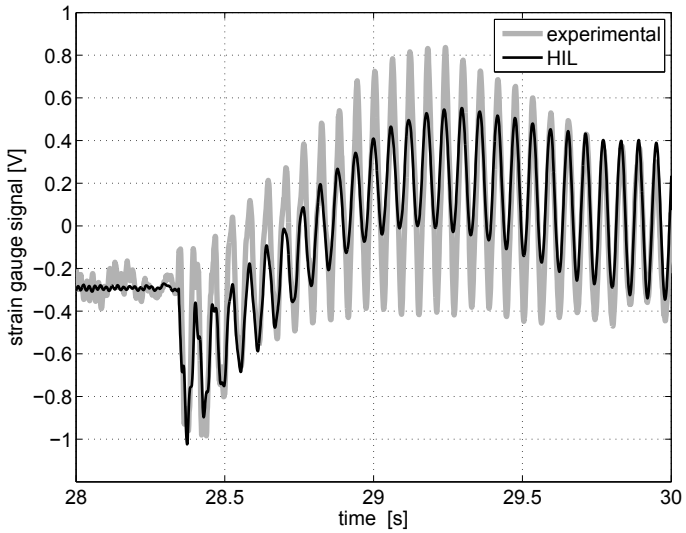

Figure 5.14: Optimal control: experimental validation of the strain gauge signal closed-loop response - detailed view of transient

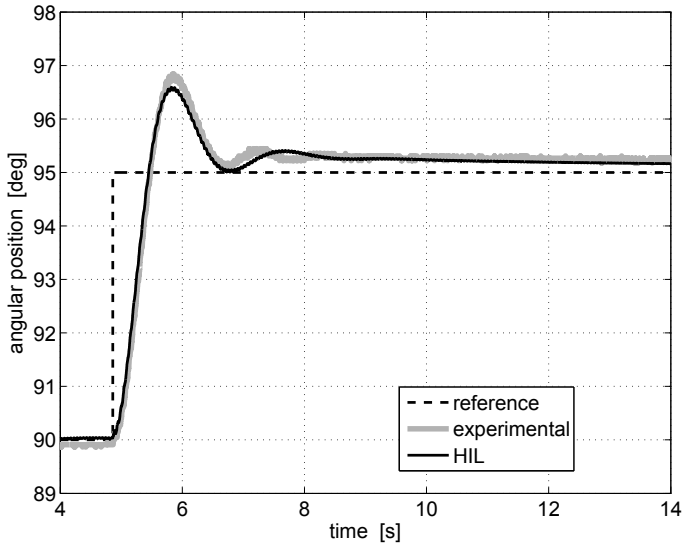

Figure 5.15: Optimal control: experimental validation of the angular position closed-loop response

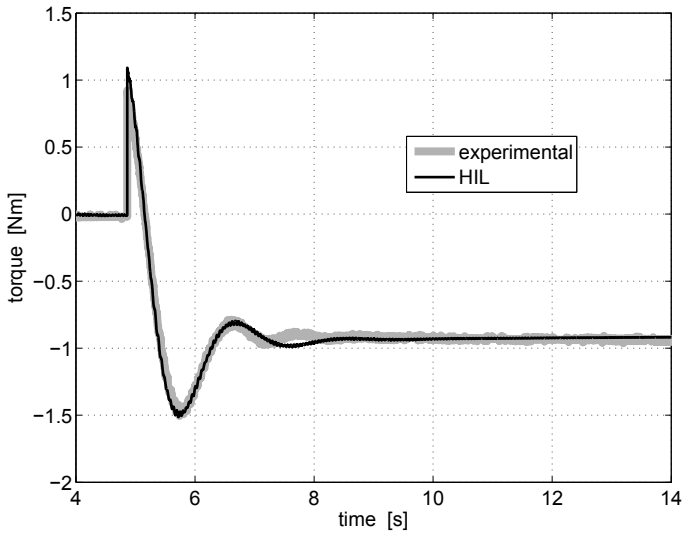

Figure 5.16: Optimal control: experimental validation of the torque closed-loop response

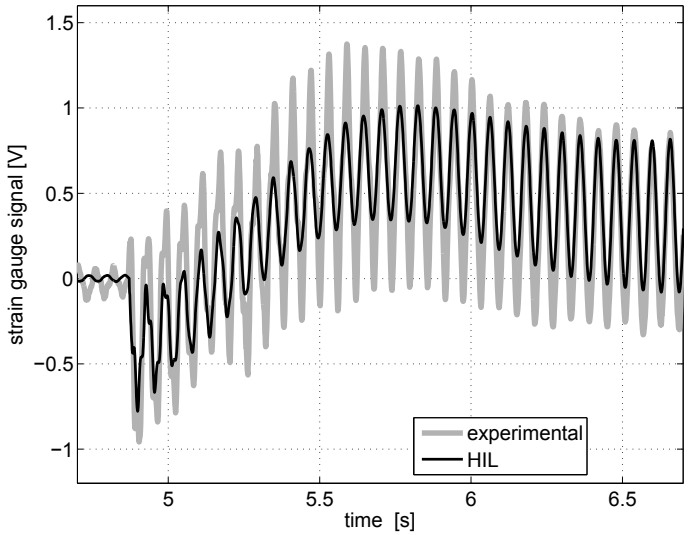

Figure 5.17: Optimal control: experimental validation of the strain gauge signal closed-loop response - detailed view of transient

6 MPC control: experimental results

Vibration suppression in flexible link manipulator is a recurring problem in most robotic applications. Solving this problem would allow to increase many times both the operative speed and the accuracy of manipulators. In this chapter an innovative controller for flexible-links mechanism based on MPC (Model Predictive Control) with constraints is proposed. So far this kind of controller has been employed almost exclusively for controlling slow processes, like chemical plants, but the authors' aim is to show that this approach can be successfully adapted to plants whose dynamical behavior is both nonlinear and fast changing. Therefore in this chapter such controller will be applied to control both the position and elastic displacements of different examples of flexible-links mechanisms. The mechanisms under investigation are:

- single-link mechanism with gravity
- four-bar mechanism
- five-bar mechanism

The effectiveness of this control system will be compared to the performance obtained with other classical control systems, such as PID and linear quadratic regulators.

6.1 MPC control of a four-bar linkage

In this section a model predictive control with constraints is proposed for vibration control in a four-link flexible mechanism. The choice of this control strategy

has been motivated by different factors. First, the prediction ability based on an internal model can be a very effective advantage in fast-dynamic systems. Then MPC is well suited to MIMO plants (in this case the mechanical system will be modeled as a SIMO plant), since the outputs are computed by solving a minimization problem which can take account of different variables. Another strong plus of this control strategy is represented by its ability to handle constraints on both control and controlled variables. This can be very effective in real-world control strategies were actuators limitations, such as maximum torque, or maximum speed of motors cannot be neglected.

The MPC controller has been implemented in software simulation using Matlab/Simulink^{TM}. Exhaustive simulations have been made to prove the accuracy, the effectiveness and the robustness of this control approach. An FPGA implementation of this MPC controller is now being studied, following the results proposed by Ling in [97]. The control system proposed in this paper will be employed to control both the position and the vibration in a four-link flexible mechanism laying on the horizontal plane. The crank is actuated by a torque-controlled electric motor, while the vibration phenomena are measured in the mid-span of the follower link. This work follows a previous work, [103], in which the same authors have experimentally tested the effectiveness of this kind of control system for controlling the position and the vibration in a single-link flexible mechanism. The robustness of the controller with respect to the modeling uncertainties is proven by exhaustive simulations, while the effects of choosing different tuning parameters are also shown investigated. Numerical results of a comparison between the proposed MPC controller and a classical PID controller are presented as well.

6.2 Reference mechanism

The mechanism chosen as the basis of the simulations is a four-link mechanism, made by three steel rods, see fig. 6.2. The fourth link of the mechanism is the ground link. The section of the rods is square, and their side is 6 mm wide. These three rods are connected in a closed-loop planar chain employing four revolute joints. The first and the third link (counting anticlockwise) are connected to the chassis, which can be considered to be perfectly rigid. The rotational motion of the first link, which is the shortest one, can be imposed through a torque-controlled actuator. The whole chain can swing along the horizontal plane, so the effects of gravity on both the rigid and elastic motion of the mechanism can

be neglected. The length of the links and the other geometrical dimensions of the mechanism has been chosen to replicate the actual mechanism prototype.

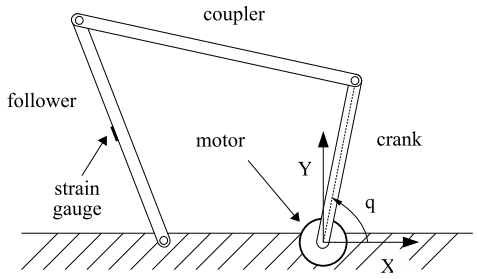

Figure 6.1: The four-link mechanism used for simulations

The crank, whose length is $L_1 = 0.3728m$, has been modeled, like the coupler, with a single finite-element (Fig. 6.2). For the follower, two finite elements have been used, since it is the longest one. Increasing the number of finite elements would certainly improve the overall accuracy of the model, but also includes some drawbacks, in particular it increases the computational effort required for the simulation. Each link described with 1 finite-element has 6 elastic degrees of freedom, whereas the one described by 2 finite-element has 9 degrees of freedom. After putting together the 3 links on the frame, considering the constraints fixed by the kinematic couplings and neglecting one of the nodal displacements in order to make the system solvable (see [1]), the resulting flexible system is described by 12 nodal elastic displacements and one rigid degree of freedom.

Table 6.1: Kinematic and dynamic characteristics of reference mechanism

	symbol	value
Young's modulus	E	210×10^9 [Pa]
Flexural inertia moment	J	11.102×10^{-10} $[m^4]$
Beams width	a	6×10^{-3} [m]
Beams thickness	b	6×10^{-3} [m]
Mass/unit of length of links	m	272×10^{-3} $[Kg/m]$
Crank length	L_1	0.3728 [m]
Coupler length	L_2	0.525 [m]
Follower length	L_3	0.632 [m]
Ground length	L_4	0.3595 [m]
Rayleigh damping constants	α	8.72×10^{-2} $[s^{-1}]$
	β	2.1×10^{-5} [s]

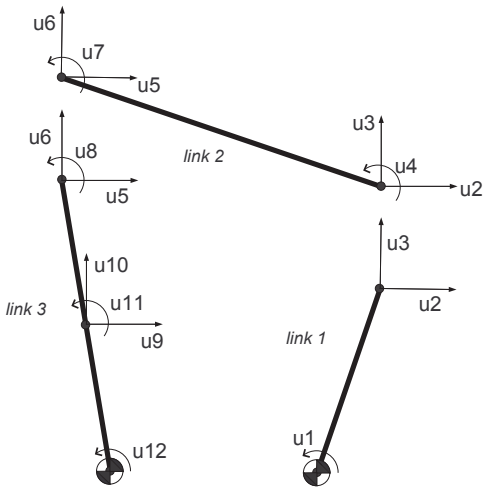

Figure 6.2: Elastic displacements in the four-link mechanism

6.3 Linear state-space dynamic model

The dynamic model presented in chapter 2 is strongly nonlinear, due to the quadratic relation between the nodal accelerations and the velocities of the free coordinates. Thus it cannot be used as a prediction model for a linear MPC controller. In order to develop a state-space form linearized version of the aforementioned dynamic system a linearization procedure has been developed by Gasparetto in [166]. Here this procedure will be briefly recalled.

From the basics of system theory, a linear time-invariant model expressed in state-space can be written as:

$$\begin{cases} \dot{\mathbf{x}}(t) = \mathbf{F}_{lin}\mathbf{x}(t) + \mathbf{G}_{lin}\mathbf{v}(t) \\ \mathbf{y}(t) = \mathbf{H}_{lin}\mathbf{x}(t) + \mathbf{D}_{lin}\mathbf{v}(t) \end{cases} \tag{6.1}$$

where $\mathbf{x}(t)$ is the state vector, $\mathbf{y}(t)$ is the output vector, $\mathbf{v}(t)$ represents the input vector and $\mathbf{F}_{lin}$, $\mathbf{G}_{lin}$, $\mathbf{H}_{lin}$ and $\mathbf{D}_{lin}$ are time-invariant matrices. Taking $\mathbf{x} = [\dot{\mathbf{u}}, \dot{\mathbf{q}}, \mathbf{u}, \mathbf{q}]^T$ as the state vector, linearized state-space form of the dynamic model in (6) can be written as:

$$\mathcal{A}_{lin}\dot{\mathbf{x}} = \mathcal{B}_{lin}\ \mathbf{x} + \mathcal{C}_{lin}\tau \tag{6.2}$$

Now a steady equilibrium configuration $\mathbf{x}_e$ where $\mathbf{u} = \mathbf{u}_e$ under the system input $\mathbf{v} = \mathbf{v}_e$ can be chosen. In the neighborhood of this point holds:

$$\begin{cases} \mathbf{x}(t) = \mathbf{x}_e + \Delta\mathbf{x}(t) \\ \mathbf{v}(t) = \mathbf{v}_e + \Delta\mathbf{v}(t) \end{cases} \tag{6.3}$$

Bringing this relations into (2.80) the following relationship turns out:

$$\mathcal{A}_{lin}(\mathbf{x}_e)\Delta\dot{\mathbf{x}} = \mathcal{B}_{lin}(\mathbf{x}_e + \Delta\mathbf{x})(\mathbf{x}_e + \Delta\mathbf{x}) + \mathcal{C}_{lin}(\mathbf{x}_e + \Delta\mathbf{x})(\mathbf{v}_e + \Delta\mathbf{x}) \tag{6.4}$$

After some steps that can be found in major detail in [166], $\mathcal{A}_{lin}$ and $\mathcal{B}_{lin}$ matrices in (6.2) can be written as:

$$\mathcal{A}_{lin} = \begin{bmatrix} \mathbf{M} & \mathbf{MS} & \mathbf{0} & \mathbf{0} \\ \mathbf{S}^T\mathbf{M} & \mathbf{S}^T\mathbf{MS} & \mathbf{0} & \mathbf{0} \\ \mathbf{0} & \mathbf{0} & \mathbf{I} & \mathbf{0} \\ \mathbf{0} & \mathbf{0} & \mathbf{0} & \mathbf{I} \end{bmatrix} \tag{6.5}$$

$$\mathcal{B}_{lin} = \begin{bmatrix} -2\mathbf{M}_G - \alpha\mathbf{M} - \beta\mathbf{K} & \mathbf{0} & -\mathbf{K} & 0 \\ \mathbf{S}^T(-2\mathbf{M}_G - \alpha\mathbf{M} - \beta\mathbf{K}) & \mathbf{0} & \mathbf{0} & 0 \\ \mathbf{I} & \mathbf{0} & \mathbf{0} & \mathbf{0} \\ \mathbf{0} & \mathbf{I} & \mathbf{0} & \mathbf{0} \end{bmatrix} \tag{6.6}$$

$\mathcal{C}_{lin}$ remains unchanged after the linearization process, since it is composed of only zeros and ones. The standard form of the state-space system can be easily found from $\mathcal{A}_{lin}$, $\mathcal{B}_{lin}$ and $\mathcal{C}_{lin}$:

$$\begin{cases} \Delta\dot{\mathbf{x}} = \mathbf{F}_{lin}\Delta\mathbf{x} + \mathbf{G}_{lin}\Delta\mathbf{v} \\ \mathbf{y} = \mathbf{H}_{lin}\mathbf{x} + \mathbf{D}_{lin}\mathbf{v} \end{cases} \tag{6.7}$$

where:

$$\begin{aligned} \mathbf{F}_{lin} &= {\mathcal{A}_{lin}}^{-1}\mathcal{B}_{lin} \\ \mathbf{G}_{lin} &= {\mathcal{A}_{lin}}^{-1}\mathcal{C}_{lin} \end{aligned} \tag{6.8}$$

6.3.1 Accuracy of the linearized model

In order to estimate the accuracy of the linearized model, a simple comparison between the impulsive responses for linear and nonlinear models will be set. A more detailed investigation on the accuracy of the linear model can be found on the previous work by Caracciolo et al. [86]. The mechanism will be fed with a 5 Nm torque impulse applied to the crank. The initial configuration has been arbitrarily chosen as $q_0 = 0$ (but the effectiveness of the linearization model holds for any configuration of choice). Here a comparison of the two nodal displacements u_2 and u_{10} is set, but the results extend also to all the other nodal displacements belonging to the model.

As it can be seen from Figure 6.3 the linearized model shows a very high level of accuracy as far as the rigid rotation q is concerned. Figure 6.3.b shows that the error increases as the mechanism moves from the linearization configuration, nevertheless it remains very low. After two seconds of simulation the

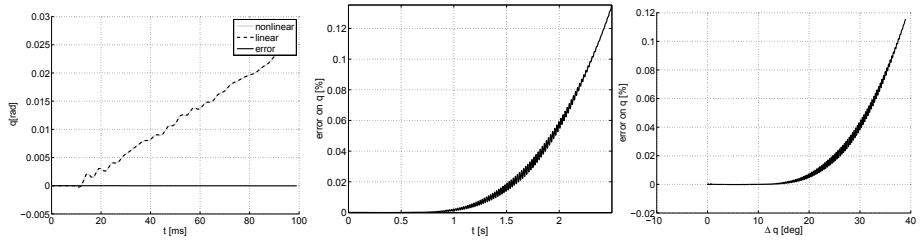

(a) (b) (c)

Figure 6.3: Crank angular position q. (a) Comparison of the nonlinear and linearized system impulsive responses. (b) Error in per cent vs. time. (c) Error in per cent vs. angular motion from the "equilibrium" configuration

error between the linear and nonlinear dynamic responses is still lower than 0.1%. Notice that the error reaches the threshold of 0.1% when the crank angular position has moved more or less 40 degrees from the original position (Figure 6.3.c). The response of the two models show more discrepancies if the nodal elastic displacements u_i are considered. In this situation the kinematic and dynamic nonlinearities affect more heavily the differences between the two responses.

Figure 6.4 shows the comparison of the nonlinear and linearized system impulsive responses in terms of the nodal displacement u_2. As it can be seen from Figure 6.4.a the differences are negligible during the transient. Nevertheless they increase as the mechanism moves from the "equilibrium" configuration (Figures 6.4.b and 6.4.d) . In particular the differences on u_2 between the linearized and the nonlinear models are less than the ± 20 per cent as long as the motion from the original position is kept less than 80 degrees (Figure 6.4.c).

A similar behavior can be observed for the all the other displacements. In particular Figure 6.5 shows a comparison on the nodal displacement u_{10}. Here the differences between the linearized and the nonlinear models are less than the ± 20 per cent as long as the motion from the original position is kept less than 40 degrees (Figure 6.5.c). This deterioration may be due to the nonlinear effects on the sensitivity matrix $\mathbf{S}(q)$. From the graph in Figure 6.4.b it can be seen that the absolute linearization error converges to a zero value: it should be stated that this error does not affect the closed-loop control system when it is less than the minimum value that can be measured the acquisition system.

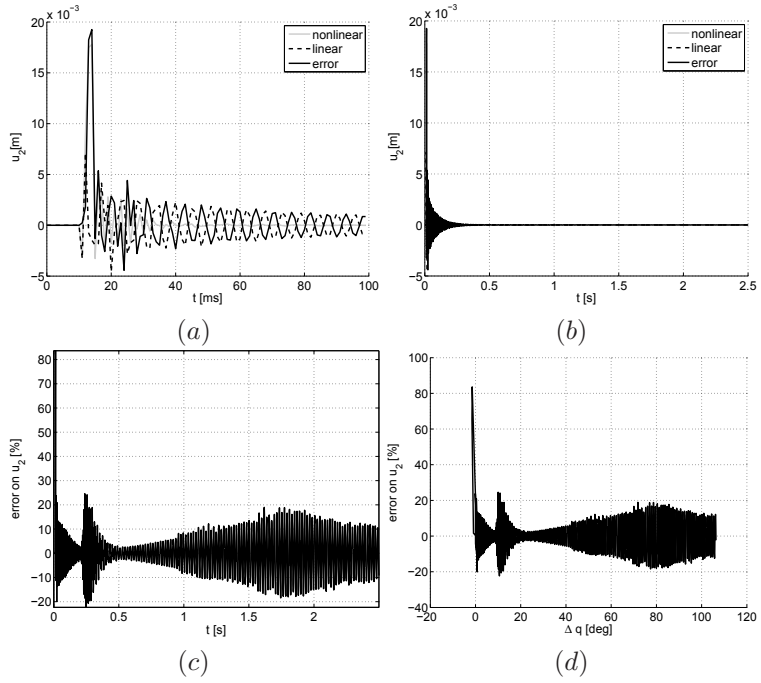

Figure 6.4: Comparison of the nonlinear and linearized system impulsive responses for the nodal displacement u_2. (a) Transient responses. (b) Steady state responses. (c) Error in per cent vs. time. (d) Error in per cent vs. angular motion from the "equilibrium" configuration.

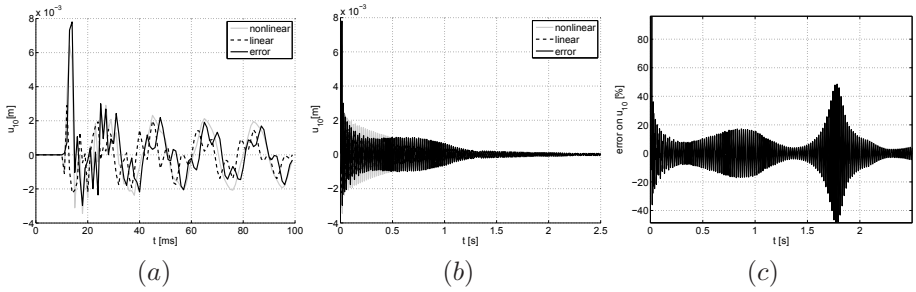

Figure 6.5: Nodal displacement u_{10}. (a) Comparison of the nonlinear and linearized system impulsive responses. (b) Absolute error vs. time. (c) Error in per cent vs. angular motion from the "equilibrium" configuration.

6.3.2 State observer

The MPC controller that will be presented and discussed in next sections requires for the whole state vector $\mathbf{x}$ to be available at each sampling time. Nev-

ertheless in practical applications it is impossible to measure all the 12 nodal displacements (and their time derivatives) belonging to the state vector. Hence the need of the state observer to obtain an estimate of the full state vector from a subset of it. Here a standard Kalman asymptotic estimator has been chosen. An estimation of $\mathbf{x}(k)$ and $\mathbf{x}_m(k)$ (where $\mathbf{x}(k)$ is the state of the plant model and $\mathbf{x}_m(k)$ is the state of the measurement noise model) can be computed from the measured output $\mathbf{y}_m(k)$ trough:

$$\begin{aligned}
\begin{bmatrix} \hat{\mathbf{x}}(k|k) \\ \hat{\mathbf{x}}_m(k|k) \end{bmatrix} &= \begin{bmatrix} \hat{\mathbf{x}}(k|k-1) \\ \hat{\mathbf{x}}_m(k|k-1) \end{bmatrix} + \mathbf{M}(\mathbf{y}_m(k) - \hat{\mathbf{y}}_m(k)) \\
\begin{bmatrix} \hat{\mathbf{x}}(k+1|k) \\ \hat{\mathbf{x}}_m(k+1|k) \end{bmatrix} &= \begin{bmatrix} \mathbf{A}\hat{\mathbf{x}}(k|k) + \mathbf{B}_u\mathbf{u}(k) \\ \tilde{\mathbf{A}}\hat{\mathbf{x}}_m(k|k) \end{bmatrix} \\
\hat{\mathbf{y}}_m(k) &= \mathbf{C}_m\hat{\mathbf{x}}(k|k-1)
\end{aligned} \tag{6.9}$$

The gain matrix $\mathbf{M}$ is designed using Kalman filtering techniques, see [127]. Figures 6.6-6.9 demonstrate the effectiveness of the proposed observer, by comparison of the impulsive responses of the nonlinear system and the observer. An error on the observer initial state has been assumed, in this way the nonlinear system and the observer started from different initial conditions. In particular each component on the observer initial state vector was different from that of the nonlinear system both in magnitude and in phase: the observer initial condition has been overestimated of 30 per cent, and the sign was changed too. It can be seen that the observer is able both to reduce in few milliseconds the initial error and to keep it below the 10 per cent. Therefore the observer can reproduce with a minimal error the full state vector of the system from the knowledge of u_{10} and q.

6.3.3 Results of the Model Predictive Controller

In this section the effectiveness of the developed MPC controlled is tested in a simulation environment. This controller acts as a MISO (Multiple-Input, Single-Output) system: the MPC relies on the knowledge of the instantaneous values of the displacements u_{10} and crank angular position q. u_{10} and q are the two controlled variables, while the torque applied to the crank acts as the control variable. The tuning of the MPC depends on 5 variables:

1. weight on u_{10}: w_{10}
2. weight on q: w_q

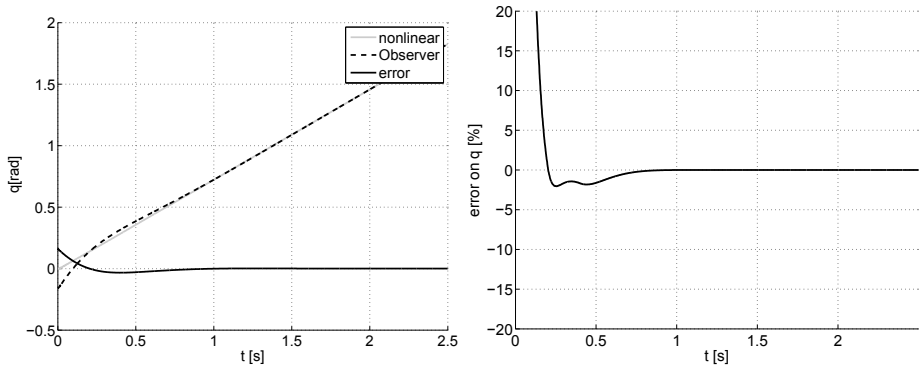

(a) (b)

Figure 6.6: Displacement q. (a) Comparison of the nonlinear system and observer impulsive responses. (b) Error in per cent vs. time

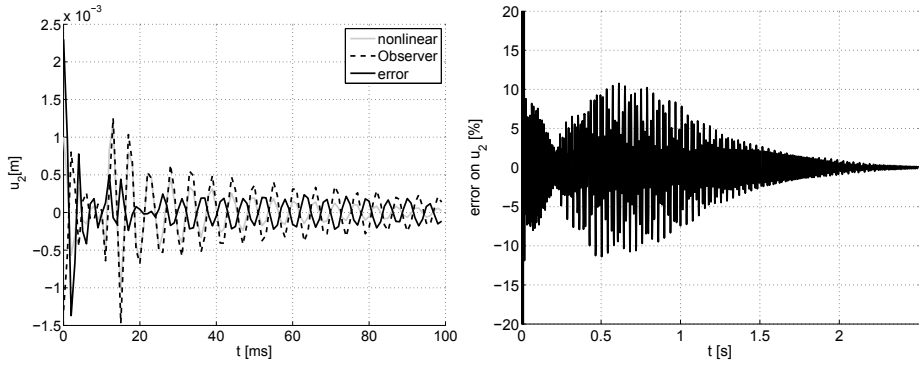

(a) (b)

Figure 6.7: Nodal displacement u_2. (a) Comparison of the nonlinear system and observer impulsive responses. (b) Error in per cent vs. time

3. sampling time: T_s

4. prediction horizon: H_p

5. control horizon: H_c

Then constraints on both control and controlled variables should to be taken into account. Here inequalities constraints have been used:

1. $u_{10_{min}} \leq u_{10} \leq u_{10_{max}}$

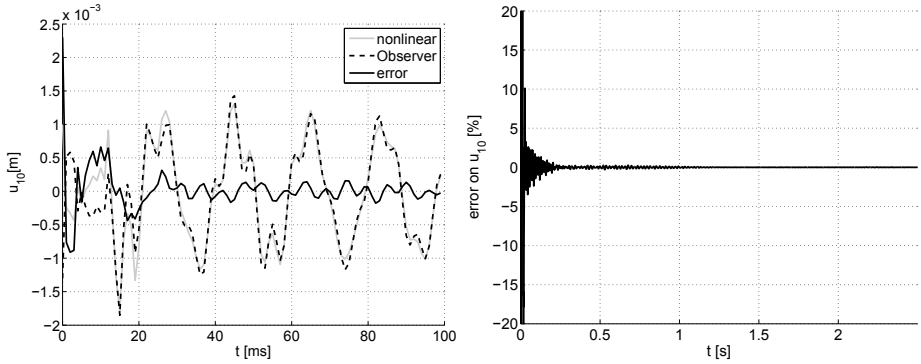

(a) (b)

Figure 6.8: Nodal displacement u_{10}. (a) Comparison of the nonlinear system and observer impulsive responses. (b) Error in per cent vs. time

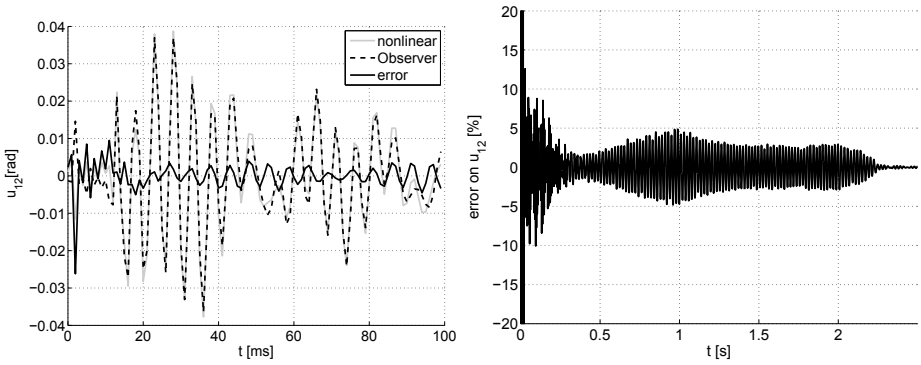

(a) (b)

Figure 6.9: Nodal displacement u_{12}. (a) Comparison of the nonlinear system and observer impulsive responses. (b) Error in per cent vs. time

2. $q_{min} \leq q \leq q_{max}$

3. $\tau_{min} \leq \tau \leq \tau_{max}$

The overall behavior of the controller depends on a large set of variables. While τ_{min} and τ_{max} depends on actuator peak torque, all the others parameters can be tuned quite freely. As a simple rule of thumb, the inequalities constraints should be chosen thinking about the desired performance of the closed-loop system, but always taking care of not setting them too tight, otherwise the system may behave unexpectedly.

Values of T_s, H_p and H_c should, in practical applications, be chosen according to the available computational resources. Every choice of T_s requires to solve the optimization problem $1/T_s$ times every second, and the computational cost of every evaluation is directly proportional to both H_p and H_c.

Referring to [97], Ling proved that a 1.5 million gates FPGA can handle values of T_s around 20 ms without using particular optimization strategies and high-level FPGA programming (the dynamic system size was 2, $T_s = 20ms$, $H_c = 3$, $H_p = 10$). On the other side, Bleris in [93] proved that using more specialized hardware and optimization techniques allows to set T_s as low as 1 ms (the size of the dynamic system was 4, $H_c = 3$, $H_p = 10$).

The model obtained from linearization (evaluated on the initial configuration of the mechanism) will be used to develop the MPC linear controller. Then the MPC will be employed to control the position of the nonlinear mechanism, keeping as small as possible the deformations during the overall motion. The tuning of the MPC controller is chosen to be: $T_s = 1$ms, $H_p = 55$ and H_c =5. By using these values very high performances can be obtained both in terms of the crank angular position tracking and of the vibrations damping. The final angular position is reached in a very short time (more or less 100 ms), while the elastic displacements reaches a negligible level after less than 500 ms.

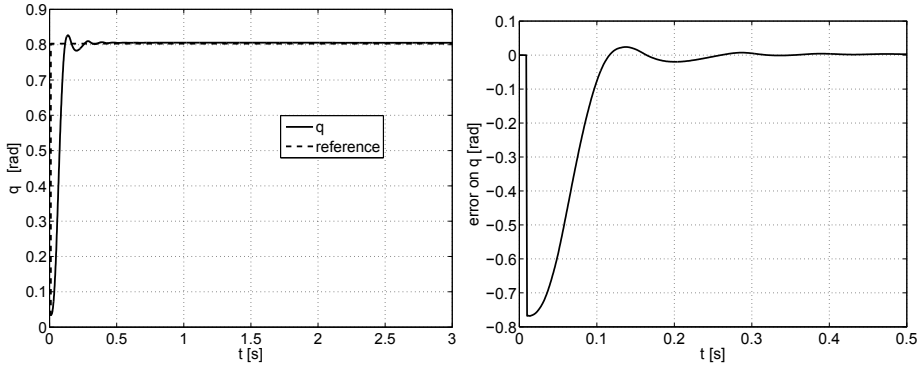

(a) (b)

Figure 6.10: Angular position of the crank q. (a) Response of the MPC control (b) Error on q

In Figure 6.12 the mechanism is shown at $t = 0$, in $t = 0.120$ s and in $t = 1$ s, hence respectively before the motion, during the transient, and when the mechanism is steady at its final configuration. The elastic displacements,

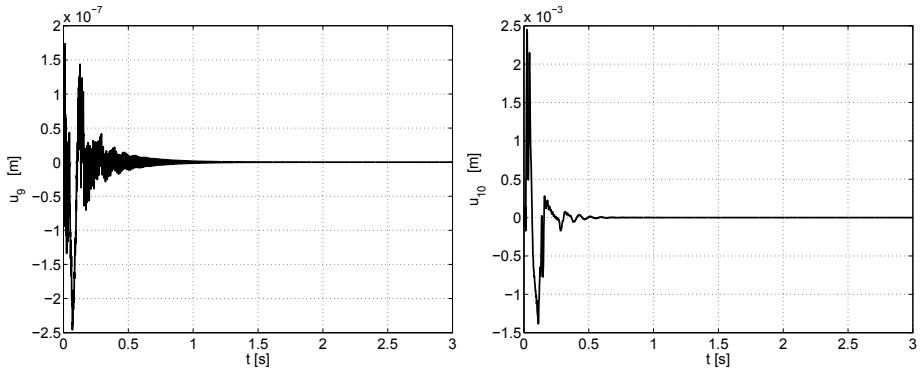

(a) (b)

Figure 6.11: Elastic displacements measured in the local reference frame employing the MPC control. (a) Elastic displacement u_9 (b) Elastic displacement u_{10}

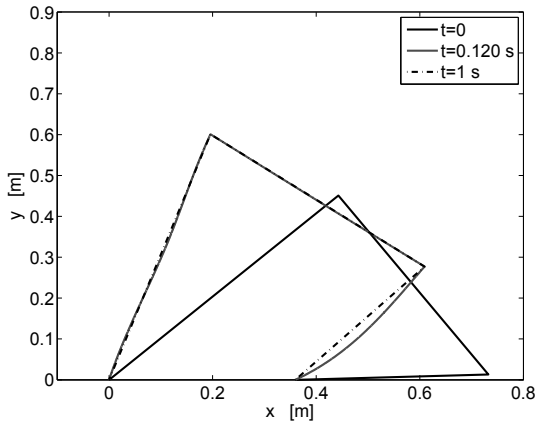

Figure 6.12: Mechanism configurations: initial, during the motion, final. Elastic deformation is displayed with a $\times 10$ gain

calculated using some interpolation functions, are amplified 10 times in order to make links deformation more evident. As it can be seen in Figure 6.12, the largest displacements are the located along the crank, while the vibration along the follower are kept small by the control action.

6.3.4 Robustness

In order to verify the robustness of the proposed control scheme, exhaustive tests have been made. A set of simulations have been made employing the same control system on different perturbed nonlinear model. The purpose of these perturbation is to mimic the effects of uncertainties in the model. A great deal of experimental tests have been made with uncertainties of different sign (i.e. +20%, -20%) on the parameters that have greater influence on the response of the nonlinear model, such as the value of the length of the first link L_1, the linear mass density m of the links, the elastic modulus E. Moreover, further tests have been made by altering the accuracy of the torque provided by the closed-loop control system: in this way the torque fed to the motor differs to both the optimal torque value computed by the MPC controller and the torque used by the state observer to estimate the actual state of the plant. This approach to robustness analysis has been used in other works, such as [167], where different non-nominal plant are employed to show the capabilities of the proposed control over a classical one by means of software simulation tests.

In Figure 6.13 the effects of altering the linear mass density m of all the links belonging to the mechanism are tested. As it can be clearly seen, an underestimation of the linear mass density by the controller does not bring the closed loop to an unstable behavior: when the actual mass of the links is 30% more than the nominal case the response of the system gets more damped. The same variation in the other direction (-30%) of the m parameter does not lead to instability, as it just increases the overshoot of the angular position tracking. In the two perturbed cases the influence on the vibration damping is quite subtle, especially when the transient is over.

The change to the parameter L_1, which represents the length of the first link, can be harmful to the stability of the closed-loop system, as can be seen in Figure 6.14. A 30 % overestimation of the parameter L_1 has little or no effects on the response of the system: in this case the evolution of variables q and u_{10} are the same as the nominal plant's one. In case of a 20 % underestimation of L_1 (here the actual length of the link is 20 % longer than the same link of the modeled plant) the closed-loop system is no more stable: the evolution of the values represented in Figure 6.14 resembles the evolution of an unstable plant.

The closed-loop system retains its performance even in presence of a mismatch between the actual and the estimated elasticity of the links, which is represented by the means of the elastic modulus E. In Figure 6.15 it can be

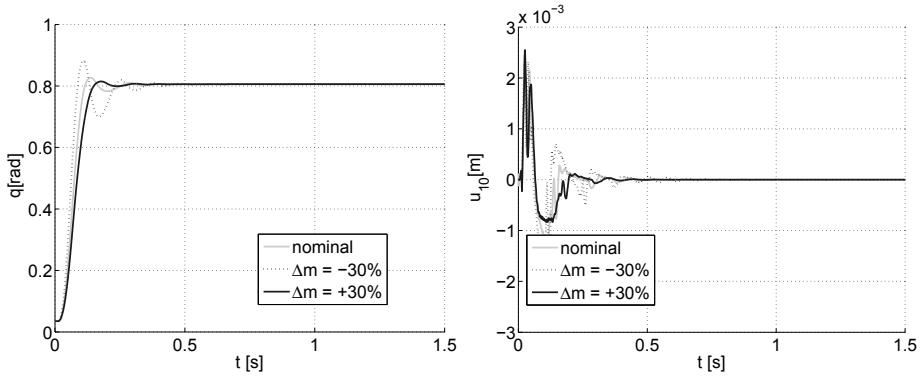

(a) (b)

Figure 6.13: Robustness analysis to the change of linear mass density m. (a) Angular position q. (b) Elastic displacement u_{10} measured in the local reference frame.

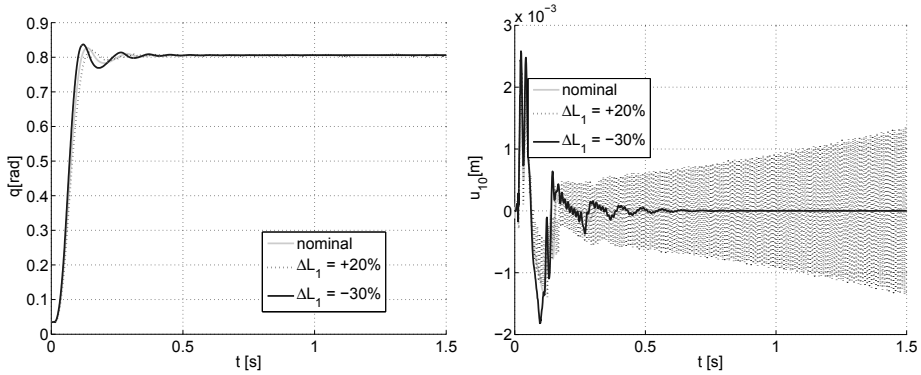

(a) (b)

Figure 6.14: Robustness analysis to the change of length of the first link L_1 (a) Angular position q. (b) Elastic displacement u_{10} measured in the local reference frame.

seen that altering this value of a $\pm$ 30 % factor does not affect the performance of the control system: this means that the proposed controller is robust to a change of the vibration modes of the plant.

In Figure 6.16 the effects of a gain error in the estimation of the applied torque is tested. As can be seen in Figure 6.16 the performance of the closed-loop system are almost not affected by a $\pm$30 % factor. In case of an overestimation

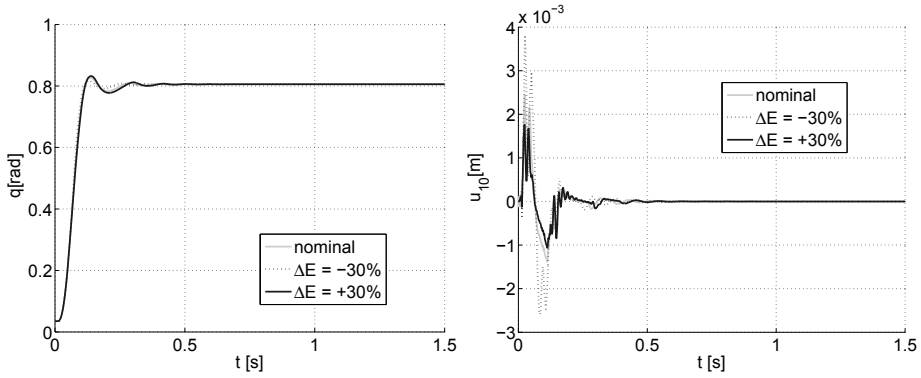

(a) (b)

Figure 6.15: Robustness analysis to the change of elastic modulus E (a) Angular position q. (b) Elastic displacement u_{10} measured in the local reference frame.

of the applied torque (the actuator provides less torque than the desired one) the response of the system is slower. When the torque is underestimated by the observer and by the control system, the closed-loop response has more overshoot but the plant remains stable.

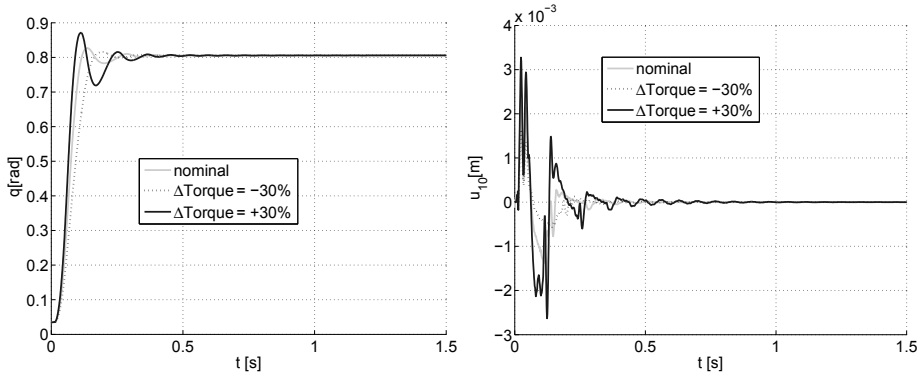

(a) (b)

Figure 6.16: Robustness analysis to the change of applied torque: (a) Angular position q. (b) Elastic displacement u_{10} measured in the local reference frame.

In Figure 6.17 the results of three tests are displayed in the same graphs: the nominal plant is first controlled with the nominal torque, then a + 30 % gain error is introduced, then also an additive white gaussian noise is added to

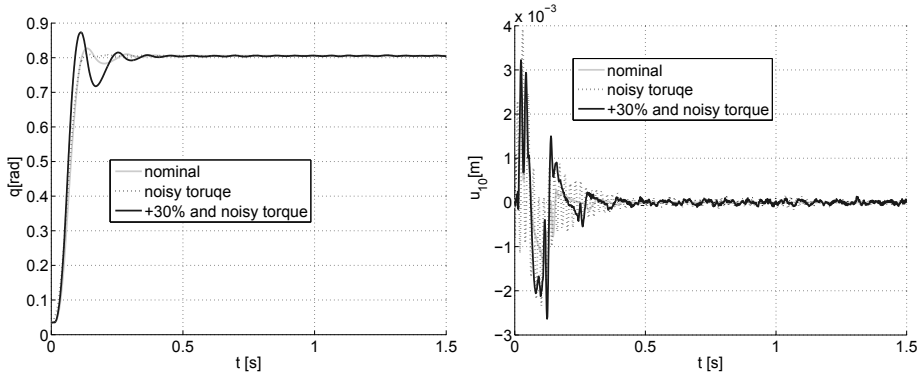

(a) (b)

Figure 6.17: Robustness analysis to the change of applied torque and noisy torque: (a) Angular position q. (b) Elastic displacement u_{10} measured in the local reference frame.

the torque. Again, the MPC controller shows its robust behavior: even when noise is added the response of the system has just a small degradation of the performances.

6.4 Effects of H_c, H_p and f_c on the closed-loop system

In this section the effects of choosing different values for the tuning parameters of the MPC controlled are investigated by the means of simulation tests. In Figure 6.18 the effectiveness of the controller is evaluated for different values of the sampling frequency of the control system, in order to test the effects of using a control system with less computational demands. It can be seen that the performance of the system are less satisfactory for f_c=100 Hz. This performance reduction might be due to the the lesser efficacy of the system observer at lower frequency, since this has been tuned for a 1 ms refresh time.

In Figure 6.19 the effects of choosing different control horizon is investigated: it can be seen that this tuning parameter has a limited effect on the response of the closed-loop system. In particular reducing the control horizon H_p to 5 introduces a small degradation of the performances: the overshoot is slightly increased and the transient response is a little slower. H_c can be increased up to the length of the prediction horizon (here $H_p = 55$) but this choice does not

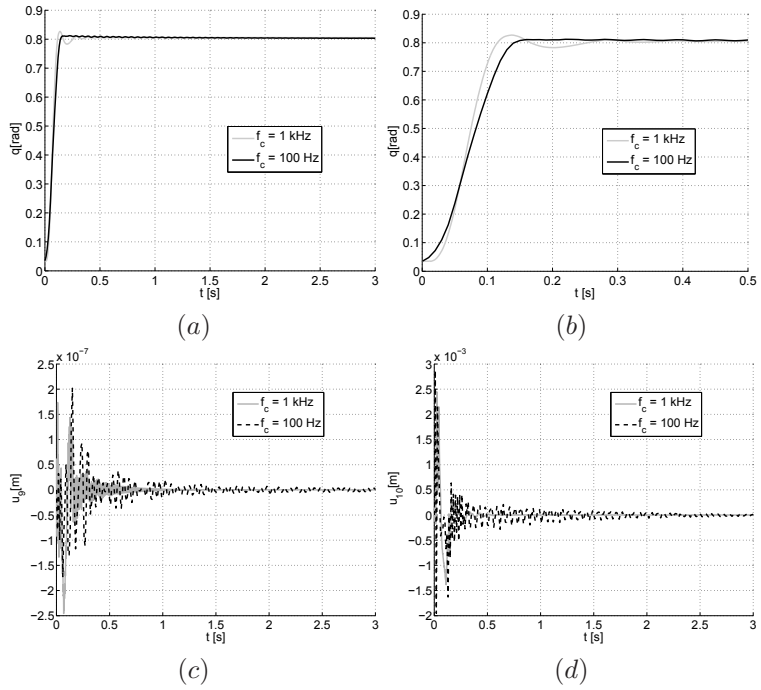

Figure 6.18: Response of the control system at with different sampling frequency: 1 Khz and 100 Hz(a) Angular position q. (b) Angular position q: zoom view (c) Elastic displacement u_{10} measured in the local reference frame (d) Elastic displacement u_9 measured in the local reference frame.

improve the performances of the controller. In practical situations H_c should be kept quite small, since a longer control horizon increases the computational weight of the minimization problem solved by the MPC controller.

Changing the length of the prediction horizon H_p has little or no effects on the performance of the controller when dealing with a nominal plant, since it affects mainly the robustness of the closed-loop system. Here some results on a perturbed plant are presented, just to show that a longer prediction horizon can be used to increase the robustness of the controller. In Figure 6.20 the results of a set of experimental test are presented: the original control system (with H_p=55 and H_c=15) is employed to control a plant with some parametric mismatches: in the model used for prediction there is a 10 % overestimation of the length of the first link L_1, a 30 % overestimation of the linear mass density of the links m and of the Young's modulus E, while the torque actually applied to the plant is 30 % more than the desired one. It can be seen that this perturbed

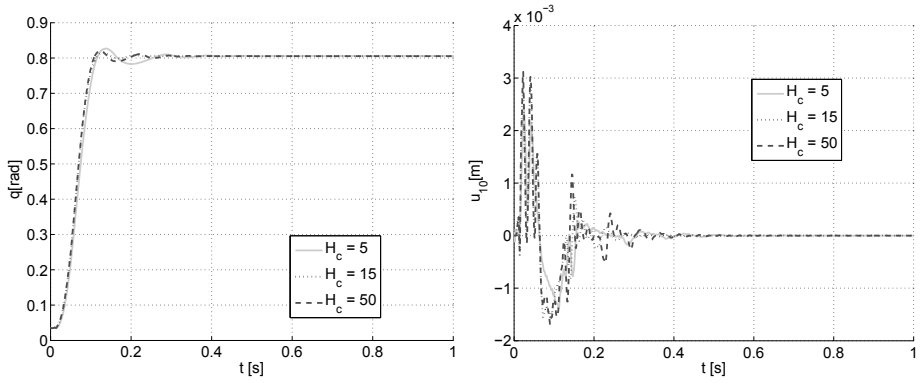

(a) (b)

Figure 6.19: Analysis of the effects of different control horizon H_c: (a) Angular position q. (b) Elastic displacement u_{10} measured in the local reference frame.

plant is no more stable when the prediction horizon is H_p=55. By increasing this value (in Figure 6.20 the results are presented for H_p=155 and H_c=255) stability and good performance can be obtained. It should also be noticed that increasing the prediction horizon has less effects on the increasing of the overall computational weight required by the MPC controller than the increasing of the control horizon H_c.

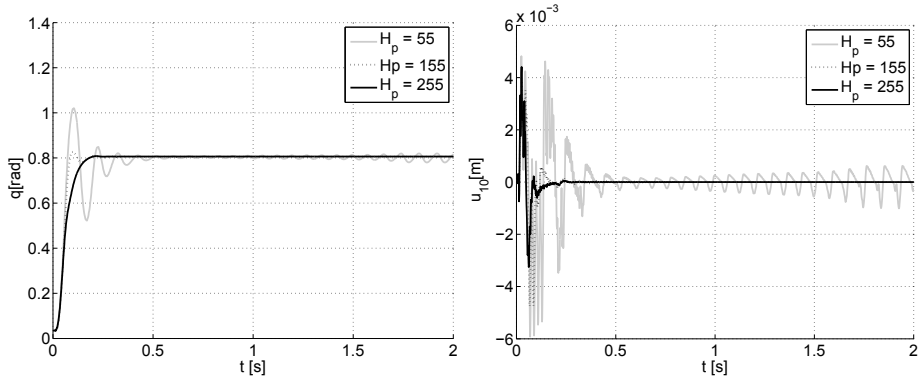

(a) (b)

Figure 6.20: Analysis of the effects of different prediction horizon H_p on a perturbed version of the plant: (a) Angular position q. (b) Elastic displacement u_{10} measured in the local reference frame.

6.4.1 Position Control (PID): simulation results

Here a PID control is implemented and tested: the simulation results are used to compare the proposed MPC controller with a traditional and commonly used control technique. The target of the tuning of the PID is to move the mechanism at the same speed that can be obtained with the MPC controller. This is because the maximum amplitude of the vibration phenomena are directly proportional to the moving speed of the mechanism.

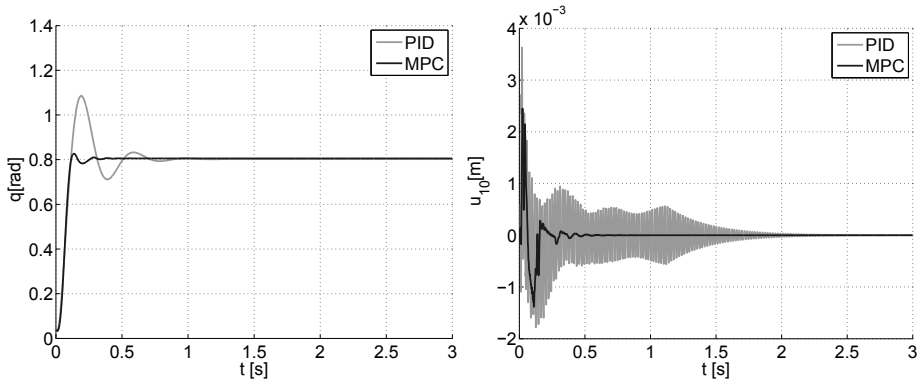

Figure 6.21: Comparison of the response of the system with PID and MPC control. (a) Angular position q. (b) Elastic displacement u_{10}.

As it can be seen in Figure 6.21 PID control has a very subtle effects on vibration damping in a four-link mechanism. Looking at Fig. 6.21 it can be seen that PID allows the mechanism to follow with high speed and no permanent error the reference trajectory, but a noticeable overshoot (≈ 35 %) is still present. This overshoot phenomenon can be eliminated, but at the cost of reducing the rise time of the system, namely decreasing the overall speed of the mechanism. A comparison of the effective time required to keep the vibration under certain tresholds are presented in Table 6.2, but it also can be clearly seen from 6.21.b that the MPC controller has a superior vibration reduction capability.

Comparison of effective vibration damping

Here a comparison of the damping effects obtained with the PID control, the MPC controller with $f_c = 1kHz$ and the MPC controller with $f_c = 100Hz$ is presented. Considering the time required to keep transverse displacement inside

Table 6.2: Comparison of vibration damping times and % overshoot

Controller	$\lvert\Delta u_{10}\rvert < 1mm$	$\lvert\Delta u_{10}\rvert < 0.1mm$	$\lvert\Delta u_{10}\rvert < 0.02mm$	overshoot %
PID	244 ms	1860 ms	3215 ms	34.74
MPC @ 1 kHz	119 ms	294 ms	480 ms	2.54
MPC @ 100 Hz	140 ms	1530 ms	2645 ms	0.7

a ± 1 mm, both MPC behave considerably better than the PID: this requires a 244 ms to respect this limit, while the two MPC need only 119 ms and 140. Then, PID takes 1.86 s to reduce vibration below 0.1 mm and 2.65 s to get under 0.02 mm, while the "slow" MPC requires respectively 1.53 s and 2.645 s. The best performances can be obtained with the MPC operating at 1 kHz: 294 ms after the reference step u_{10} is kept below 0.1 mm and after a mere 480 ms below 0.02 mm. PID has 34.74 % overshoot, which can be unaxceptable in some practical situations. The "fast" MPC has a mere 2.54 % overshoot, meanwhile the slower MPC has even less overshoot (0.7 %), but it should be pointed out that the slow MPC controller has also a slightly slower rise time than the MPC operating at 1 kHz.

Conclusion

A high accuracy FEM-based dynamical model of a four-bar flexible link mechanism has been presented in this section. This model has been employed in software simulation environment to investigate the effectiveness of MPC control strategy for vibration damping in flexible closed-loop planar mechanisms. In order to implement the control system, a linearized model of the dynamic system has been developed. This linearized state-space model is capable of a high precision approximation of mechanism dynamic behavior, on both position and vibration dynamics. A constrained Model Predictive Control (MPC) system has been employed to control both the angular position and the vibrations of the mechanism. The optimal performance have been tested on the nominal plant, meanwhile a robustness analysis has been conducted by the means of exhaustive tests conducted on different perturbed plants. The performances of this control systems have been then compared to the ones that can be obtained trough a standard PID control. MPC control has proved to be very effective both for reference position tracking and vibration suppression, and has exposed a good level of robustness to uncertainties on the plant and to mismatches between the actual and the measured control variable.

6.5 Trajectory tracking and vibration suppression in a 5-link mechanism

In this section the system under investigation is a 5-bar linkage controlled with an MPC controller. The aim of this study is to make the mechanism move the end-effector of the mechanism along a predefined trajectory. In particular, extensive simulation results are presented to show precisely how the main tuning parameters of the MPC controller (H_p and H_c) influence the trajectory tracking of the closed-loop system. Also a reference lookahead strategy is implemented, and the advantages brought by this choice are shown trough simulations. Tracking in the joint space is investigated as well.

6.5.1 Reference mechanism

The mechanism under consideration is the two dofs manipulator shown in Figure 6.22, carried out at the Mechatronics Laboratory. It is made up of four steel rods connected in a closed-loop chain by using five revolute joints. The motion of the cranks (namely the first and the fourth link counting anti-clockwise) is governed by two torque-controlled actuators. The ground link can be considered to be perfectly rigid without affecting the accuracy of the model. The mechanical characteristics of the mechanism are shown in Table 6.1. As it can be seen, the links are very thin (their square section is just 6 mm wide) so the whole mechanism is quite prone to vibration.

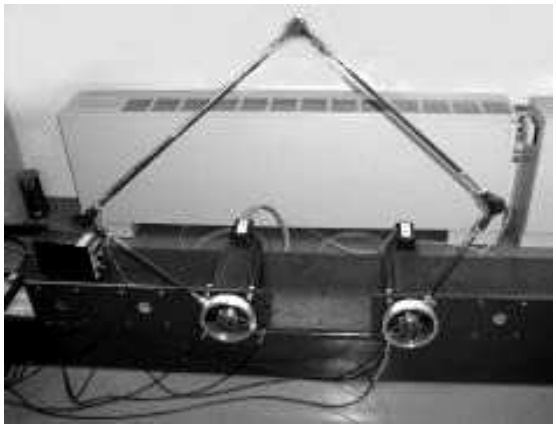

Figure 6.22: Five-link manipulator (Mechatronics Lab, University of Udine)

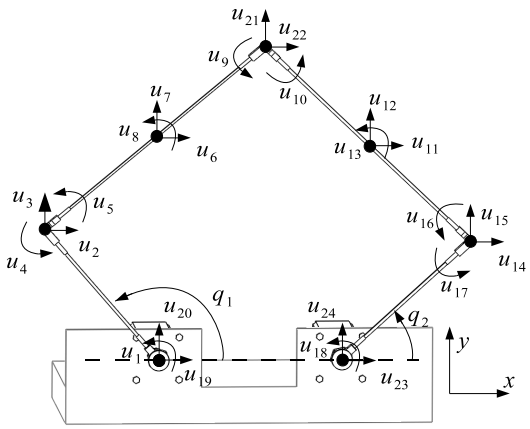

Figure 6.23: Elastic displacements and angular position in the five-link mechanism

The second and the third link have been modeled with two beam elements, since they are the longest. Increasing the number of finite elements in each link will certainly improve the overall accuracy of the model, however this also increases the computational effort required to execute the simulations. Each link that has been modeled with a single-beam element has 6 elastic degrees of freedom, whereas the 2 finite-element link has 9 degrees of freedom. The overall FEM model is described by 24 nodal displacements, as it can be seen in Figure 6.23. However, in order to make solvable the dynamic system in eq. (2.80), nodal displacements from u_{19} to u_{24} must be forced to zero, see [1]. Therefore, the overall motion of the mechanism is described by 18 nodal elastic displacements ($\mathbf{u} = [u_1, u_2, \ldots, u_{18}]^T$) and two rigid degrees of freedom ($\mathbf{q} = [q_1, q_2]^T$).

Table 6.3: Kinematic an dynamic characteristics of the flexible link mechanism

	symbol	value
Young's modulus	E	200×10^9 [Pa]
Flexural inertia moment	J	1.08×10^{-10} $[m^4]$
Beams width	a	6×10^{-3} [m]
Beams thickness	b	6×10^{-3} [m]
Mass/unit of length of links	m	0.282 $[kg/m]$
Length of first link	L_1	0.3 [m]
Length of second link	L_2	0.6 [m]
Length of third link	L_3	0.6 [m]
Length of fourth link	L_4	0.3 [m]
Ground length	L_5	0.3 [m]
Rayleigh damping constants	α	8.72×10^{-2} $[s^{-1}]$
	β	2.1×10^{-5} [s]

6.5.2 Linearized model

The dynamic model in eq. (2.80) is nonlinear, since matrix $\dot{\mathbf{S}}$ contains the values of the velocities $\dot{\mathbf{q}}$ of the free coordinates (i.e. $\dot{\mathbf{S}} = \dot{\mathbf{S}}(\dot{\mathbf{q}}, \mathbf{q})$), which yield a quadratic term $\dot{\mathbf{q}}^2$ in the velocities of the free coordinates, see [166]. As such, it cannot be used as a prediction model for linear MPC controllers. In order to obtain a linear version of the dynamic system, the linearization procedure developed by Gasparetto in [166] has been followed. From the basics of system theory, a linear time-invariant model expressed in state-space form can be written as:

$$\begin{cases} \dot{\mathbf{x}}(t) = \mathbf{F}_{lin}\mathbf{x}(t) + \mathbf{G}_{lin}\mathbf{w}(t) \\ \mathbf{y}(t) = \mathbf{H}_{lin}\mathbf{x}(t) \end{cases} \tag{6.10}$$

where $\mathbf{x}(t)$ is the state vector, $\mathbf{y}(t)$ is the output vector, $\boldsymbol{w}(t)$ represents the input vector and $\mathbf{F}_{lin}$, $\mathbf{G}_{lin}$ and $\mathbf{H}_{lin}$ are time-invariant matrices. The input $\mathbf{w}(t)$ for the system is a vector that includes the torques applied to the first and the fourth link: $\mathbf{w}(t) = [\tau_1, \tau_2]^T$, being τ_1 and τ_2 the torques provided by the actuators. The state vector is $\mathbf{x}(t) = [\dot{u}_1, \ldots, \dot{u}_{18}, \dot{q}_1, \dot{q}_2, u_1, \ldots, u_{18}, q_1, q_2]^T$. The output vector is $\mathbf{y}(t) = [u_1, u_{18}, q_1, q_2]^T$, since this is the subset of the state that is available to the control system as measured variables. In practical applications, u_1 and u_{18} are measured by means of strain gauges, while q_1 and q_2 can be measured by using rotary encoders.

Equation (2.80) can be written in the following form:

$$\mathbf{A}(\mathbf{q}, \dot{\mathbf{q}}, t)\dot{\mathbf{x}}(t) = \mathbf{B}(\mathbf{q}, \dot{\mathbf{q}}, t)\mathbf{x}(t) + \mathbf{C}(\mathbf{q}, \dot{\mathbf{q}}, t)\mathbf{w}(t) \tag{6.11}$$

to point out that the matrices involved in eq. (6.11) are time-variant and they depend also on $\mathbf{q}$ and $\dot{\mathbf{q}}$, i.e. the position and the velocity of the degrees of freedom. Matrices $\mathbf{A}(\mathbf{q}, \dot{\mathbf{q}}, t)$, $\mathbf{B}(\mathbf{q}, \dot{\mathbf{q}}, t)$ and $\mathbf{C}(\mathbf{q}, \dot{\mathbf{q}}, t)$ can be linearized around an equilibrium point $\mathbf{x}_e$, yielding from eq. (6.12) to eq (6.13):

$$\mathcal{A}_{lin}\dot{\mathbf{x}}(t) = \mathcal{B}_{lin}\mathbf{x}(t) + \mathcal{C}_{lin}\mathbf{w}(t) \tag{6.12}$$

After some steps that can be found in detail in [166], $\mathcal{A}_{lin}$ and $\mathcal{B}_{lin}$ in Eq. (6.12) can be written as:

$$\mathcal{A}_{lin} = \begin{bmatrix} \mathbf{M} & \mathbf{MS} & \mathbf{0} & \mathbf{0} \\ \mathbf{S}^T\mathbf{M} & \mathbf{S}^T\mathbf{MS} & \mathbf{0} & \mathbf{0} \\ \mathbf{0} & \mathbf{0} & \mathbf{I} & \mathbf{0} \\ \mathbf{0} & \mathbf{0} & \mathbf{0} & \mathbf{I} \end{bmatrix}_{\mathbf{x}=\mathbf{x_e}} \tag{6.13}$$

$$\mathcal{B}_{lin} = \left[\begin{array}{cccc} -2\mathbf{M}_G - \alpha\mathbf{M} - \beta\mathbf{K} & \mathbf{0} & -\mathbf{K} & \mathbf{0} \\ \mathbf{S}^T(-2\mathbf{M}_G - \alpha\mathbf{M} - \beta\mathbf{K}) & \mathbf{0} & \mathbf{0} & \mathbf{0} \\ \mathbf{I} & \mathbf{0} & \mathbf{0} & \mathbf{0} \\ \mathbf{0} & \mathbf{I} & \mathbf{0} & \mathbf{0} \end{array} \right]_{\mathbf{x}=\mathbf{x_e}} \tag{6.14}$$

$$\mathcal{C}_{lin} = \left[\begin{array}{c} \mathbf{I} \\ \mathbf{S^T} \\ \mathbf{0} \\ \mathbf{0} \end{array} \right]_{\mathbf{x}=\mathbf{x_e}} \tag{6.15}$$

So equation (2) can be rewritten in terms of $\mathcal{A}_{lin}$, $\mathcal{B}_{lin}$ and $\mathcal{C}_{lin}$ as:

$$\left\{ \begin{array}{l} \dot{\mathbf{x}}(t) = \mathcal{A}_{lin}^{-1}\mathcal{B}_{lin}\mathbf{x}(t) + \mathcal{A}_{lin}^{-1}\mathcal{C}_{lin}\mathbf{w}(t) \\ \mathbf{y}(t) = H_{lin}\mathbf{x}(t) \end{array} \right. \tag{6.16}$$

State observer

The algorithm used by the MPC requires the whole state vector $\mathbf{x}$ be available at every iteration of the controller. Since in practical situations it is impossible to measure all the 18 nodal displacements that belong to the state vector, a state observer must be used. As already done to produce the results presented in the previous section, a Kalman asymptotic estimator has been used. An estimation of $\mathbf{x}(k)$ and $\mathbf{x}_m(k)$ (where $\mathbf{x}(k)$ is the state of the plant model and $\mathbf{x}_m(k)$ is the state of the measurement noise model) can be computed from the measured output $\mathbf{y}(k)$ through:

$$\left\{ \begin{array}{l} \left[\begin{array}{c} \hat{\mathbf{x}}(k|k) \\ \hat{\mathbf{x}}_m(k|k) \end{array} \right] = \left[\begin{array}{c} \hat{\mathbf{x}}(k|k-1) \\ \hat{\mathbf{x}}_m(k|k-1) \end{array} \right] + \mathcal{M}(\mathbf{y}(k) - \hat{\mathbf{y}}(k)) \\ \\ \left[\begin{array}{c} \hat{\mathbf{x}}(k+1|k) \\ \hat{\mathbf{x}}_m(k+1|k) \end{array} \right] = \left[\begin{array}{c} \mathbf{F}\hat{\mathbf{x}}(k|k) + \mathbf{F}_w\mathbf{w}(k) \\ \tilde{\mathbf{F}}\hat{\mathbf{x}}_m(k|k) \end{array} \right] \\ \\ \hat{\mathbf{y}}(k) = \mathbf{H}\hat{\mathbf{x}}(k|k-1) \end{array} \right. \tag{6.17}$$

$\mathcal{M}$, $\mathbf{F}_w$, $\tilde{\mathbf{F}}$ have been designed using Kalman filtering techniques. In this way, the state observer can give an accurate estimation of the full state $\mathbf{x}$ from the knowledge of u_1, u_{18}, q_1 and q_2. This observer presents a very high level of accuracy: some results that prove its performances are shown in Figures (6.25 - 6.27). The results shown in this graph have been derived by stimulating the nonlinear plant with the impulsive torques, as shown in Figure 6.24. These graphs compare the actual nodal displacement and angular positions with their estimated values.

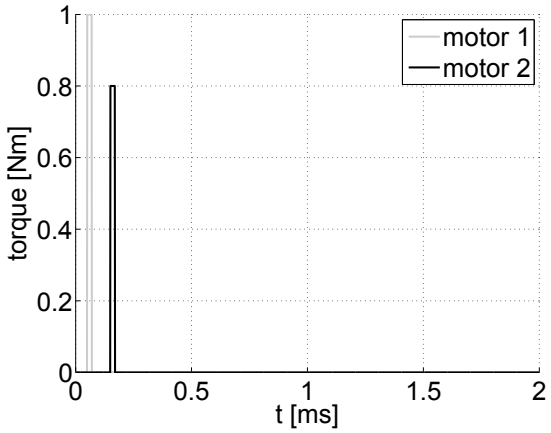

Figure 6.24: Torques applied to derive plots in Figures 6.25, 6.26, 6.27

Here the results are shown only for two rigid rotations and one nodal displacement, but the likeness holds also for all the other nodal displacements belonging to the state vector.

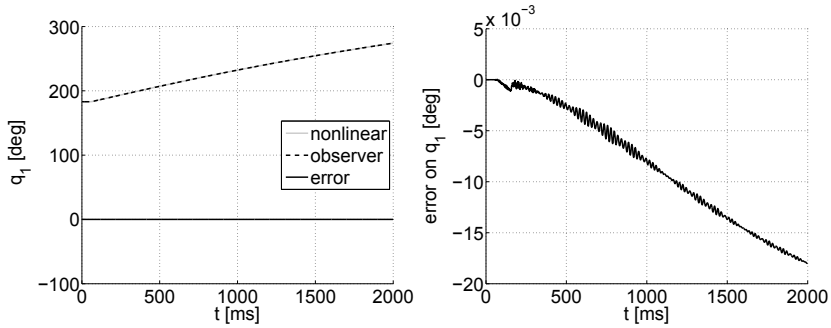

(a) (b)

Figure 6.25: (a) Comparison of actual and estimated angular position, estimation error for q_1 (b) absolute error on q_1

6.5.3 MPC control: numerical results of trajectory tracking in the joints space

In this section the effectiveness of the proposed control strategy for simultaneous path following and vibration reduction will be demonstrated and discussed, by showing the results of several simulations obtained in MATLAB/Simulink environment. The effectiveness of the MPC controller as a regulator has already

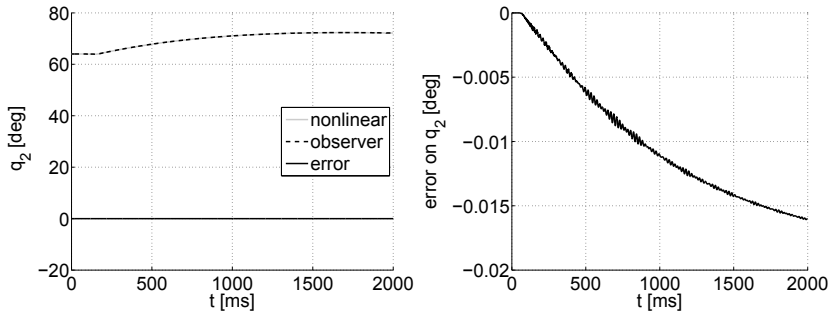

(a) (b)

Figure 6.26: (a) Comparison of actual and estimated angular position, estimation error for q_2 (b) absolute error on q_2

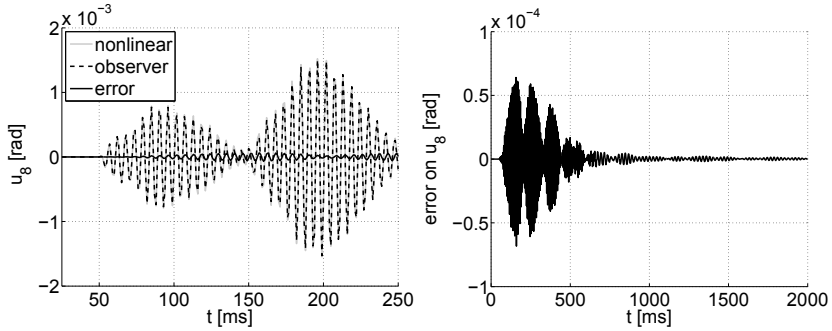

(a) (b)

Figure 6.27: (a) Comparison of actual and estimated nodal displacement, estimation error for u_8 (b) absolute error on u_8

been proven in [103], [105], but here the focus moves from regulation problem to tracking problem. Moreover, it should be pointed out that the problem of position control in a multi dofs system is non-trivial, since a lack of synchronization between the motion of the axis leads to severe worsening to the accuracy. For this reason, a reference lookahead strategy has been included in the predictive control, and the effective improvement is shown. Effects of different choices for some of the tuning parameters of the controller, namely the two horizons H_p and H_c, are investigated in terms of accuracy of reference tracking and vibration damping by the means of extensive sets of simulations.

To test the capabilities of the MPC controller for both position control and vibration damping, some tests have been conducted feeding the controller with two reference signals for q_1 and q_2, as they can be seen in Figure 6.30. In

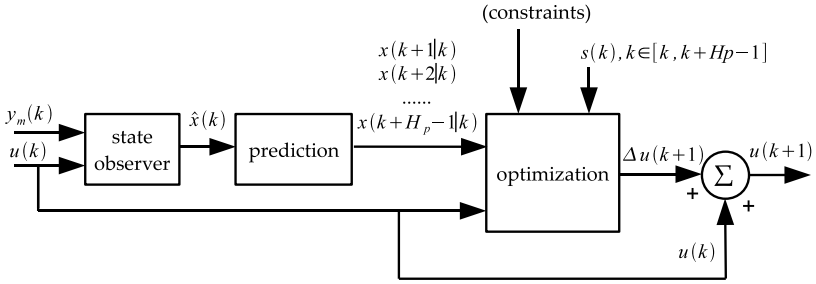

Figure 6.28: Structure of the MPC controller

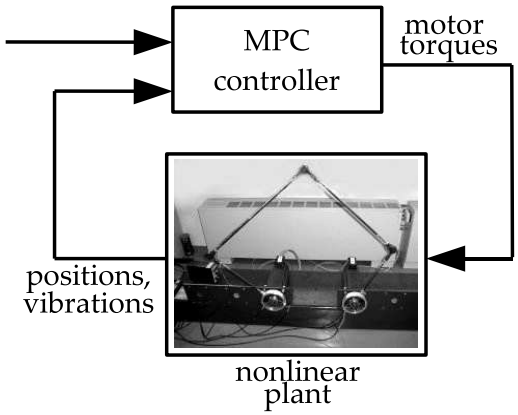

Figure 6.29: Closed-loop system

these tests, the mechanism performs two high-speed rotation of the first and the fourth link: q_1 rotates of 45 degrees, while q_2 rotates of 30, degrees in 500 ms. As it can be seen in Figure 6.30, the closed-loop system exhibits optimal performances: the reference tracking is very good and has almost no delay. The torques provided by the two actuators are displayed in Figure 6.31. In Figure 6.30, it can be seen that the closed-loop system damps very efficiently the vibration that arises in the mechanism when the two angular position q_1 and q_2 have discontinuous velocities and accelerations.

6.5.4 Effects of the reference lookahead and control tuning

The promptness in reference tracking exhibited in Figure 6.30 is heavily influenced by the reference lookahead system used by the MPC controller. As already stated in Eq. (18), the optimal control sequence is calculated ad every iteration

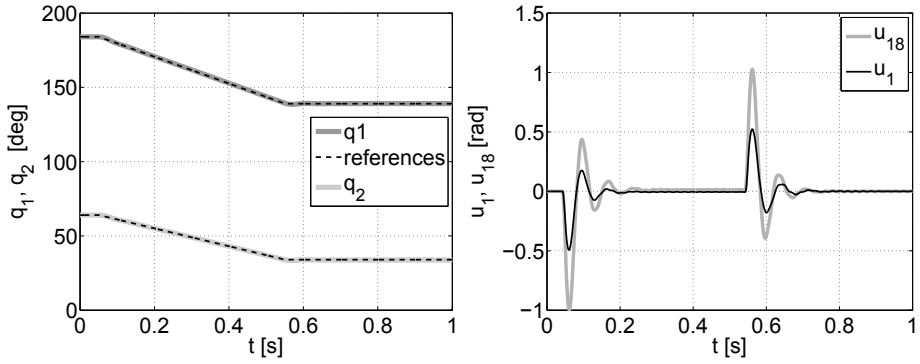

(a) (b)

Figure 6.30: Closed-loop performances: (a) evolution of angular positions q_1 and q_2 (b) angular displacements u_1 and u_{18} for reference tracking in the operational space

in order to minimize (also) the quadratic norm $\|\mathcal{Z}(k) - \mathcal{T}(K)\|^2$, which is the quadratic norm of the tracking error, i.e. of $\mathcal{E}(k) = \mathcal{Z}(k) - \mathcal{T}(K)$, in which $\mathcal{Z}(k)$ and $\mathcal{T}(k)$ are the evolution of controlled outputs and the reference from actual time k to $k + H_p$.

When reference look-ahead is not implemented, the future reference values are estimated simply by: $r(k+i) = r(k)\ \forall i \in [1, H_p - 1]$, so $\mathcal{T}(k) = r(k)$, which is the exact prediction only for constant or step-changing reference signals. The enhancing in terms of reference tracking obtainable with reference lookahead can be seen in Figure 6.32: the same test presented in Figure 6.30 is here compared with the results obtained without reference lookahead. It can be seen that the adoption of a lookahead strategy reduces the delay of the response. This effects is even more evident when the change rate of the reference trajectory and the prediction horizon are increased.

The tuning of the MPC controller is also influenced by the values of the weights used in the minimization problem (see eq. 17) as the diagonal entries of matrices $\mathbf{Q}$ and $\mathbf{R}$. These weights are:

- w_{τ_1} and w_{τ_2}: weights on the two torques applied to the first and the third link, respectively
- $w_{\delta\tau_1}$ and $w_{\delta\tau_2}$: weights on the change rate of the two torques applied to the first and the third link, respectively
- w_{u_1}, $w_{u_{18}}$: weights on the two controlled nodal displacements u_1 and u_{18},

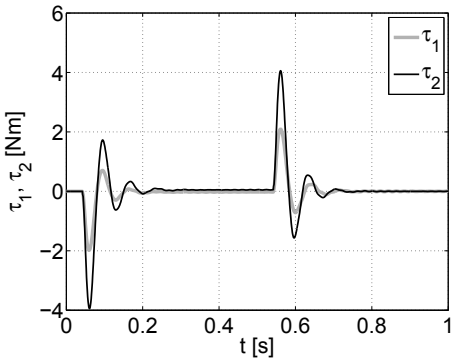

Figure 6.31: Closed-loop performances: torques τ_1 and τ_2 applied by the two actuators

respectively

- w_{q_1}, w_{q_2}: weights on the angular positions q_1 and q_2, respectively

Then, the behavior of the controller depends also on the length of the two horizons: the prediction horizon H_p and the control horizon H_c. For all the tests conducted, the sampling frequency is $T_s = 1$ ms. The tuning for the test shown in Figures 6.30,6.31,6.32 is: $w_{\tau_1} = w_{\tau_2} = w_{\delta\tau_1} = w_{\delta\tau_2} = 0.1$; $w_{u_1} = 3000$, $w_{u_{18}} = 2000$, $w_{q_1} = 4000$, $w_{q_2} = 7000$, $H_p = 10$, $H_c = 5$.

Influence of the control horizon H_c on closed-loop performance

In oder to show how the choice of the control horizon and the prediction horizon affects the closed-loop response, extensive sets of simulations have been conducted. A few results are displayed in Figures 6.33 and 6.34, in which the effects of altering only the length of the control horizon are reported. From Figure 6.33 it can be seen that altering the control horizon has a limited effect on the reference tracking of the two angular positions q_1 and q_2: with lower values of H_c the angular movement appears to be slightly less accurate. The parameter H_c influences mainly the readiness of the system in terms of vibration reduction: as can be inferred from Figure 6.34 the choice of higher values of the control horizon lead to higher vibration peak but with a more fast damping. This effect can be thought as a higher gain of the controller. Results are shown with H_c up to 5, since further increase does lead to little or no improvements.

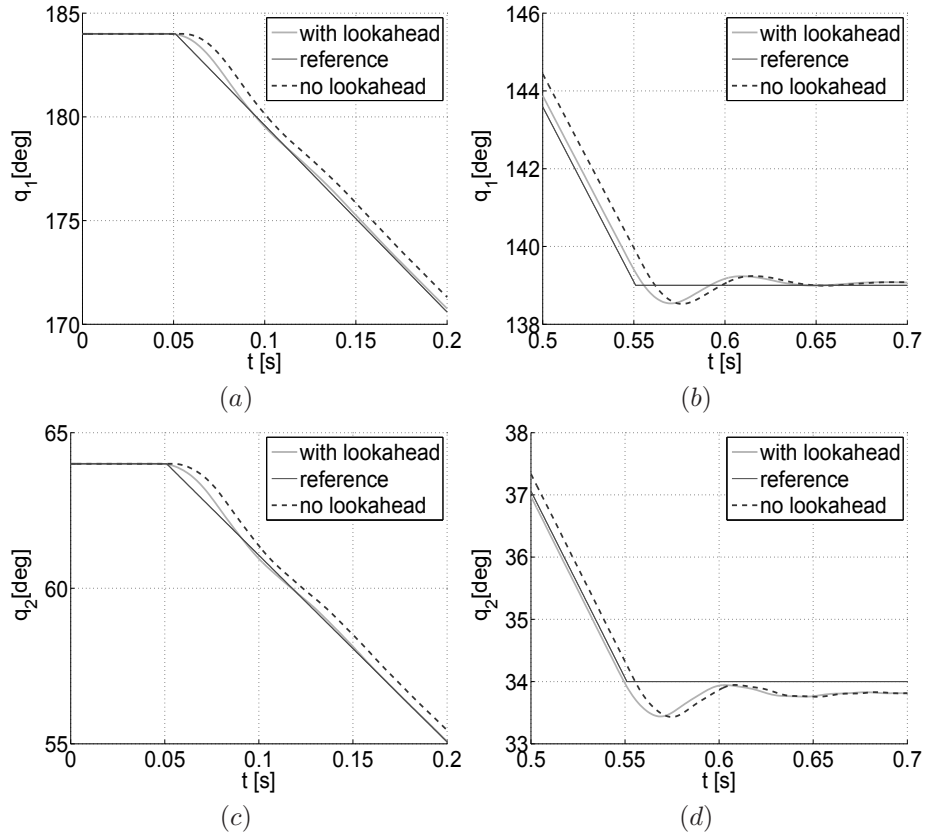

Figure 6.32: Comparison of reference tracking with and without reference lookahead (a),(b) angular position q_1 (c),(d) angular position q_2

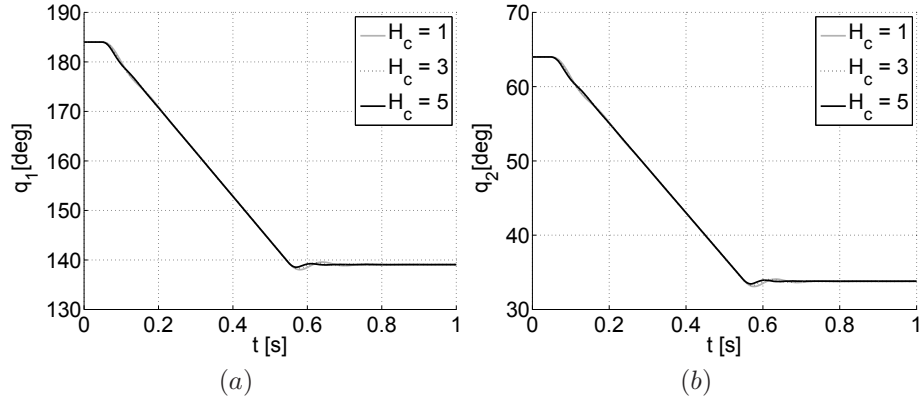

Figure 6.33: Effects of different values of the control horizon H_c ($H_p = 10$): (a) angular position q_1 of the first link (b) angular position q_2 of the fourth link

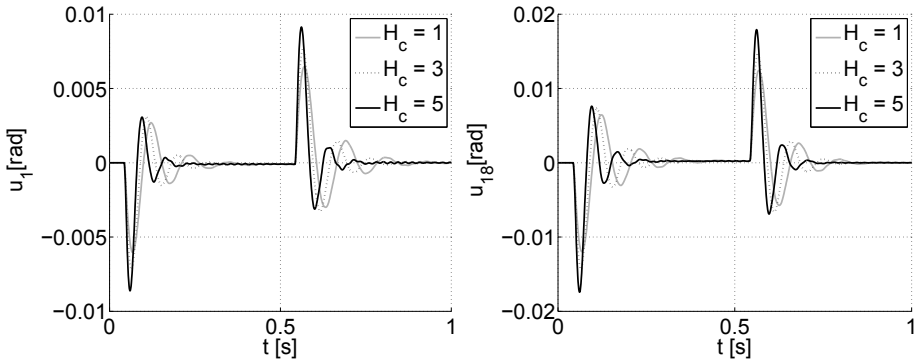

(a) (b)

Figure 6.34: Effects of different values of the control horizon H_c ($H_p = 10$): (a) angular displacement u_1 along the first link (b) angular displacement u_{18} along the fourth link

Influence of the prediction horizon H_p on closed-loop performance

In Figures 6.35 and 6.36 the effects of altering the prediction horizon H_p are shown. From those graphs it can be inferred that H_p influences mainly the damping performances of the closed-loop system. From Figure 6.35, that vibration of u_1 and u_{18} require more time to be damped when choosing shorter H_p. At the same time, the reference tracking of q_1 and q_2 is more accurate when H_p is higher. Here the results are shown with H_p up to 20, since it has been proven that the performance enhancing is very slight when going beyond this threshold.

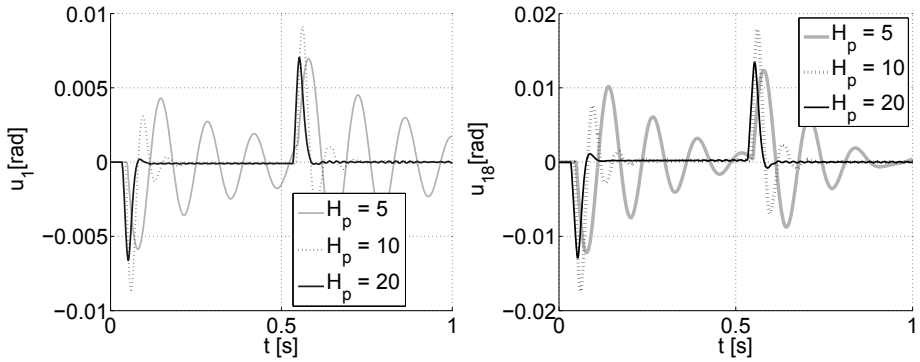

(a) (b)

Figure 6.35: Effects of different values of the prediction horizon H_p ($H_c = 10$): (a) angular displacement u_1 (b) angular displacement u_{18}

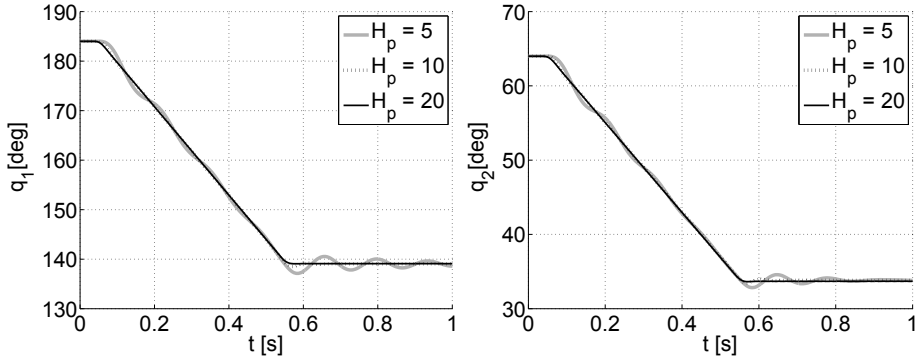

(a) (b)

Figure 6.36: Effects of different values of the prediction horizon H_p ($H_c = 10$): (a) angular position q_1 of the first link (b) angular position q_2 of the fourth link

The previous observations can be summarized by the graphs in Figure 6.37, which report the results of several simulations obtained by changing the values of the prediction and control horizons. A large number of tests have been conducted by performing the same tests whose results are displayed in Figures 10 and 11, but here the prediction horizon ranges from 3 to 20, and the control horizon ranges from 1 to H_p, since it makes no sense to set $H_p > H_c$. All the values of the other parameters of the controller are kept the same as the previous simulations. For sake of simplicity, two indices have been defined, as follows:

$$\begin{aligned} k_1 &= \|\Delta\mathbf{q}(t)\|_\infty \\ k_2 &= \|\Delta\mathbf{q}(t)\|_\infty \quad with \quad t \in [0.9s, 1s] \end{aligned} \tag{6.18}$$

being $\Delta\mathbf{q}(t)$ the tracking error, i.e. $\Delta\mathbf{q}(t) = \|\mathbf{q}_D(t) - \mathbf{q}(t)\|$, in which $\mathbf{q}_D(t) = [q_{1D}(t), q_{2D}(t)]$ and $\mathbf{q}(t) = [q_1(t), q_2(t)]$ are the desired and actual angular positions of the cranks, respectively. The index k_1 describes the infinity norm of the quadratic error. Namely, it measures the error (evaluated in the joint space) between the desired and the actual position of the controlled cranks, while the index k_2 is defined as the infinity norm of the tracking error at the end of the test. Therefore it is closely related to the steady-state error. As it can be inferred by comparing the two graphs, the value of H_p affects in different ways the mentioned indices.

In Figure 6.37a it can be seen that the maximum path error can be minimized by choosing $H_p = 14$ and $H_c > 4$. It can also be noticed that the maximum tracking error is highly sensitive to the prediction horizon, as long as the ratio between H_c and H_p is sufficiently high. In Figure 6.37b the value of performance index k_2 is plotted versus H_p and H_c: it can be seen that, in order to reduce the steady-state error, H_p should be chosen to be around 7. Again, H_c has less influence than H_p on the performances of the closed-loop system when position accuracy is the main concern.

6.5.5 Evaluation of robustness

Exhaustive numerical tests have been conduced to test the robustness of the controller to mismatches between the plant and its model used for prediction and observation. This approach to robustness evaluation has been employed in other papers, such as [168, 105]. Simulation results show that the MPC controller can withstand severe plant-model parametric mismatches. In Figures 6.38 and 6.39 the response of the nominal plant is compared to the response of two different

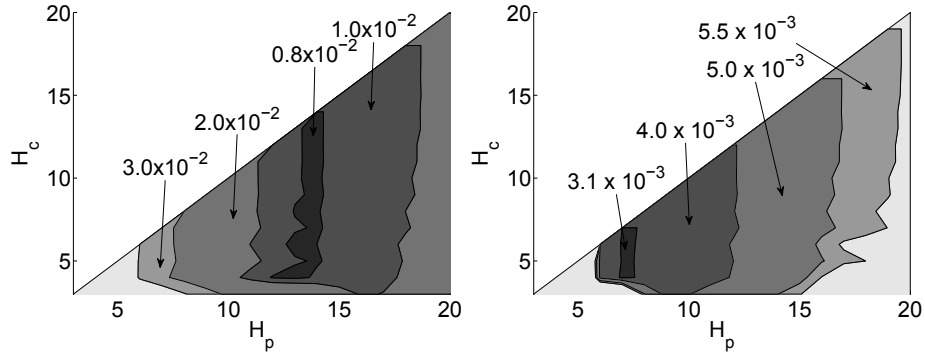

(a) (b)

Figure 6.37: Effects of different values of H_p and H_c: (a) performance index k_1 (b) performance index k_2

mismatched plants. In the perturbed plant, some fundamental parameters have been changed, such as the elastic modulus E and the linear mass density m of the links. Moreover two uncorrelated noise signals have been added to the torques. These two noisy disturbance act as severe unmeasured noises, since the state observer cannot measure them. The three plotted simulation in Figures (6.38,6.39) refer to: (1) plant with E and m reduced by 20%, uncorrelated torque noise with PSD = 1 $\times 10^{-4}$; (2) plant with E and m increased by 20%, uncorrelated torque noises with PSD = 1 $\times 10^{-4}$; (3) nominal plant.

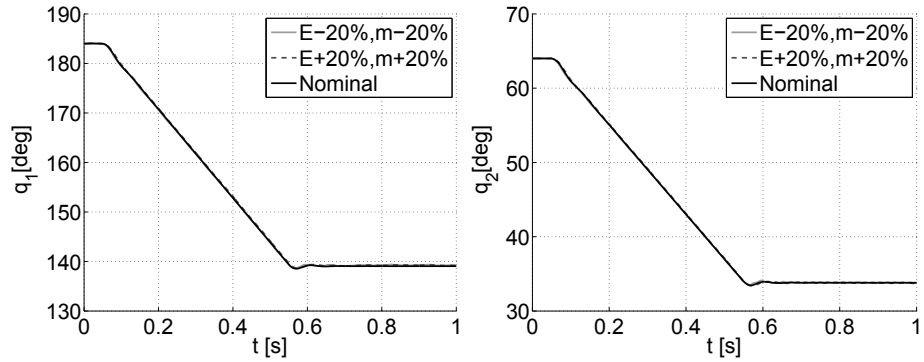

(a) (b)

Figure 6.38: Comparison of the response of the nominal and of two perturbed plants with added noise: (a) angular position q_1 of the first link (b) angular position q_2 of the fourth link

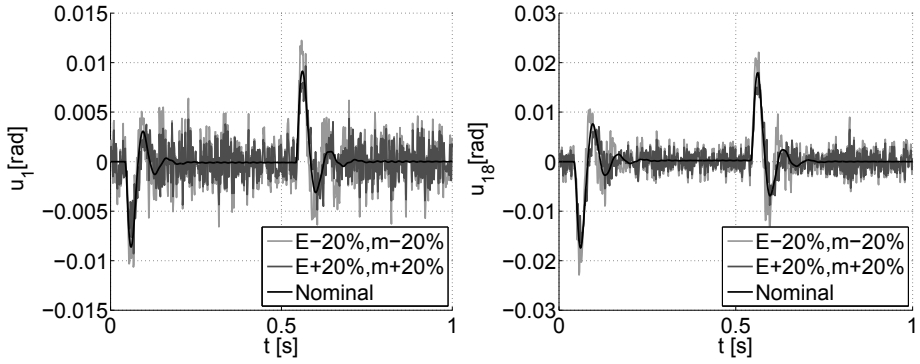

(a) (b)

Figure 6.39: Comparison of the response of the nominal and two perturbed plants with added noise: (a) angular displacement u_1 (b) angular displacement u_{18}

The MPC controller shows a robust behavior: even when noise is added the response of the system has just a small degradation of the performances, nevertheless the stability as been preserved. As it is evident in Figure 6.39, the increased level of vibration are caused solely by the torque disturbances, since the reference tracking of q_1 and q_2 (see Figure 6.38) has an almost undetectable degradation, and the closed-loop system retains its stability. It should be pointed out that the magnitudes of both the additive noises and the parametric mismatches artificially added to the closed-loop system are far beyond the unavoidable mismatches that arise in typical experimental tests.

6.5.6 Numerical investigation of end-effector trajectory tracking

In the previous sections the effectiveness of the proposed control strategy has been proved for tasks defined in the joint space. Nevertheless, the manipulator tasks are defined, in general, in the operational space. In such a space the control requirements become much stricter, since small errors in joint position could cause large errors in the end-effector position, owing to the kinematic structure of the manipulator. In this section a suitable test-bench will be carried out to prove the effectiveness of the proposed control approach for a task defined in the operational space, as well. The end effector (assumed to be fixed to the joint C) should move from the position C_0 (-100mm, 460mm) toward position C_f (400mm, 460mm) following the straight line which passes between the mentioned

points (Figure 6.40). The movement must be executed in $T = 1$ s and the vibrations as well as the position errors should be kept as small as possible.

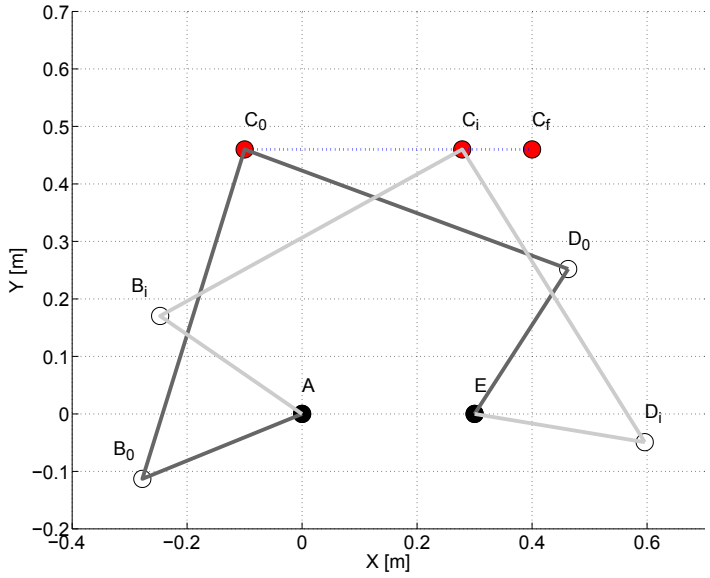

Figure 6.40: Reference trajectory for the end effector in the operational space

The trajectory in the Cartesian space has been planned by using a 3rd degree polynomial function, whose coefficients have been set by the constraints on the final and initial positions and the related velocities (forced to zero). Figure 6.41 shows the resultant joints position, velocity and acceleration, obtained trough the inverse kinematic algorithm. It can be observed that the desired motion of each controlled joint is wider than 80 degrees. Therefore, the task looks to be heavy since the movement has to be completed very quickly (T = 1 s). In Figure 6.42 four surfaces show the sensibility coefficients w_{ij} end-effector C of the ERLS as a function of the rigid coordinate's values q_1 and q_2, defined by the following equation:

$$\dot{\mathbf{C}} = \mathbf{S}_C(\mathbf{q})\dot{\mathbf{q}} = \begin{bmatrix} w_{11} & w_{12} \\ w_{21} & w_{22} \end{bmatrix}_{(q_1,q_2)} \begin{bmatrix} \dot{q}_1 \\ \dot{q}_2 \end{bmatrix} \tag{6.19}$$

The curves in black show the w_{ij} values corresponding to the planned trajectory. It can be seen that for the chosen trajectory the sensibility coefficients vary rather slowly. This behavior helps the effectiveness of the assumed linear

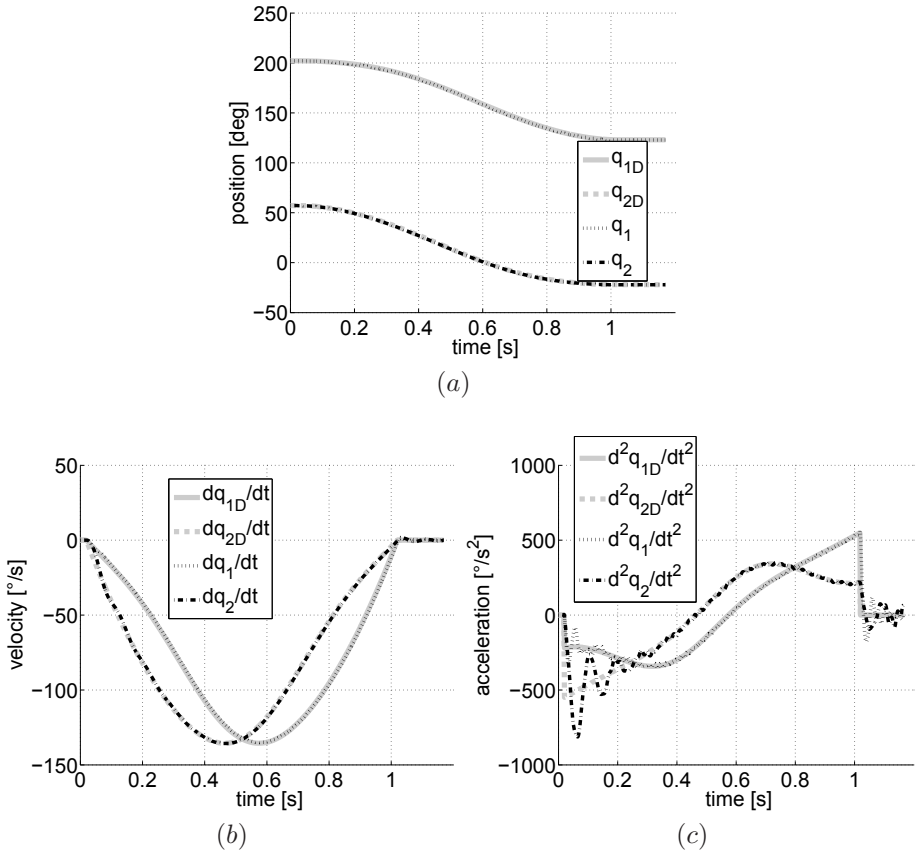

Figure 6.41: Actual q_i and planned q_{iD} trajectories: positions (a), velocities(b) and acceleration (c)

observer, even if the mechanism moves far away from the linearization configuration.

Figure 6.41 proves the efficiency of suggested control approach, by displaying the real versus planed trajectories, while Figure 6.43 shows the related u_1 and u_{18} nodal displacements and proves the MPC effectiveness in keeping small the manipulator vibration. It can be shown that both position and velocity trajectories are followed quite accurately, while some discrepancies appear as far as the acceleration signals are concerned. Figure 6.44 shows the end-effector tracking error that the manipulator makes while following the trajectory. It can be shown that the latter is always less than 0.6 mm for $T = 1$ s. It increases up to the middle region of the desired trajectory and decreases towards the final

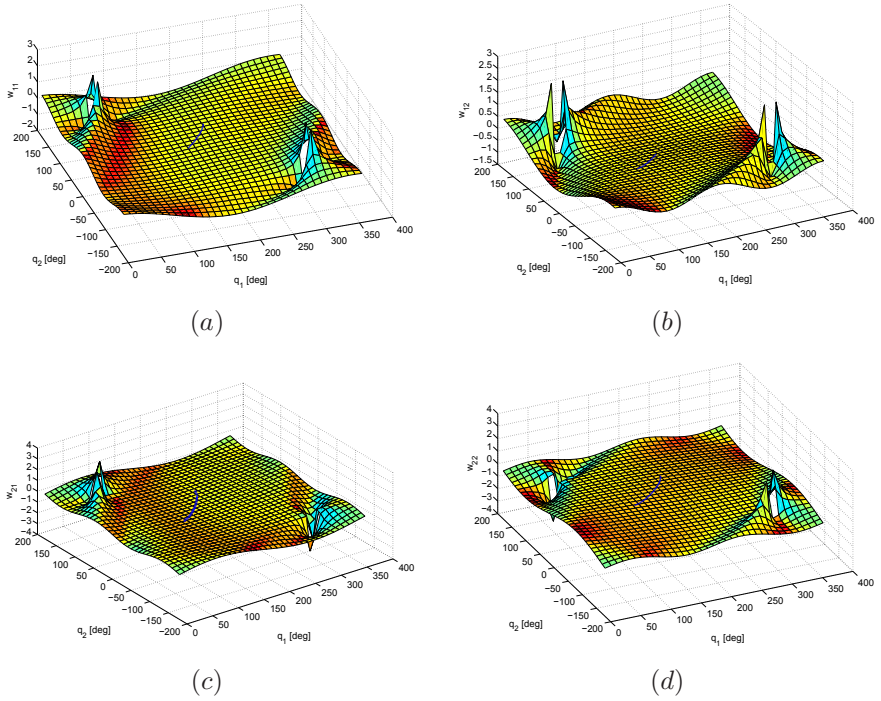

Figure 6.42: Evolution of sensitivity coefficients for the end effector position along the planned trajectories: (a) w_{11} (b) w_{12} (c) w_{21} (d) w_{22}

position. This behavior can be easily explained if the controller behavior, which tends to slow down any velocity change, so as to reduce the vibration amplitude, is considered. Therefore, the MPC smooths the trajectories and delays the trajectory tracking. Its action affects the movements of the rigid coordinates in two different ways, owing to the complex behavior of the mechanism. As a result, errors on q_1 and q_2 cause an amplified error on current end-effector position, following eq. 32:

$$\Delta\mathbf{C} = \begin{bmatrix} w_{11} & w_{12} \\ w_{21} & w_{22} \end{bmatrix}_{(q_1, q_2)} \begin{bmatrix} \Delta q_1 \\ \Delta q_2 \end{bmatrix} \tag{6.20}$$

The controller effects on vibration minimization become more comprehensible by looking at Figures 6.44 and 6.45. Figure 6.44 displays the tracking error when the task is executed in a shorter time. Since, in this case, changes in velocity and acceleration are greater than in the previous simulation, the MPC controller delays much more the path following. On the other hand, Figure

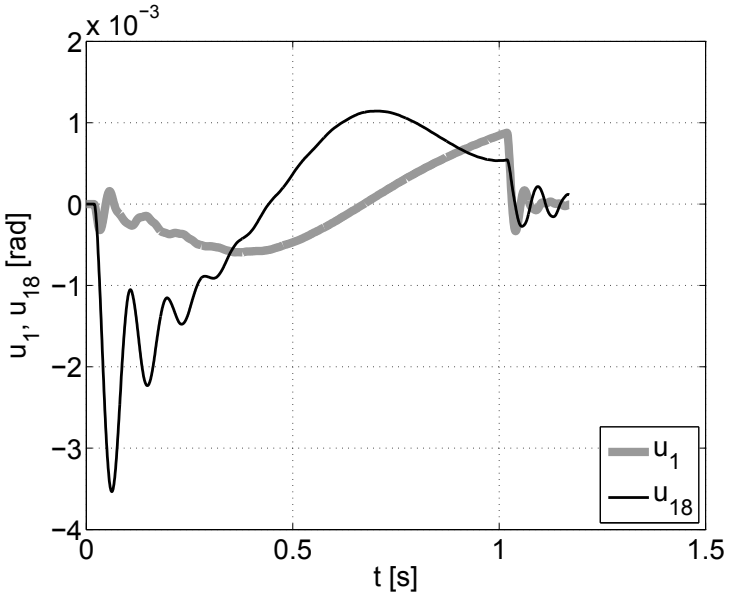

Figure 6.43: Nodal displacements u_1 and u_{18}

6.45 shows what happens if the MPC weights on the vibration amplitude are changed. It can be seen that by augmenting the weights on the deformations, a clear degrading effect occurs on the end-effector accuracy. Therefore, much attention must be paid in selecting the MPC weights: the behavior of the overall mechanism strongly depends on their values and a suitable trade-off between the requirements on trajectory error and vibration reduction must be found.

Figure 6.46 shows the effects of different choiches on the interpolating function. It is well known that for a compliant mechanism, discontinuities on the reference trajectory should be limited to derivatives of the highest order and, in any case, these should be kept as small as possible. Figure 6.47 seems to contradict this guideline: increasing the interpolating function order (therefore, reducing the discontinuities to the highest order derivatives) decreases the controller performances. This behavior might be interpreted by considering that any increment of the interpolating function order increases the maximum values of the velocities and acceleration increase as well. Therefore, it requires a heavier controller action which raises the delay on the path following.

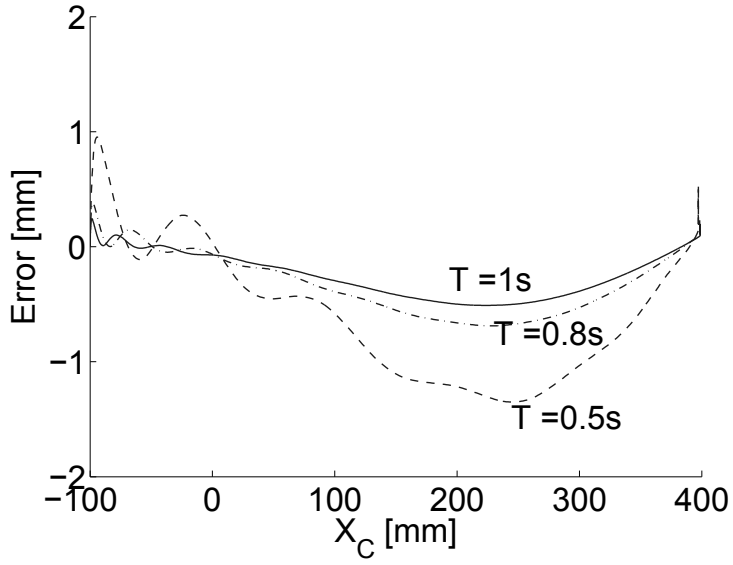

Figure 6.44: Path following errror of the manipulator end-effector C along the desired trajectory with different task execution times

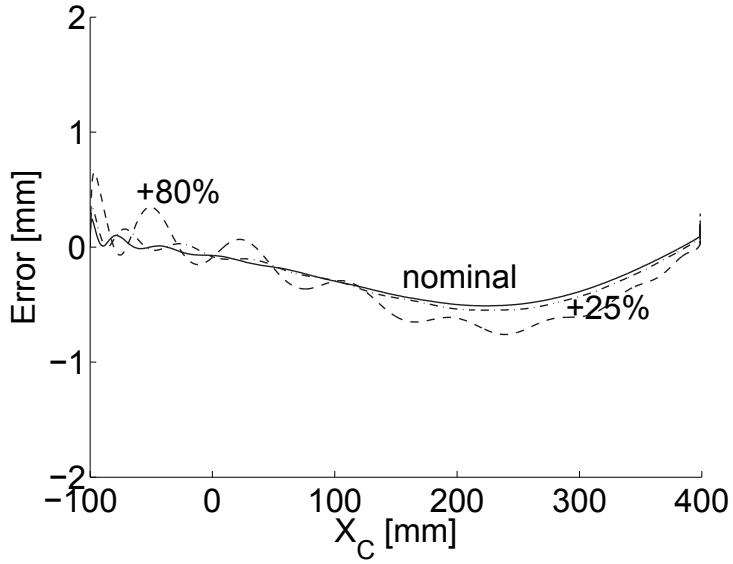

Figure 6.45: Effects on the trajectory error of increments on deformation weights

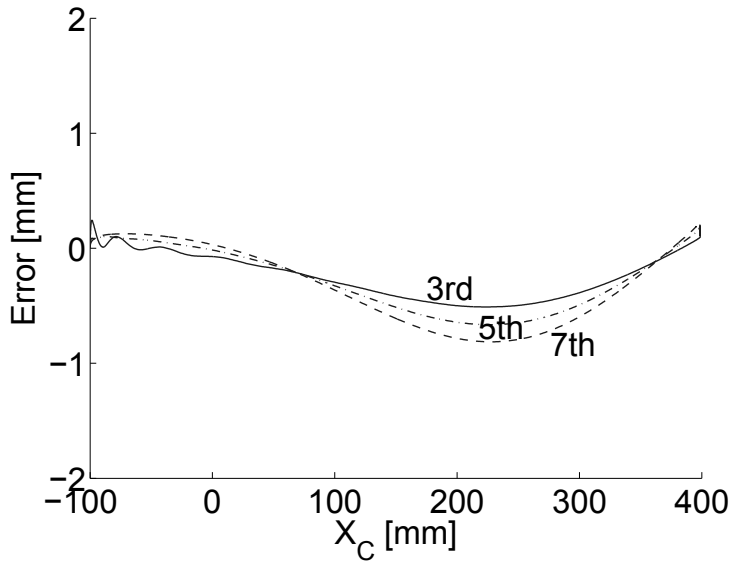

Figure 6.46: Effects of the interpolating function on the trajectory error

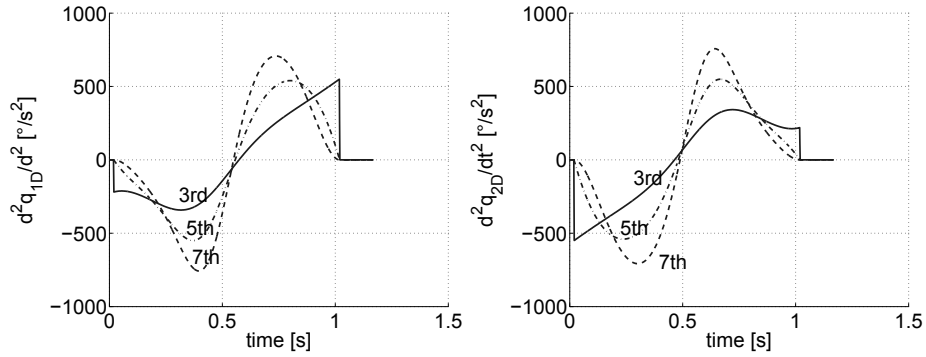

(a) (b)

Figure 6.47: Velocities (a) and acceleration (b) of q_1 and q_2 with 3^{rd}, 5^{th} and 7^{th} order interpolation functions

6.5.7 End effector tracking of a closed trajectory

Simulation results: trajectory tracking

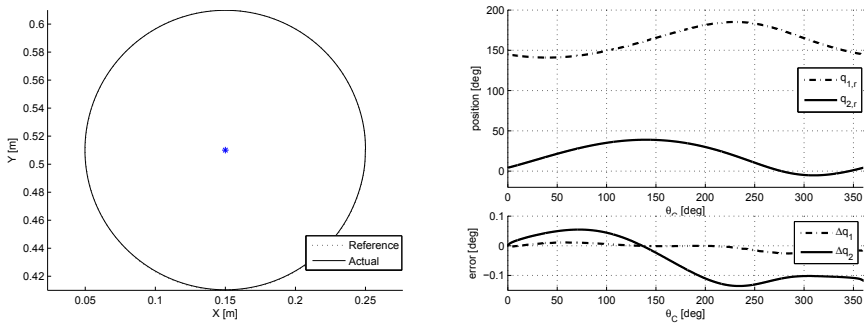

(a) (b)

Figure 6.48: (a) Trajectory in the Cartesian space; (b) Trajectory and position errors of the joints

In this subsection, the effectiveness of the MPC as a suitable controller for multi-actuated flexible-link manipulators will be proven and discussed by investigating the behavior of the 5-R mechanism by a different task, which consists on tracking the circumference with the center in $\mathbf{C}_c = [0.150m, 0.510m]^T$ and radius $r_c = 0.10m$: $C : \mathbf{X}(\theta_c) = \mathbf{C}_c + r_c \begin{bmatrix} \cos\theta_c & \sin\theta_c \end{bmatrix}^T$, $\theta_c \in [0, 2\pi]$

The trajectory has been planned as in [169]. This procedure, indeed, allows for the computation of the optimal trajectory depending on jerk and execution

time. Figure 6.48.(a) shows the trajectory in the Cartesian space, while Figure 6.48.(b) shows the trajectories of the related joints. The MPC controller has been tuned with the following values: $H_p = 5$, $H_c = 5$,$w_{u_1} = w_{u_{18}} = 2 \times 10^3$, $w_{q_1} = w_{q_2} = 4 \times 10^4$.

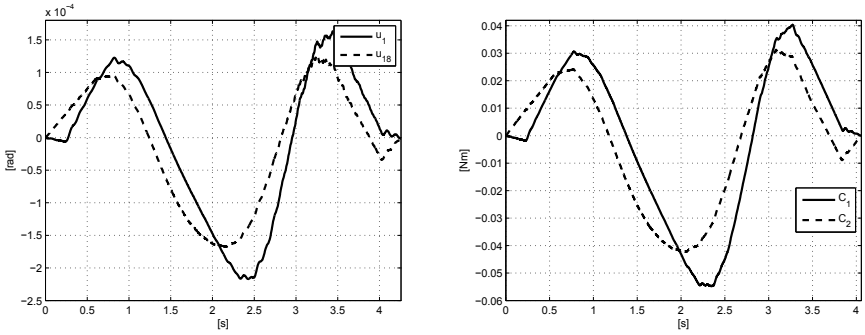

(a) (b)

Figure 6.49: (a) Nodal displacements u_1, u_{18}; (b) Input torques

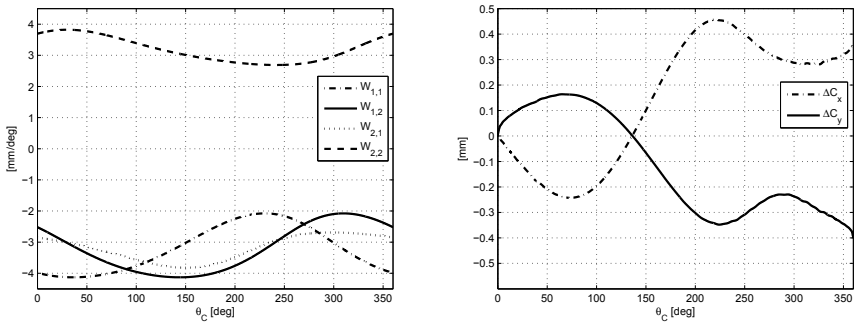

(a) (b)

Figure 6.50: (a) Sensibility's coefficients; (b) Position error

The main simulation results are shown in Figures 3 through 5. In particular, Figure 6.48.b shows the angular positions of cranks q_1 and q_2 and their corresponding errors. It should be pointed out that the joint errors are never more than 1.2 tenths of degree, which proves the considerable performance of the controller. At the same time, the elastic displacements u_1 and u_{18} are shown in Figure 6.49.a. By comparing Figure 6.49.a with Figure 6.49.b (where the input torques are shown); it is possible to evaluate the capabilities of such a controller

much more clearly. The vibration affecting the nodal displacements is, indeed, kept very minimal and the main displacements can be attributed largely to the accelerating torques input; therefore, the MPC controller is able to reduce vibration as well. As far as the position errors in the Cartesian space are concerned, the MPC seems to be a little less high-performance (Figure 6.50.b). This can be imputed to the kinematic structure of the mechanism, as well as to the physiological behavior of the proposed controller. The kinematics of the manipulator, indeed, amplifies the joint errors as follows: $\Delta\mathbf{C} = \mathbf{S}_C(\mathbf{q})\Delta\mathbf{q} = [w_{ij}]\,\Delta\mathbf{q}$, where $\mathbf{S}_C(\mathbf{q})$ is the sensibility coefficients' matrix of the end-effector. It should be noted that this matrix depends on the current manipulator configuration. As such, the amplification of the joint errors varies as the manipulator changes configuration. Figure 6.50.a shows the values of the four elements of $\mathbf{S}_C$. By considering the joint errors of Figure 6.48.b and the coefficients of Figure 6.50.a, it is possible to infer the error of the end-effector shown in Figure 6.50.b. As a result, in order to reduce the position error in the Cartesian space, a high-performance control action must be settled on the joints. This issue is dependent on the physiological behavior of the controller, which can only handle the end-effector position through the kinematic structure of the manipulator. Neither does a position's feedback exist nor does the MPC controller have an internal kinematic model of the structure. The kinematic model would enormously complicate the controller and would require a much higher computational effort. A better solution for MPC control is currently being investigated by the authors. It will permit forcing the axes to behave in a more synchronized way. Although the resulting trajectory will be slightly slowed down , the position performance appears to be very promising.

6.5.8 Conclusions

In this section a predictive control strategy has been proposed as an effective solution to the problem of simultaneous trajectory tracking and vibration suppression for compliant mechanisms with multiple actuators. The control system is based on receding horizon strategy, reference lookahead and accurate prediction model. The mechanism chosen to validate trough extensive sets of numerical simulations the effectiveness of the controller is a flexible five-link planar mechanism. Numerical results are provided to investigate the effects of different choices for the tuning parameters on vibration damping and reference tracking in both the joint space and the operational space. The effects of choosing

different trajectory planning algorithms for point-to-point motion in the operational space are investigated as well. Moreover an evaluation of the robustness of the controller to severe parametric mismatches is provided by the means of exhaustive simulations. It has been proved that the control system is very effective in both trajectory tracking and vibration suppression even in high-speed and extensive movement range task, and it is robust to both parametric mismatches between the actual and the modeled plant and to unmeasured input disturbances.

6.6 Experimental validation of MPC control

This section presents an experimental validation of the Model Predictive Control scheme (MPC) for active vibration damping in flexible-link robotic manipulators (FLM). The design of this controller is based on an accurate dynamic model of the mechanisms, able to take into account the coupled rigid-flexible dynamics of the system. Experimental results on a single-link manipulator affected by gravity force show that the proposed controller achieves a good position tracking performance and an effective vibration suppression. The evaluation of such a controller is done experimentally by comparing it with classical controllers with the performance of a Linear Quadratic (LQ) control with integral action. Experimental results confirm the far better accuracy of the proposed Model Predictive Control.

6.6.1 Experimental setup

The plant used to evaluate the effectiveness of the proposed predictive control strategy is a single-link flexible mechanism. It is made by a long and thin steel rod, actuated by a brushless motor. No reduction gears are used, so one end of the link is rigidly coupled to the motor shaft. The flexible link can rotate on the vertical plane, so the mechanism dynamics is heavily affected by the gravity force. The structural and dynamic characteristics of the flexible rod can be found in Table 6.4. Owing to the overall dimensions, the mechanism has a limited movement range (around ± 25 [deg]) from the vertical position. The motion of the link is governed trough an Indramat DKC-MKD brushless servo drive system. This drive is used as a torque generator, i.e. the instant value of the torque applied by the motor can be controlled by using an analog signal. Such a signal is supplied by a National Instruments PCI-6259 DAQ board, controlled by a Core 2 Quad PC. The angular position is measured by a 4000 cpr quadrature encoder is read with a National Instruments PCI-6602 board. The strain gauge signal is measured with the same PCI-6259 board used to generate the torque reference signal, as it is visible in Figure 6.52. The data acquisition and the control softwares run over the LabVIEW Real-Time OS.

The dynamic model can be described with a good accuracy it with four finite elements. This discretization is sufficient to describe accurately the first four modes of vibration: 23 Hz, 63 Hz, 124 Hz, 206 Hz. Higher order modeds can be neglected as they have low energy and high damping values.

Figure 6.51: The flexible-link mechanism used for experimental tests

6.7 State observer

The control strategy explained above can be applied only when a measure of the whole state $\mathbf{x}$ is available. In this application, there are only two measured values, so a state observer must be used. Here a Kalman asymptotic estimator has been chosen. An estimation of $\mathbf{x}(k)$ and $\mathbf{x}_m(k)$ (where $\mathbf{x}(k)$ is the state of the plant model and $\mathbf{x}_m(k)$ is the state of the measurement noise model) can be computed from the measured output $\mathbf{y}_m(k)$ as:

$$\begin{bmatrix} \hat{\mathbf{x}}(k|k) \\ \hat{\mathbf{x}}_m(k|k) \end{bmatrix} = \begin{bmatrix} \hat{\mathbf{x}}(k|k-1) \\ \hat{\mathbf{x}}_m(k|k-1) \end{bmatrix} + \mathbf{L}(\mathbf{y}_m(k) - \hat{\mathbf{y}}_m(k))$$

$$\begin{bmatrix} \hat{\mathbf{x}}(k+1|k) \\ \hat{\mathbf{x}}_m(k+1|k) \end{bmatrix} = \begin{bmatrix} \mathbf{A}\hat{\mathbf{x}}(k|k) + \mathbf{B}\mathbf{z}(k) \\ \tilde{\mathbf{A}}\hat{\mathbf{x}}_m(k|k) \end{bmatrix} \tag{6.21}$$

$$\hat{\mathbf{y}}_m(k) = \mathbf{C}_m\hat{\mathbf{x}}(k|k-1)$$

The gain matrix $\mathbf{L}$ has been designed by using Kalman filtering techniques

Table 6.4: Structral and dynamics characteristics of the flexible rod

	Symbol	Value
Young's modulus	E	230×10^9 [Pa]
Flexural stiffness	EJ	191.67 [Nm^4]
Beam width	a	1×10^{-2} [m]
Beam thickness	b	1×10^{-2} [m]
Mass/unit length	m	0.7880 [kg/m]
Flexible Link length	l	1.5 [m]
Strain sensor position	s	0.75 [m]
First Rayleigh damping constant	α	4.5×10^{-1} [s^{-1}]
Second Rayleigh damping constant	β	4.2×10^{-5} [s^{-1}]

(see [127]).

The design of both the estimator and the prediction model is based on a linear state-space model of the FLM which has been obtained by applying the linearization procedure developed in [166] to Eq. (6). The resulting state-space model can be rewritten as:

$$\begin{cases} \dot{\mathbf{x}}(t) = \mathbf{A}\mathbf{x}(t) + \mathbf{B}\mathbf{z}(t) \\ \mathbf{y}(t) = \mathbf{C}\mathbf{x}(t) \end{cases} \tag{6.22}$$

where $\mathbf{A} \in \mathbb{R}^{26} \times \mathbb{R}^{26}$, $\mathbf{B} \in \mathbb{R}^{26} \times \mathbb{R}^{1}$, $\mathbf{C} \in \mathbb{R}^{2} \times \mathbb{R}^{26}$ are time-invariant matrices. The state vector $\mathbf{x}$ includes all the nodal displacements and the angular position q, as well as their time derivatives:

$$\mathbf{x}(t) = [u_1, u_2, \ldots, u_{13}, q, \dot{u_1}, \dot{u_2}, \ldots, \dot{u}_{13}, \dot{q}]^T$$

The output vector of the LTI system consists of two elements: $\mathbf{y}(t) = [u_6, q]^T$, being u_6 the rotational displacement at the midspan of the link. The input vector $\mathbf{z}(t)$ includes the torque applied to the link as single element.

A comparison of measured and estimated values of the link curvature is reported in Figure 6.54. As it can be seen, the value of the elastic displacement can be evaluated with a good accuracy. It must be pointed out that the state observer has the availability of only the quadrature encoder signal and the nominal torque applied to the rod. In this way, the robustness of the closed-loop system can be improved, since the measure of the strain gauge signal is heavily affected by noise. Moreover, the reduced number of sensor make this control strategy suitable to most robotic manipulators for industrial use, since sensors

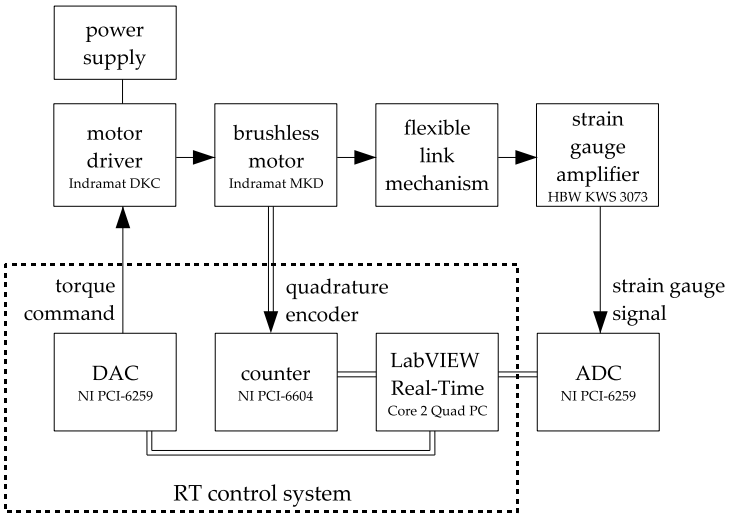

Figure 6.52: Experimental setup

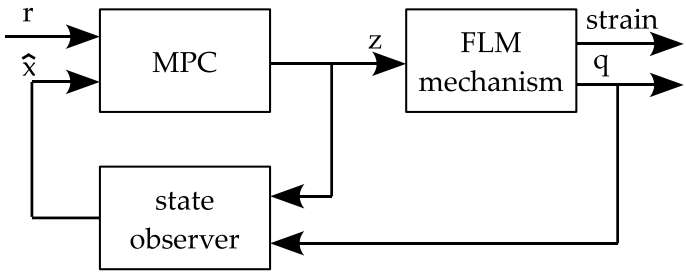

Figure 6.53: MPC control: block diagram

such as accelerometers and strain gauge bridges are usually unavailable on these systems.

6.8 Experimental results: MPC control

The proof of the accuracy of the controller is given in this section. The position regulation and the vibration damping are evaluated from the results of two different experimental tests. In the first test, indicated as "Test 1" in Table 6.5 and in Figures 6.55(a-c), the reference angular position signal is an ideal step that decreases form $+15$ [deg] to -15 [deg]. As it can be seen in figure 6.55(a) the 30-degrees movement is performed in 2 seconds, with a very small overshoot

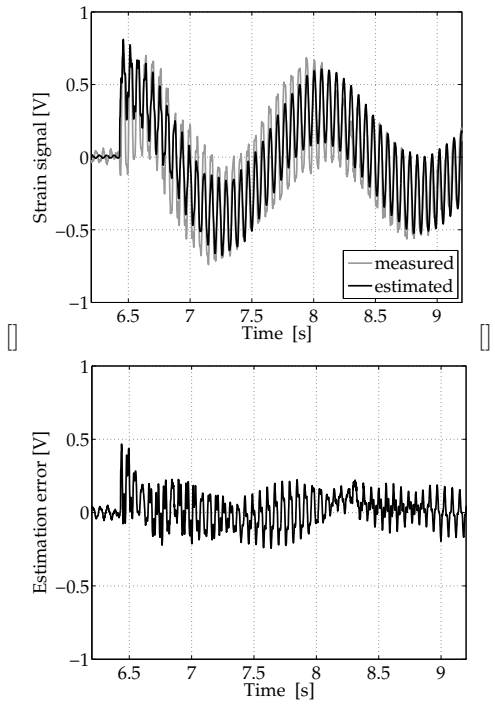

Figure 6.54: State observer; (a) measured and estimated strain gauge signals (b) estimation error

and without any steady state error. As it is clear form Figure 6.55(c), the value of the torque command is kept inside the allowable range of the actuator. The closed-loop system shows a good damping, since the vibration is kept below the minimum detectable amplitude within 3 seconds from the transient. Vibration damping can be improved at the cost of a scarce degradation of the accuracy on the angular position accuracy. In "Test 2" the weight on the angular position, $\mathbf{Q}(1,1)$, is reduced by 33 %, while the weight on vibration amplitude, $\mathbf{Q}(2,2)$ is increased by 33 %, with respect to "Test 1". At the same time, the prediction horizon is changed from 400 to 500. The increasing of H_p leads to a more damped response, and can improve the robustness of the system, as highlighted in [106]. Moreover, the vibration damping can be enhanced by increasing the weight on u and reducing the weight on q. As it is evident form figure 6.55(d), the tracking of the angular position is less fast, but the overshoot is reduced. Vibration damping is slightly improved from Test 1, as it can be seen in figure 6.55(e). In the Test 2 the range of the position reference is reduced to 20 degrees to show how the performance of the MPC controller is not affected by the width of the reference step signal.

In all the tests, the angular position is evaluated by the quadrature encoder mounted on the motor shaft, while the strain signal is measured using a Hottinger Baldwin Messtechnik KWS 3073 strain gauge signal amplifier, as in Figure 6.52.

Table 6.5: MPC tuning parameters

	q_0 $[deg]$	q_f $[deg]$	H_p	H_c	$\mathbf{Q}(1,1)$	$\mathbf{Q}(2,2)$	$\mathbf{R}$
Test 1	15	-15	400	10	300	3000	1
Test 2	-10	10	500	10	200	4000	1

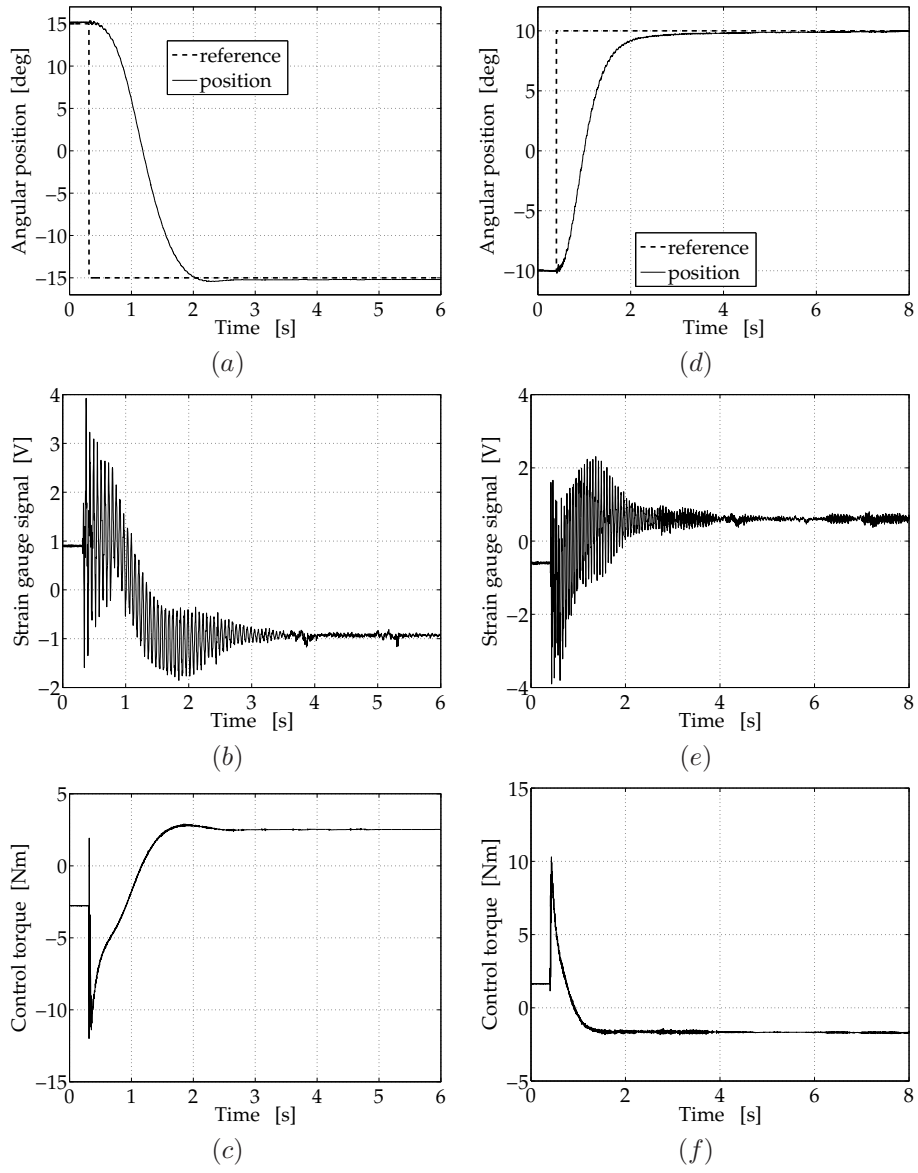

Figure 6.55: MPC control: closed-loop response to a step position reference. Test 1 (a,b,c) and Test 2 (d,e,f)

6.9 Experimental results: comparison between MPC and LQ performance

In this section the performance of the proposed MPC controlled are evaluated by comparing them with those of a Liner Quadratic controller with an integral action. All the tests have been conducted by providing the angular position reference signal with ideal steps of different amplitudes.

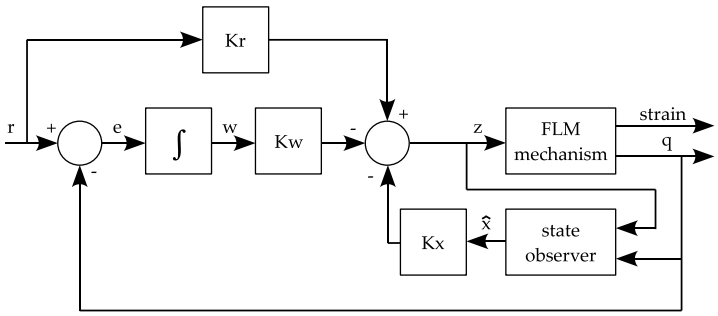

Figure 6.56: LQ control with integral action: block diagram

Here just a brief overview of the Linear Quadratic (LQ) control strategy for flexible link mechanism is given. Such a controller is used to set up a comparison between the MPC controller and a classic control system based on the same model and the same controlled variables. In this way the features of the predictive control strategy can be clearly highlighted.

A graphic representation of the control's loop structure is reported in Figure 6.56. Owing to the space constraints of this paper, just a basic overview of this controller will be given (for more details see [128]).

In order to add an integral action into the LQ controller, the state-space model must be augmented. The tracking error can be defined so that its time derivative obeys to the following differential equation:

$$\dot{\mathbf{w}}(t) = \mathbf{r}(r) - \mathbf{y}(t) = \mathbf{r}(t) - \mathbf{C}\mathbf{x}(t) \tag{6.23}$$

where $\mathbf{r}(t)$ is the desired trajectory that the plant output $\mathbf{y}(t)$ should follow. In this way, $\mathbf{w}(t)$ is the integral of the tracking error. An augmented state vector $\hat{\mathbf{x}}$ can be defined such as: $\hat{\mathbf{x}} = \begin{bmatrix} \mathbf{x} \\ \mathbf{w} \end{bmatrix}$, then the augmented state equation is:

$$\dot{\hat{\mathbf{x}}}(t) = \underbrace{\begin{bmatrix} \mathbf{A} & 0 \\ -\mathbf{C} & 0 \end{bmatrix}}_{\hat{\mathbf{A}}} \hat{\mathbf{x}} + \underbrace{\begin{bmatrix} \mathbf{B} \\ 0 \end{bmatrix}}_{\hat{\mathbf{B}}} \mathbf{z} + \underbrace{\begin{bmatrix} 0 \\ \mathbf{r} \end{bmatrix}}_{\mathbf{d}} \tag{6.24}$$

while the augmented output equation is:

$$\mathbf{y} = \underbrace{\begin{bmatrix} \mathbf{C} & 0 \end{bmatrix}}_{\hat{\mathbf{C}}} \hat{\mathbf{x}} \tag{6.25}$$

The LQ tracking controller calculates the optimal control sequence $\mathbf{z}(t)$ which minimizes the performance index J defined as:

$$J = \frac{1}{2} \int_0^\infty \left\{ (\mathbf{y} - \mathbf{r})^T \mathbf{Q}_y (\mathbf{y} - \mathbf{r}) + \mathbf{w}^T \mathbf{Q}_w \mathbf{w} + \mathbf{z}^T \mathbf{R} \mathbf{z} \right\} dt \tag{6.26}$$

The first term inside the integral minimizes the absolute value of the tracking error and the elastic displacement. Whereas, the second term takes into account the absolute value of integral error of q. The last one minimizes the system input: in this case the torque applied to the link.

In this case $\mathbf{Q}_y$ is a diagonal matrix of weights, while $\mathbf{Q}_w$ and $\mathbf{R}$ are scalar values. The control action obeys to:

$$z(t) = -\mathbf{K}_x \mathbf{x} - \mathbf{K}_w w + \mathbf{K}_r \mathbf{r} \tag{6.27}$$

where the optimal value of the gain matrices $\mathbf{K}_x$, $\mathbf{K}_w$, $\mathbf{K}_r$ are found trough the solution of a suitable Riccati equation.

Here, a comparison of the closed loop performance by using the LQ and the MPC controller is set. The two control systems are tuned to obtain the same rise time. As it can be seen from figure 6.57(a), the LQ control has a poor accuracy on the position tracking: the overshoot is 1.3 degrees wide and the settling time is more or less 3 seconds long. The improved angular tracking error of MPC is highlighted by the much smaller settling time (less than 1 second) and by the negligible overshoot, as it can be seen in figure 6.57(b).

As far as the vibration damping is concerned, the MPC again performs better: the elastic displacement is kept below the minimum detectable amplitude range ± 70 [mV] after less than 2 seconds from the change in reference, while the same occurs for the LQ controller after more than 5 seconds. The comparison between the two controllers is limited to a 5-degree-wide step, since the LQ controller cannot preserve satisfactory performance over this reference step

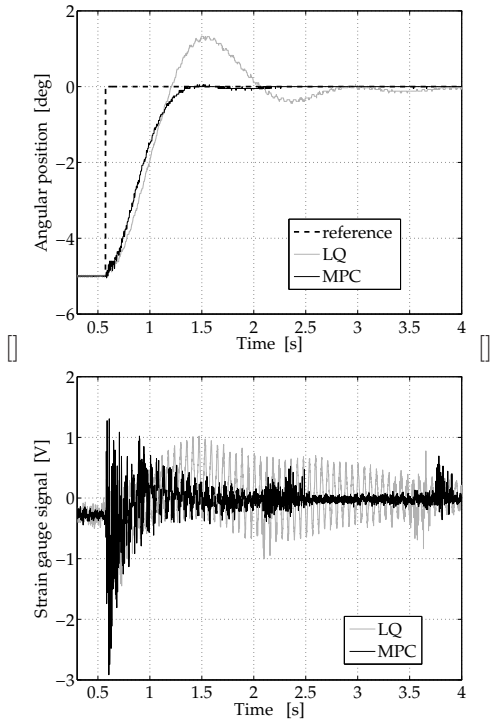

Figure 6.57: LQ vs MPC: (a) comparison of angular position tracking (b) comparison of strain gauge signal

without a strong slowing down of the closed-loop response of the system. The strain signal is very noisy. Figure 6.57(b) shows how the strain signal if affected by a periodic disturbance which occurs every 1.2 seconds. This disturbance is due mainly to the noise irradiated from the motor power supply and by the motor driver. It must be pointed out that this large amount of disturbance does not affect the performance of neither the LQ nor the MPC controller, since the state estimator used in both cases does not rely on this measurement.

6.10 Conclusion

An MPC controller for the simultaneous position and vibration control of flexible-link mechanisms has been implemented and tested on a real single-link mechanism. It has been proved that the proposed control strategy can be very effective, and it outperforms classical control strategies, such as the Linear Quadratic (LQ) optimal control investigated here, both in terms of tracking of angular po-

sition tracking and vibration damping.

The state estimator used for all the experimental tests has been shown to be capable of providing an accurate estimation of the plant dynamics with a very limited set of sensors. Such an estimator needs the measure of the angular position only and the torque applied by the brushless motor. For this reason, the proposed controller can be easily adapted to most of the industrial manipulators, which usually do not have sensors for measuring the elastic displacement of the links.

Conclusion

In this thesis, the subject of control of flexible links robots has been treated and solutions for some of the problems related to it have been presented and evaluated. The problem of dynamic modeling and simulation have been approached using a highly accurate nonlinear dynamic model based on Finite Element Model (FEM) and and Equivalent Rigid Link System (ERLS). It has been verified that such model can produce accurate results even if a small number of elements is used. Such results are used as the basis for the development of a Real-Time simulator of flexible-link mechanisms, which constitutes the core of an Hardware-In-the-Loop testbench for single-link mechanisms affected by gravity. The experimental validation of the proposed HIL simulator is performed by comparing the response of the real and of the simulated system using the same real-time controller. The comparison shows a good agreement of results.

The problem of feedback control of flexible-link mechanisms is dealt trough the use of predictive control technique. In particular, two different strategies of Model Predictive Control (MPC) are used to simultaneously control the position and the deflection of fast flexible link mechanisms. Both an constrained and an unconstrained formulation are investigated. Results are provided for a single-link mechanisms, for a four bar linkage and a five-bar mechanisms. The capability MPC to produce a forecast on the plant dynamics can provide, as shown trough extensive numerical and experimental tests, results which outperforms classical control strategies (PID) and model-based control, such as linear quadratic optimal control.

Moreover, the problem of choosing the most suitable trajectory planning

algorithm and the best values for the control tuning parameters has been investigated trough several numerical trials. Such problem has been formulated as and end-effector tracking system with vibration damping. A five-bar mechanisms has been chosen as the testbench for this application. Results indicated that generally, higher values of the prediction horizon lead to an improved vibration damping and to a slower response of the control system. High bandwidth can be restored by the use of small control horizon, therefore by 'concentrating' the control action in a limited lapse of time. The choice of the weights for the cost function on which MPC is based, can be operated as in the linear quadratic control framework, at least as long as the weighting matrices are kept constant along the prediction and control horizons.

Also experimental results have been produced to show the superior capabilities of MPC to perform high-speed movements with limited vibration trough the comparison with traditional control strategies, such as PID and optimal linear quadratic control.

Future development of this work could include an analysis of the stability properties of the proposed control systems. Such task however appears to be quite complex, given the nonlinear characteristics of flexible-link mechanisms. The development of new predictive control strategies especially tailored for flexible-link mechanisms is possible as well, and this research could lead to improve even the very good results shown in this work. The design of the control systems used for this work has been based on linearized models, but a nonlinear model can be used as well, therefore leading to a Nonlinear Model Predictive Control (NMPC) formulation. However, such task is made quite complex by the difficulty of solving nonlinear optimization control problems with complex plant dynamics, as in the case of flexible-link mechanisms. In this cases the convergence of the optimization procedure is not guaranteed, given the non convex nature of the problem, especially if real-time capability is required.

Appendix: Finite Elements for the analysis of elastic beams

A.1 Finite Elements for the analysis of elastic beams

In this section a discretization based on Finite Elements will be applied to elastic beams. The discretized beam will be used as the main building block for representing both the static and the dynamic behavior of flexible-link mechanisms. Finite Element has been chosen as an effective way to bring into finite dimension an otherwise infinite-dimension problem, such as the dynamics of an elastic element. The theoretical results on the theory of elasticity is based on the Ritz analysis. An excellent reference can be found in the book [170].

A.1.1 The beam element

A beam can be defined as a straight element, delimited by two nodes (placed at the two ends), at which the beam element exchanges forces with the surroundings. The beam element is usually associated with a local reference frame (x, y), in which x is the longitudinal axis and y is normal to x. The behavior of the beam element can be thought as the superposition of three basic elements:

- truss element
- beam element
- torsion bar

The behavior as torsion bar will not be analyzed here, since the dynamic model that will be introduced in the next section neglects this kind of solicitation. Therefore, from here to all the rest of this work, it will be intended that all the torques acting on the mechanisms will have an axis of application perpendicular to the plane in which the flexible-link mechanism moves.

Truss element

The behavior of a beam subject to only longitudinal forces can be effectively described as a truss element element. In particular, our aim is to describe the elastic displacement of the two endpoint of the beam along the x axis. Let us consider a single beam, and fix one of its endpoints (the 'left' one, for example). If a force with magnitude F is applied along the positive direction of the x axis (as in figure A.1.1), the elastic displacement along the element, $u_x(x)$, can be calculated as:

$$u_x(x) = \frac{F}{EA}x$$

in which F is the static force, A the area of the section of the beam, E the elastic constant of the material which constitutes the beam.

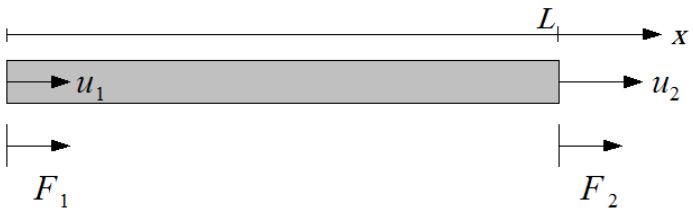

Figure A.1: Truss element

More generally, the finite element method is based on the definition of some specific functions $u_x(x)$ in the form:

$$u_x(x) = \sum f_i(x)\alpha_i \tag{A.1}$$

Therefore the elastic displacement is represented by a linear combination of some functions $f_i(x)$ weighted by the coefficients α_i. The functions $f_i(x)$ are called Ritz functions and the coefficients α_i are called Ritz coefficients. The number of Ritz coefficients and function is always equal to the number of

degrees of freedom off the beam element. Referring to the previous example, the interpolating function is simply x, weighted by an unitary coefficient. The more general formulation which includes the forces acting longitudinally on both the ends of the rod is presented in the following.

Interpolating function for the truss element

Given a longitudinal element whose length is L, a linear solution can be chosen as:

$$u_x(x) = \alpha_0 + \alpha_1 x \tag{A.2}$$

The coefficients α_0 and α_1 can be calculated in order to impose that the Ritz solution for the two nodes equals the elastic displacements u_1 and u_2 at the two nodes. In this way it will be obtained that:

$$u_1 = u_x(0) = \alpha_0$$

and

$$u_2 = u_x(L) = \alpha_0 + \alpha_1 L$$

The resulting system of equation is:

$$\begin{bmatrix} \alpha_0 \\ \alpha_1 \end{bmatrix} = \begin{bmatrix} 1 & 0 \\ -1/L & 1/L \end{bmatrix} \begin{bmatrix} u_1 \\ u_2 \end{bmatrix} \tag{A.3}$$

Rewriting it as:

$$u_x(x) = \begin{bmatrix} 1 & x \end{bmatrix} \begin{bmatrix} \alpha_0 \\ \alpha_1 \end{bmatrix}$$

and using A.3, one obtains:

$$u_x(x) = (1 - x/L)u_1 + (x/L)u_2 \tag{A.4}$$

This result represents a Ritz function, which can be used to evaluate the elastic displacement for a generic point belonging to the a beam, on which a constant force acts along its longitudinal direction. The two interpolating functions:

$$h_1(x) = 1 - x/L \qquad h_2(x) = x/L \tag{A.5}$$

should be used as explained here: $h_1(x)$ represents the elastic displacement inside the beam when u_1 is unitary and u_2 equals zero. The elastic displacement in the symmetric situation ($u_1 = 0$ and $u_2 = 0$) is measured by $h_2(x)$, instead.

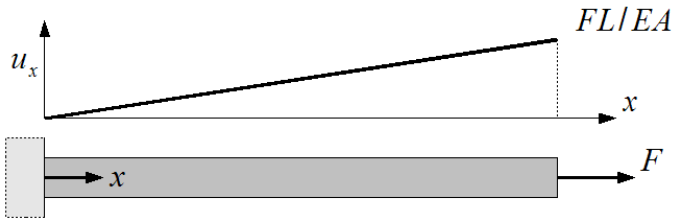

Figure A.2: Elastic displacement for a truss element with a fixed end

A.1.2 Stiffness matrix

Let us consider the same beam elements on which the two longitudinal static forces F_1 and F_2 are acting on both the nodes. The elastic displacement $\epsilon_{xx} = du_x/dx = (-1/L)u_1 + (1/L)u_2$ will be constant, since a linear description has been chosen for the interpolating function. The virtual displacement is therefore:

$$\delta u_x(x) = (1 - x/L)\delta u_1 + (x/L)\delta u_2$$

while the virtual deformation is:

$$\delta\epsilon_{xx} = d\delta u_x/dx = (-1/L)\delta u_1 + (1/L)\delta u_2$$

By applying the virtual works principle to this situation, one obtains:

$$\int_L \frac{d\delta u_x(x)}{dx}\frac{du_x(x)}{dx}EAdx = F_1\delta u_x(0) + F_2\delta u_x(L) \tag{A.6}$$

Introducing the deformation, the virtual deformation and the virtual displacements of the point of application of the force, we obtain, given the choice of interpolating functions made before:

$$\int_L [(-1/L)\delta u_1 + (1/L)\delta u_2][(-1/L)u_1 + (1/L)u_2]EAdx = F_1\delta u_1 + F_2\delta u_2 \tag{A.7}$$

Chosing $\delta u_1 \neq 0$ and $\delta u_2 = 0$ yields:

$$\int_L (-1/L)[(-1/L)u_1 + (1/L)u_2]EAdx = F_1$$

Chosing $\delta u_1 = 0$ and $\delta u_2 \neq 0$ brings:

$$\int_L (1/L)[(-1/L)u_1 + (1/L)u_2]EAdx = F_2$$

After the evaluation of the integrals in the two equations above, one obtains the linear system:

$$\begin{bmatrix} EA/L & -EA/L \\ -EA/L & EA/L \end{bmatrix} \begin{bmatrix} u_1 \\ u_2 \end{bmatrix} = \begin{bmatrix} F_1 \\ F_2 \end{bmatrix} \tag{A.8}$$

The resulting matrix is the stiffness matrix of the element, usually denoted by the **K** symbol. It allows to evaluate the displacements of the nodes of the beam element as a function of the forces acting on the two nodes. In fact, equation A.8 can be rewritten as:

$$\mathbf{Ku} = \mathbf{F} \tag{A.9}$$

or, inverting **K**:

$$\mathbf{u} = \mathbf{K}^{-1}\mathbf{F} \tag{A.10}$$

with $\mathbf{u} = [u_1, u_2]'$ and $\mathbf{F} = [F_1, F_2]'$ as the vector of elastic displacements and external forces, respectively. The evaluation of the displacements for all the points belonging to the beam requires to use the matrix of interpolating functions $\mathbf{H}(x)$. The equation to use is:

$$u_x(x) = \mathbf{H}(x)\mathbf{u} \tag{A.11}$$

with **H** including the interpolating function defined in A.5:

$$\mathbf{H}(x) = [h_1(x), h_2(x)] \tag{A.12}$$

A.1.3 Equivalent nodal loads

Some situations requires to analyze the effects of a generic force whose distribution is not limited to the two nodes. Since we want to keep the 'compatibility' to the kind of formulation provided in equation A.9, a vector of equivalent nodal forces will be used to represent the equivalent effects of distributed loads. In order to do this, we consider the equation of virtual works:

$$\int_L \delta\epsilon_{xx}\epsilon_{xx}EAdx = \int_L \delta u_x f_x dx + \sum_i F_i x \delta u_{ix} \tag{A.13}$$

The work of the distributed force can be calculated using the interpolating functions. This brings to:

$$\int_L \delta u_x(x) f_x(x) = \int_L \delta u^T H^T f_x(x) dx \tag{A.14}$$

The vector $\mathbf{P}$ of equivalent nodal loads can be defined as:

$$\mathbf{P} = \int_L H^T(x) f_x(x) dx \tag{A.15}$$

The use of $\mathbf{P}$ allows us to rewrite equation A.13 as:

$$\delta \mathbf{u}^T \mathbf{K} \mathbf{u} = \delta \mathbf{u}^T \mathbf{P} + \delta \mathbf{u}^T \mathbf{F} \tag{A.16}$$

so the resulting equilibrium of forces is:

$$\mathbf{K}\mathbf{u} = \mathbf{P} + \mathbf{F} \tag{A.17}$$

From the equations derived before, it can be seen how a distributed load f_x can be 'transformed' into an equivalent concentrated vector of loads $\mathbf{P}$, whose value should be added to the vector of nodal forces $\mathbf{F}$. The equivalence between $\mathbf{P}$ and f_x is established in order to conserve the produced work. In the simple case of a struct-and-tie element subject to a constant solicitation $f_x(x) = c$ acting on the whole element along the longitudinal direction, vector $\mathbf{P}$ can be evaluated through the equation:

$$\mathbf{P} = \int_L \begin{bmatrix} 1 - x/L \\ x/L \end{bmatrix} c dx = \begin{bmatrix} cL/2 \\ cL/2 \end{bmatrix} \tag{A.18}$$

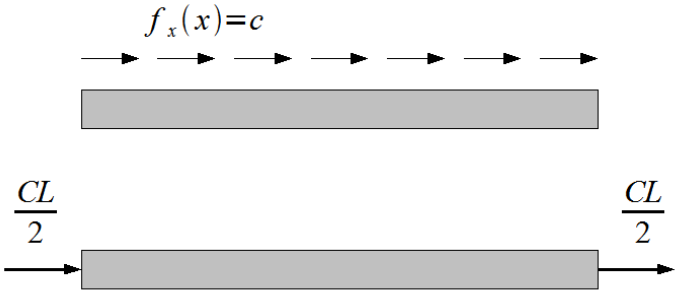

Figure A.3: Equivalent nodal load for a 2 d.o.f. truss element

Mass matrix

Here, in order to completely define the truss element, we define its mass matrix. Let's consider a beam element constituted by an isotropic material whose volumetric mass density is ρ. Therefore the mass per unit of length of the beam element is $m = \rho A$, being A the area of its section. Taking the second derivative of the displacement $u_x(x) = H(x)u$ one obtains:

$$\ddot{\mathbf{u}}_x(x) = \mathbf{H}(x)\ddot{\mathbf{u}} \tag{A.19}$$

We can consider the inertial forces $-m\ddot{\mathbf{u}}_x(x)$ distributed along the beam element as a function of the nodal accelerations $\ddot{\mathbf{u}}$:

$$\mathbf{f}_{inertia} = -m\mathbf{H}(x)\ddot{\mathbf{u}} \tag{A.20}$$

and evaluate the corresponding equivalent nodal loads:

$$\mathbf{P}_{inertia} = -\int_L \mathbf{H}^T(x)\mathbf{H}(x)\ddot{\mathbf{u}}m dx \tag{A.21}$$

Since $\mathbf{P}_{inertia} = -\mathbf{M}\ddot{\mathbf{u}}$, we can obtain a relation that can be used to express the mass matrix $\mathbf{M}$:

$$\mathbf{M} = \int_L \mathbf{H}^T(x)\mathbf{H}(x)m dx \tag{A.22}$$

which becomes, for the struct and tenon element:

$$\mathbf{M} = \int_L \begin{bmatrix} 1 - x/L \\ x/L \end{bmatrix} \begin{bmatrix} 1 - x/L & x/L \end{bmatrix} m dx = \begin{bmatrix} mL/3 & mL/6 \\ mL/6 & mL/3 \end{bmatrix} \tag{A.23}$$

A.1.4 The beam element

As explained before, an accurate description of elastic beams requires to take into account also the flexural behavior of the rods. In particular here the aim is to find a formulation able to describe the effects of moments acting on the beam, and also of forces not acting along the longitudinal direction of the element.

According to the procedure used before, here we investigate the stiffness matrix, the mass matrix, the vector of equivalent nodal loads and the interpolation functions. In particular, here we start from the definition of the matrix of interpolating functions H. Now we are considering a 4 degrees of freedom (d.o.f.) element, which are: lateral displacements on the two nodes, and angular

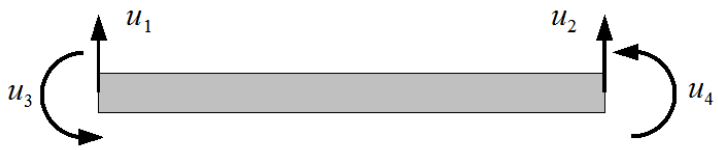

Figure A.4: 4 d.o.f. beam element

displacements at the same nodes. Since there are 4 d.o.f., the deformation of the beam element can be defined as a third degree polynomial function:

$$u(x) = \alpha_0 + \alpha_1 x + \alpha_2 x^2 + \alpha_3 x^3 \tag{A.24}$$

Similarly to the procedure adopted for the struct-and-tenon we can express the relation between the Ritz coefficients and the degrees of freedom of the beam, yielding to this matrix relation:

$$\begin{bmatrix} 1 & 0 & 0 & 0 \\ 0 & 1 & 0 & 0 \\ 1 & L & L^2 & L^3 \\ 0 & 1 & 2L & 3L^2 \end{bmatrix} \begin{bmatrix} \alpha_0 \\ \alpha_1 \\ \alpha_2 \\ \alpha_3 \end{bmatrix} = \begin{bmatrix} u_1 \\ u_2 \\ u_3 \\ u_4 \end{bmatrix} \tag{A.25}$$

The inverse relation between the u_i and the α_i is:

$$\begin{bmatrix} \alpha_0 \\ \alpha_1 \\ \alpha_2 \\ \alpha_3 \end{bmatrix} = \begin{bmatrix} 1 & 0 & 0 & 0 \\ 0 & 1 & 0 & 0 \\ -3/L^2 & -2/L & 3/L^2 & -1/L \\ 2/L^3 & 1/L^2 & -2/L^3 & 1/L^2 \end{bmatrix} \begin{bmatrix} u_1 \\ u_2 \\ u_3 \\ u_4 \end{bmatrix} \tag{A.26}$$

Using equation (A.24) together with (A.26):

$$u(x) = \begin{bmatrix} 1 & x & x^2 & x^3 \end{bmatrix} \begin{bmatrix} 1 & 0 & 0 & 0 \\ 0 & 1 & 0 & 0 \\ -3/L^2 & -2/L & 3/L^2 & -1/L \\ 2/L^3 & 1/L^2 & -2/L^3 & 1/L^2 \end{bmatrix} \begin{bmatrix} u_1 \\ u_2 \\ u_3 \\ u_4 \end{bmatrix} \tag{A.27}$$

Therefore the relation between the lateral displacement and the nodal displacement is:

$$u(x) = h_1(x)u_1 + h_2(x)u_2 + h_3(x)u_3 + h_4(x)u_4 \tag{A.28}$$

with the four interpolating functions:

$$\begin{aligned} h_1(x) &= 1 - 3(x/L)^2 + 2(x/L)^3 \\ h_2(x) &= x - 2x^2/L + x^3/L^2 \\ h_3(x) &= 3(x/L)^2 - 2(x/L)^3 \\ h_4(x) &= -x^2/L + x^3/L^2 \end{aligned} \tag{A.29}$$

The interpolating functions are plotted in figure A.5. The first interpolating function allows to evaluate the deformation of the beam element when the lateral displacement at the left node is unitary and all the other three displacements equals zero. The same applies symmetrically for $h_2(x)$. $h_3(x)$ and $h_4(x)$ allows to evaluate the deformation when the tangent of the angle of rotation of the first and second node is unitary, respectively, and all the other nodal displacements are equal to zero.

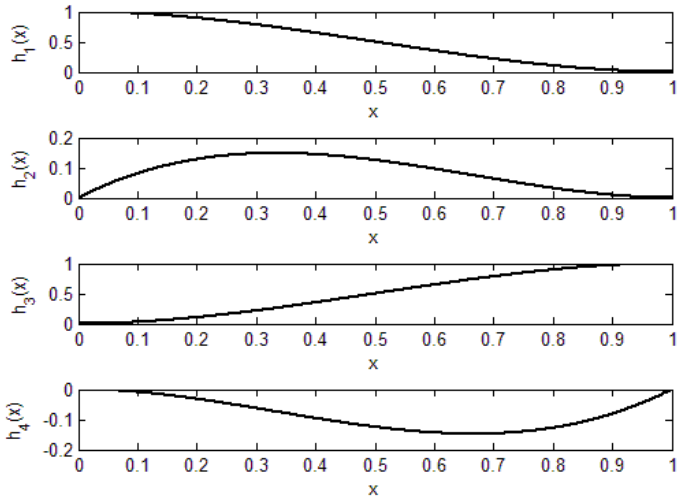

Figure A.5: Interpolating function for the 4 d.o.f. beam element

Stiffness matrix

Again, the stiffness matrix can be evaluated starting from the matrix of interpolating function $\mathbf{H}(x) = [h_1(h), h_2(x), h_3(x), h_4(x)]$ and its second derivative of the longitudinal coordinate x. We indicate such derivative as $\mathbf{H}''(x)$. By defining the vector of the generalized nodal loads:

$$\mathbf{F}^T = [f_1, m_2, f_3, m_4]$$

we can express the equation of virtual works as:

$$\int_L \delta u^T \mathbf{H}''^T \mathbf{H}'' \mathbf{u} EJ dx = \delta \mathbf{u}^T \mathbf{F} \tag{A.30}$$

in which, taking each time only one nonzero element of $\delta \mathbf{u}^T$, one obtains the equilibrium equation:

$$\int_L \mathbf{H}''^T \mathbf{H}'' EJ dx) \mathbf{u} = \mathbf{F}$$

therefore the stiffness matrix for the 4 d.o.f. element is:

$$\mathbf{K} = \int_L \mathbf{H}''^T(x) \mathbf{H}''(x) EJ dx \tag{A.31}$$

Calculating each element of such matrix yields:

$$\mathbf{K} = \frac{EJ}{L^3} \begin{bmatrix} 12 & 6L & -12 & 6L \\ 6L & 4L^2 & -6L & 2L^2 \\ -12 & -6L & 12 & -6L \\ 6L & 2L^2 & -6L & 4L^2 \end{bmatrix} \tag{A.32}$$

Equivalent loads vector and mass matrix

The vector of equivalent nodal loads, useful when distributed loads are present, can be in the general situation calculated from the definition:

$$\mathbf{P} = \int_L \mathbf{H}^T(x) f(x) dx \tag{A.33}$$

which takes different forms according to the particular configuration taken into consideration. When a transversal distributed load $f(x) = c$ is present, equation (A.33) takes the form:

$$\mathbf{P} = \int_L \begin{bmatrix} h_1(x) \\ h_2(x) \\ h_3(x) \\ h_4(x) \end{bmatrix} f(x) dx = \begin{bmatrix} cL/2 \\ cL^2/12 \\ cL/2 \\ cL^2/12 \end{bmatrix} \tag{A.34}$$

Following the same procedure already used for the struct-and-tenon element, the following mass matrix $\mathbf{M}$ can be evaluated:

$$\mathbf{M} = \int_L \mathbf{H}^T(x) \mathbf{H}(x) m dx = \frac{mL}{420} \begin{bmatrix} 156 & 22L & 54 & -13L \\ 22L & 4L^2 & 13L & -3L^2 \\ 54 & 13L & 156 & -22L \\ -13L & -3L^2 & -22L & 4L^2 \end{bmatrix} \tag{A.35}$$

A.1.5 Artbitrary Orientation

The matrices **M**, **K** and **P** as expressed in the previous paragraphs can only describe the behavior of a beam placed with an axis along the x-axis. In order to take into consideration an arbitrary orientation, both the nodal displacements and the forces acting on the beam element must be referred to a reference system external to the beam. Therefore, from here to the end of the entire work, we will refer to a local reference frame or to a global reference frame. The first is referred to the single beam taken into consideration, while the latter refers to an arbitrary reference frame which is external to the flexible element.

Let's take into consideration a 4 d.o.f. element, as displayed in figure (A.6):

Figure A.6: D.o.f. in the local reference frame

Let's consider also two reference systems, the local system L, whose orientation is fixed to the beam, and a global reference frame G, which forms an angle γ with L. γ is measured in anti-clockwise direction from the axis x_G to the axis x_L, as it can be seen in figure (A.7). The relation between the force F_i and the displacements u_i in the local reference frame L is expressed trough the stiffness matrix K_L:

$$\mathbf{K}_L\mathbf{u}_L = \begin{bmatrix} EA/L & 0 & -EA/L & 0 \\ 0 & 0 & 0 & 0 \\ -EA/L & 0 & EA/L & 0 \\ 0 & 0 & 0 & 0 \end{bmatrix} \begin{bmatrix} u_1 \\ u_2 \\ u_3 \\ u_4 \end{bmatrix}_L = \begin{bmatrix} F_1 \\ F_2 \\ F_3 \\ F_4 \end{bmatrix}_L$$

In order to express the rotation of the vectors of forces and displacement in the global reference frame G, the following relation can be used:

$$\mathbf{u}_G = \mathbf{T}_{GL}\mathbf{u}_L = \begin{bmatrix} \cos\gamma & -\sin\gamma & 0 & 0 \\ \sin\gamma & \cos\gamma & 0 & 0 \\ 0 & 0 & \cos\gamma & -\sin\gamma \\ 0 & 0 & \sin\gamma & \cos\gamma \end{bmatrix}$$

The rotation matrix $\mathbf{T}_{GL}$ allows to 'move' from the local to the global reference frame. Therefore it can be called: 'local-to-global' rotation matrix. Such

matrix expresses the rotation of a rigid body around the z axis. More reference on rotation matrix can be found in the excellent book [171]. The inverse relation is obtained by taking the 'global-to-local' rotation matrix ($\mathbf{T}_{LG}$) as the transpose of $\mathbf{T}_{GL}$:

$$\mathbf{u}_L = \mathbf{T}_{GL}^T \mathbf{u}_G$$

with

$$\mathbf{T}_{GL}^T = \mathbf{T}_{LG}$$

This very same matrix can also be used to 'rotate' the stiffness matrix, the vector of external loads and the mass matrix ($\mathbf{K}_G$, $\mathbf{F}_G$ and $\mathbf{M}_G$) trough the relations:

$$\begin{aligned} \mathbf{M}_G &= \mathbf{T}_{GL}\mathbf{M}_L\mathbf{T}_{GL}^T \\ \mathbf{K}_G &= \mathbf{T}_{GL}\mathbf{K}_L\mathbf{T}_{GL}^T \\ \mathbf{P}_G &= \mathbf{T}_{GL}\mathbf{P}_L \end{aligned} \tag{A.36}$$

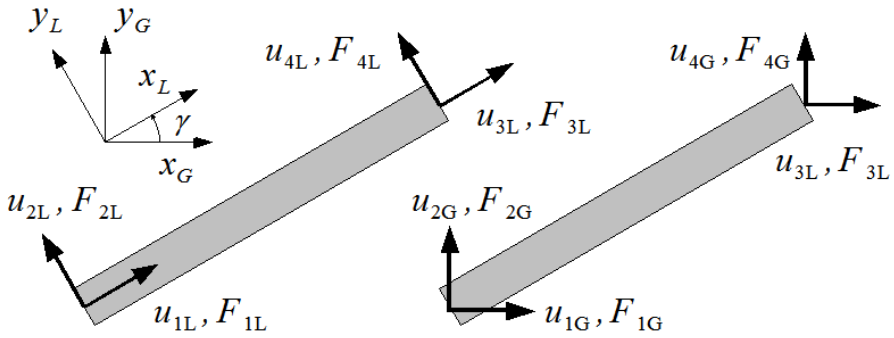

Figure A.7: Global and local reference frames

A.1.6 Matrices for the 6 d.o.f. beam

In order to describe the behavior of a 6 d.o.f. beam elements, it is necessary to merge the description of the struct-and-tenon element and of the 4 d.o.f. element. As a first step, we enumerate the the 6 d.o.f. in the local reference frame as in figure (A.8). The longitudinal displacements are take as the first and fourth element of the displacement vector u, while the lateral displacement

(measured along the y axis) are taken as the second and the fifth. The angular d.o.f., i.e. the rotations around the z axis, are taken as the third and sixth element.

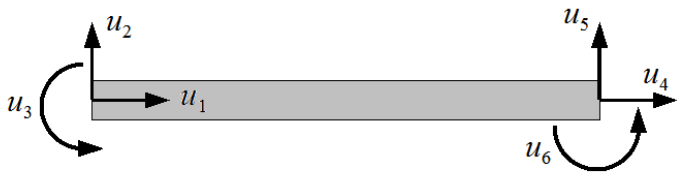

Figure A.8: 6 d.o.f. beam element: nodal displacements

The principle of superimposition of effect allows to express the stiffness matrix $\mathbf{K}_L$ just by merging the expressions of $\mathbf{K}$ in equations (A.8) and (A.32). The same applies for the mass matrix evaluated in the local reference frame, $\mathbf{M}_L$, whose expression is derived from equations (A.23) and (A.35). The resulting matrices are:

$$\mathbf{M}_L = mL \begin{bmatrix} 1/3 & 0 & 0 & 1/6 & 0 & 0 \\ 0 & 156/420 & 22L/420 & 0 & 54/420 & -13L/420 \\ 0 & 22L/420 & 4L^2/420 & 0 & 13L/420 & -3L^2/420 \\ 1/6 & 0 & 0 & 1/3 & 0 & 0 \\ 0 & 54/420 & 13L/420 & 0 & 156/420 & -22L/420 \\ 0 & -13L/420 & -3L^2 420 & 0 & -22L/420 & 4L^2/420 \end{bmatrix} \tag{A.37}$$

$$\mathbf{K}_L = \begin{bmatrix} EA/L & 0 & 0 & -EA/L & 0 & 0 \\ 0 & 12EJ/L^3 & 6EJ/L^2 & 0 & -12EJ/L^3 & 6EJ/L^2 \\ 0 & 6EJ/L^2 & 4EJ/L & 0 & -6EJ/L^2 & 2EJ/L \\ -EA/L & 0 & 0 & EA/L & 0 & 0 \\ 0 & -12EJ/L^3 & -6EJ/L^2 & 0 & 12EJ/L^3 & -6EJ/L^2 \\ 0 & 6EJ/L^2 & 2EJ/L & 0 & -6EJ/L^2 & 4EJ/L \end{bmatrix} \tag{A.38}$$

The expression of the stiffness and of the mass matrix in the global reference frame can be derived, as in equation (A.36), using the local-to-global rotation matrix:

$$\mathbf{T}_{GL} = \begin{bmatrix} \cos\gamma & -\sin\gamma & 0 & 0 & 0 & 0 \\ \sin\gamma & \cos\gamma & 0 & 0 & 0 & 0 \\ 0 & 0 & 1 & 0 & 0 & 0 \\ 0 & 0 & 0 & \cos\gamma & -\sin\gamma & 0 \\ 0 & 0 & 0 & \sin\gamma & \cos\gamma & 0 \\ 0 & 0 & 0 & 0 & 0 & 1 \end{bmatrix} \tag{A.39}$$

Bibliography

[1] M. Giovagnoni, "A numerical and experimental analysis of a chain of flexible bodies," *Journal of Dynamic Systems, Measurement, and Control*, vol. 116, pp. 73–80, 1994.

[2] W. Book, *Modeling, design and control of flexible manipulator arms*. Massachusetts Institute of Technology., 1974.

[3] S. Dwivedy and P. Eberhard, "Dynamic analysis of flexible manipulators, a literature review," *Mechanism and Machine Theory*, vol. 41, no. 7, pp. 749–777, 2006.

[4] R. Theodore and A. Ghosal, "Comparison of the assumed modes and finite element models for flexible multilink manipulators," *The International journal of robotics research*, vol. 14, no. 2, p. 91, 1995.

[5] R. Cannon and E. Schmitz, "Initial experiments on the end-point control of a flexible one-link robot," *The International Journal of Robotics Research*, vol. 3, no. 3, p. 62, 1984.

[6] E. Bayo, "Timoshenko versus bernoulli-euler beam theories for the inverse dynamics of flexible robots.," *International Journal of Robotics & Automation*, vol. 4, no. 1, pp. 53–56, 1989.

[7] P. Wang and J. Wei, "Vibrations in a moving flexible robot arm," *Journal of sound and vibration*, vol. 116, no. 1, pp. 149–160, 1987.

[8] V. Feliu, K. Rattan, and H. Brown Jr, "Modeling and control of single-link flexible arms with lumped masses," *Journal of dynamic systems, measurement, and control*, vol. 114, p. 59, 1992.

[9] B. Nagaraj, B. Nataraju, and D. Chandrasekhar, "Nondimensional parameters for the dynamics of a single flexible link," in *International Conference on Theoretical, Applied, Computational and Experimental Mechanics (ICTACEM)*, 2001.

[10] S. Tso, T. Yang, W. Xu, and Z. Sun, "Vibration control for a flexible-link robot arm with deflection feedback," *International journal of non-linear mechanics*, vol. 38, no. 1, pp. 51–62, 2003.

[11] F. Rakhsha and A. Goldenberg, "Dynamics modelling of a single-link flexible robot," in *Robotics and Automation. Proceedings. 1985 IEEE International Conference on*, vol. 2, pp. 984–989, IEEE, 1985.

[12] E. Barbieri and U. Ozguner, "Unconstrained and constrained mode expansions for a flexible slewing link," in *American Control Conference, 1988*, pp. 83–88, IEEE, 1988.

[13] B. Tabarrok, C. Leech, and Y. Kim, "On the dynamics of an axially moving beam," *Journal of the Franklin Institute*, vol. 297, no. 3, pp. 201–220, 1974.

[14] K. Buffinton, "Dynamics of elastic manipulators with prismatic joints," *Journal of dynamic systems, measurement, and control*, vol. 114, p. 41, 1992.

[15] S. Tadikonda and H. Baruh, "Dynamics and control of a translating flexible beam with a prismatic joint," *Journal of dynamic systems, measurement, and control*, vol. 114, p. 422, 1992.

[16] S. Nagarajan and D. Turcic, "Lagrangian Formulation of the Equations of Motion for Elastic Mechanisms With Mutual Dependence Between Rigid Body and Elastic Motions: Part II - System Equations," *Journal of dynamic systems, measurement and control*, vol. 112, p. 215, 1990.

[17] S. Nagarajan and D. Turcic, "Lagrangian formulation of the equations of motion for elastic mechanisms with mutual dependence between rigid body and elastic motions: Part I - element level equations," *ASME J. Dynamic Systems, Measurement and Control*, 1990.

[18] J. Bricout, J. Debus, and P. Micheau, "A finite element model for the dynamics of flexible manipulators," *Mechanism and Machine Theory*, vol. 25, no. 1, pp. 119–128, 1990.

[19] L. Chang and K. Gannon, "A dynamic model on a single-link flexible manipulator," *Journal of Vibration and Acoustics*, vol. 112, p. 138, 1990.

[20] M. Giovagnoni, "Linear decoupled models for a slewing beam undergoing large rotations," *Journal of sound and vibration*, vol. 164, no. 3, pp. 485–501, 1993.

[21] M. Tokhi, A. Azad, H. Poerwanto, S. Kourtis, and M. Baxter, "A simulink environment for simulation and control of flexible manipulator systems," in *Control'96, UKACC International Conference on (Conf. Publ. No. 427)*, vol. 1, pp. 210–215, IET, 1996.

[22] M. Tokhi, Z. Mohamed, S. Amin, and R. Mamat, "Dynamic characterisation of a flexible manipulator system: theory and experiments," in *TENCON 2000. Proceedings*, vol. 3, pp. 167–172, IEEE, 2000.

[23] J. Martins, M. Ayala Botto, and J. Sá da Costa, "Modeling of flexible beams for robotic manipulators," *Multibody System Dynamics*, vol. 7, no. 1, pp. 79–100, 2002.

[24] J. Martins, Z. Mohamed, M. Tokhi, J. Sá da Costa, and M. Botto, "Approaches for dynamic modelling of flexible manipulator systems," in *Control Theory and Applications, IEE Proceedings-*, vol. 150, pp. 401–411, IET, 2003.

[25] J. Lee and B. Wang, "Optimal control of a flexible robot arm," *Computers & structures*, vol. 29, no. 3, pp. 459–467, 1988.

[26] Q. Liu, "Dynamic analysis of a spatial robot manipulator with a flexible prismatic link," 1993.

[27] G. Zhu, S. Ge, and T. Lee, "Simulation studies of tip tracking control of a single-link flexible robot based on a lumped model," *Robotica*, vol. 17, no. 1, pp. 71–78, 1999.

[28] W. Khalil and M. Gautier, "Modeling of mechanical systems with lumped elasticity," in *Robotics and Automation, 2000. Proceedings. ICRA'00. IEEE International Conference on*, vol. 4, pp. 3964–3969, IEEE, 2000.

[29] S. Megahed and K. Hamza, "Modeling and simulation of planar flexible link manipulators with rigid tip connections to revolute joints," *Robotica*, vol. 22, no. 3, pp. 285–300, 2004.

[30] R. Milford and S. Asokanthan, "Configuration dependent eigenfrequencies for a two-link flexible manipulator: Experimental verification," *Journal of sound and vibration*, vol. 222, no. 2, pp. 191–207, 1999.

[31] A. De Luca and B. Siciliano, "Explicit dynamic modeling of a planar two-link flexible manipulator," in *Decision and Control, 1990., Proceedings of the 29th IEEE Conference on*, pp. 528–530, IEEE.

[32] W. Sunada and S. Dubowsky, "On the dynamic analysis and behavior of industrial robotic manipulators with elastic members," in *American Society of Mechanical Engineers, Design and Production Engineering Technical Conference, Washington, DC*, p. 1982, 1982.

[33] A. Morris and A. Madani, "Static and dynamic modelling of a two-flexible-link robot manipulator," *Robotica*, vol. 14, no. 3, pp. 289–300, 1996.

[34] A. Morris and A. Madani, "Computed torque control applied to a simulated two-flexible-link robot," *Transactions of the Institute of Measurement and Control*, vol. 19, no. 1, p. 50, 1997.

[35] A. Morris and A. Madani, "Quadratic optimal control of a two-flexible-link robot manipulator," *Robotica*, vol. 16, no. 01, pp. 97–108, 1998.

[36] H. Lee, "New dynamic modeling of flexible-link robots," *Journal of dynamic systems, measurement, and control*, vol. 127, p. 307, 2005.

[37] V. Gamarra-Rosado and E. Yuhara, "Dynamic modeling and simulation of a flexible robotic manipulator," *Robotica*, vol. 17, no. 5, pp. 523–528, 1999.

[38] V. Gamarra-Rosado, "A planar flexible robotic manipulator," *Kybernetes*, vol. 29, no. 5/6, pp. 787–797, 2000.

[39] W. Book, "Recursive lagrangian dynamics of flexible manipulator arms," *The International Journal of Robotics Research*, vol. 3, no. 3, p. 87, 1984.

[40] B. Siciliano and W. Book, "A singular perturbation approach to control of lightweight flexible manipulators," *The International Journal of Robotics Research*, vol. 7, no. 4, p. 79, 1988.

[41] P. Chedmail, Y. Aoustin, and C. Chevallereau, "Modelling and control of flexible robots," *International journal for numerical methods in engineering*, vol. 32, no. 8, pp. 1595–1619, 1991.

[42] M. Arteaga, "On the properties of a dynamic model of flexible robot manipulators," *Journal of dynamic systems, measurement, and control*, vol. 120, p. 8, 1998.

[43] H. Asada, Z. Ma, and H. Tokumaru, "Inverse dynamics of flexible robot arms: modeling and computation for trajectory control," *Journal of dynamic systems, Measurement, and Control*, vol. 112, p. 177, 1990.

[44] R. Vidoni, A. Gasparetto, M. Giovagnoni, and P. Boscariol, "A novel 3D equivalent rigid link system approach for flexible-link mechanisms: formulation and comparison with the floating frame of reference approach," in *Multibody dynamics 2011, ECCOMAS thematic conference, Brussels, Belgium, 4-7 July*, 2011.

[45] W. Beres and J. Sasiadek, "Finite element dynamic model of multilink flexible manipulators," *Applied Mathematics and Computer Science*, vol. 5, no. 2, pp. 231–262, 1995.

[46] W. Beres, J. Sasiadek, and G. Vukovich, "Control and dynamic analysis of multilink flexible manipulator," in *Robotics and Automation, 1993. Proceedings., 1993 IEEE International Conference on*, pp. 478–483, IEEE, 1993.

[47] A. Gasparetto, "On the modeling of flexible-link planar mechanisms: Experimental validation of an accurate dynamic model," *Journal of dynamic systems, measurement, and control*, vol. 126, p. 365, 2004.

[48] M. Benosman and G. Le Vey, "Control of flexible manipulators: A survey," *Robotica*, vol. 22, no. 05, pp. 533–545, 2004.

[49] D. Torfs, R. Vuerinckx, J. Swevers, and J. Schoukens, "Comparison of two feedforward design methods aiming at accurate trajectory tracking of the end point of a flexible robot arm," *Control Systems Technology, IEEE Transactions on*, vol. 6, no. 1, pp. 2–14, 1998.

[50] T. Looke, M. Bayoumi, and M. Farooq, "Simulation of computed torque controllers for flexible manipulators," in *Circuits and Systems, 1991., Proceedings of the 34th Midwest Symposium on*, pp. 505–508, IEEE, 1993.

[51] D. Kwon and W. Book, "A time-domain inverse dynamic tracking control of a single-link flexible manipulator," *J. Dynamic Systems, Measurement, and Control*, vol. 116, pp. 193–200, 1994.

[52] C. Menq and J. Chen, "Dynamic modeling and payload-adaptive control of a flexible manipulator," in *Robotics and Automation, 1988. Proceedings., 1988 IEEE International Conference on*, pp. 488–493, IEEE.

[53] V. Feliu, K. Rattan, and H. Brown Jr, "Adaptive control of a single-link flexible manipulator," *Control Systems Magazine, IEEE*, vol. 10, no. 2, pp. 29–33, 1990.

[54] J. Feliu, V. Feliu, and C. Cerrada, "Load adaptive control of single-link flexible arms based on a new modeling technique," *Robotics and Automation, IEEE Transactions on*, vol. 15, no. 5, pp. 793–804, 1999.

[55] J. Yang, F. Lian, and L. Fu, "Adaptive robust control for flexible manipulators," in *Robotics and Automation, 1995. Proceedings., 1995 IEEE International Conference on*, vol. 1, pp. 1223–1228, IEEE, 1995.

[56] J. Yang, F. Lian, and L. Fu, "Nonlinear adaptive control for flexible-link manipulators," *Robotics and Automation, IEEE Transactions on*, vol. 13, no. 1, pp. 140–148, 1997.

[57] K. Rattan and V. Feliu, "A robust control scheme for flexible manipulators," in *Aerospace and Electronics Conference, 1991. NAECON 1991., Proceedings of the IEEE 1991 National*, pp. 1090–1095, IEEE, 1991.

[58] F. Karray, S. Tafazolli, and W. Gueaieb, "Robust tracking of a lightweight manipulator system," *Nonlinear Dynamics*, vol. 20, no. 2, pp. 169–179, 1999.

[59] S. Pal, H. Stephanou, and G. Cook, "Optimal control of a single link flexible manipulator," in *Robotics and Automation, 1988. Proceedings., 1988 IEEE International Conference on*, pp. 171–175, IEEE, 1988.

[60] J. Lee, "Application of optimal control theory to flexible robotic manipulations," *Robotics and Computer-Integrated Manufacturing*, vol. 7, no. 3-4, pp. 327–335, 1990.

[61] O. Smith, "Posicast control of damped oscillatory systems," *Proceedings of the IRE*, vol. 45, no. 9, pp. 1249–1255, 1957.

[62] W. Singhose, W. Seering, and N. Singer, "Shaping inputs to reduce vibration: a vector diagram approach," in *Robotics and Automation, 1990. Proceedings., 1990 IEEE International Conference on*, pp. 922–927, IEEE, 1990.

[63] W. Singhose and N. Singer, "Effects of input shaping on two-dimensional trajectory following," *Robotics and Automation, IEEE Transactions on*, vol. 12, no. 6, pp. 881–887, 1996.

[64] K. Liu, W. You, and Y. Li, "Combining a feedback linearization approach with input shaping for flexible manipulator control," in *Machine Learning and Cybernetics, 2003 International Conference on*, vol. 1, pp. 561–565, IEEE, 2003.

[65] S. Rhim and W. Book, "Noise effect on adaptive command shaping methods for flexible manipulator control," *Control Systems Technology, IEEE Transactions on*, vol. 9, no. 1, pp. 84–92, 2001.

[66] H. Kim, S. Choi, and B. Thompson, "Compliant control of a two-link flexible manipulator featuring piezoelectric actuators," *Mechanism and machine theory*, vol. 36, no. 3, pp. 411–424, 2001.

[67] S. Choi, "Compliant motion control of a three-link manipulator with link flexibility and joint constraints," *Proceedings of the Institution of Mechanical Engineers, Part C: Journal of Mechanical Engineering Science*, vol. 219, no. 11, pp. 1207–1217, 2005.

[68] S. Ge, T. Lee, and Z. Wang, "Model-free regulation of multi-link smart materials robots," *Mechatronics, IEEE/ASME Transactions on*, vol. 6, no. 3, pp. 346–351, 2001.

[69] E. Bayo, "Computed torque for the position control of open-chain flexible robots," in *Robotics and Automation, 1988. Proceedings., 1988 IEEE International Conference on*, pp. 316–321, IEEE, 1988.

[70] J. Cheong, W. Chung, Y. Yoom, and S. Oh, "Control of two-link flexible manipulator using disturbance observer with reaction torque feedback," in *Advanced Robotics, 1997. ICAR'97. Proceedings., 8th International Conference on*, pp. 227–232, IEEE, 1997.

[71] Y. Aoustin and A. Formal'sky, "On the feedforward torques and reference trajectory for flexible two-link arm," *Multibody System Dynamics*, vol. 3, no. 3, pp. 241–265, 1999.

[72] Y. Wang, Y. Feng, X. Yu, and N. Zhang, "Terminal sliding mode control of mimo linear systems with unmatched uncertainties," in *Industrial Electronics Society, 2003. IECON'03. The 29th Annual Conference of the IEEE*, vol. 2, pp. 1146–1151, IEEE, 2003.

[73] N. Zhang, Y. Feng, and X. Yu, "Optimization of terminal sliding control for two-link flexible manipulators," in *Industrial Electronics Society, 2004. IECON 2004. 30th Annual Conference of IEEE*, vol. 2, pp. 1318–1322, IEEE, 2004.

[74] A. Yigit, "On the stability of pd control for a two-link rigid-flexible manipulator," *Journal of dynamic systems, measurement, and control*, vol. 116, p. 208, 1994.

[75] S. Lin, S. Tosunoglu, and D. Tesar, "Control of a six-degree-of-freedom flexible industrial manipulator," *Control Systems Magazine, IEEE*, vol. 11, no. 3, pp. 24–30, 1991.

[76] F. Boyer and W. Khalil, "An efficient calculation of flexible manipulator inverse dynamics," *The International Journal of Robotics Research*, vol. 17, no. 3, p. 282, 1998.

[77] P. Gallina, A. Gasparetto, G. Rosati, and A. Rossi, "Design of a pid controller for a flexible five-bar closed-chain planar manipulator," in *RoManSy 14: theory and practice of robots and manipulators: proceedings of the Fourteenth CISM-IFToMM Symposium*, vol. 438, p. 141, Springer Verlag, 2002.

[78] V. Utkin, "Control of elastic multi-link manipulators based on the dynamic compensation method," in *Circuits and Systems, 1998. ISCAS'98. Proceedings of the 1998 IEEE International Symposium on*, vol. 6, pp. 594–597, IEEE, 1998.

[79] M. Isogai, F. Arai, and T. Fukuda, "Modeling and vibration control with neural network for flexible multi-link structures," in *Robotics and Automation, 1999. Proceedings. 1999 IEEE International Conference on*, vol. 2, pp. 1096–1101, IEEE, 1999.

[80] G. Zhu and S. Ge, "A model-free approach for regulation of multi-link flexible robots," in *American Control Conference, 1997. Proceedings of the 1997*, vol. 3, pp. 1417–1421, IEEE, 1997.

[81] Z. Wang, S. Ge, and T. Lee, "Non-model-based robust control of multi-link smart material robots," in *Asian Conference on Robotics and Its Application, Singapore*, pp. 268–273, 2001.

[82] S. Ge, T. Lee, J. Gong, and Z. Wang, "Model-free controller design for a single-link flexible smart materials robot," *International Journal of Control*, vol. 73, no. 6, pp. 531–544, 2000.

[83] A. Trevisani and M. Valcher, "Adaptive control of a flexible-link mechanism using an energy-based approach," in *American Control Conference, 2004. Proceedings of the 2004*, vol. 6, pp. 5256–5261, IEEE.

[84] A. Trevisani and M. Valcher, "An energy-based adaptive control design technique for multibody-mechanisms with flexible links," *Mechatronics, IEEE/ASME Transactions on*, vol. 10, no. 5, pp. 571–580, 2005.

[85] A. Gasparetto and V. Zanotto, "Vibration reduction in a flexible-link mechanism through synthesis of an optimal controller," *Meccanica*, vol. 41, no. 6, pp. 611–622, 2006.

[86] R. Caracciolo, D. Richiedei, A. Trevisani, and V. Zanotto, "Robust mixed-norm position and vibration control of flexible link mechanisms," *Mechatronics*, vol. 15, no. 7, pp. 767–791, 2005.

[87] R. Caracciolo, D. Richiedei, and A. Trevisani, "Design and experimental validation of piecewise-linear state observers for flexible link mechanisms," *Meccanica*, vol. 41, no. 6, pp. 623–637, 2006.

[88] R. Caracciolo, D. Richiedei, and A. Trevisani, "Robust piecewise-linear state observers for flexible link mechanisms," *Journal of Dynamic Systems, Measurement, and Control*, vol. 130, p. 031011, 2008.

[89] R. Caracciolo, D. Richiedei, and A. Trevisani, "Experimental validation of a model-based robust controller for multi-body mechanisms with flexible links," *Multibody System Dynamics*, vol. 20, no. 2, pp. 129–145, 2008.

[90] S. Qin and T. Badgwell, "A survey of industrial model predictive control technology," *Control engineering practice*, vol. 11, no. 7, pp. 733–764, 2003.

[91] X. Chen, Q. Li, and S. Fei, "Constrained model predictive control in ball mill grinding process," *Powder Technology*, vol. 186, no. 1, pp. 31–39, 2008.

[92] T. Perez, G. Goodwin, and C. Tzeng, "Model predictive rudder roll stabilization control for ships," in *Proc. 5th IFAC Conf. on Manoeuvring and Control of Marine Craft*, 2000.

[93] L. Bleris, P. Vouzis, M. Arnold, and M. Kothare, "A co-processor fpga platform for the implementation of real-time model predictive control," in *American Control Conference, 2006*, pp. 6–pp, IEEE, 2006.

[94] M. Morari, M. Baotic, and F. Borrelli, "Hybrid systems modeling and control," *European Journal of Control*, vol. 9, no. 2-3, pp. 177–189, 2003.

[95] R. Murray, J. Hauser, A. Jadbabaie, *et al.*, "Online control customization via optimization-based control," 2003.

[96] G. Hassapis, "Implementation of model predictive control using real-time multiprocessing computing," *Microprocessors and microsystems*, vol. 27, no. 7, pp. 327–340, 2003.

[97] K. Ling, S. Yue, and J. Maciejowski, "A fpga implementation of model predictive control," in *American Control Conference, 2006*, pp. 6–pp, Ieee, 1930.

[98] M. He, C. Chen, and X. Zhang, "Fpga implementation of a recursive rank one updating matrix inversion algorithm for constrained mpc," in *Intelligent Control and Automation, 2006. WCICA 2006. The Sixth World Congress on*, vol. 1, pp. 733–737, IEEE, 2006.

[99] M. Hassan, R. Dubay, C. Li, and R. Wang, "Active vibration control of a flexible one-link manipulator using a multivariable predictive controller," *Mechatronics*, vol. 17, no. 6, pp. 311–323, 2007.

[100] K. Zmeu and E. Shipitko, "Predictive controller design with offline model learning for flexible beam control," in *Physics and Control, 2005. Proceedings. 2005 International Conference*, pp. 345–350, 2005.

[101] L. Bossi, C. Rottenbacher, G. Mimmi, and L. Magni, "Multivariable predictive control for vibrating structures: An application," *Control Engineering Practice*, 2011.

[102] T. Fan and C. De Silva, "Dynamic modelling and model predictive control of flexible-link manipulators," *International Journal of Robotics and Automation*, vol. 23, no. 4, pp. 227–234, 2008.

[103] P. Boscariol, A. Gasparetto, and V. Zanotto, "Vibration reduction in a flexible link mechanism through the synthesis of an mpc controller," in *Proceedings of the 5th IEEE Iternational Conference on Mechatronics (ICM2009)*, (Malaga, Spain), 14-17 April 2009.

[104] P. Boscariol, A. Gasparetto, M. Giovagnoni, A. Lanzutti, R. Vidoni, and V. Zanotto, "Receding horizon control of a compliant manipulator: experimental analysis," in *Proceedings of the 13th IFToMM World Congress in Mechanism and Machine Science, Guanajuato, Mexico*, pp. 1–10, IFToMM, June 19-25 2011.

[105] P. Boscariol, A. Gasparetto, and V. Zanotto, "Model predictive control of a flexible links mechanism," *Journal of Intelligent and Robotic Systems*, vol. 58-2, pp. 125–147, 2010.

[106] P. Boscariol, A. Gasparetto, and V. Zanotto, "Active position and vibration control of a flexible links mechanism using model-based predictive control," *Journal of Dynamic Systems, Measurement, and Control*, vol. 132, January 2010.

[107] P. Boscariol, "Experimental validation of a special state observer for a class of flexible link mechanisms," *Annals of Faculty Engineering Hunedoara - International Journal of Engineering*, vol. XI, no. 1, pp. 179–182, 2011.

[108] P. Boscariol and V. Zanotto, "Design of a controller for trajectory tracking for compliant mechanisms with effective vibration suppression," *Robotica*, vol. 30, no. 1, pp. 15–29, 2012.

[109] P. Boscariol, A. Gasparetto, and V. Zanotto, "Trajectory following and vibration control for flexible-link manipulators," *ROMANSY 18 Robot Design, Dynamics and Control*, pp. 299–306, 2010.

[110] P. Boscariol, A. Gasparetto, A. Lanzutti, R. Vidoni, and V. Zanotto, "Flimhils: A hardware-in-the-loop simulator of flexible links mechanisms," *Acta Mechanica Slovaca*, vol. 2-A, pp. 81–94, June 2008.

[111] P. Boscariol, A. Gasparetto, and V. Zanotto, "Design and experimental validation of a hardware-in-the-loop simulator for mechanisms with link flexibility," in *Proceedings of the 10th Biennial Conference on Engineeing and System Design and Analysis - ESDA2010-24254, July 12-14*, (Istanbul, Turkey), July 12-14 2011.

[112] G. Lowen and W. Jandrasits, "Survey of investigations into the dynamic behavior of mechanisms containing links with distributed mass and elasticity," *Mechanism and Machine theory*, vol. 7, no. 1, pp. 3–17, 1972.

[113] A. Erdman and G. Sandor, "Kineto-elastodynamics–A review of the state of the art and trends," *Mechanism and Machine Theory*, vol. 7, no. 1, pp. 19–33, 1972.

[114] G. Lowen and C. Chassapis, "The elastic behavior of linkages: an update," *Mechanism and machine theory*, vol. 21, no. 1, pp. 33–42, 1986.

[115] D. Turcic and A. Midha, "Generalized equations of motion for the dynamic analysis of elastic mechanism systems," *Journal of dynamic systems, measurement, and control*, vol. 106, no. 4, pp. 243–248, 1984.

[116] F. Liou and A. Erdman, "Analysis of a high-speed flexible four-bar linkage: Part I - formulation and solution.," *TRANS. ASME J. VIBRAT. ACOUST. STRESS RELIAB. DES.*, vol. 111, no. 1, pp. 35–41, 1989.

[117] B. Jonker, "Linearization of dynamic equations of flexible mechanismsa finite element approach," *International journal for numerical methods in engineering*, vol. 31, no. 7, pp. 1375–1392, 1991.

[118] K. Hsiao and R. Yang, "Effect of member initial curvature on a flexible mechanism response," *Journal of sound and vibration*, vol. 190, no. 2, pp. 177–194, 1996.

[119] W. Yoo and E. Haug, "Dynamics of flexible mechanical systems using vibration and static correction modes," *Journal of Mechanisms, Transmissions and Automation in Design*, vol. 108, pp. 315–322, 1986.

[120] C. Damaren and I. Sharf, "Simulation of flexible-link manipulators with inertial and geometric nonlinearities," *Journal of dynamic systems, measurement, and control*, vol. 117, p. 74, 1995.

[121] R. Gregorio and V. Parenti-Castelli, "On the characterization of the dynamic performances of planar manipulators," *Meccanica*, vol. 40, no. 3, pp. 267–279, 2005.

[122] H. Attia, "Dynamic analysis of spatial linkages: a recursive approach," *Meccanica*, vol. 40, no. 1, pp. 1–18, 2005.

[123] R. Caracciolo and A. Trevisani, "Simultaneous rigid-body motion and vibration control of a flexible four-bar linkage," *Mechanism and machine theory*, vol. 36, no. 2, pp. 221–243, 2001.

[124] L. Chang and J. Hamilton, "The kinematics of robotic manipulators with flexible links using an equivalent rigid link system (ERLS) model," *Journal of dynamic systems, measurement, and control*, vol. 113, p. 48, 1991.

[125] M. Giovagnoni, "Simplifications using isoparametric elements in flexible linkage analysis," *International Journal for Numerical Methods in Engineering*, vol. 28, no. 4, pp. 967–977, 1989.

[126] T. Wasfy and A. Noor, "Computational strategies for flexible multibody systems," *Applied Mechanics Reviews*, vol. 56, p. 553, 2003.

[127] G. Franklin, M. Workman, and D. Powell, *Digital control of dynamic systems*. Addison-Wesley Longman Publishing Co., Inc. Boston, MA, USA, 1997.

[128] B. Anderson, J. Moore, and D. Naidu, *Optimal control: linear quadratic methods*. Prentice Hall Englewood Cliffs, NJ, 1990.

[129] K. Ogata, *Modern control engineering*. Prentice Hall PTR, 2001.

[130] M. Moallem, *Control and Design of Flexible-Link Manipulators*. PhD thesis, Concordia University, 1996.

[131] M. Spong, "Underactuated mechanical systems," *Control Problems in Robotics and Automation*, pp. 135–150, 1998.

[132] L. Sciavicco and B. Siciliano, "Robotica industriale: modellistica e controllo di manipolatori," *Robotica Industriale: Modellistica e Controllo di Manipulatori*, 1995.

[133] B. Siciliano and O. Khatib, *Springer handbook of robotics*. Springer-Verlag New York Inc, 2008.

[134] A. De Luca and B. Siciliano, "An asymptotically stable joint pd controller for robot arms with flexible links under gravity," in *Decision and Control, 1992., Proceedings of the 31st IEEE Conference on*, pp. 325–326, IEEE, 1992.

[135] J. Bobrow, S. Dubowsky, and J. Gibson, "Time-optimal control of robotic manipulators along specified paths," *The International Journal of Robotics Research*, vol. 4, no. 3, p. 3, 1985.

[136] B. Martin and J. Bobrow, "Minimum-effort motions for open-chain manipulators with task-dependent end-effector constraints," *The International Journal of Robotics Research*, vol. 18, no. 2, p. 213, 1999.

[137] Z. Sun and J. Reif, "On energy-minimizing paths on terrains for a mobile robot," in *Robotics and Automation, 2003. Proceedings. ICRA'03. IEEE International Conference on*, vol. 3, pp. 3782–3788, IEEE, 2003.

[138] D. Miu and S. Bhat, "Minimum power and minimum jerk position control and its applications in computer disk drives," *Magnetics, IEEE Transactions on*, vol. 27, no. 6, pp. 4471–4475, 1991.

[139] Z. Shiller, "Time-energy optimal control of articulated systems with geometric path constraints," in *Robotics and Automation, 1994. Proceedings., 1994 IEEE International Conference on*, pp. 2680–2685, IEEE, 1994.

[140] L. Van Willigenburg, "Computation and implementation of digital time-optimal feedback controllers for an industrial xy robot subjected to path, torque, and velocity constraints," *The International journal of robotics research*, vol. 12, no. 5, p. 420, 1993.

[141] F. Lin and R. Brandt, "An optimal control approach to robust control of robot manipulators," *Robotics and Automation, IEEE Transactions on*, vol. 14, no. 1, pp. 69–77, 1998.

[142] R. Theodore and A. Ghosal, "Robust control of multilink flexible manipulators," *Mechanism and machine theory*, vol. 38, no. 4, pp. 367–377, 2003.

[143] D. Kirk, *Optimal control theory: an introduction*. Dover Pubns, 2004.

[144] B. Anderson and J. Moore, *Optimal control: linear quadratic methods*. Prentice-Hall Englewood Cliffs (NJ):, 1989.

[145] H. Kwakernaak and R. Sivan, *Linear optimal control systems*, vol. 188. Wiley-Interscience New York, 1972.

[146] J. Richalet, A. Rault, J. Testud, and J. Papon, "Model predictive heuristic control:: Applications to industrial processes," *Automatica*, vol. 14, no. 5, pp. 413–428, 1978.

[147] J. Maciejowski, *Predictive Control with Constraints*. Prentice Hall. Harlow, UK., 2001.

[148] C. Cutler and B. Ramaker, "Dynamic matrix control-a computer control algorithm," in *Proceedings of the joint automatic control conference*, pp. 13–15, 1980.

[149] D. Prett and R. Gillette, "Optimization and constrained multivariable control of a catalytic cracking unit," in *Proceedings of the joint automatic control conference*, vol. 1, 1980.

[150] G. M. Bitmead G. and W. V., "Adaptive optimal control, the thinking man's GPC," 1990.

[151] D. Mayne, "Optimization in model based control 1," *Dynamics and Control of Chemical Reactors, Distillation Columns and Batch Processes*, p. 229, 1995.

[152] L. Wang, *Model Predictive Control System Design and Implementation using MATLAB*. Springer Verlag, 2009.

[153] E. Camacho and C. Bordons, *Model predictive control*. Springer Verlag, 2004.

[154] C. Bordons and E. Camacho, "A generalized predictive controller for a wide class of industrial processes," *Control Systems Technology, IEEE Transactions on*, vol. 6, no. 3, pp. 372–387, 1998.

[155] J. Richalet, *Pratique de la Commande Prèdictive*. Edition Hermès, Paris, 1993.

[156] J. Leitner, "Space technology transition using hardware in the loop simulation," in *Aerospace Applications Conference, 1996. Proceedings., 1996 IEEE*, vol. 2, pp. 303–311, IEEE, 1996.

[157] H. Hanselmann, "Hardware-in-the-loop simulation testing and its integration into a cacsd toolset," in *Computer-Aided Control System Design, 1996., Proceedings of the 1996 IEEE International Symposium on*, pp. 152–156, IEEE, 1996.

[158] G. Pritschow and S. R
"ock, "hardware in the loop simulation of machine tools," *CIRP Annals-Manufacturing Technology*, vol. 53, no. 1, pp. 295–298, 2004.

[159] G. Stoeppler, T. Menzel, and S. Douglas, "Hardware-in-the-loop simulation of machine tools and manufacturing systems," *Computing & Control Engineering Journal*, vol. 16, no. 1, pp. 10–15, 2005.

[160] X. Hu, "Applying robot-in-the-loop-simulation to mobile robot systems," in *Advanced Robotics, 2005. ICAR'05. Proceedings., 12th International Conference on*, pp. 506–513, IEEE, 2005.

[161] F. Aghili and J. Piedboeuf, "Contact dynamics emulation for hardware-in-loop simulation of robots interacting with environment," in *Robotics and Automation, 2002. Proceedings. ICRA'02. IEEE International Conference on*, vol. 1, pp. 523–529, IEEE, 2002.

[162] R. Chhabra and M. Emami, "Concurrent design of robot manipulators using hardware-in-the-loop simulation," in *2008 IEEE International Conference on Technologies for Practical Robot Applications (TePRA)*, 2008.

[163] A. Martin, E. Scott, and M. Emami, "Design and development of robotic hardware-in-the-loop simulation," in *Control, Automation, Robotics and Vision, 2006. ICARCV'06. 9th International Conference on*, pp. 1–6, IEEE.

[164] E. Bringmann and A. Kramer, "Model-based testing of automotive systems," in *Software Testing, Verification, and Validation, 2008 1st International Conference on*, pp. 485–493, Ieee.

[165] R. Isermann, J. Schaffnit, and S. Sinsel, "Hardware-in-the-loop simulation for the design and testing of engine-control systems," *Control Engineering Practice*, vol. 7, no. 5, pp. 643–653, 1999.

[166] A. Gasparetto, "Accurate modelling of a flexible-link planar mechanism by means of a linearized model in the state-space form for design of a vibration controller," *Journal of Sound and vibration*, vol. 240, no. 2, pp. 241–262, 2001.

[167] Y. Chang and H. Yen, "Design of a robust position feedback tracking controller for flexible-joint robots," *Control Theory & Applications, IET*, vol. 5, no. 2, pp. 351–363, 2011.

[168] N. Ghahramani and F. Towhidkhah, "Constrained incremental predictive controller design for a flexible joint robot," *ISA transactions*, vol. 48, no. 3, pp. 321–326, 2009.

[169] A. Gasparetto and V. Zanotto, "A technique for time-jerk optimal planning of robot trajectories," *Robotics and Computer-Integrated Manufacturing*, vol. 24, no. 3, pp. 415–426, 2008.

[170] L. Meirovitch, *Principles and techniques of vibrations*. Prentice Hall Upper Saddle River, NJ, 1997.

[171] J. Craig, *Introduction to robotics*, vol. 7. Addison-Wesley Reading, MA, 1989.

List of Figures

2.1 Kinematic definitions 14

3.1 Elastic deformation of a single link mechanism with an external load F_y = -10 N applied to the free end 26
3.2 Position vectors for the four-bar mechanism under investigation . 27
3.3 Finite element discretization for the 4-bar mechanism 28
3.4 Matrix assembling for multi-element discretization 28
3.5 Nodes after the imposition of constraints 29
3.6 EULA PacDrive D2 robot 31
3.7 Position vectors for the 5-link mechanism 32
3.8 Nodal discretization for the whole mechanism 33
3.9 Static deformation of a 5-bar linkage under gravity and external loads 34
3.10 Static deformation of a 5-bar mechanism under a 10 N load applied to the end-point 35
3.11 Simulink model for single link mechanism, discretized with a single finite element 36
3.12 S-function: execution flowchart 39
3.13 Free response of the single-link mechanisms with initial condition $q_0 = -\pi/3$: rigid displacement q 40
3.14 Free response of the single-link mechanisms with initial condition $q_0 = -\pi/3$: elastic displacements u_1, u_2 and u_3 40

3.15 Torque impulse applied to the FLM 41
3.16 Forced response: angular position q 42
3.17 Forced response: elastic displacements 42
3.18 Applied torque 43
3.19 Elastic displacement with 1 and 2 finite elements: elastic displacement u_x 44
3.20 Elastic displacement with 1 and 2 finite elements: elastic displacement u_y 45
3.21 Elastic displacement with 1 and 2 finite elements: elastic displacement u_z 45
3.22 Elastic displacement with 2 and 3 elements discretization: elastic displacement u_x 46
3.23 Elastic displacement with 2 and 3 elements discretization: elastic displacement u_y 46
3.24 Elastic displacement with 2 and 3 elements discretization: elastic displacement u_z 47
3.25 Four-bar mechanisms: finite element discretization 48
3.26 Simulink model for the flexible 4-bar mechanisms 49
3.27 Free response: elastic displacement u_9 along the x axis 50
3.28 Free response: elastic displacement u_{10} along the y axis 50
3.29 Free response: elastic displacement u_{11} along the z axis 51
3.30 Free response: crank position q 51
3.31 Torque sollicitation 52
3.32 Angular position of the crank, q 52
3.33 Elastic displacement at the 6^{th} node: u_9 along the x axis 53
3.34 Elastic displacement at the 6^{th} node: u_{10} along the y axis 53
3.35 Elastic displacement at the 6^{th} node: u_{11} along the z axis 54
3.36 5 bar mechanism: finite element discretization 55
3.37 Free response with initial conditions: $q_1(0) = 2/3\pi$ and $q_2(0) = \pi/2$: angular positions q_1 and q_2 56
3.38 Free response eith initial conditions: $q_1(0) = 2/3\pi$ and $q_2(0) = \pi/2$: elastic displacement u_6 57
3.39 Free response eith initial conditions: $q_1(0) = 2/3\pi$ and $q_2(0) = \pi/2$: elastic displacement u_7 58
3.40 Free response with initial conditions: $q_1(0) = 2/3\pi$ and $q_2(0) = \pi/2$: elastic displacmenet u_8 58
3.41 Torque sollicitations to the two cranks 59

3.42 Evolution of angular positions q_1 and q_2 60
3.43 Elastic displacement alog the x axis at the midspan of the second link 61
3.44 Elastic displacement alog the y axis at the midspan of the second link 61
3.45 Elastic displacement alog the z axis at the midspan of the second link 62

4.1 Generic control in the joint space 64
4.2 Generic control in the operative space 64
4.3 Feedback control 65
4.4 Feedforward control 65
4.5 Block diagram of a single joint actuation system 66
4.6 Generic control for each independent joint 67
4.7 PD control with gravity compensation: block diagram 68
4.8 LQG control: block diagram 71
4.9 Block diagram of discrete-time model predictive control 83
4.10 Unconstrained MPC with state observer: block diagram 87
4.11 Predictive control: the basic idea 89
4.12 Structure of unconstrained control 99

5.1 Experimental tests: traditional approach 105
5.2 Experimental tests: Hardware-In-the-Loop approach 106
5.3 The mechanisms used for experimental tests 109
5.4 Frequency spectrum of strain signal: comparison between experimental results and HIL simulation 110
5.5 Finite-element discretization: nodal displacements 110
5.6 The HIL test bench: PXI-based simulator and Real-Time controller 112
5.7 PI position control: control diagram 115
5.8 PI position control: experimental validation of the angular position closed-loop response 116
5.9 PI position control: experimental validation of the torque closed-loop response 117
5.10 PID position control: experimental validation of the strain gauge signal closed-loop response - detailed view of the transient 118
5.11 LQY with integral action position and vibration control: control diagram 119

5.12 Optimal control: experimental validation of the angular position closed-loop response 120
5.13 Optimal control: experimental validation of the torque closed-loop response 121
5.14 Optimal control: experimental validation of the strain gauge signal closed-loop response - detailed view of transient 121
5.15 Optimal control: experimental validation of the angular position closed-loop response 122
5.16 Optimal control: experimental validation of the torque closed-loop response 122
5.17 Optimal control: experimental validation of the strain gauge signal closed-loop response - detailed view of transient 123

6.1 The four-link mechanism used for simulations 127
6.2 Elastic displacements in the four-link mechanism 128
6.3 Crank angular position q. (a) Comparison of the nonlinear and linearized system impulsive responses. (b) Error in per cent vs. time. (c) Error in per cent vs. angular motion from the "equilibrium" configuration 130
6.4 Comparison of the nonlinear and linearized system impulsive responses for the nodal displacement u_2. (a) Transient responses. (b) Steady state responses. (c) Error in per cent vs. time. (d) Error in per cent vs. angular motion from the "equilibrium" configuration. 131
6.5 Nodal displacement u_{10}. (a) Comparison of the nonlinear and linearized system impulsive responses. (b) Absolute error vs. time. (c) Error in per cent vs. angular motion from the "equilibrium" configuration. 131
6.6 Displacement q. (a) Comparison of the nonlinear system and observer impulsive responses. (b) Error in per cent vs. time . . . 133
6.7 Nodal displacement u_2. (a) Comparison of the nonlinear system and observer impulsive responses. (b) Error in per cent vs. time 133
6.8 Nodal displacement u_{10}. (a) Comparison of the nonlinear system and observer impulsive responses. (b) Error in per cent vs. time 134
6.9 Nodal displacement u_{12}. (a) Comparison of the nonlinear system and observer impulsive responses. (b) Error in per cent vs. time 134

6.10 Angular position of the crank q. (a) Response of the MPC control (b) Error on q 135
6.11 Elastic displacements measured in the local reference frame employing the MPC control. (a) Elastic displacement u_9 (b) Elastic displacement u_{10} 136
6.12 Mechanism configurations: initial, during the motion, final. Elastic deformation is displayed with a $\times 10$ gain 136
6.13 Robustness analysis to the change of linear mass density m. (a) Angular position q. (b) Elastic displacement u_{10} measured in the local reference frame. 138
6.14 Robustness analysis to the change of length of the first link L_1 (a) Angular position q. (b) Elastic displacement u_{10} measured in the local reference frame. 138
6.15 Robustness analysis to the change of elastic modulus E (a) Angular position q. (b) Elastic displacement u_{10} measured in the local reference frame. 139
6.16 Robustness analysis to the change of applied torque: (a) Angular position q. (b) Elastic displacement u_{10} measured in the local reference frame. 139
6.17 Robustness analysis to the change of applied torque and noisy torque: (a) Angular position q. (b) Elastic displacement u_{10} measured in the local reference frame. 140
6.18 Response of the control system at with different sampling frequency: 1 Khz and 100 Hz(a) Angular position q. (b) Angular position q: zoom view (c) Elastic displacement u_{10} measured in the local reference frame (d) Elastic displacement u_9 measured in the local reference frame. 141
6.19 Analysis of the effects of different control horizon H_c: (a) Angular position q. (b) Elastic displacement u_{10} measured in the local reference frame. 142
6.20 Analysis of the effects of different prediction horizon H_p on a perturbed version of the plant: (a) Angular position q. (b) Elastic displacement u_{10} measured in the local reference frame. 142
6.21 Comparison of the response of the system with PID and MPC control. (a) Angular position q. (b) Elastic displacement u_{10}. . . 143
6.22 Five-link manipulator (Mechatronics Lab, University of Udine) . 145

6.23 Elastic displacements and angular position in the five-link mechanism . . . 146
6.24 Torques applied to derive plots in Figures 6.25, 6.26, 6.27 149
6.25 (a) Comparison of actual and estimated angular position, estimation error for q_1 (b) absolute error on q_1 . . . 149
6.26 (a) Comparison of actual and estimated angular position, estimation error for q_2 (b) absolute error on q_2 . . . 150
6.27 (a) Comparison of actual and estimated nodal displacement, estimation error for u_8 (b) absolute error on u_8 . . . 150
6.28 Structure of the MPC controller . . . 151
6.29 Closed-loop system . . . 151
6.30 Closed-loop performances: (a) evolution of angular positions q_1 and q_2 (b) angular displacements u_1 and u_{18} for reference tracking in the operational space . . . 152
6.31 Closed-loop performances: torques τ_1 and τ_2 applied by the two actuators . . . 153
6.32 Comparison of reference tracking with and without reference lookahead (a),(b) angular position q_1 (c),(d) angular position q_2 154
6.33 Effects of different values of the control horizon H_c ($H_p = 10$): (a) angular position q_1 of the first link (b) angular position q_2 of the fourth link . . . 154
6.34 Effects of different values of the control horizon H_c ($H_p = 10$): (a) angular displacement u_1 along the first link (b) angular displacement u_{18} along the fourth link . . . 155
6.35 Effects of different values of the prediction horizon H_p ($H_c = 10$): (a) angular displacement u_1 (b) angular displacement u_{18} 156
6.36 Effects of different values of the prediction horizon H_p ($H_c = 10$): (a) angular position q_1 of the first link (b) angular position q_2 of the fourth link . . . 156
6.37 Effects of different values of H_p and H_c: (a) performance index k_1 (b) performance index k_2 . . . 158
6.38 Comparison of the response of the nominal and of two perturbed plants with added noise: (a) angular position q_1 of the first link (b) angular position q_2 of the fourth link . . . 158
6.39 Comparison of the response of the nominal and two perturbed plants with added noise: (a) angular displacement u_1 (b) angular displacement u_{18} . . . 159

6.40 Reference trajectory for the end effector in the operational space 160
6.41 Actual q_i and planned q_{iD} trajectories: positions (a), velocities(b) and acceleration (c) 161
6.42 Evolution of sensitivity coefficients for the end effector position along the planned trajectories: (a) w_{11} (b) w_{12} (c) w_{21} (d) w_{22} . 162
6.43 Nodal displacements u_1 and u_{18} 163
6.44 Path following errror of the manipulator end-effector C along the desired trajectory with different task execution times 164
6.45 Effects on the trajectory error of increments on deformation weights 164
6.46 Effects of the interpolating function on the trajectory error . . . 165
6.47 Velocities (a) and acceleration (b) of q_1 and q_2 with 3^{rd}, 5^{th} and 7^{th} order interpolation functions 166
6.48 (a) Trajectory in the Cartesian space; (b) Trajectory and position errors of the joints 166
6.49 (a) Nodal displacements u_1, u_{18}; (b) Input torques 167
6.50 (a) Sensibility's coefficients; (b) Position error 167
6.51 The flexible-link mechanism used for experimental tests 171
6.52 Experimental setup 173
6.53 MPC control: block diagram 173
6.54 State observer; (a) measured and estimated strain gauge signals (b) estimation error 174
6.55 MPC control: closed-loop response to a step position reference. Test 1 (a,b,c) and Test 2 (d,e,f) 176
6.56 LQ control with integral action: block diagram 177
6.57 LQ vs MPC: (a) comparison of angular position tracking (b) comparison of strain gauge signal 179

A.1 Truss element 184
A.2 Elastic displacement for a truss element with a fixed end 186
A.3 Equivalent nodal load for a 2 d.o.f. truss element 188
A.4 4 d.o.f. beam element 190
A.5 Interpolating function for the 4 d.o.f. beam element 191
A.6 D.o.f. in the local reference frame 193
A.7 Global and local reference frames 194
A.8 6 d.o.f. beam element: nodal displacements 195

List of Tables

3.1 Characteristics of the FLM 24
3.2 Nodal displacement in the 4-bar linkage with $q = \pi/6$ 30

5.1 Structural and dynamics characteristics of the flexible rod 108
5.2 Dynamic characteristics of the actuator 111

6.1 Kinematic and dynamic characteristics of reference mechanism . 127
6.2 Comparison of vibration damping times and % overshoot 144
6.3 Kinematic an dynamic characteristics of the flexible link mechanism 146
6.4 Structral and dynamics characteristics of the flexible rod 172
6.5 MPC tuning parameters 175

UNIVERSITÀ DEGLI STUDI DI UDINE
DIPARTIMENTO DI INGEGNERIA ELETTRICA, GESTIONALE E MECCANICA

Udine, 26 gennaio 2012

Presentazione e giudizio finale sull'attività svolta da Paolo Boscariol nell'ambito del XIV Ciclo del Corso di Dottorato in Ingegneria Industriale e dell'Informazione

Negli anni accademici 2009, 2010, 2011, il dott. Paolo Boscariol ha frequentato presso il Dipartimento di Ingegneria Elettrica, Gestionale e Meccanica dell'Università di Udine il corso di Dottorato in **Ingegneria Industriale e dell'Informazione, XIV ciclo.**

Attività didattica

Corsi mutuati dai corsi di laurea dell'Università di Udine

- Regolazione e controllo in tempo reale – Prof. D. Casagrande

Partecipazione a scuole e corsi esterni

- Scuola Sidra 2009 – Controllo robusto e vincolato, Bertinoro 13/07/09-18/07/09
- Corso PCDIMS CAD++ - 14/12/2009 – 18/12/2009

Altri seminari seguiti

- Workshop Robcast – Università di Siena – 04/05/09

Partecipazione a Conferenze Internazionali

- ICM 2009 - IEEE International Conference on Mechatronics, 14-17 April 2009 Malaga – Spain
- CISM-IFToMM Symposium on Robot Design, Dynamics, and Control - Romansy 2010 July 5-8, Udine – Italy
- 13th IFToMM World Congress in Mechanism and Machine Science, Guanajuato (Mexico), June 19-25, 2011
- INTERNATIONAL SYMPOSIUM on ADVANCED ENGINEERING & APPLIED MANAGEMENT – 40th ANNIVERSARY in HIGHER EDUCATION – Hunedoara (Romania) 4-5 Novembre 2010

Partecipazione a Conferenze Nazionali

- XIX Congresso Aimeta - Ancona 14-17 settembre 2009

Periodi di Attività all'estero

DIEGM – via Delle Scienze, 208 – 33100 Udine – Italia – tel. + 39 - 0432 558253 – fax + 39 -0432 558251
e-mail: segreteria.diegm@amm.uniud.it – c.f. 80014550307 – p. IVA 01071600306

- 31 Agosto 2011-18 Dicembre 2011 visiting PhD student presso Menrva Lab – Simon Fraser University, Vancouver, Canada

Riconoscimenti

- Premio "Nicola Chiari" 2010 per la migliore applicazione di controllo e di misura, NIDays 2010, Roma

Attività di Ricerca

L'attività di Ricerca dell' Ing. Boscariol ha riguardato diverse problematiche legate alla modellizzazione ed il controllo di meccanismi a membri flessibili. Lo studio di modelli dinamici di meccanismi flessibili ha portato allo sviluppo di applicazioni di controllo predittivo model-based (MPC) per questo tipo di dispositivi, ed allo sviluppo di simulatori Real-Time per applicazioni Hardware-In-the-Loop.
In particolare, si è dimostrato tramite prove sia numeriche che sperimentali la validità dell'approccio scelto.
Parallelamente sono state affrontate alcune problematiche riguardanti lo sviluppo di tecniche per la pianificazione di traiettorie per manipolatori flessibili, basate sulle tecniche del controllo ottimo e della modellizzazione dinamica agli elementi finiti. Partendo da una accurata descrizione del modello dinamico di un manipolatore è pertanto possibile definire una traiettoria ottima secondo una arbitraria legge di costo.
Inoltre l'ing. Boscariol, in collaborazione con il gruppo di ricerca Menrva Lab, Simon Fraser University, Vancouver – Canada, si è dedicato alla ricerca di tecniche numeriche per l'ottimizzazione dell'andatura di climbing robot che utilizzano dry adhesive.

Elenco Pubblicazioni

[1] P Boscariol, V. Zanotto "Design of a controller for trajectory tracking for compliant mechanisms with effective vibration suppression" Robotica, Volume 30, pp. 15–29 (2012)

[2] P. Boscariol, A. Gasparetto, V. Zanotto "Simultaneous position and vibration control system for flexible link mechanisms" Meccanica, vol. 46 (4), August 2011, pp. 723-737, DOI: 10.1007/s11012-010-9333-9

[3] P. Boscariol "Experimental validation of a special state observer for a class of flexible link mechanisms"Annals of Faculty Engineering Hunedoara – International Journal of Engineering. Vol. XI-1 pp. 179-182 (2011)

[4] P. Boscariol, A. Gasparetto, A. Lanzutti, R. Vidoni, V. Zanotto "Neumesy: A special robot for neurosurgery" Annals of Faculty Engineering Hunedoara – International Journal of Engineering. Vol. IX-2 pp. 65-72 (2011)

[5] P. Boscariol, A. Gasparetto, A. Lanzutti, R. Vidoni, V. Zanotto "Experimental validation of minimum time-jerk algorithms for industrial robots" Journal of Intelligent & Robotic Systems, Volume 64, Number 2, November 2011, pp. 197-219, DOI: 10.1007/s10846-010-9533-5

[6] P. Boscariol, A. Gasparetto, V. Zanotto "A HIL simulator of Flexible-Link Mechanisms" Journal of Intelligent & Robotic Systems, Volume 64, Number 3-4, December 2011, pp. 427-446, DOI: 10.1007/s10846-011-9547-7

[7] V. Zanotto, P. Boscariol, A. Gasparetto, A. Lanzutti, R. Vidoni, N. Di Lorenzo, P. Gallina, A. Dalla Via , A. Rossi "A master-slave haptic system for neurosurgery" Applied Bionics and Biomechanics 8 (2011), pp- 209-220

[8] P. Boscariol, A. Gasparetto, A. Lanzutti, R. Vidoni, V. Zanotto "Sistema di controllo Real-Time per un robot cartesiano" Proc. of NIDays2011, Milano, 23 Febbraio 2011

[9] P. Boscariol, A. Canderan, A. Gasperetto, R. Vidoni "An advanced manufacturing system based on MARS (multi agent robotic system)" Proc. of the 9th International Conf. on Advanced Manufacturing Systems and Technology AMST '11, Mali Losinj (Croatia), June 16-17 2011, pp.295-306

[10] P. Boscariol, A. Gasparetto, M. Giovagnoni, R. Vidoni "Experimental validation of an innovative haptic system for surgical robotics" Proc. of the 9th International Conf. on Advanced Manufacturing Systems and Technology AMST '11, Mali Losinj (Croatia), June 16-17 2011, pp.271-282

[11] R. Vidoni, A. Gasparetto, M. Giovagnoni and P. Boscariol "A novel 3D equivalent rigid link system approach for flexible-link mechanisms: formulation and comparison with the floating frame of reference approach" Proc. of the ECCOMAS Thematic Conference on Multibody Dynamics 2011, Brussels, July 4-7 2011, pp.1-13

[12] P. Boscariol, A. Gasparetto, M. Giovagnoni, A. Lanzutti, R. Vidoni, V. Zanotto "Receding horizon control of a compliant manipulator: experimental analysis" Proceedings of the 13th IFToMM World Congress in Mechanism and Machine Science, Guanajuato (Mexico), June 19-25, 2011, pp.1-10

[13] R. Vidoni, A. Gasparetto, M. Giovagnoni, P. Boscariol "Dynamic analysis and simulation of spatial flexible-link manipulators by means of a novel Equivalent Rigid Link System approach" Atti del XX Congresso Nazionale AIMETA, Bologna, 12-15 settembre 2011

[14] A. Gasparetto, P. Boscariol, A. Lanzutti, R. Vidoni "Trajectory planning in Robotics" Proc. of the Int.l Workshop on Mathematics and Algorithms for CAM, Engineering and Numerical Control (MAMENC), Beijing, Oct. 24-26, 2011, pp. 1-13

[15] P Boscariol "Sistema meccatronico intelligente per meccanismi flessibili" Proc. of NIDays2011, Milano, 23 Febbraio 2011

[16] P. Boscariol, A. Gasparetto, V. Zanotto "Model Predictive Control of a Flexible Links Mechanism" Journal of Intelligent & Robotic Systems: Volume 58, Issue 2 (May 2010), Page 125-147

[17] P. Boscariol, A.Gasparetto and Vanni Zanotto "Active Position and Vibration Control of a Flexible Links Mechanism Using Model-Based Predictive Control" ASME Journal of Dynamic Systems, Measurement, and Control, January 2010, Vol. 132, DOI: 10.1115/1.4000658

[18] P. Boscariol, V. Zanotto, A. Gasparetto, F. Parere, O. Toscano, D. Baggio "Hardware-in-the-Loop Simulator for the rapid development of domestic dryers" Proceedings of the NIDays 2010. Roma, 24 febbraio 2010, pp. 61-62

[19] V. Zanotto, A. Gasparetto, P. Boscariol, A. Lanzutti, R. Vidoni, A. Rossi "A haptic master-slave robotic system for minimally invasive neurosurgery with NI cRIO and NI LabVIEW" Proceedings of the NIDays 2010. Roma, February, 24 (2010), pp. 63-64 (2010 Best Appl. 'N.Chiari' Award Winner)

[20] P. Boscariol, A. Gasparetto, V. Zanotto "Trajectory Following and Vibration Control for Flexible-link Manipulators" Proceedings of the 18th CISM-IFToMM Symposium on Robot Design, Dynamics, and Control - Romansy 2010 July 5-8, 2010 pp. 299-306

[21] P. Boscariol, A. Gasparetto, V. Zanotto "Design and Experimental Validation of a Hardware-In-the-Loop Simulator for Mechanisms with Link Flexibility" Proceedings of the 10th Biennial Conference on Engineeing and System Design and Analysis - ESDA2010-24254, July 12-14

[22] Boscariol, P. Gasparetto, A. Zanotto, V."Vibration reduction in a flexible link mechanism through the synthesis of an MPC controller" ICM 2009 - IEEE International Conference on Mechatronics, 14-17 April 2009 pp. 1-6 DOI 10.1109/ICMECH.2009.4957182

[23] A Antoniolli, P. Boscariol, A. Gasparetto, A. Lanzutti, R. Vidoni, V. Zanotto "Sistema meccatronico intelligente per dispositivi di apertura e chiusura automatici" Proceedings of NIDays 09 - Forum Tecnologico sulla Progettazione Grafica di Sistemi, Milano 25 Febbraio 2009

[24] P. Boscariol, A. Gasparetto, M. Giovagnoni, A. Lanzutti, R. Vidoni, V. Zanotto "Innovative Control Techniques for Mechatronic Systems" XIX Congresso Aimeta - Ancona 14-17 settembre 2009

[25] A. Dalla Via, G. Boschetti, P. Boscariol, A. Gasparetto, A. Lanzutti, R. Vidoni, V. Zanotto "FLIMHILS: A Hardware-in-the-Loop Simulator of Flexible Links Mechanisms" Acta Mechanica Slovaca vol 12 no. 2 A, 2008, pp. 81-94

UNIVERSITÀ DEGLI STUDI DI UDINE
DIPARTIMENTO DI INGEGNERIA
ELETTRICA, GESTIONALE E MECCANICA

Giudizio complessivo del Collegio:

Sulla base dell'attività del dottorando nel triennio, delle relazioni annuali presentate al collegio, della valutazione del tutor, che ha presentato anche i commenti di esperti esterni, il collegio giudica positivamente l'operato del dottorando, e lo ammette all'esame finale per il conseguimento del titolo.
In rappresentanza del Collegio Docenti del Dottorato di Ricerca in Ingegneria Industriale e dell'Informazione

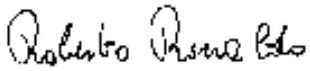

Prof. Roberto Rinaldo

Coordinatore del Collegio Docenti del Dottorato di Ricerca in Ingegneria Industriale e dell'Informazione

DIEGM – via Delle Scienze, 208 – 33100 Udine – Italia – tel. + 39 - 0432 558253 – fax + 39 -0432 558251
e-mail: segreteria.diegm@amm.uniud.it – c.f. 80014550307 – p. IVA 01071600306